BINGO
a better future under
CLIMATE CHANGE

BRINGING INNOVATION TO ONGOING
WATER MANAGEMENT

D3.5

Improved model applications/descriptions based on field data

March 2019

www.projectbingo.eu

The BINGO project has received funding from the European Union's Horizon 2020 Research and Innovation programme, under the Grant Agreement number 641739.

Horizon 2020 Societal challenge 5:
Climate action, environment, resource efficiency and raw materials

BINGO

Bringing INnovation to onGOing water management – a better future under climate change

Grant Agreement n° 641739, Research and Innovation Action

Deliverable number:	**D3.5**
Deliverable name:	**Improved model applications/descriptions based on field data**
WP / WP number:	WP3: Integrated analysis of the water cycle
Delivery due date:	Project month 45 (31/03/2019)
Actual date of submission:	29/03/2019
Dissemination level:	Public
Lead beneficiary:	CYI
Responsible scientist/administrator:	Adriana Bruggeman (CYI)
Estimated effort (PM):	24.7
Contributor(s):	T. aus der Beek (IWW), R. Becker (IWW), A. Bruggeman (CYI), H. Djuma (CYI), M. Eliades (CYI), M.L. Forcadell (AjBDN), A. Fortunato (LNEC), P. Freire (LNEC), M.H.J. van Huijgevoort (KWR), E. Kristvik (NTNU), C. Kübeck (IWW), L. Locatelli (AQUATEC), P. Lorza (WV), T. Merete Muthanna (NTNU), J. Montes (AjBDN), S. Pflug (KWR), M. Rodrigues (LNEC), B. Russo (AQUATEC), M. Scheibel (WV), A. Seifu Gragne (NTNU), D. Sunyer (AQUATEC), E. Teneketzi (WV), B.R. Voortman (KWR, Moisture Matters), J.P.M. Witte (KWR);
Estimated effort contributor(s) (PM):	AQUATEC: 0.8; AjBDN (Municipality of Badalona): 0.2; CYI: 12; IWW: 1; KWR: 12; LNEC: 0.5; NTNU: 1; WUPPERVERBAND: 4.
Internal reviewer:	H. Djuma (CYI), A. Fortunato (LNEC), M.H.J. van Huijgevoort (KWR), E. Kristvik (NTNU), L. Locatelli (AQUATEC), P. Lorza (WV)

Changes with respect to the DoA
Not applicable

Dissemination and uptake
This report is public.

Short Summary of results (<250 words)
D3.5 – Improved model applications/descriptions based on field data was developed by CYI, IWW, LNEC, NTNU, KWR, AQUATEC with support of the local stakeholder partners, within WP3 - Integrated analysis of the water cycle. The aim of the BINGO field research was to improve our understanding of hydrologic processes and to integrate this knowledge in the hydrologic model applications at the six research sites. Within the scope of the BINGO Project, soil moisture was monitored in Wupper Basin (Germany) and Troodos (Cyprus). Evapotranspiration of natural vegetation was monitored by lysimeters and in large pot experiments for the Veluwe (Netherlands) and by sapflow sensors in Troodos. Combined sewage water flows, sediment and sea water quality was monitored in Badalona (Spain), estuary water and salinity levels were monitored in Tagus (Portugal) and rainfall variability was monitored in Bergen. The field work observations were used for model calibrations (Troodos, Wupper, Badalona), validations (Tagus) and improvement of model input data (Veluwe). Field research methods and experience were exchanged between the research sites and valuable experience was gained by all project partners. The monitoring and analysis of water balance components led to an improved understanding of hydrologic processes and an improved capacity for the modelling of climate change impacts and adaptation options. Further field observations, modelling and analysis are foreseen at all sites.

Evidence of accomplishment
This report as well as the model output.

TABLE OF CONTENTS

TABLE OF FIGURES

TABLE OF TABLES

1. INTRODUCTION

This document is developed as part of the BINGO (Bringing INnovation to onGOing water management – a better future under climate change) project, which has received funding from the European Union's Horizon 2020 Research and Innovation programme, under the Grant Agreement number 641739. The Project website (www.projectbingo.eu) represents Deliverable 3.5 of Work Package 3 (WP3) – Improved model applications/descriptions based on field data.

……..

2. Overall aim of field work in BINGO

Hydrologic models are parameterized based on field observations. These field observations can include physically-based observations such as soil physical properties; parameters obtained from field experiments such as crop coefficients; and empirical or conceptual parameters, derived from model calibration with water levels, water flows or water quality observations. Climate change and socio-economic changes are affecting our environment and the hydrologic processes in our models. Thus, the observation and analysis of hydrologic properties and processes is important for improving the modelling of climate change impacts, especially for climate-water extremes such as floods and droughts. The aim of the here presented research is to improve our understanding of hydrologic processes through field observations and to integrate these observations in the hydrologic models applied at the six research sites. Evapotranspiration processes are investigated in Troodos (Cyprus) and in the Veluwe (Netherlands). Soil moisture is monitored in the Wupper Basin (Germany) and Troodos. Rainfall variability was monitored and analysed in Bergen (Norway). Estuary water and salinity levels were monitored in Tagus (Portugal) and combined sewage water flows, sediment and sea water quality were monitored in Badalona (Spain). The field work observations were used for model improvements and an outlook for further research is presented.

3. Cyprus

3.1. Introduction and objectives

The steep mountain slopes along the northern slopes of the Troodos Mountains in Cyprus are dominated by *Pinus brutia* forests. The *P. brutia* forests can be found on very shallow, steeply sloping soils. Even though little rain falls during the long and hot summer months, the trees remain green year round. However, in recent drought years die back of pine trees has been observed by the Cyprus Department of Forests. It is obvious that standard hydrologic models do not represent the hydrologic processes of these open hillslope forests. Thus, our capacity to model the effects of climate change on the hydrologic cycle in this semi-arid Mediterrenana environment is severely compromised.

P. brutia is a light demanding, fast-growing and drought resistant tree species, with a deep rooting-system, which can grow in areas with mean annual rainfall as low as 350 mm (Boydak, 2004; Nahal, 1983). *P. brutia* are systematically close species to the better known *P. halepensis* (Frankis, 1998). Both species grow under similar meteorological conditions in the Mediterranean basin (Frankis, 1998), but *P. brutia* is more water demanding and less thermophilic than *P. halepensis* (Chambel et al., 2013). There is no scientific literature on *P. brutia* transpiration and on their role in the forest water balance, in contrast to *P. halepensis,* which have been studied extensively (e.g., Schiller and Cohen, 1998; Ungar et al., 2013).

Tree roots in semi-arid regions generally extend far beyond the projected crown radius (Wu et al., 1985). Transpiration in water-limited environments would be overestimated if calculated by using the crown projected area and total evapotranspiration would exceed rainfall, leading to significant errors in water balance calculations (Crosbie et al., 2007). As an alternative, the areal extent of the roots of the trees is often approximated with the use of geometric methods (Walker et al., 1989; Wu et al., 1985). Voronoi polygons (also known as Thiessen polygons) have been applied in ecological modelling, plant growth and competition studies (e.g., Abellanas et al., 2016; Burkhart and Tomé, 2012; Gspaltl et al., 2012; Liao et al., 2013). Voronoi polygons obey the basic axiom of “configuration” in plant competition (Berger et al., 2008). These polygons divide the forest planar area by allocating it to the nearest tree. Voronoi polygons have the potential to represent the below-ground plant competition for resources (water, nutrients), but this potential has not been exploited (Berger et al., 2008; Czárán, 1998).

The GR4J model (Perrin et al., 2003) was used to analyze drought risks related to streamflow inflow to the groundwater recharge check dams in the downstream area of Peristerona Watershed WP4 (D4.3). The GR4J is a conceptual, four-parameter rainfall-runoff model. The model parameters are fitted, using daily precipitation, potential evapotranspiration and streamflow records. The model has been found suitable for simulating the streamflow for Troodos watersheds (Le Coz et al., 2016). However, the best fit of the four-parameter model does not close the water balance of the watersheds.

The main goal of the hydrologic field research in Cyprus was to improve our understanding of the effect of climate change, especially droughts, on the water balance components of the watersheds along the northern hillslopes of the Troodos Mountains. The northern slopes watersheds are located in the rain shadow of the mountains and expected to be more strongly affected by climate change than the southern slopes. The specific objectives of the field research are (i) to monitor and model the water balance components of a *P. brutia* forest; (ii) to use field observations to modify the GR4J model to simulate streamflow and evapotranspiration in the Peristerona Watershed.

The Peristerona Watershed was selected as a representative rural and forested watershed along the northern slopes of the Troodos Mountains. The forest ecohydrologic research was the subject of the PhD of Marinos Eliades (Eliades, 2018). The forestry research site and the results of 2015-2017 are described in detail in Eliades et al. (2018a, 2018b). Here we summarize the field and modeling research and present the water balance components of the forestry research site for the period 2015-2018. In addition, stream flow and meteorological parameters were monitored to improve the simulation of hydrologic processes in the watershed.

3.2. Methods

3.2.1. Study site description

The Peristerona River flows from the northern slopes of the Troodos mountain massif into the Western Mesaoria plain Figure 3.1). The Peristerona Watershed covers an area of 112 km^2. The highest point of the watershed is Papoutsa Mountain at 1540 m above sea level (asl). The river is deeply incised throughout the watershed. The 78-km^2 upstream and upper-midstream area of the Peristerona Watershed, upstream of the Panagia Bridge streamflow monitoring station, is the main water producing area of the watershed. In the downstream area a series of seven check dams have been constructed across the wide streambed to recharge the groundwater. The river connects with the Serrachis River at the Masari recharge dam (135 m asl), just north of the buffer zone. A full description of the watershed was presented in D3.1.

The steep hillslopes in the upper-midstream area of the watershed are covered with coniferous *Pinus brutia* forests. These pine forests cover 26% of the 78-km^2 up and upper-midstream watershed area, according to the 2012 Corine Land Cover map. Sclerophyllous vegetation covers 38% of this watershed area and is dominant at the higher elevations. The remaining areas are transitional woodland-shrub and agriculture lands with significant areas of natural vegetation (20%). Cultivated areas, mainly on drystone wall terraces, cover 14%.

The forestry research site is located on the edge of Peristerona Watershed, at 620 m asl. The forest is a natural, homogeneous, open stand of *Pinus brutia* trees. Long-term annual rainfall at the site is 425 mm. The forestry site is located on the fractured diabase formation of the Troodos ophiolite. The site has an average slope of 25 degrees, with a northern aspect. The soil has a loam texture, has an average depth of 14 cm and is covered with a thick layer of pine needles. A small number of rockrose bushes (*Cistus sp.)* can be found in the rocky and open areas of the forest that are not shaded by the canopies of the *P. brutia* trees. (Eliades et al., 2018a).

Figure 3.1 Peristerona watershed with the BINGO field research locations, stretching north from the Troodos mountain massif (dark color) into the Western Mesaoria plain in Cyprus.

3.2.2. Field work

For the BINGO Project, four sap flow sensors (ICT International) and 20 soil moisture and temperature sensors (5TM, Decagon) were installed at the Agia Marina-Xyliatos forestry research site (Figure 3.2). Meteorological sensors (LUFFT) and tipping bucket rain gauges (Lambrecht) were installed in Alona at 1300 m asl in the upstream area of Peristerona Watershed, at the Agia Marina-Xyliatos forestry research site at 620 m asl and downstream in Peristerona at 180 m asl (Figure 3.3). Streamflow observations were made at Platanistasa Water Mill, at Platanistasa Forest, at Panagia Bridge (continuous) and at Orounda Bridge Figure 3.4).

Figure 3.2 *Pinus brutia* trees, sap flow sensors, soil moisture sensors, throughfall gauges at the Agia Marina_Xyliatou forestry research site.

Figure 3.3 Meteorological station in Alona upstream (left) and in Peristerona in the downstream area of Peristerona Watershed (right).

Figure 3.4 Manual streamflow observations (left) and Panagia Bridge station (right) in Peristerona Watershed.

The research at Agia Marina-Xyliatos forestry site started in fall 2014 and was strengthened and expanded with the above BINGO Project sensors. The capacitance-based soil moisture and temperature sensors measure volumetric soil moisture content. The sensors were installed at 12-cm depth at 1 and 2 m north and south of four trees (TM2, TM4, TM6, TM7) to capture the effects of shading and of the strong north–south slope. These trees were also equipped with sap flow sensors. Additional sensors were installed 3-m south of tree TM2 and 1-m west of tree TM6. One sensor was installed in a deeper soil pocket at 30-cm depth near tree TM7 and two sensors were installed in an open rocky area between the trees. All soil moisture observations were recorded hourly. No significant effect of tree and location respective to tree on the soil moisture at 12-cm depth were found with a two-way analysis of variance (Eliades et al., 2018a). Therefore, the average soil moisture content of the 18 12-cm depth sensors was used for the forest water balance computations. The volumetric soil moisture observations were multiplied with the average soil depth (14.25 cm), obtained from observations taken at a 1-m grid around the four trees, to obtain the soil moisture storage.

The sap flow sensors are Heat Ratio Method (HRM) instruments and can measure low sap flow rates, including reverse flows (Burgess and Downey, 2014). The HRM consists of a set of two measurement needles (downstream and upstream) and one central needle (heater) that releases a heat pulse. The two measurement needles have thermistors positioned exactly at 7.5 mm and 22.5 mm from the tip of the measurement needles. The HRM determines the increase in temperature at these two points after the

release of the heat pulse. Sapflow sensors were installed in the stem of the trees at 1.3-m height facing north. An increment borer and indicator dye was used to determine the sapwood depth of the trees. The installation procedure, computations and corrections for natural thermal gradients, wound and misalignment of the needles were conducted according to Burgess et al. (1998, 2001) and Vandegehuchte et al. (2015). The sap velocity (*Vs*) was calculated according to Burgess et al. (2001) with the use of the Sap Flow Tool software (Burgess and Downey, 2014). For the conversion of sap velocity to sap flow, we multiplied the sap velocity (V_s) with the corresponding cross-sectional area of the sapwood (A_x). All sap flow measurements were recorded hourly.

Linear regression equations were established between the sap flow observations from the 14 trees that were monitored during the four year monitoring period, to obtain a complete four year record for all trees. The total Voronoi forest ground area of the 14 trees is 547 m^2. The monitored trees and Voronoi polygons are pictured in Figure 3.5.

Temperature, relative humidity, wind speed, solar radiation and rainfall are recorded by the meteorological station. Throughfall was measured by 28 manual rain gauges, randomly located under the canopy of four trees (Figure 3.2). A linear relation between daily rainfall and throughfall was established, using all daily observations (Eliades et al., 2018a).

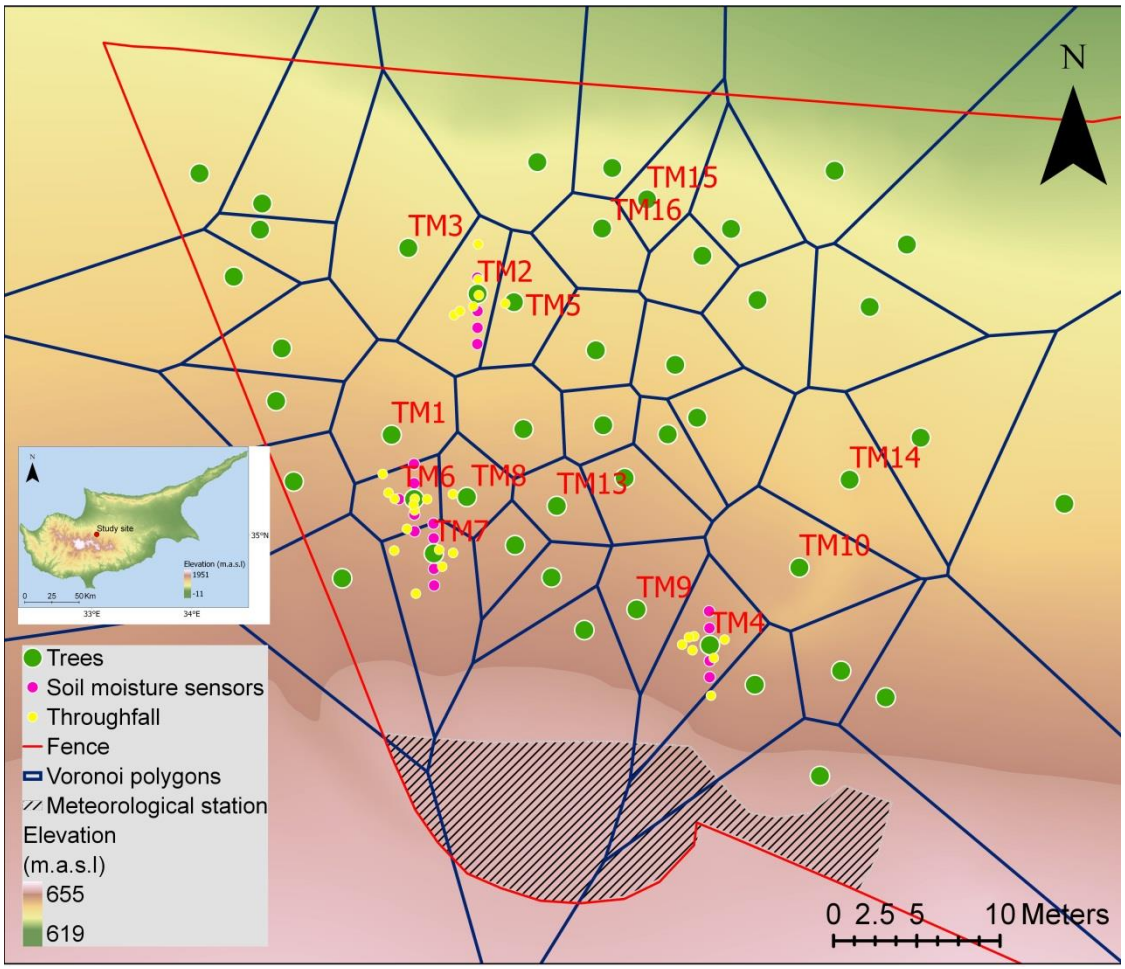

Figure 3.5 Agia-Marina-Xyliatou forestry research site, showing the twelve monitored trees, Voronoi polygons, soil moisture sensors and throughfall gauges.

3.2.3. Model description

Forest water balance components

A daily soil water balance model was used to derive all water balance components from the field observations, as follows:

$\Delta S = (P - I) - Ts - Es - L$

where ΔS is the daily change in soil moisture, P is the rainfall, I is the interception loss over the canopy, Ts is the tree transpiration sourced from the soil, Es is the soil evaporation and L are the drainage and runoff losses, all expressed in mm d^{-1}, over the Voronoi area (A) of the trees. It is assumed that net lateral flow across the boundaries of the Voronoi polygons is zero. Losses become either bedrock recharge or flow to the stream.

A stepwise approach is used to estimate (i) soil evaporation (*Es*), tree transpiration from the soil (*Ts*), and surface and drainage losses (*L*). Reduction coefficients for soil evaporation and transpiration from the soil are computed as linear functions of soil moisture, similar to Allen et al. (1998). The additional reduction of soil evaporation by the thick layer of pine needles was simulated by a mulch coefficient. Surface runoff and drainage losses (*L*) were assumed to occur when the soil moisture exceeds field capacity. Total daily transpiration (*T*) is observed by the sap flow sensors. Any transpiration that is not fulfilled by the soil moisture (*Ts*) is assumed to originate from the bedrock fractures (*Tb*).

Based on the soil moisture observations, the soil moisture at which the reduction of evapotranspiration starts was set at field capacity. The mulch coefficient, the field capacity, minimum soil moisture level for soil evaporation, and wilting point were obtained by calibration of the daily soil water balance model for the year 2015. The Nash-Sutcliffe Efficiency (NSE), Kling-Gupta Efficiency (KGE), Mean Absolute Error (MAE) and percent bias were used as model evaluation criteria. The model is implemented in Excel; full details are presented by Eliades et al. (2018a).

Streamflow

The GR4J model was used for the Peristerona Watershed streamflow simulations. The GR4J is a lumped, four-parameter, daily rainfall-runoff model. A detailed presentation of the model is given by Perrin et al. (2003). The four parameters represent the watershed production (soil moisture) storage (*X1*), groundwater exchange acting on streamflow (*X2*), stream flow storage (*X3*), and a time parameter for the unit hydrograph (*X4*). The groundwater exchange coefficient can be positive (inflow to stream) or negative (recharge losses). The parameters are imbedded in exponential equations, which are used to represent the hydrologic processes. All input data and model parameters are expressed in mm over the watershed area, except for *X4*, which is expressed in days. Daily rainfall (*P)* and reference evapotranspiration (ET_o) are the inputs to the model. The four model parameters are determined by calibration with daily streamflow observations (*Q*).

The model has been implemented in both R and in Excel (https://webgr.irstea.fr/en/modeles/journalier-gr4j-2/fonctionnement_gr4j/). The Excel model can be automatically optimized using the Solver tool in Excel, with the use of four metrics: the standard Nash Sutcliffe Efficiency (NSE), the NSE on square roots of the flow (NSE-sqrt), the NSE on natural logs of the flows (NSE-ln) and the percent Bias. The percent Bias is relative to 100%, where a bias of 100% indicates that the total observed streamflow is equal to the modeled streamflow over the modeling time period.

The GR4J model was modified to be calibrated with the evapotranspiration data obtained from Agia-Marina-Xyliatou forestry site. Monthly instead of daily data were used to reduce the effect of the spatial variability in meteorological conditions over the watershed. The observed evapotranspiration in Agia-Marina-Xyliatou forestry site was normalized by the total computed evapotranspiration over the watershed. The same set of efficiency criteria as for the flow simulations were added for calibrating and evaluating the evapotranspiration pattern in the GR4J Excel model. Here the assumption is that the evapotranspiration in the watershed behaves similar as in the forest site.

Daily rainfall and reference evapotranspiration over the watershed were computed from the installed meteorological sensors and the stations from the Cyprus Department of Meteorology. Both the Penman-Monteith equation and the Hargreaves equation were used for the computation of the reference evapotranspiration (Allen et al., 1998). The Penman-Monteith computed evapotranspiration shows a similar temporal pattern as the Hargreaves computed evapotranspiration. However, the first is more sensitive to the specific location of meteorological station (e.g., valley versus hill top), especially in this very heterogeneous topographic environment. Thus, the Hargreaves equation was used to compute the reference evapotranspiration for the watershed simulations, considering also that this equation was used for the long-term simulations of the past and future (D4.3). The daily precipitation, maximum and minimum temperatures for the period 1980 to 2010 were extracted from the 1-km gridded data sets for Cyprus (Camera et al., 2014) and averaged over the watershed area. These data were also used for the downscaling of the future climate change scenarios (2020-2050).

3.3. Results

3.3.1. Field work results

The coefficient of determination (R^2) for the regression relations between the sapflow observations of the 14 trees during 2015-2018 ranged between 0.78 and 0.98, allowing the gap-filling of all trees for the full four year monitoring period. The transpiration of the 14 trees, averaged over the Voronoi area of the trees, is presented in Figure 3.6. In the 2016 and 2017 drought years, transpiration nearly stopped at the end of the long dry summer, reaching a minimum of 0.02 mm/d in October 2016. Reverse flow was observed during cold periods in January 2015 and 2016. This could be an indication of the trees' frost protection (Eliades et al., 2018b). The year 2018 had high rainfall events at the end of May and in September, during periods of high atmospheric evapotranspiration demand, resulting in the highest annual sapflow (267 mm) of the four monitored years. A peak sapflow rate of 2.0 mm/d was observed on 8 June 2018. The observed daily precipitation, soil moisture and reference evapotranspiration (ETo) at the research site are presented in Figure 3.7.

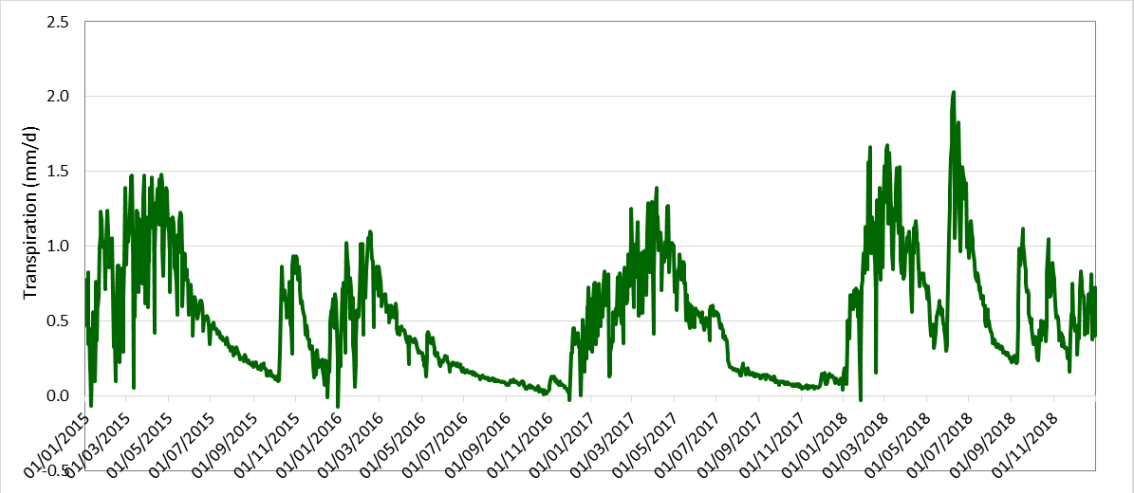

Figure 3.6 Observed daily transpiration (mm/d) averaged over the Voronoi area of the 1~~42~~ monitored trees at the forestry research site in Agia Marina-Xyliatou, during 2015-2018.

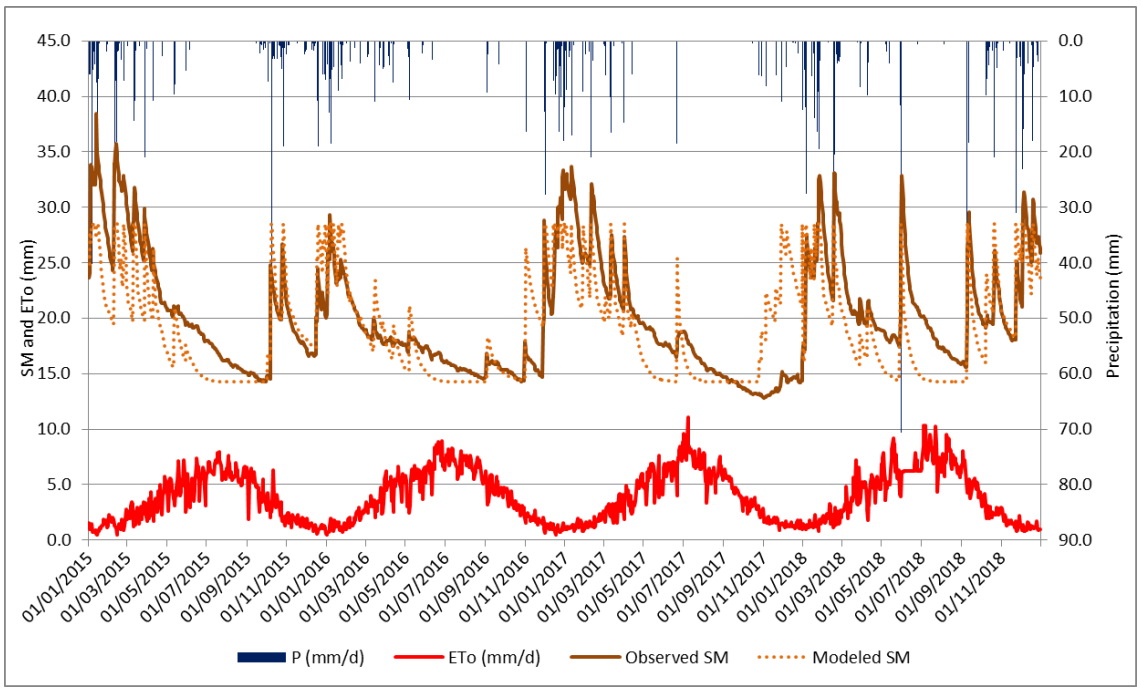

Figure 3.7 Observed daily precipitation (P), reference evapotranspiration (ETo) (mm/d) and observed and modeled soil moisture (SM) (mm) at the forestry research site in Agia Marina-Xyliatou, during 2015-2018.

Average stream flow at Platanistasa Forest (0.12 m^3/s) was higher than at the upstream location at Platanistasa Water Mill (0.09 m3/s). This indicated a stream flow contribution from the forest along the 7-km long stream stretch. However, nearly 20% of the stream observations showed higher streamflow upstream than downstream, indicating occurrence of stream flow recharge losses, especially during low flows.

Stream flow observations at Orounda Bridge in the downstream area were linked with the continuous observations at Panagia Bridge station. The streamflow observations showed substantial recharge losses in the alluvial aquifer and sedimentary formations downstream of Panagia Bridge station (Figure 3.8). The relation between the midstream and downstream streamflow observations can be expressed with a linear

relation (R^2 = 0.88), shown in Figure 3.8. A minimum streamflow of 0.26 m^3/s at Panagia Bridge is needed for streamflow to reach the groundwater recharge check dams, downstream of Orounda Bridge. The obtained equation was used to model the streamflow from the long-term observations at Panagia Bridge. Figure 3.9presents the 3-year moving averages of the annual streamflow at Orounda Bridge. During the dry hydrologic years 1997/1998 – 2000/2001 the 3-year average remained below 5 Mm^3 for four years in a row. Again in 2007/07 and 2008/09 the 3-year average stream flow fell below 5 Mm^3, stressing the groundwater recharge for the downstream communities.

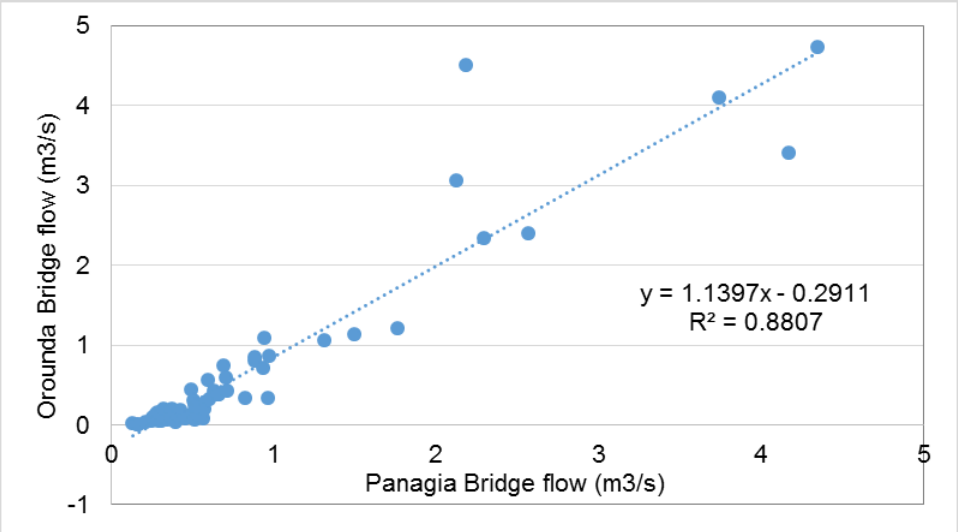

Figure 3.8 Relation between stream flow at Orounda Bridge and Panagia Bridge stations.

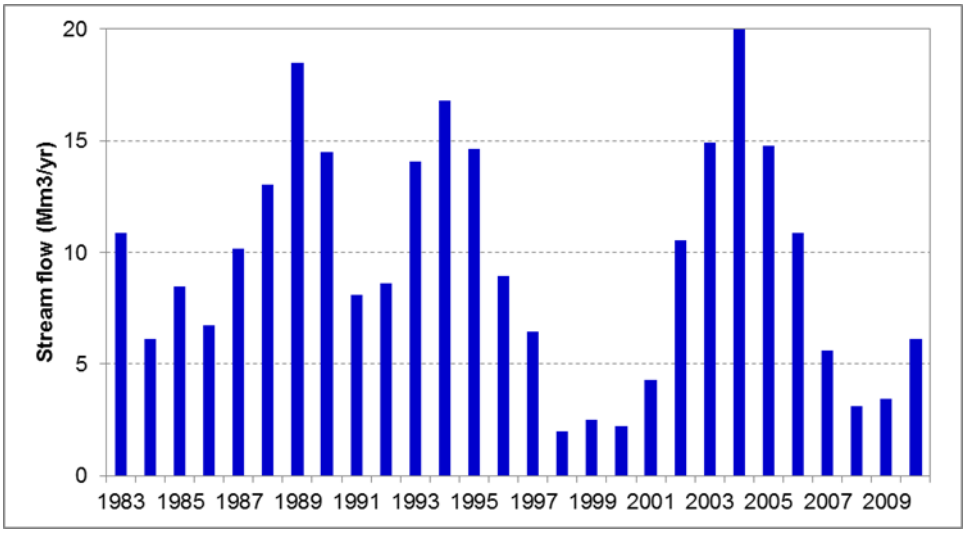

Figure 3.9 Three-year moving average of the annual stream flow at Orounda Bridge.

3.3.2. Model results

The water balance components and model evaluation criteria for 2015-2018 are summarized in Table 3.1. The soil moisture was modelled with a mean absolute error ranging between 1.7 (2016) and 3.5 mm (2017). The modeled soil moisture is also shown in Figure 3.5. The values of the calibrated parameters were 0.2 for the mulch coefficient, 20% for the field capacity, 15% for the wilting point and 10% for the minimum evaporation soil moisture content. The year 2017 was extremely dry, with rain was just 52% of the long-term average annual rainfall. Total evapotranspiration, made up of interception, soil evaporation

and transpiration from soil and bedrock amounted to 132% of the rain in 2017. The evapotranspiration of the trees is maintained with water taken up from the bedrock fractures, resulting in a net water loss for the forests. In the other three years total evapotranspiration ranged between 84 and 88% of the rain. The net loss (surface and drainage loss minus the transpiration uptake from the bedrock fractures) was positive, ranging between 10% in 2018 to 14% in 2016. This shows the contribution of the forest to the recharge of the bedrock and the flow to the stream. Stream flow in the ditches near the recharge site was observed during exceptional wet periods with extreme rainfall events only (2012, 2019).

Table 3.1 Water balance components over the Voronoi area of the 14 trees at the Agia-Mariana-Xyliatou forestry site, precipitation is presented in mm, and all other parameters are a fraction of rainfall, and the model evaluation criteria (calibrated for 2015 and validated for 2016-2018).

Parameter	2015	2016	2017	2018
Precipitation (mm)	507	359	220	576
Interception	0.18	0.19	0.18	0.15
Soil evaporation	0.26	0.35	0.43	0.28
Transpiration from soil	0.12	0.10	0.19	0.12
Transpiration from bedrock	0.31	0.20	0.53	0.34
Soil moisture change	-0.01	0.03	-0.07	0.02
Losses	0.43	0.34	0.22	0.44
Net loss	0.12	0.14	-0.31	0.10
	Calibration		Validation	.
Nash-Sutcliffe Efficiency	0.65	0.60	0.23	0.53
Kling-Gupta Efficiency	0.78	0.77	0.53	0.67
Mean Absolute Error (mm)	3.1	1.7	3.5	2.4
Bias (%)	-10	2	0.2	-11

The results of the GR4J calibration for the years 2015-2018 are presented in Table 3.2. The standard model configuration returns all NSE coefficients above 0.80. However, when optimizing for the observed evapotranspiration pattern (Run2), the watershed production (soil) storage becomes very small, evapotranspiration is reduced and the increase in streamflow is compensated by losses, with a large exchange coefficient (X2=-10.6), to fit the observed flows. The standard NSE for the evapotranspiration is acceptable (0.56), but the other NSEs for evapotranspiration are not as good. These results led to two more runs with the streamflow exchange coefficient (X2) set to zero. Here the optimization for streamflow (Run3) and for evapotranspiration (Run4) give a nearly similar production storage and the NSEs for evapotranspiration are nearly the same for both runs. However, the Run4 optimization does not reach the same streamflow simulation performance as Run3. The simulated streamflow of Run1 and Run3 are shown in Figure 3.10.

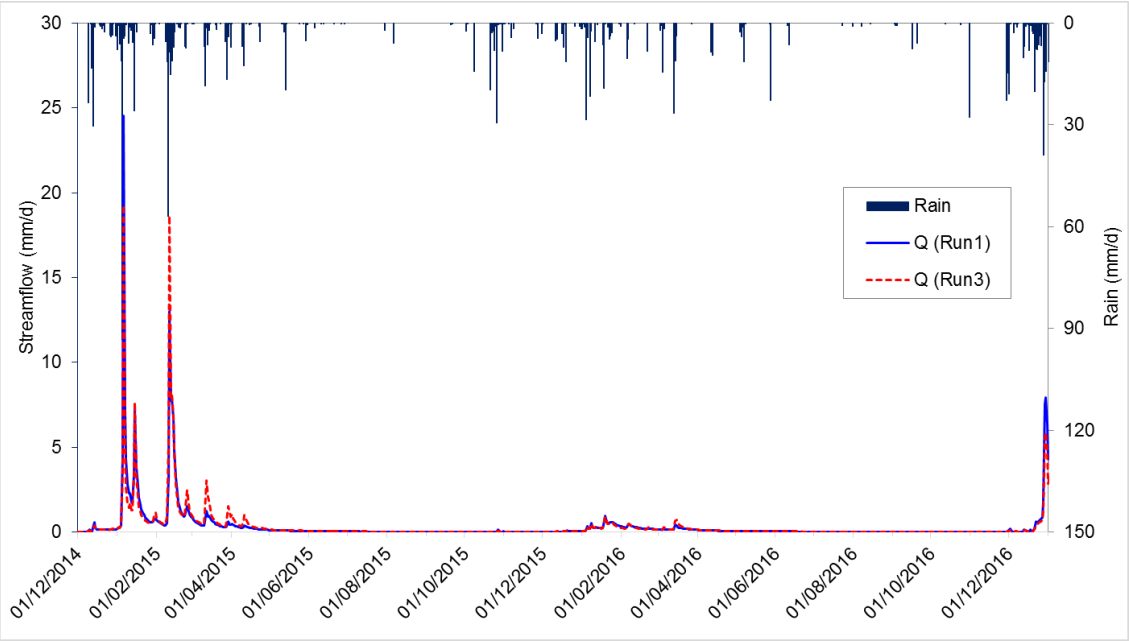

Figure 3.10 Simulated streamflow for Peristerona Watershed during 2015-2016, for Run1 and Run3 (X2=0).

Table 3.2 The GR4J model parameters, evaluation criteria for streamflow (Q) and evapotranspiration (ET) and the water balance components, as a fraction of the rain, for the Peristerona Watershed for 2014-2018, calibrated without and with the observed temporal evapotranspiration pattern of the Agia-Marina-Xyliatou forestry research site.

	Run1	Run2	Run3	Run4
Objective function	NSE(Q)	NSE(ET)	NSE(Q)	NSE(ET)
Constraint		NSE(Q)>0.6		NSE(Q)>0.6
Model			X2=0	X2=0
X1: Capacity of production store (mm)	155.0	25.4	271.2	267.3
X2: Water exchange coefficient (mm)	-2.3	-10.6	0.0	0.0
X3: Capacity of routing store (mm)	56.9	60.6	22.4	63.2
X4: Unit hydrograph time base (d)	1.6	1.4	1.7	1.4
NSE(Q)	0.88	0.60	0.82	0.60
NSE-sqrt(Q)	0.87	0.62	0.88	0.79
NSE-ln(Q)	0.84	0.59	0.84	0.66
Bias(Q) (%)	100	100	100	100
NSE(ET)	0.42	0.56	0.27	0.27
NSE-sqrt(ET)	0.52	0.40	0.49	0.49
NSE-ln(ET)	-0.40	-33.71	0.36	0.34
Bias(ET) (%)	95.3	98.2	95.1	94.8
Precipitation (mm)	511	511	511	511
Evapotranspiration	0.73	0.56	0.81	0.80
Streamflow	0.18	0.18	0.18	0.18
Loss	0.06	0.21	0.00	0.00

The results of the standard long-term streamflow simulations are presented in Table 3.3. Both the calibration for the hydrologic years 1995/96 to 2009/10 and the validation for 1980/81 to 1994/1995 show very good NSEs. The NSE-sqrt and the NSE-ln for the validation runs even outperform the calibration runs, for both model parameterizations (with X2 calibrated and with X2=0). This indicates that the model

performs well for small flows. The model performance is slightly better for the models with the calibrated X2 (Run 5 and 6), compared to the models with X2=0 (Run7 and Run8). However, the models with X2=0 show higher evapotranspiration values, 79% for 1995-2010 (Run7) and 72% for 1980-1995 (Run8), which are closer to the expected values than the evapotranspiration of the models with the calibrated X2 (71% and 83%).

The calibrated model parameters from the 2015-2018 data (Run1, 3 and 4 in Table 3.2) were validated with the long-term 1980-1995 and 1995-2010 data. These results are summarized in Table 3.4. The NSE values are either good or acceptable, but lower than the NSE values for the 1980-1995 validation with the 1995-2010 calibration (Table 3.4). This could be expected because models calibrated on long-term data sets are expected to represent the streamflow better than models calibrated on short-term data sets. However, an exception can be found in the NSE-ln values for the 1980-1995 validation years, which show that the 2015-2018 calibrated model (NSE-ln 0.87 for Run10) outperforms the long-term calibrated model (NSE-ln 0.85 for Run6) (Table 3.3 and Table 3.4). Similarly, for the model without X2, the NSE-ln values of the 2015-2018 calibrated model are higher (0.88 for Run12) than for the long-term calibrated model (0.83 for Run8) (Table 3.3 and Table 3.4). Thus, low flows are slightly better simulated with the 2015-2018 calibrated models than with the 1995-2010 calibrated models. These results are most likely an indication of the sensitivity of the GR4J model to the calibration data sets, considering that the 2015-2018 calibration years were drier (511 mm average annual rain) than the 1995-2010 calibration years (599 mm).

Table 3.3 Calibrated GR4J model parameters, evaluation criteria and water balance components, as fraction of the rain, for the Peristerona Watershed for 1995-2010 (calibration) and 1980-1995 (validation); bold numbers are referred to in the text.

	Run5	Run6	Run7	Run8
Years	1995-2010	1980-1995	1995-2010	1980-1995
Model			X2=0	X2=0
X1: Capacity of production store (mm)	225.1	225.1	364.7	364.7
X2: Water exchange coefficient (mm)	-2.5	-2.5	0.0	0.0
X3: Capacity of routing store (mm)	73.6	73.6	35.9	35.9
X4: Unit hydrograph time base (d)	1.28	1.28	1.33	1.33
NSE(Q)	0.86	0.77	0.82	0.71
NSE-sqrt(Q)	0.83	0.88	0.82	0.86
NSE-ln(Q)	0.77	**0.85**	0.75	**0.83**
Bias(Q) (%)	100	101	100	101
Precipitation (mm)	599	639	599	639
Evapotranspiration	0.71	0.63	0.79	0.72
Streamflow	0.21	0.28	0.21	0.28
Losses	0.08	-0.09	0.00	0.00

Run 9 and 10, which include the X2 exchange coefficient, show again lower evapotranspiration, 66% and 57%, respectively, than would be expected (Table 3.4). The NSE values for Run13 and Run14, where the calibrated parameters were optimized with the evapotranspiration observations are generally lower than those of the other four runs (Run9-12). An exception is the 0.60 NSE for Run 13, which is slightly higher than the 0.58 NSE of Run 11. Overall, the results show that the GR4J model with X2=0 captures the observed evapotranspiration better, while the evapotranspiration-optimized calibration did not lead to a marked improvement.

Table 3.4 Long-term model simulations with the calibrated GR4J model parameters from the 2015-2018 calibration, obtained without (Run9-12) and with (Run13-14) the observed temporal evapotranspiration pattern of the Agia-Marina-Xyliatou forestry research site; bold numbers are referred to in the text.

	Run9	Run10	Run11	Run12	Run13	Run14
Years	1995-2010	1980-1995	1995-2010	1980-1995	1995-2010	1980-1995
Obj.function	NSE(Q)	NSE(Q)	NSE(Q)	NSE(Q)	NSE(ET)	NSE(ET)
Model			X2=0	X2=0	X2=0	X2=0
X1	155.0	155.0	271.2	271.2	262.4	262.4
X2	-2.3	-2.3	0.0	0.0	0.0	0.0
X3	56.9	56.9	22.4	22.4	180.7	180.7
X4	1.6	1.6	1.67	1.7	1.50	1.5
NSE(Q)	0.61	0.59	**0.58**	0.62	**0.60**	0.53
NSE-sqrt(Q)	0.79	0.84	0.79	0.83	0.63	0.71
NSE-ln(Q)	0.81	**0.87**	0.82	**0.88**	0.34	0.46
Bias(Q)	117	116	123	122	125	125
Precipit.(mm)	599	639	599	639	599	639
Evapotransp.	0.66	0.57	0.74	0.66	0.73	0.66
Streamflow	0.25	0.32	0.26	0.34	0.27	0.34
Loss	0.09	0.11	0.00	0.00	0.00	0.00

3.4. Discussion

The field research at the forestry site is the first quantification of forest evapotranspiration in Cyprus and the first quantification of evapotranspiration of the drought-tolerant *P. brutia* species, globally. In three out of the four monitored years, evapotranspiration of the forest ranged between 84 and 88% of the annual rainfall (359-576 mm). However, in the 2017 drought year evapotranspiration exceeded the precipitation, indicating that rainfall surplus during wet years recharges the fractured bedrock. Over the Thus, the drier conditions, which are projected by climate change model simulations for the Mediterranean region, may not leave sufficient bedrock recharge during wet years to protect these hillslope forests against droughts.

The modelling of the forest water balance components is strongly empirical as it relies on the sapflow observations. Further field and modeling research is needed to relate the forest evapotranspiration to environmental parameters. Field observations and analyses should investigate the physiological mechanisms that support these drought tolerant trees and the soil and leaf water potentials at which evapotranspiration is maintained. It is especially important to observe sapflow during sequences of drought years to quantify the capacity of the tree-accessible bedrock water storage.

The long-term runoff coefficient of the Peristerona Watershed is 24% of the average annual precipitation of 619 mm (1980-2010). The ecohydrological observations, together with the Platanistasa streamflow observations, support the hypothesis that the permeable gabbro formations at the higher elevations in the watershed contribute more to the streamflow than the diabase formations in the midstream area. These findings also support the general observed hydrologic trends of a decrease in evapotranspiration fractions (fraction of rainfall) with an increase in rainfall.

The use of the evapotranspiration observations improved our understanding of the functioning of the GR4J model. The model simulations with the field observations indicated the sensitivity of the GR4J model to the

wetness of the calibration data sets. This confirms the results of the model transferability analysis of Le Coz et al. (2016). The streamflow observations in the downstream area allow the projection of streamflow into the groundwater recharge check dams to quantify possible water supply constraints for the downstream areas under climate change. Overall the model calibrations with X2=0 show a better representation of the water balance components in Peristerona Watershed and should, therefore, be used for climate change simulations.

3.5. Bibliography

Abellanas, B., Abellanas, M., Pommerening, A., Lodares, D., Cuadros, S., 2016. A forest simulation approach using weighted Voronoi diagrams. An application to Mediterranean fir Abies pinsapo Boiss stands. For. Syst. 25, 2171–9845. https://doi.org/10.5424/fs/2016252-08021

Berger, U., Piou, C., Schiffers, K., Grimm, V., 2008. Competition among plants: Concepts, individual-based modelling approaches, and a proposal for a future research strategy. Perspect. Plant Ecol. Evol. Syst. 9, 121–135. https://doi.org/10.1016/j.ppees.2007.11.002

Boydak, M., 2004. Silvicultural characteristics and natural regeneration of Pinus brutia Ten. - A review. Plant Ecol. 171, 153–163. https://doi.org/10.1023/B:VEGE.0000029373.54545.d2

Burkhart, H.E., Tomé, M., 2012. Indices of Individual-Tree Competition, in: Modeling Forest Trees and Stands. Springer Netherlands, Dordrecht, pp. 201–232. https://doi.org/10.1007/978-90-481-3170-9_9

Chambel, M.R., Climent, J., Pichot, C., Ducci, F., 2013. Mediterranean Pines (Pinus halepensis Mill. and brutia Ten.), in: Pâques, L.E. (Ed.), Forest Tree Breeding in Europe: Current State-of-the-Art and Perspectives. Springer Netherlands, Dordrecht, pp. 229–265. https://doi.org/10.1007/978-94-007-6146-9_5

Crosbie, R.S., Wilson, B., Hughes, J.D., McCulloch, C., 2007. The upscaling of transpiration from individual trees to areal transpiration in tree belts. Plant Soil 297, 223–232. https://doi.org/10.1007/s11104-007-9337-y

Czárán, T., 1998. Spatiotemporal Models of Population and Community Dynamics, Population and Community Biology Series. Chapman & Hall.

Eliades, M., 2018. The influence of Pinus brutia trees on the water balance of fractured Mediterranean mountain environments. PhD Dissertation, The Cyprus Institute, Nicosia, Cyprus.

Eliades, M., A. Bruggeman, H. Djuma, M.W. Lubczynski. 2018a. Tree Water Dynamics in a Semi-Arid, Pinus brutia Forest. Water, 10(8), 1039. https://doi.org/10.3390/w10081039

Eliades, M., A. Bruggeman, M. Lubczynski, A. Christou, C. Camera, H. Djuma. 2018b. The water balance components of Mediterranean pine trees on a steep mountain slope during two hydrologically contrasting years. J. Hydrology 562: 712-724. https://doi.org/10.1016/j.jhydrol.2018.05.048

Gspaltl, M., Sterba, H., O'hara, K.L., 2012. The relationship between available area efficiency and area exploitation index in an even-aged coast redwood (Sequoia sempervirens) stand. Forestry 85, 567–577. https://doi.org/10.1093/forestry/cps052

Le Coz, M., Bruggeman, A., Camera, C., Lange, M.A., 2016. Impact of precipitation variability on the performance of a rainfall–runoff model in Mediterranean mountain catchments. Hydrol. Sci. J. 61, 507–518. https://doi.org/10.1080/02626667.2015.1051983

Liao, J., Li, Z., Quets, J.J., Nijs, I., 2013. Effects of space partitioning in a plant species diversity model. Ecol. Modell. 251, 271–278. https://doi.org/10.1016/J.ECOLMODEL.2012.12.030

Nahal, I., 1983. Le Pin brutia (Pinus brutia Ten. subsp. brutia). For. Mediterr. 5, 165–176.

Perrin, C., Michel, C., Andréassian, V., 2003. Improvement of a parsimonious model for streamflow simulation. J. Hydrol. 279, 275–289. https://doi.org/10.1016/S0022-1694(03)00225-7

Schiller, G., Cohen, Y., 1998. Water balance of Pinus halepensis Mill. afforestation in an arid region. For. Ecol. Manage. 105, 121–128. https://doi.org/10.1016/S0378-1127(97)00283-1

Ungar, E.D., Rotenberg, E., Raz-Yaseef, N., Cohen, S., Yakir, D., Schiller, G., 2013. Transpiration and annual water balance of Aleppo pine in a semiarid region: Implications for forest management. For. Ecol. Manage. 298, 39–51. https://doi.org/10.1016/j.foreco.2013.03.003

Walker, J., Sharpe, P.J.H., Penridge, L.K., Wu, H., 1989. Ecological Field Theory: the concept and field tests, in: Progress in Theoretical Vegetation Science. Springer Netherlands, Dordrecht, pp. 81–95. https://doi.org/10.1007/978-94-009-1934-1_7

Wu, H.-I., Sharpe, P.J.H., Walker, J., Penridge, L.K., 1985. Ecological field theory: A spatial analysis of resource interference among plants. Ecol. Modell. 29, 215–243. https://doi.org/10.1016/0304-3800(85)90054-7

4. Germany

4.1. Introduction and objectives

In the scope of the BINGO project, it was examined how information gained from field measurements of soil moisture can be used to improve the performance of the hydrological models “TALSIM” and “SWAT”. TALSIM is the model used by the Wupperverband for the operational forecasting (see D3.3). SWAT (Soil & Water Assessment Tool) was chosen due to its high capability to account for environmental and climate changes in scenario simulations. The models were set-up for the “Obere Dhünn” catchment, in the Wupper study site, to simulate effects of climate and land use changes on hydrological processes. To assure a good model performance the models were calibrated against measured discharge data and their performance was evaluated using classical efficiency measures. The calibration results showed a good agreement between simulated and observed runoff values (detailed calibration results are described in BINGO deliverable D3.4).

By calibrating the TALSIM and SWAT models using measured discharge data and optimizing the fit between simulated and observed values, we followed a common procedure in hydrological modelling, which is often times considered to be sufficient to prove a “reliable” model performance. However, especially in the case of spatially distributed models, more and more studies outline, that a multi-criteria calibration should be done if the model aims to be physically consistent for processes other than just discharge alone (Rakovec et al., 2016; Sutanudjaja et al., 2014). Yet, the availability of observed data sets of several variables is required for this procedure, which is often times unfeasible and very resource-intensive to obtain in the necessary spatial and temporal resolution.

Possible parameters to observe for water-balance-model are e.g. snow, evapotranspiration, groundwater fluxes or like in this study: soil moisture and matrix potential. In first step, small scale field measurements are installed (which could be undertaken in the scope of short-term research projects) to look if they can give a better process understanding of hydrological fluxes and how they will help to re-adjust model parameters in a post-calibration process (or even online) to further improve model performance. From the first good experiences the measurements are actually extended to the whole catchment of the reservoir.

In the scope of BINGO, Wupperverband started to monitor soil parameters - formerly, only meteorological parameters (e.g., precipitation, air temperature, air humidity, radiation, and wind velocity) and discharge were continuously measured.

Determination of soil moisture (state variable) had been so far only calculated by the hydrological models. Continuous monitoring of soil moisture and tension rose from the need to achieve a better forecast and evaluation especially for floods but also regarding the inflow to the reservoirs (single events and verification of the whole water balance).

Conceptual models used by Wupperverband show high sensitivity to antecedent soil moisture conditions (see D3.3). Estimation of infiltration rate depends on initial soil wetness, and, by long-term simulations, the model shows by some events - mainly summer storms - difficulties to simulate soil moisture accurately. An improvement in the simulation of soil moisture dynamics is therefore of high importance for this study area, which leads to the following objectives:

Main objective

- To improve the hydrological models used by the Wupperverband (i.e., TALSIM and SWAT)

Specific objectives

- To compare (generalized) soil input parameters from the German Soil Service Centre to parameters from field work activities
- To adjust and improve the models (TALSIM and SWAT) based on new field data (i.e., not only considering discharge but also soil moisture)
- To generate continuous time series of soil moisture and water tension from the installed sensors.

4.2. Methods

4.2.1. Study site description

The study area is located upstream the Große Dhünn Reservoir – GDT (Figure 4.1)**,** which is the second largest drinking water reservoir in Germany. The Dhünn River is one of the main tributaries of the Wupper River. The soil type within the Wupper River Basin is mostly homogenous; brown earth is the predominant soil type followed by gley, luvisol, and alluvial soils. Land use units consist of grassland, coniferous, deciduous, and mixed forest as well as paved areas and farmland (see D3.1).

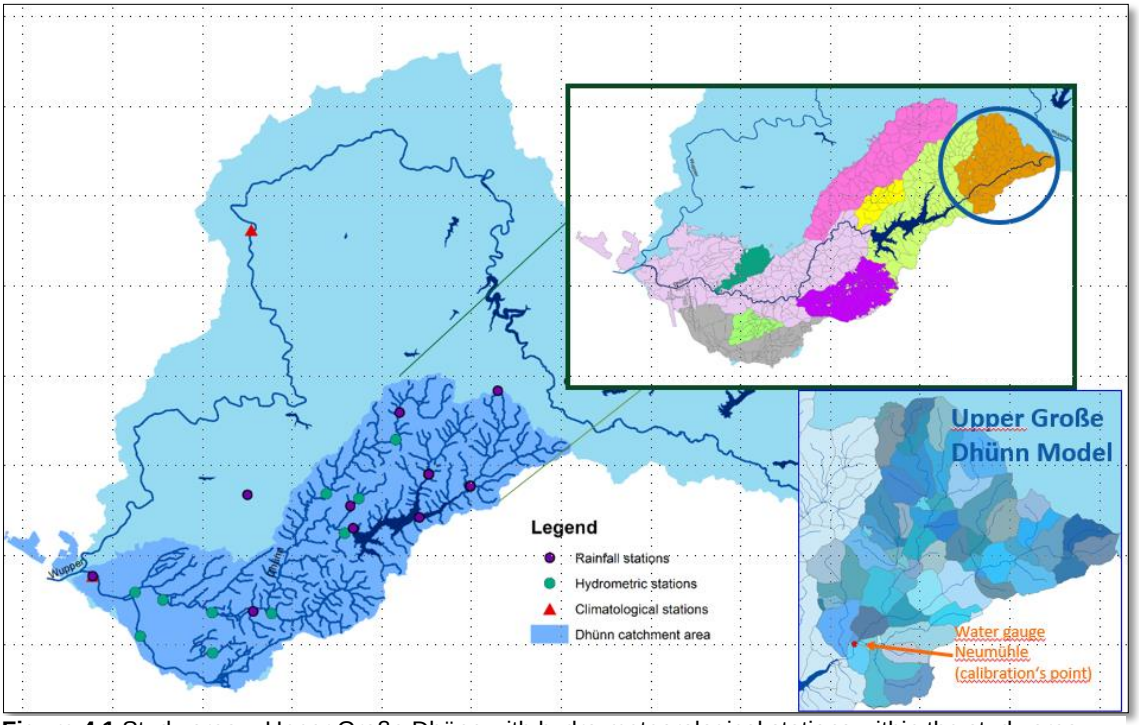

Figure 4.1 Study area – Upper Große Dhünn with hydro-meteorological stations within the study area

4.2.2. Field work

In the frame of BINGO, three soil moisture stations were installed upstream from Neumühle hydrometric station (see Figure 4.2 and Figure 4.3), for three representative land uses (i.e., grassland and coniferous and deciduous forest), as well as two representative soil types (i.e., brown earth and gley).

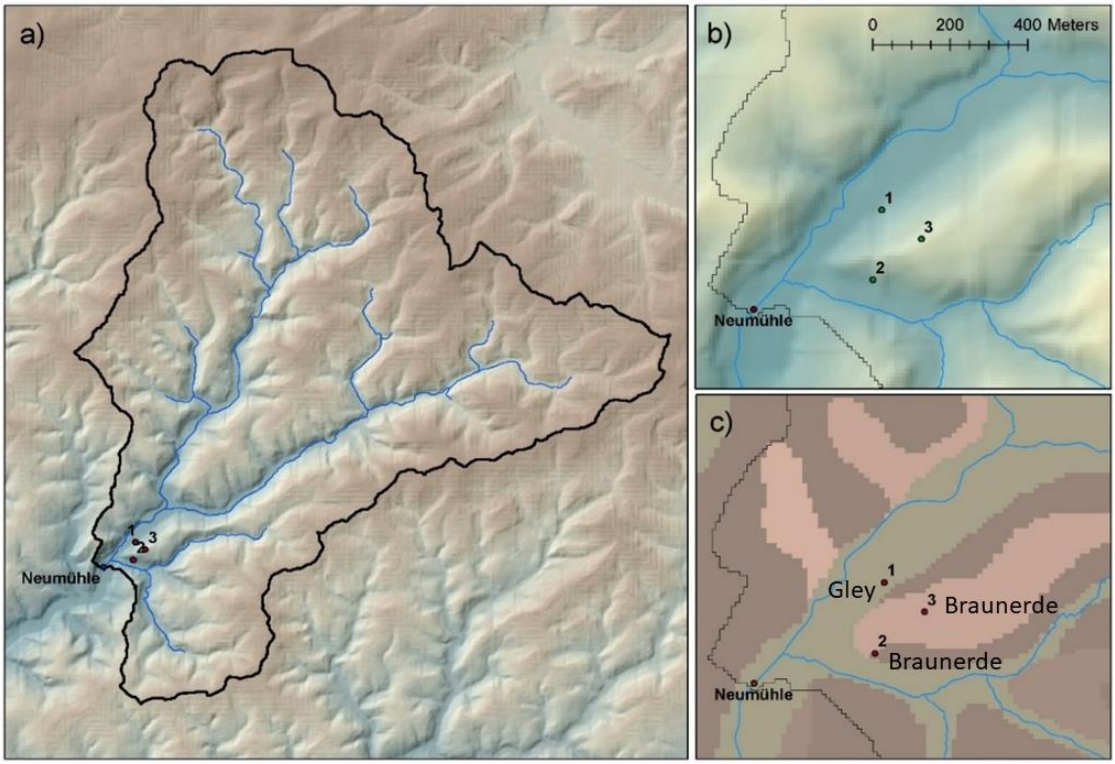

Figure 4.2 a) Obere Dhünn study area site with catchment outlet at „Neumühle“ station and the three soil moisture measuring sites, b) topographic positions of the measuring sites, and c) soil types at the respective measuring sites (box01-gley, box02 and box 03-brown earth)

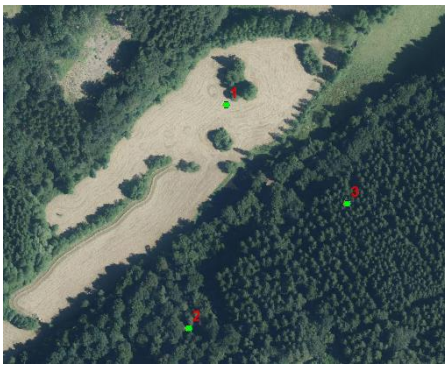

Figure 4.3. Land use classes at the respective measuring sites: box01 – grassland; box02 – deciduous forest; box03 – coniferous forest

Each station consists of a set of two soil moisture sensors SMT100 (from Truebner) and one matric potential sensor MPS-6 (from Decagon), at three different depths (5 cm, 20, cm, and 50 cm, see Figure 4.4).

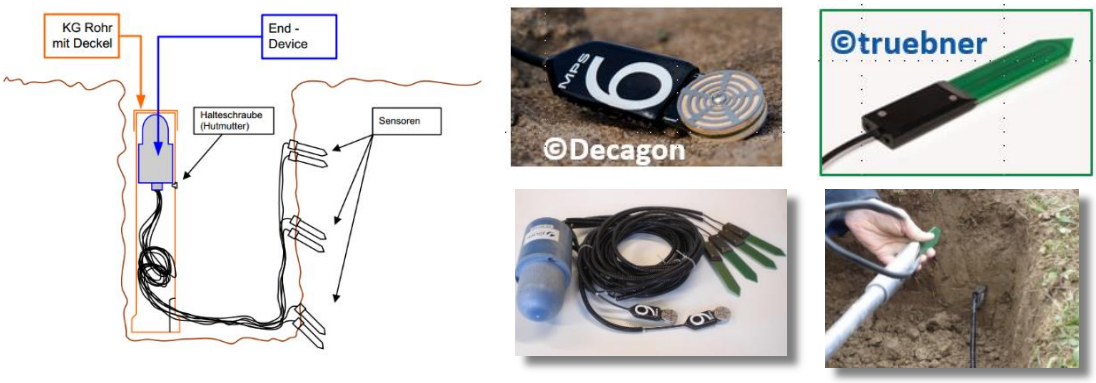

Figure 4.4. Soil moisture and matric potential sensors

The sensors were calibrated by Jülich Research Centre (see H. Bogena et al., 2010 and H. Bogena et al., 2016) and installed in December 2016

SMT100 measures soil temperature and dielectric permittivity. Dielectric permittivity is then converted into volumetric water content (in percent) with Topp's equation

$$\theta\left(\frac{m^3}{m^3}\right) = 4.3\ x\ 10^{-6} * \varepsilon^3 - 5.5\ x\ 10^{-4} * \varepsilon^2 + 2.92\ x\ 10^{-2} * \varepsilon - 5.3\ x\ 10^{-2} \qquad \text{eq. (1)}$$

Where Θ is volumetric water content and ε is dielectric permittivity. The resulting volumetric water content (calculated in percentage) ranges from 0 to 60% (Truebner, 2016).

MPS-6 (dielectric water potential sensor) measures soil water potential and temperature, with a measurement range from -9 to -100000 kPa (Decagon, 2016).

Telemetry takes place via radio from each station to a repeater unit called "coordinator". Afterwards, the data is transmitted to Jülich Research Centre via GSM. Data is sent with a 15-min time step.

Parallel, soil assessment (namely, field tests and laboratory analysis) was also carried out at the research site by the firma Botschek. Soil assessment was primarily based on detailed soil maps at a finer scale (i.e., 1:5000), which were provided by Botschek (not available in beforehand by Wupperverband).

An infiltration test (double-ring infiltrometer) was performed in situ (only at the grassland site due to field conditions, i.e., very steep slope at the two forest sites), while samples were taken for the three sites (see Figure 4.5 and Table 4.1).

Figure 4.5. Samples and double-ring infiltrometer test

Table 4.1: Soil horizons and number of samples for laboratory tests

Land use unit	Horizon [cm]	Number of samples
Grassland	0 - 14 cm	9
	14 - 32 cm	8
	32 - 55 cm	9
	55 - 75 cm	9
	75 - 100 cm	9
Coniferous forest	0 - 12 cm	8
Deciduous forest	0 - 8 cm	10

Laboratory tests included the following:

- Water tension
- Saturated hydraulic conductivity (i.e., kf values)
- Total pore volume
- pF-values
- Fraction of sand, silt[1], and clay[2]

Additionally, and not within the BINGO budget, a lysimeter was installed in September 2016. Unfortunately, it was in operation only for a few interrupted months due to several problems (bite damages, installation issues, etc.). The lysimeter was removed in 2018 and at the end there was not much data collected. Figure 4.6 shows a comparison between PET (calculated after Haude method at Neumühle station) and AET (measured by the lysimeter), from May 2017 to June 2017.

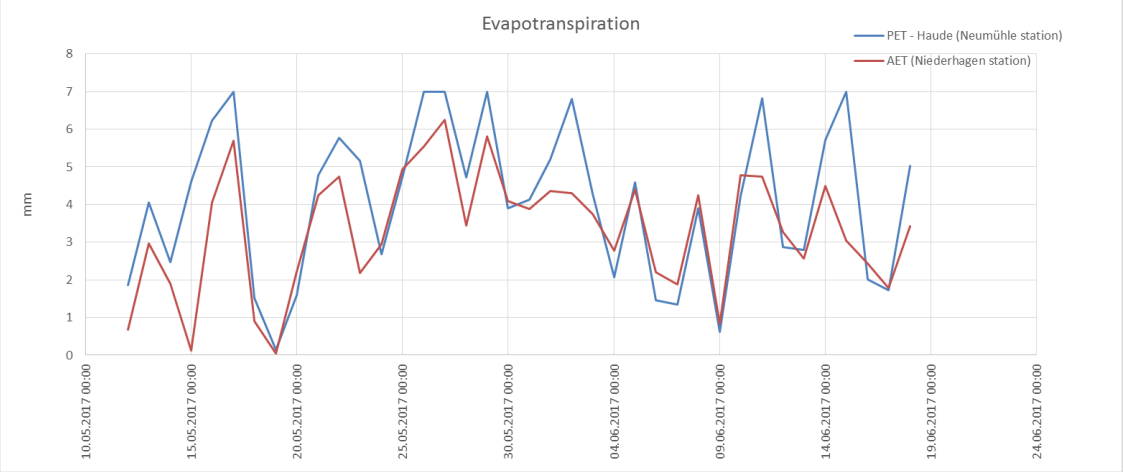

Figure 4.6. Comparison between PET (after Haude, Neumühle station) and AET (measured by the lysimeter)

[1] DE: Schluff
[2] DE: Ton

4.2.3. Model description

TALSIM

TALSIM is a lumped, physically-based, water balance model based on the water balance equation (see D3.3 for full model description). Figure 4.7shows the physical vertical and horizontal processes simulated by the model.

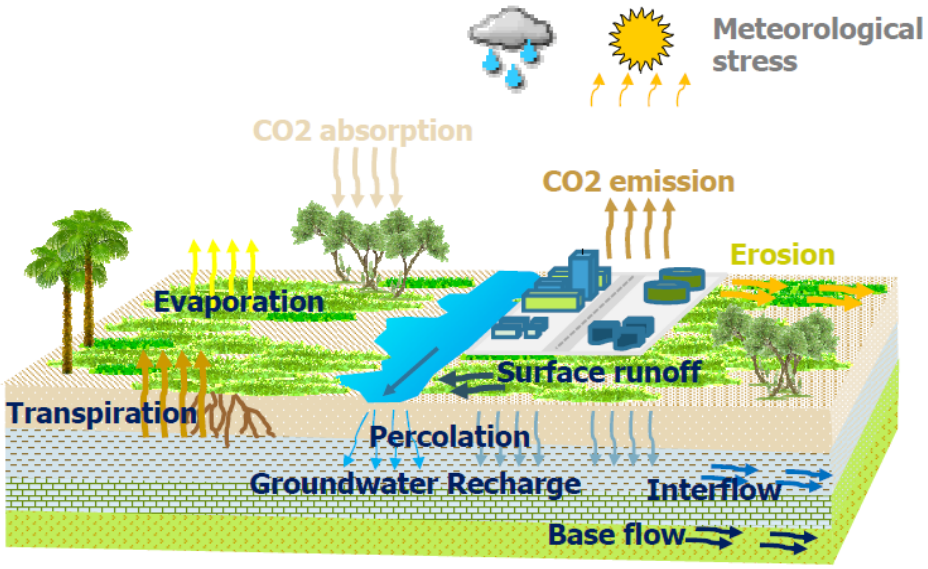

Figure 4.7 Vertical and horizontal hydrological processes simulated by TALSIM (source: TALSIM, 2016)

Surface runoff is calculated according to (see D3.3):

$$\frac{dO(t)}{dt} = P(t) - E(t) - Inf(t) - EP(t) - \frac{dS(t)}{dt} \quad \text{eq. (2)}$$

Where:

P(t): Precipitation - interception
E(t): Evaporation from free water surfaces
Inf(t): Infiltration
EP(t): Effective precipitation
O(t): Surface water storage on land (ponding)– state variable
$\frac{dO(t)}{dt}$: Change in surface water storage on land (ponding)
S(t) Snow storage – state variable
$\frac{ds(t)}{dt}$: Change in snow storage

(For sealed areas, the terms $\frac{dS(t)}{dt}$ and $Inf(t)$ are not considered).

For unsealed areas, effective precipitation is estimated either by: i) constant runoff coefficient; ii) SCS-CN procedure (depends on land cover and soil type); or iii) soil moisture simulation. The soil moisture simulation method is applied for all the models used by Wupperverband.

The input parameters for the soil moisture simulation are:

- Land cover input parameters: root depth, sealing degree, leaf area index
- Soil type input parameters: wilting point (WP), field capacity (FC), total void volume (TVV), saturated hydraulic conductivity (kf), maximum infiltration capacity, maximum capillary rise rate, and classification per soil class (e.g., sand, silt, clay)

Land cover and soil type input parameters are obtained from the German Soil Service at 1:50000 scale.

The main processes that describe the soil water storage are: infiltration (Inf), percolation (Perc), Actual evapotranspiration (AET), interflow (Int), and capillary rise (Cap), each of them depending on soil moisture, see

$$\frac{d\Theta(t)}{dt} = Inf(t) - Perc(t) - AET(t) - Int(t) + Cap(t) \quad \text{eq. (3)}$$

Where $\Theta(t)$ is soil moisture as a time dependent function.

$\Theta(t)$: Soil moisture storage (or soil water storage) – state variable

$\frac{d\Theta(t)}{dt}$: Change in soil water storage

Eq.(2) and eq.(3) are linked by the **infiltration** term. The dependency of these physical processes to soil moisture is calculated internally by the model based on the following algorithms:

a) Infiltration: estimated after Holtan approach
b) Percolation: estimated after Van Genuchten approach
c) Actual evapotranspiration: estimated after Wösten and van Genuchten
d) Interflow: runoff concentration of interflow is calculated using a single linear reservoir and storage cascade, for natural and sealed areas, respectively.
e) Capillary rise: inflow from groundwater occurs due to capillary rise. Capillary rise begins at a soil moisture content of 70% of the available field capacity[3], increasing linearly until it reaches its maximum value (maximum capillary rise rate). Simultaneously, soil moisture decreases linearly.

Although the dependency of these physical processes to soil moisture is in nature non-linear, the model offers the possibility to simulate soil water storage with a linear algorithm. The linear approach solves the continuity equation for several processes simultaneously (TALSIM, 2016). A simulation using this option was carried out in the frame of D3.5 in order to compare the results with the non-linear approach and in order to carry out a sensitivity analysis (see Figure 32 of this report).

The model input time series are described in depth in D3.3. Output time series – which include discharge and soil moisture - are produced per sub-catchment. The physical range of values of simulated soil moisture is shown on Figure 4.8, where they range from WP (wilting point, minimum possible value) to total pore volume[4] (maximum possible value, which represents saturated conditions). This is reflected in the model output, where minimum and maximum values remain under a certain threshold.

[3] Available field capacity (nFC) = FC – WP
[4] DE: GPV = Gesamtporenvolumen

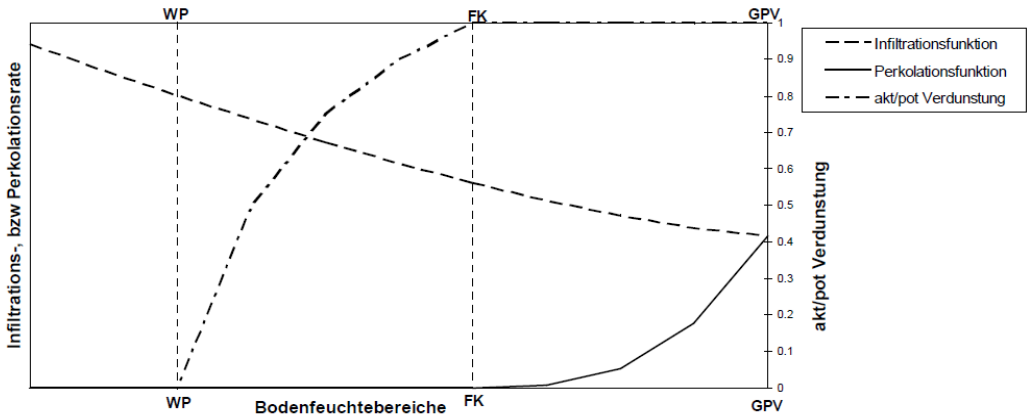

Figure 4.8. Physical range of simulated soil moisture values (y-axis: infiltration and percolation rates; x-axis: soil moisture range; WP = wilting point; FK = field capacity; GPV = total pore volume); Infiltrationsfunktion = infiltration function; Perkolationsfunktion = percolation function; akt/pot Verdunstung = actual / potential Evapotranspiration) – output time series (source: TALSIM, 2016)

In TALSIM, soil moisture resulting time series are given in [mm/m], as volumetric water content. Thus, it is possible to compare them easily with field measurements (given in percentage).

Physical parameters as result of field measurements and from German Soil Service Centre (e.g, wilting point, field capacity, etc.) were not modified. Rather, soil parameters were globally modified by decreasing or increasing e.g., maximal infiltration and kf values (i.e., hydraulic conductivity) by factors (see Table 4.4). Evaluation of modified parameters was based by comparing simulated to observed discharge and soil moisture, respectively. The model for the Upper Große Dhünn had been previously calibrated based on observed discharge (current state).

SWAT

The Soil & Water Assessment Tool (SWAT) is a spatially distributed, physically based, river basin scale model, which was primarily developed to study changes in hydrological processes due to alterations of land-management practices, in complex catchments with heterogeneous soil, land-use and management types (Neitsch et. al, 2011). Nowadays, SWAT is also widely used to assess climate change impacts on catchment hydrology and future water resources availability, as it is done in this study.

The underlying calculation of the hydrological fluxes in SWAT are based on the water balance equation:

$$SW_t = SW_0 + \sum_{i=1}^{t}(P_{day} - Q_{surf} - ET_a - Q_{lat} - Perc - Q_{gw})$$

where SW_t is the final soil water content of time step *t* (e.g. end of the day), SW_0 is the soil water content at the beginning of time t, P_{day} is the amount of precipitation, Q_{surf} is the surface runoff, ET_a is the actual evapotranspiration, Q_{lat} is lateral flow, $Perc$ is the amount of water percolating to groundwater and Q_{gw} is the groundwater return flow (adapted from Neitsch et. al, 2011). All units are given in [mm/H_2O].

Soil moisture itself therefore depends on a range of variables controlling the amount of soil moisture gains through infiltration (a) and storage capacities (b) as well as losses through plant water uptake (c), soil evaporation (d), lateral flow (e) and percolation (f):

a. Infiltration is calculated in SWAT indirectly, by using the SCS curve number method to estimate surface runoff and then subtracting the daily runoff amount from the daily precipitation sum.

b. Storage capacities are defined by soil physical characteristics, given as model parameter values, such as pore space/bulk density, grain size distribution, layer depths, and hydraulic conductivity etc., which indirectly define soil water storage capacities by controlling plant water uptake, lateral flow and percolation.

c. Plant water uptake: SWAT uses the soil physical parameters of clay content and bulk density to estimate field capacity, permanent wilting point volumetric water contents and therefore plant available water capacity.

d. Soil evaporation is estimated by calculating potential ET using the Penman-Monteith method, adjusting it for evaporation of free water in the canopy and then multiplying it with a soil cover index. The soil cover index defines the degree of soil surface shading and depends on the above ground biomass.

e. Lateral flow is calculated in SWAT using a kinematic storage model for subsurface flow, accounting for slope steepness and hence considering subsurface flow characteristics depending on the local topography.

f. Percolation amount are calculated in SWAT as the water amount exceeding the field capacity water content. If the soil layer below a saturated layer is unsaturated, the water is allowed to percolate to the lower layer.

In the context of this study is it worth to recall, that infiltration into the soil highly depends on antecedent soil moisture conditions and decreases exponentially with increasing soil moisture content. A correct simulation of soil moisture conditions is therefore of high importance for hydrological variables, such as runoff.

For an improvement of the SWAT model using the collected field data, first, the in-situ data was analyzed in order to gain a deeper understanding of the soil moisture processes at the respective measuring sites. To be temporally consistent with the time resolution of the SWAT model, we aggregated the field data of 30-sec measuring intervals to daily time steps. A time frame of two years, starting from 01.01.2017 until 31.12.2018 was examined.

Following, the previously calibrated SWAT model, which had been set-up with climate data until 2014, was updated with more recent climate data until 31.12.2018. We re-run the model to generate model results for the time frame of 01.01.2017-31.12.2018. Furthermore, the model output settings were adjusted in the way that soil water storage information is written out for each soil layer separately. Soil water storage is given by SWAT in mm per soil layer. We converted the depth of water column into volumetric water content (VWC) by dividing the water column depth by the depth of the respective soil layer. This enables a comparison of observed and simulated volumetric soil moisture information at each respective depth of the soil profile. To compare observed and simulated values, we selected the three HRUs (Hydrological Response Units), which locations correspond to the location of the measuring sites. The SWAT soil profiles and their respective soil layers, as well as the depths of the soil moistures sensors used for comparison are displayed in Figure 4.9.

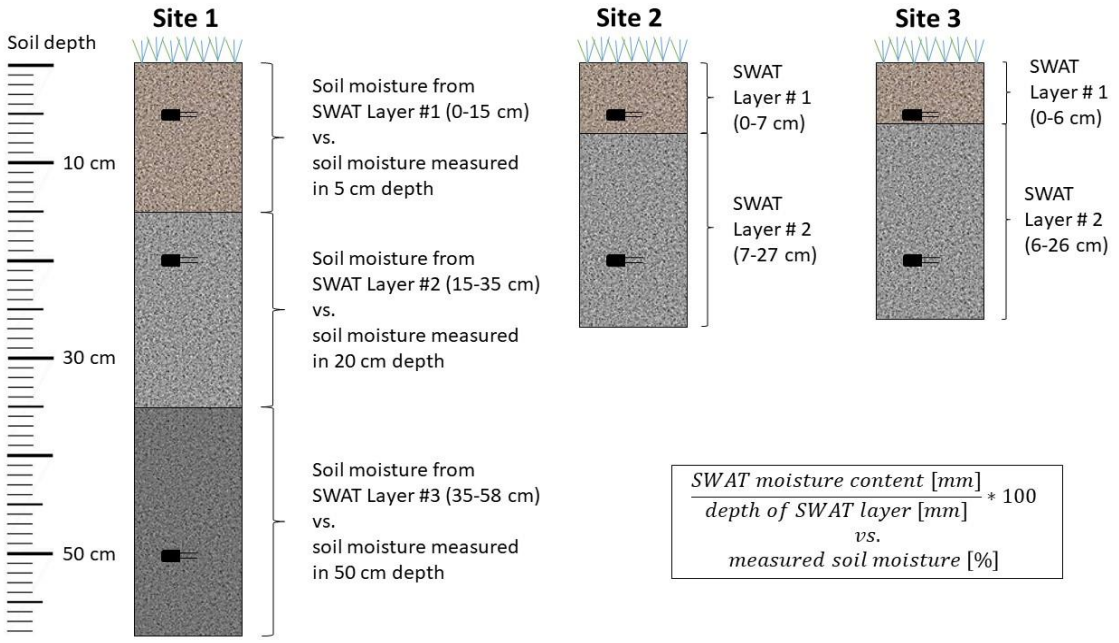

Figure 4.9: Soil layer depths as represented in SWAT at the three measuring sites, and the depth location of the soil moisture sensors, which data was used as reference for re-calibrating the SWAT model.

Through the comparative analysis of observed and simulated soil moisture processes at each soil depths, model weaknesses could be identified. These model weaknesses were then related to specific model parameters, which are dominating parameters in the estimation of soil moisture fluxes. In a manual post-calibration procedure these identified model parameters were adjusted to improve the simulation of soil moisture dynamics.

The improved parameter set was then adapted for all HRUs of the same slope, soil and land-use type. Finally, the model was re-run with the updated parameter set, which yielded the best fit between observed and simulated values and the overall model improvement was evaluated by analyzing changes in catchment discharge values.

4.3. Results

4.3.1. Field work results

The field work results include laboratory analysis, in situ tests, and soil moisture and water tension time series from the three stations.

Laboratory results

Findings showed a high fraction of clay on the three sites (ca. 64%), followed by silt (ca. 22%), with 14% of sand (see Table 4.2). Different model input parameters were obtained at different depths (i.e., total pore volume, air capacity, field capacity (by a pF value of 1.5), available field capacity, and permanent wilting point), enabling the comparison to data obtained from German Soil Service for the corresponding hydrological response units (HRUs). The results from the infiltration test (i.e., infiltration rate) at grassland are also shown in Table 2.

Table 4.2. Laboratory results at the study area

Site	Depth [cm]	No. of samples	kf-values [cm/d]	kf-values [mm/h]	Infilt. rate [cm/d]	Infilt. rate [mm/h]	Sand fraction [%]	Silt fraction [%]	Clay fraction [%]
Grass	0 - 14	9	154	64	55	23	13,3	62,2	23,6
	14 - 32	8	20	9	-	-	13,1	63,5	21,7
	32 - 55	9	20	8	-	-	15,2	64,2	20,1
	55 - 75	9	24	10	-	-	17,9	61,8	18,6
	75 - 100	9	43	18	-	-	16,6	63,3	17,3
Con. forest	0 - 12	8	3294	1373	-	-	13,1	63,0	22,7
	12 - 40	-	-	-	-	-	11,5	67,6	19,7
Dec. forest	0 - 8	10	2909	1212	-	-	15,3	61,9	22,8
	8 - 27	-	-	-	-	-	13,8	66,0	20,3

Site	Depth [cm]	No. of samples	Total pore volume [Vol%]	Air capacity [%]	Field capacity [%]	Available field capacity [%]	PWP [%]
Grass	0 - 14	9	60,8	5,0	55,8	42,5	13,3
	14 - 32	8	48,6	4,4	44,2	29,2	15,1
	32 - 55	9	45,1	3,9	41,2	26,4	14,9
	55 - 75	9	44,6	4,1	40,5	26,0	14,5
	75 - 100	9	44,7	5,3	39,4	27,3	12,1
Con. forest	0 - 12	8	71,3	29,8	41,6	31,7	9,8
	12 - 40	-	-	-	-	-	-
Dec. forest	0 - 8	10	72,3	27,7	44,5	31,9	12,6
	8 - 27	-	-	-	-	-	-

Additionally, pF curves were obtained for the three sites (see Figure 4.10 and Figure 4.11); it is important to point out that these curves are determined for each sample from saturation to dry state. In nature, the soil undergoes both cycles, i.e., from saturation to dryness and from dryness again to saturation. This is well captured by the water tension sensors, in which the hysteretic behaviour can be observed (see Figure 4.18).

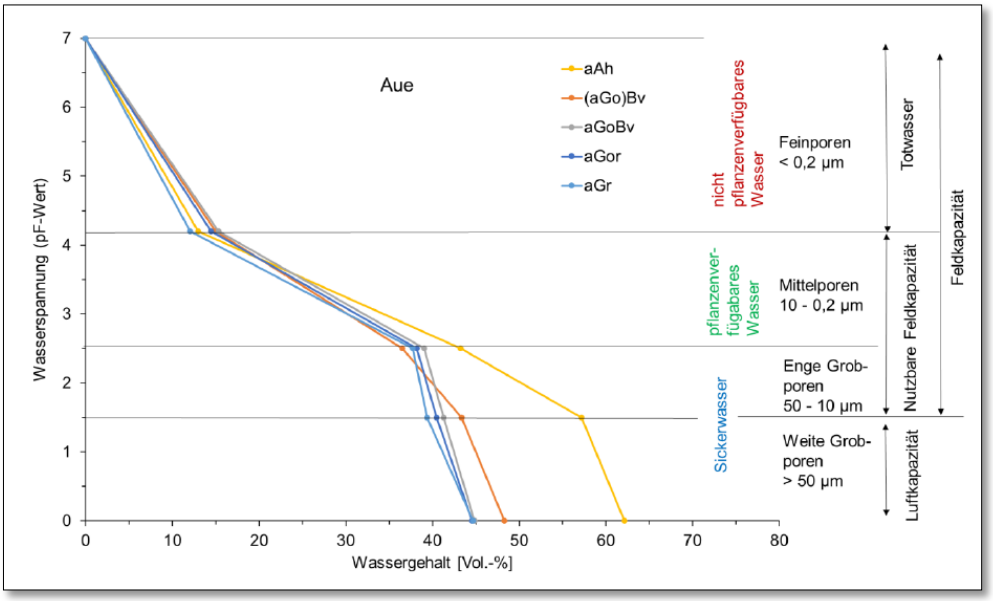

Figure 4.10 pF curve – grassland

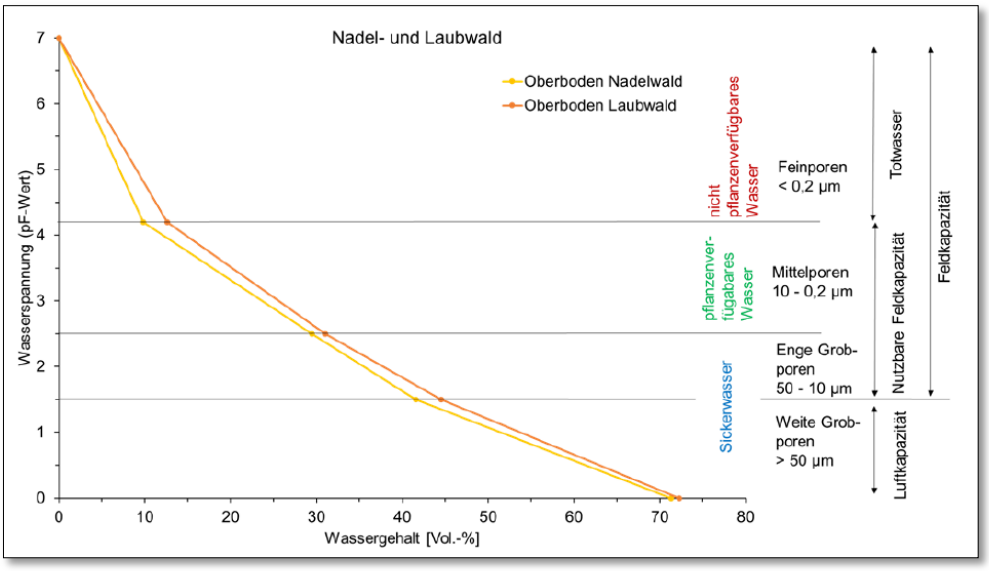

Figure 4.11. pF curve – coniferous und deciduous forest

Field measurements results

Soil moisture, soil temperature, and water tension have been continuously measured since December 2016. A pair of soil moisture sensors were installed in order to monitor significant deviations. It can be seen that at shallowest depths (e.g., 5 cm), variations between the pair of sensors are higher than at greater depths. The reason is that the surface is more influenced by natural processes like e.g., evapotranspiration. At greater depths, the data shows a more stable behaviour (see Figure 4.12 to Figure 4.14).

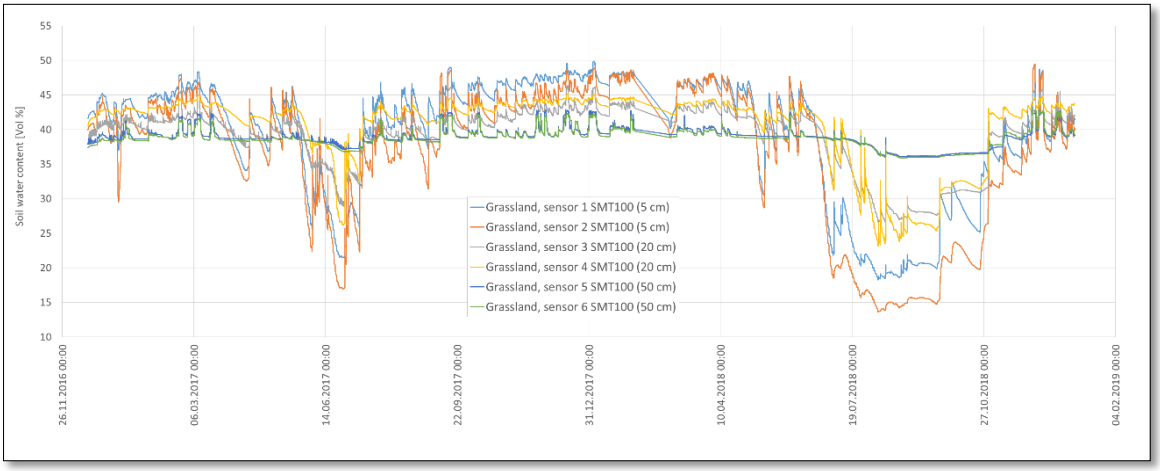

Figure 4.12. Soil moisture time series – box01 (grassland)

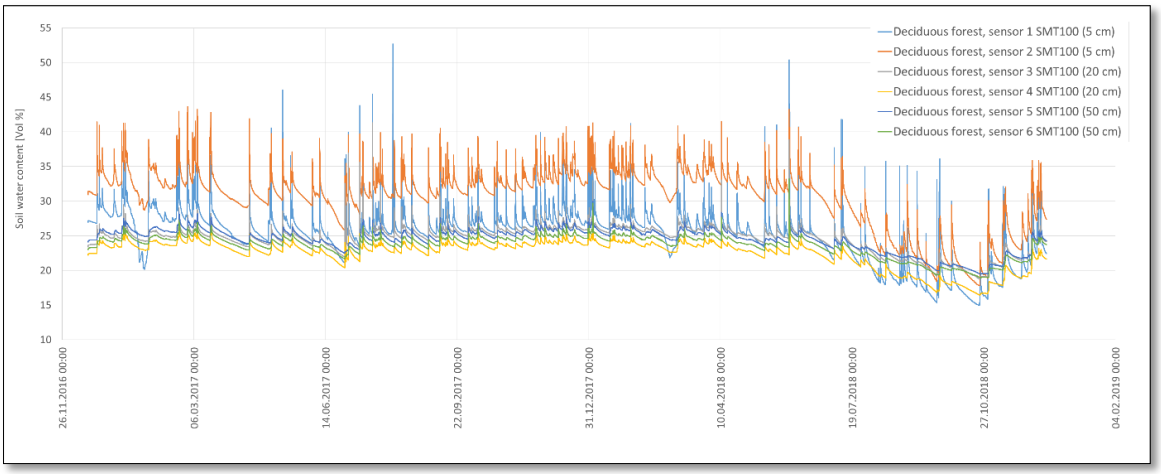

Figure 4.13. Soil moisture time series – box02 (deciduous forest)

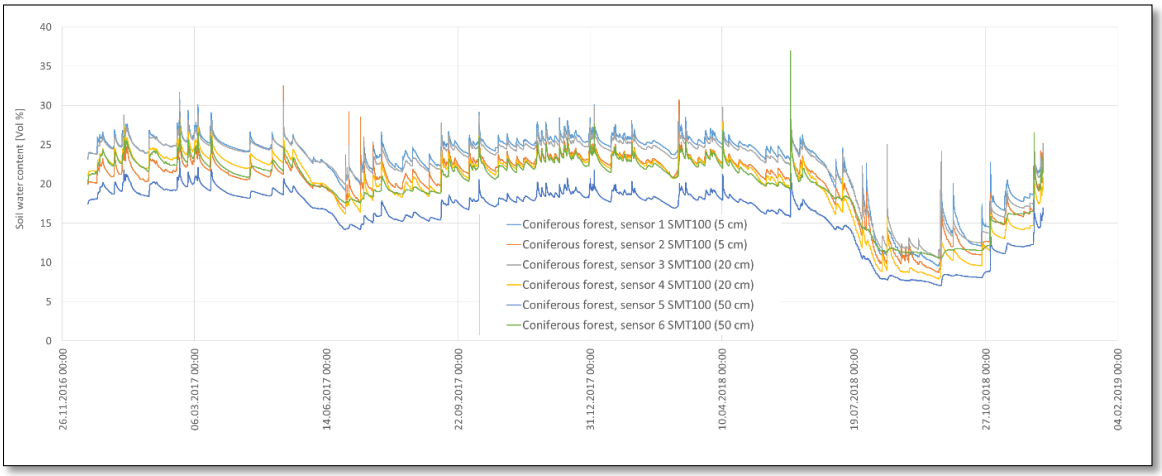

Figure 4.14. Soil moisture time series – box03 (coniferous forest)

Water tension shows the lower values during the summer months, as expected, with the highest variations taking place at the surface. Figure 4.15 to Figure 4.17 show the resulting time series. Water tension at coniferous forest demonstrated to be the greatest, especially in summer of 2018, which registered abnormally high temperatures.

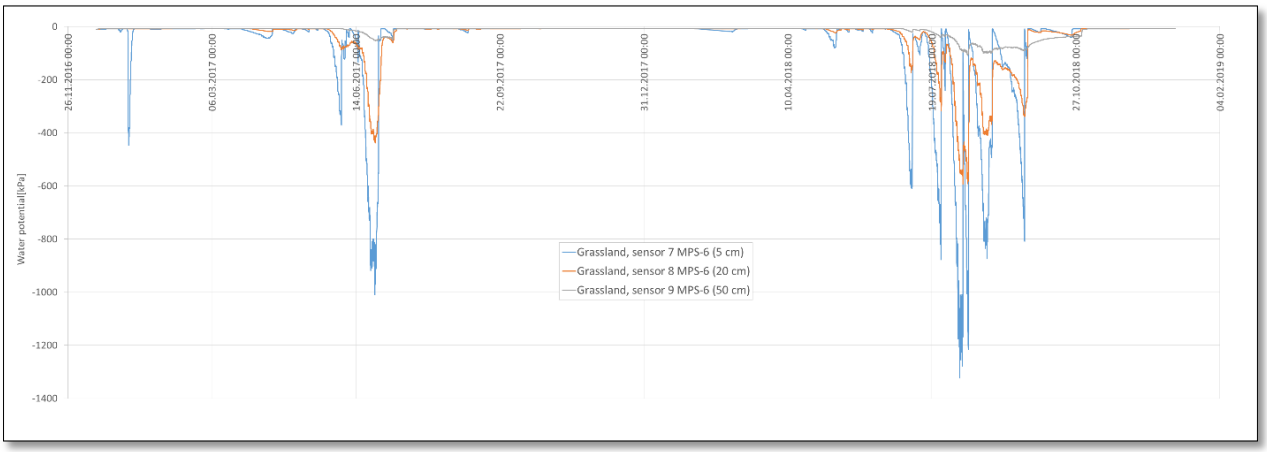

Figure 4.15. Water potential time series – box01 (grassland)

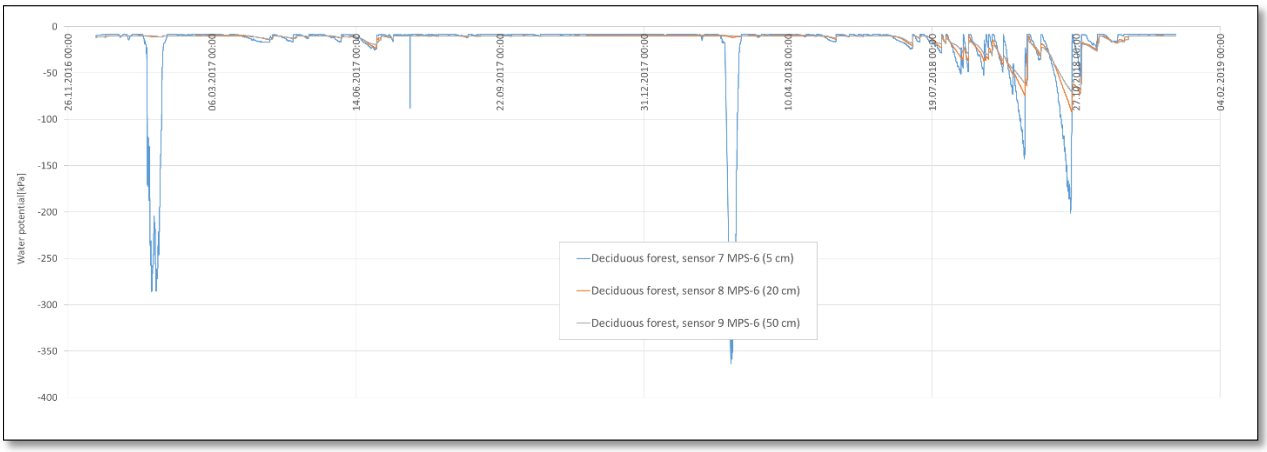

Figure 4.16. Water potential time series – box02 (deciduous forest)

Figure 4.17. Water potential time series – box03 (coniferous forest)

The measurement could be used to compare the measured transient situation against the lab values (see also Figure 4.10), whereby the lab results are only related to the emptying of the soil and not the filling process (example for box 1, depth 5 cm in Figure 4.18). The difference between both situations can be seen by the hysteresis in Figure 4.19: the soil drying process shows a more stable behaviour compared to the filling process.

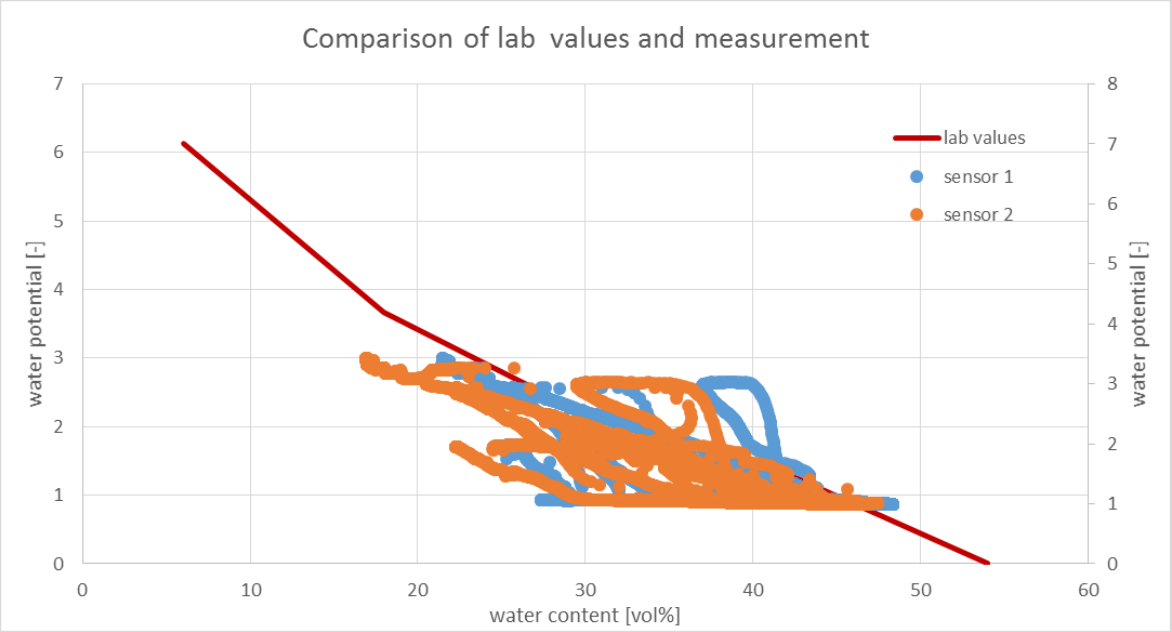

Figure 4.18. Water potential vs. water content – box01, 5 cm depth

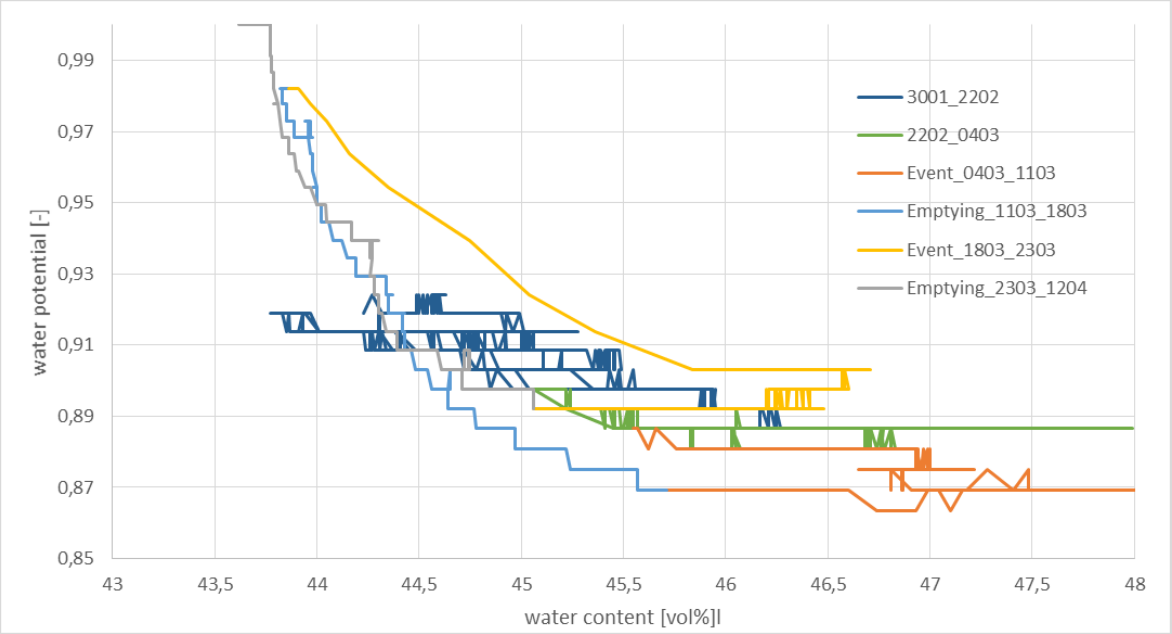

Figure 4.19. Water potential vs. water content – box01, 5 cm depth

Precipitation, discharge, and soil moisture were also compared, showing the dependency and sensitivity of discharge to antecedent soil moisture conditions and proof the plausibility of the measurements (see Figure 4.20).

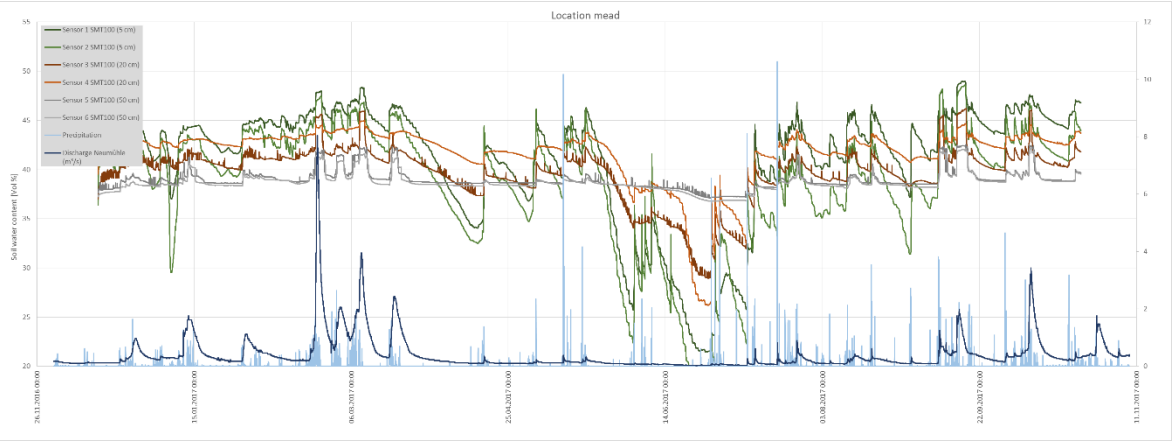

Figure 4.20. Water potential vs. water content – box01, 5 cm deepth

Comparison between soil assessment and model soil input parameters from German Soil Service

HRUs (for TALSIM and SWAT) for the study area were determined based on soil type data from the German Soil Service Centre as well as land use units (see Figure 4.21). Input data from the German Soil Service Centre was compared to the data obtained with the soil assessment based on soil type of the HRUs defined for the sub-catchment where the stations are located for the same depths (seeTable 4.3).

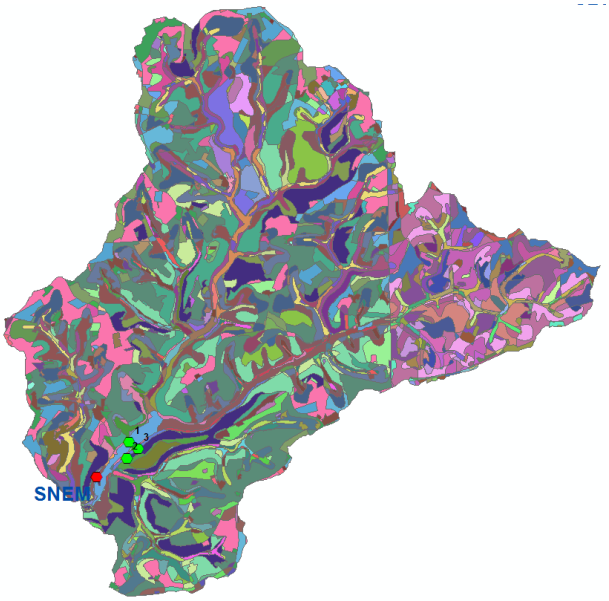

Figure 4.21. HRUs at the study area

Table 4.3. Comparison between German Soil Service and soil assessment data (field and laboratory measurements)

Box No.	HRU No.	Soil type	Land use unit	Thickness [m]	WP [mm/m]	FC [mm/m]	GPV [mm/m]	kf [mm/h]	Max. infilt. [mm/h]
German Soil Service Centre									
1	717	L4908_G-A342GS3_Wiese_II	Grassland	1,1	160	340	430	20,8	61,9
2	709	L4908_B331_Mwald_VI	Dec. forest	0,7	140	290	360	20,8	36,3
3	726	L4908_B311_Mwald_VI	Con. forest	0,3	90	220	270	12,5	22,7
Soil assessment									
1	717	Brown earth / gley	Grassland	0,75 - 1	121	394	447	18,0	NA
2	709	Brown earth / gley	Dec. forest	0,12 - 0,40	NA	NA	NA	NA	NA
3	726	Brown earth / gley	Con. forest	0,08 - 0,27	NA	NA	NA	NA	NA

*not meas. = Not measured at this depth

For grassland, the parameters obtained from the German Soil Service are very similar to those obtained with the soil assessment. On account of the parameters similarity, the soil physical properties for the calibration process were not modified. Due to site conditions, it was difficult to carry out measurements and tests at the two forest sites (too steep and rocky), so a direct comparison was not carried out.

4.3.2. Model results

TALSIM

Since the model output is given per sub-catchment, field soil moisture data was averaged for comparison purposes. Figure 4.22 presents the average volumetric water content at the research site. Figure 4.23 and Figure 4.24 show the sub-basins of the Dhünn River Basin (TALSIM model) and the TALSIM model computational domain.

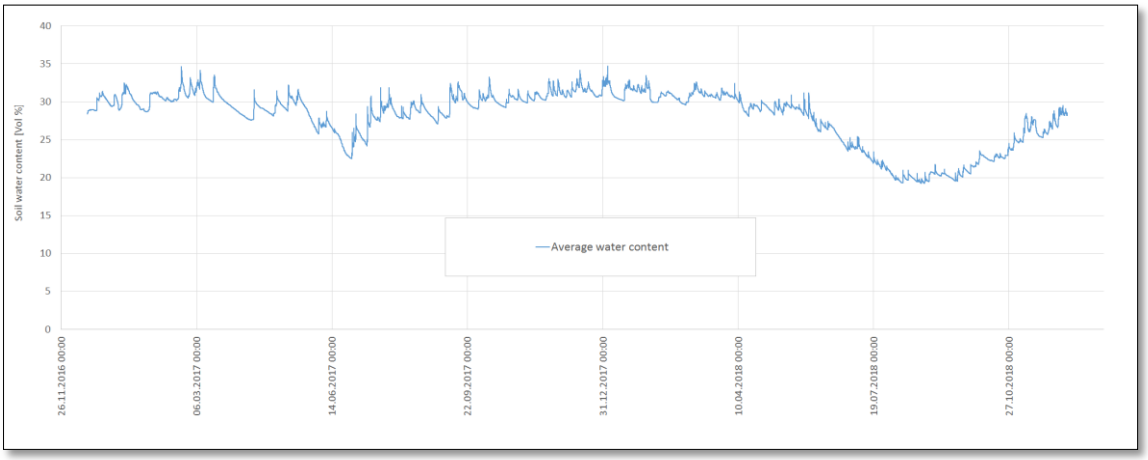

Figure 4.22 Average volumetric water content at the research site

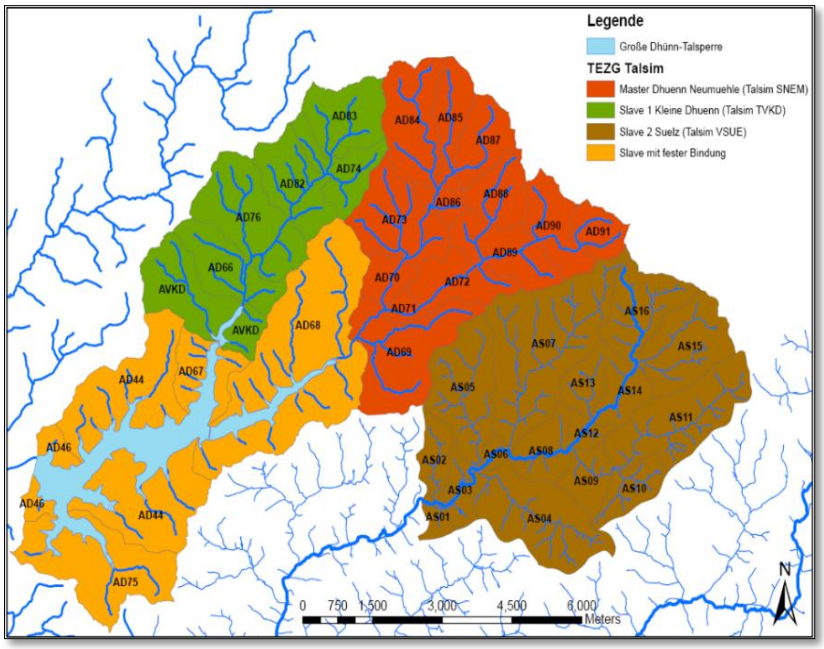

Figure 4.23. Sub-basins of Dhünn catchment area – TALSIM model (study area Upper Große Dhünn in red)

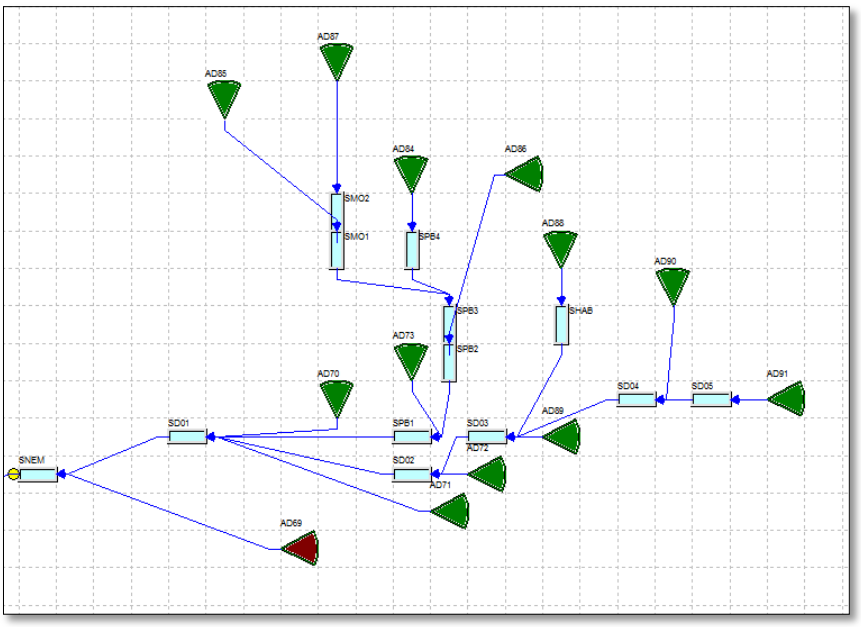

Figure 4.24. TALSIM computational domain – Upper Große Dhünn (study area located at sub-catchment AD69, in red)

Results

After several trials, the final calibration was obtained with the set of values producing the best fit between observed and simulated soil moisture and discharge. Table 4.4 presents the modified parameters.

Table 4.4. Modified parameters – model calibration

	Current state	Variant 1	Variant 2
Description (dimensionless)	**Values**		
Factor max. infiltration [-]	1	1	1
Scaling kf layer 1 [-]	1	1	0,5
Scaling kf layer 2 [-]	20	1	0,5
Scaling kf layer 3 [-]	75	1	0,5
Scaling interflow [-]	0,8	1	1
Scaling deep interflow [-]	0,8	1	1

Hydraulic conductivity proved to be one of the most sensitive parameters. The best results (variant 2) were obtained by diminishing kf values by 50 % at the three defined soil layers (the definition of the soil layers is performed internally by the model).

Figure 4.25 shows observed and simulated soil moisture (current state, variant 1, and variant 2).

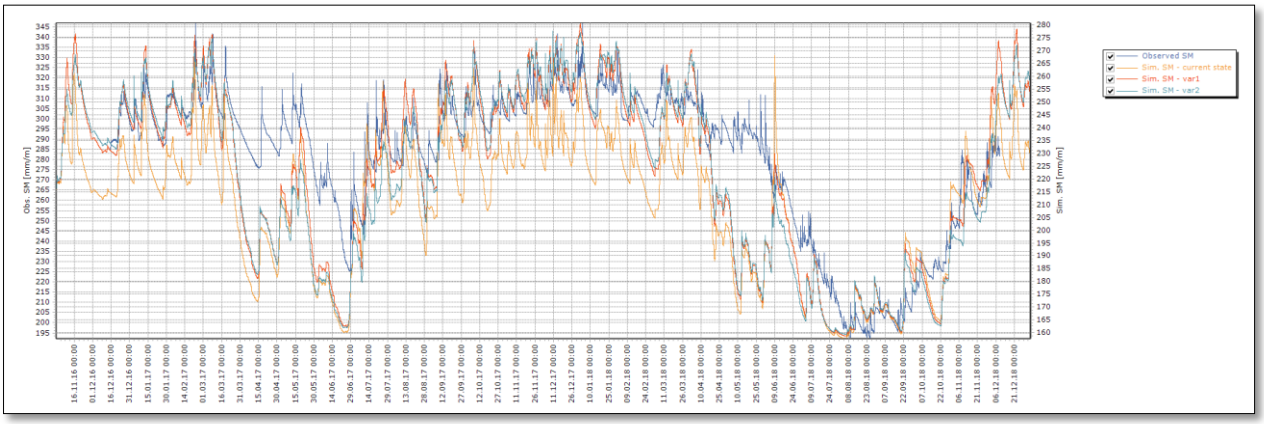

Figure 4.25. Observed and simulated soil moisture (current state, variant 1, and variant 2)

Model performance

Model performance is assessed with several metrics, previously described in D3.3. Goodness-of-fit (GOF) of observed and computed soil moisture are shown in

Figure **4.26** to Figure 4.28.

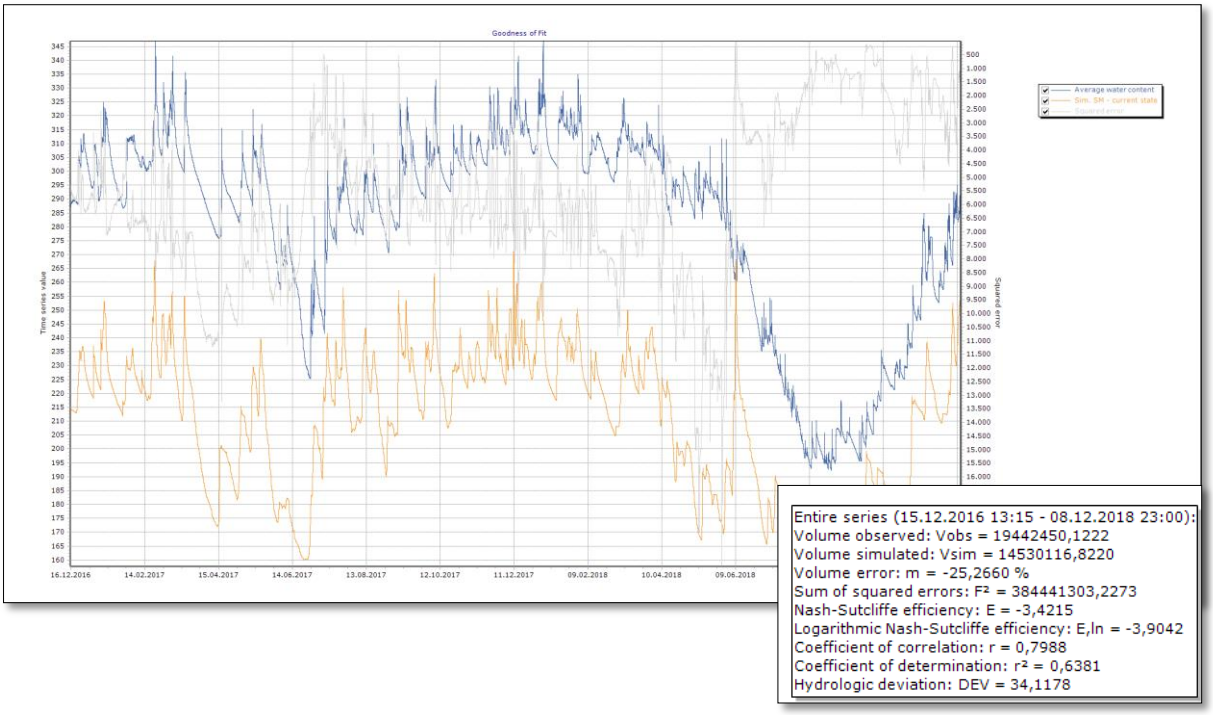

Figure 4.26. Goodness-of-fit (GoF) – observed and simulated soil moisture (current state)

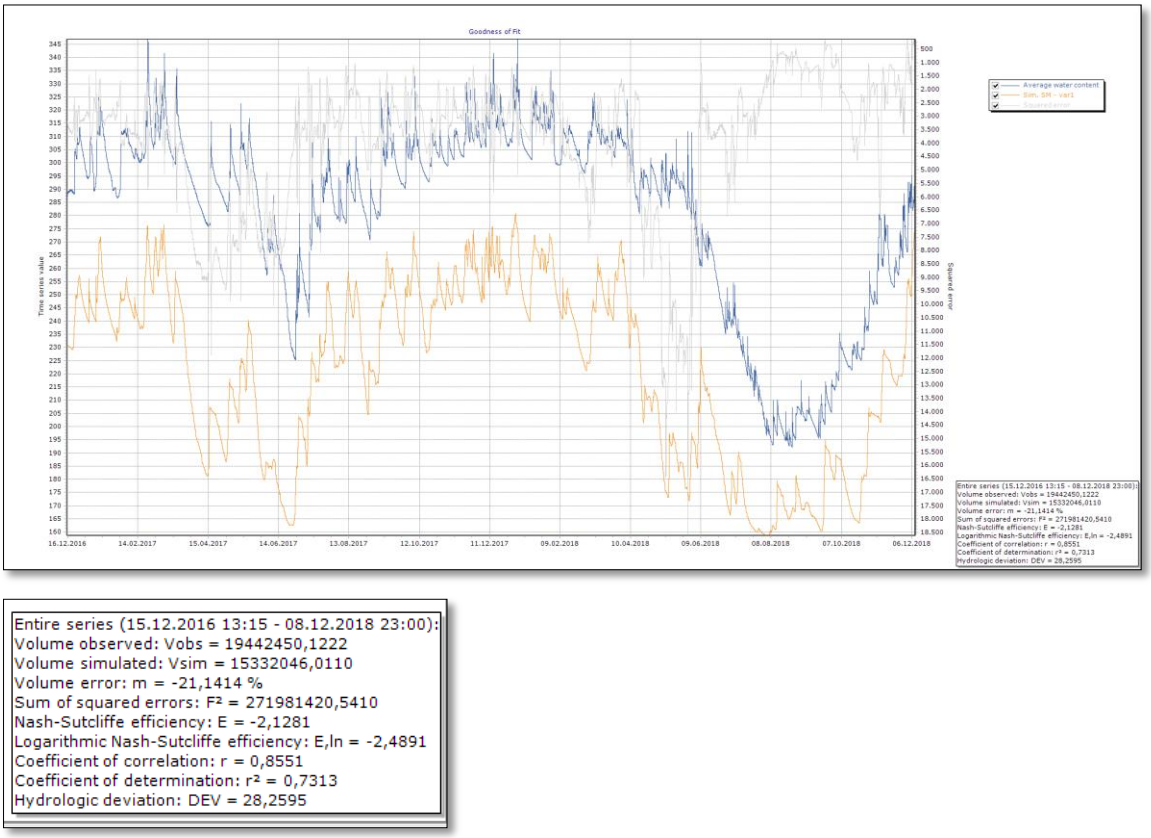

Figure 4.27. Goodness-of-fit (GoF)– observed and simulated soil moisture (variant 1)

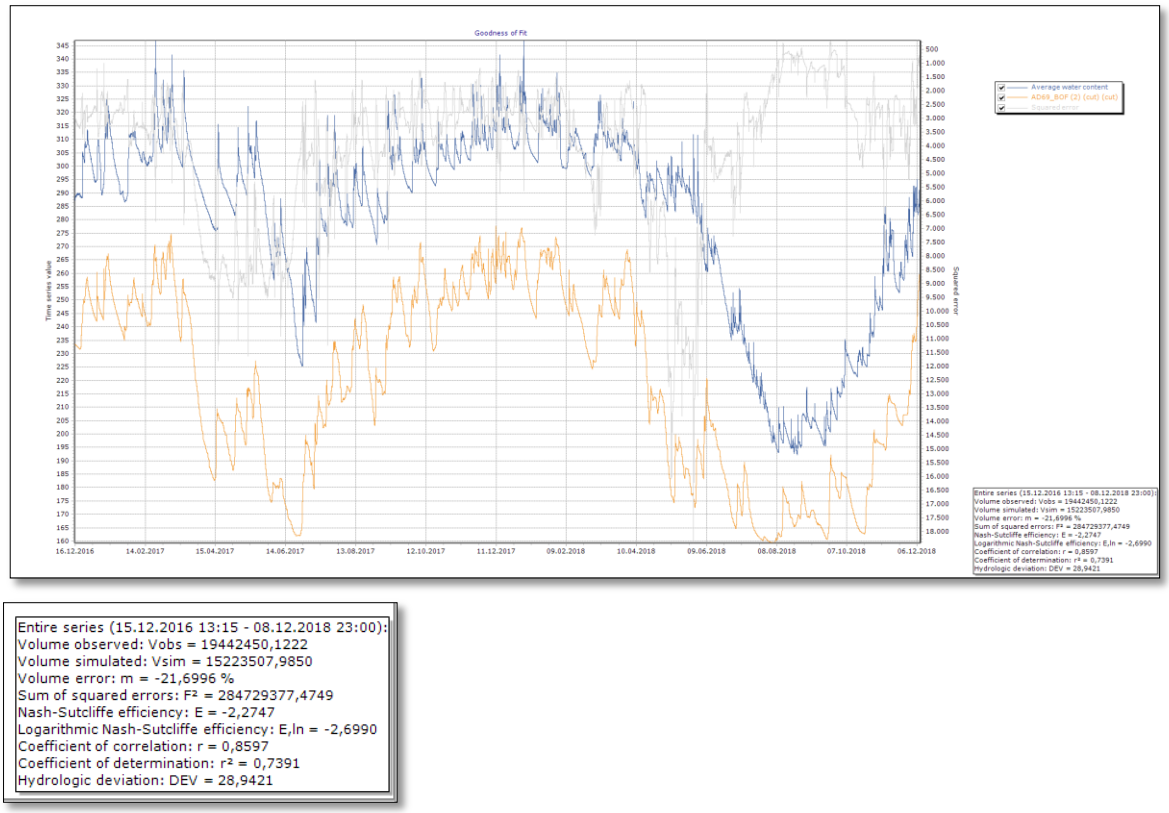

Figure 4.28. Goodness-of-fit (GoF)– observed and simulated soil moisture (variant 2)

Variant 2 showed the best agreement in terms of coefficient of correlation and determination. However, on once absolute observed data was plotted against simulated soil moisture (see Figure 4.29), a bias can be observed along the simulation period.

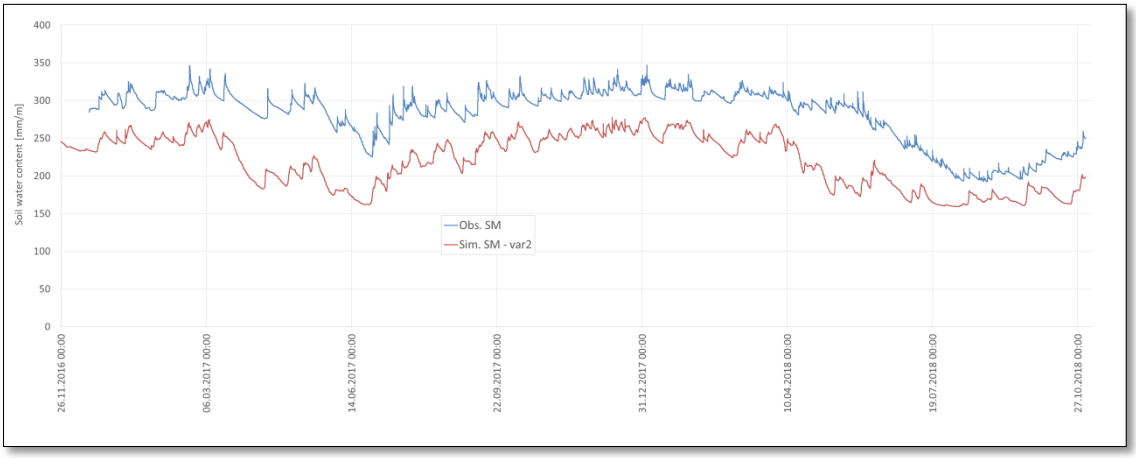

Figure 4.29. Absolute values – observed soil moisture and simulated soil moisture (variant 2)

It is assumed that this bias takes place since model output corresponds to an internal calculation based on the influence of each HRU (weight by area of each physical parameter on the sub-catchment). Thus, simulated time series are considered to be very coarse. Nevertheless, drying and wetting cycles are captured properly as well as seasonal variability and small time scale variations. The difference between the two time series seems to decrease at the lowest observed soil moisture, which indicates especially an

adequate value of WP (wilting point, minimum possible value of simulated soil moisture) from the German Soil Service in comparison to total pore volume (maximum possible value).

Figure 4.30 presents observed and simulation discharge with the same variants (i.e., current state, variant 1, and variant 2). Figure 4.31 to Figure 4.33 show GoF for observed discharge and the corresponding simulations.

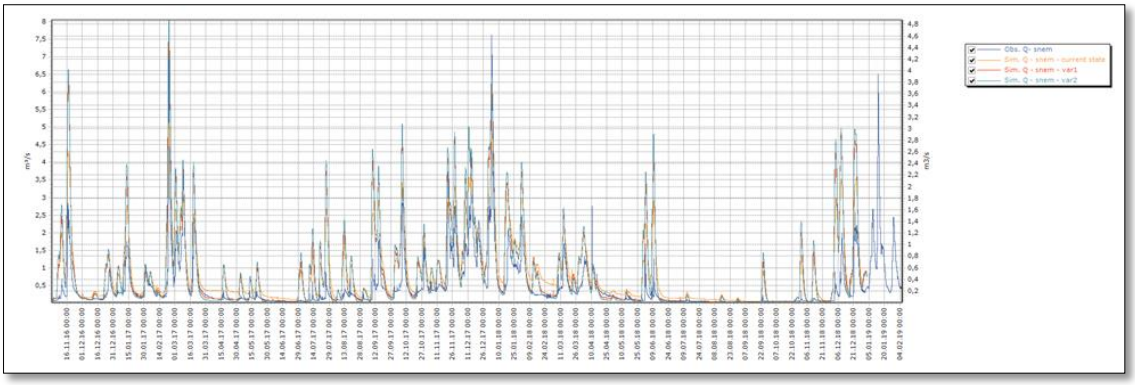

Figure 4.30. Observed and simulated discharge – Neumühle hydrometric station (SNEM)

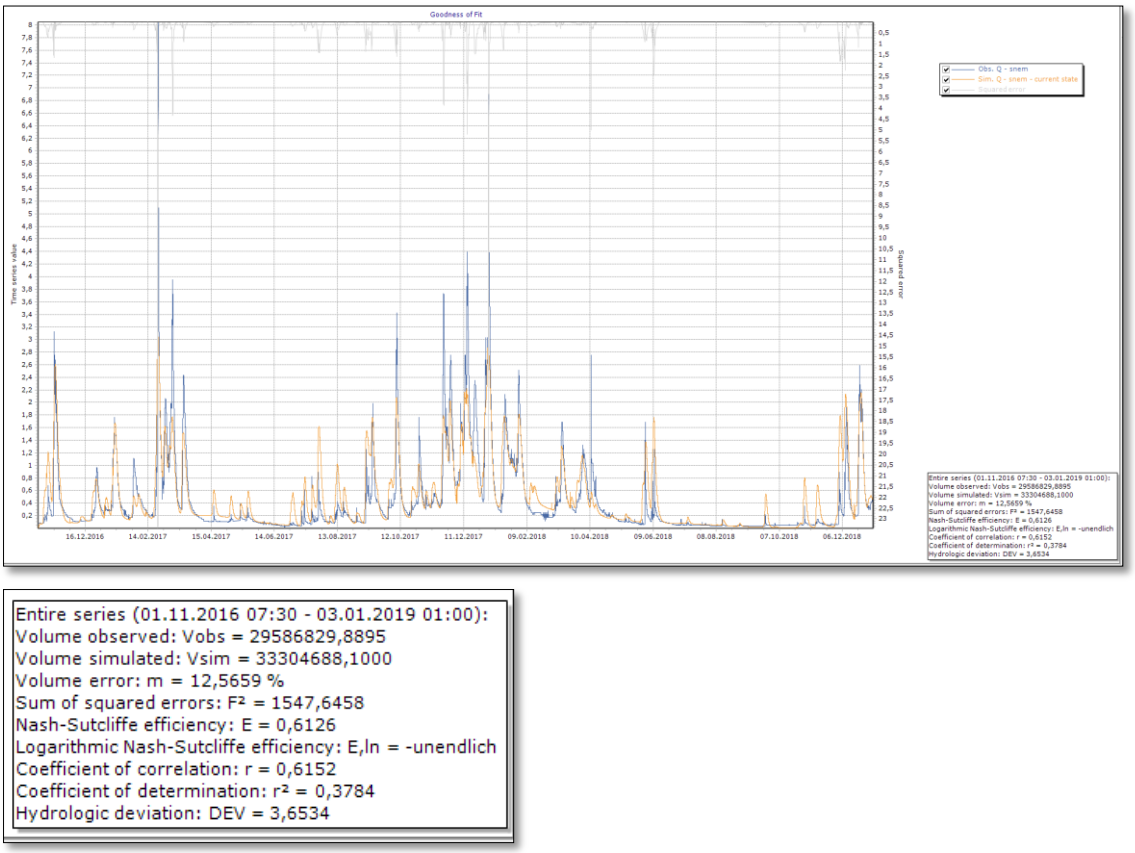

Figure 4.31. Goodness-of-fit (GoF)– observed and simulated discharge (current state)

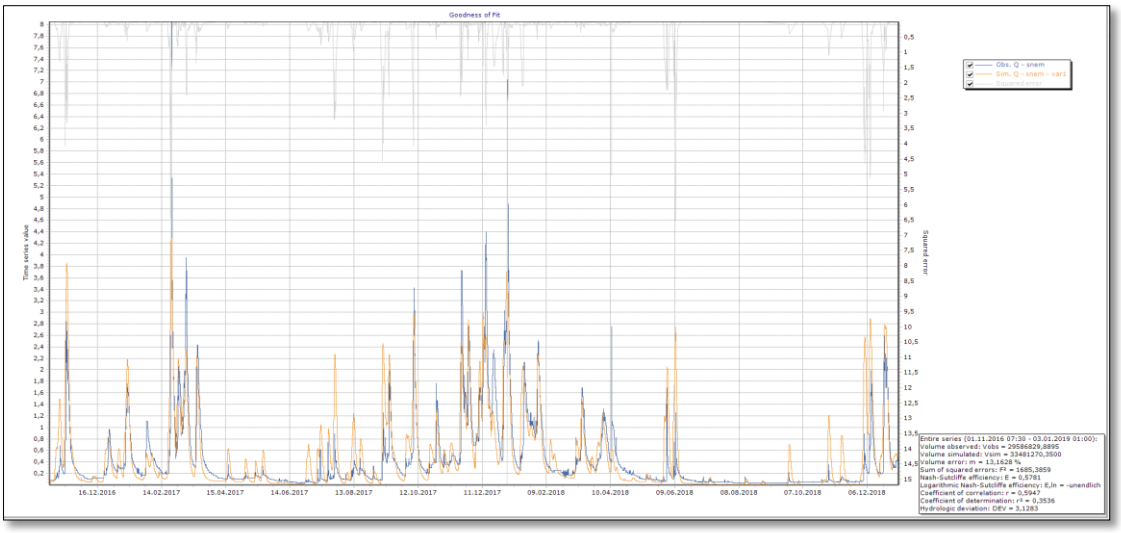

Entire series (01.11.2016 07:30 - 03.01.2019 01:00):
Volume observed: Vobs = 29586829,8895
Volume simulated: Vsim = 33481270,3500
Volume error: m = 13,1628 %
Sum of squared errors: F² = 1685,3859
Nash-Sutcliffe efficiency: E = 0,5781
Logarithmic Nash-Sutcliffe efficiency: E,ln = -unendlich
Coefficient of correlation: r = 0,5947
Coefficient of determination: r² = 0,3536
Hydrologic deviation: DEV = 3,1283

Figure 4.32. Goodness-of-fit (GoF)– observed and simulated discharge (variant 1)

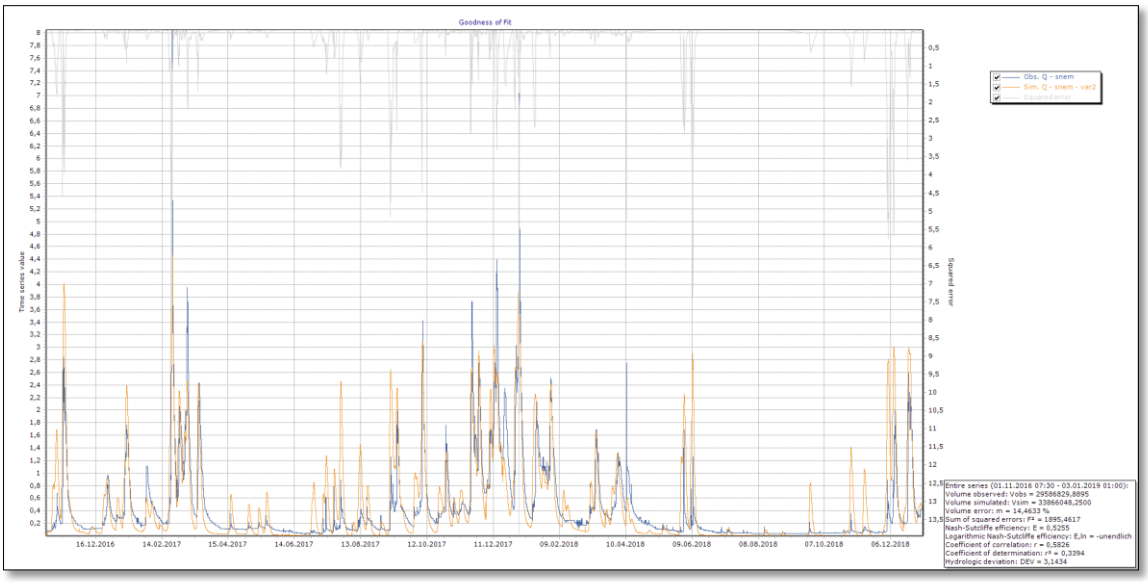

Figure 4.33. Goodness-of-fit (GoF)– observed and simulated discharge (variant 2)

Model performance indicated a slight worsening of Goodness-of-fit (GoF) metrics such as volume error, Nash-Sutcliffe efficiency, coefficient of correlation, and coefficient of determination. However, they are not considered significant. In conclusion, variant 2 results in the following:

- Improvement of high peaks magnitude
- Improvement of soil moisture
- Worsening of hydrograph volume
- Worsening of low peaks magnitude (low flow)
-

Simulation using a linear algorithm – sensitivity analysis

Figure 4.34 presents the results of two simulations: non-linear (blue) and linear solution of soil physical equations (orange). The results show that there is no difference between the two options.

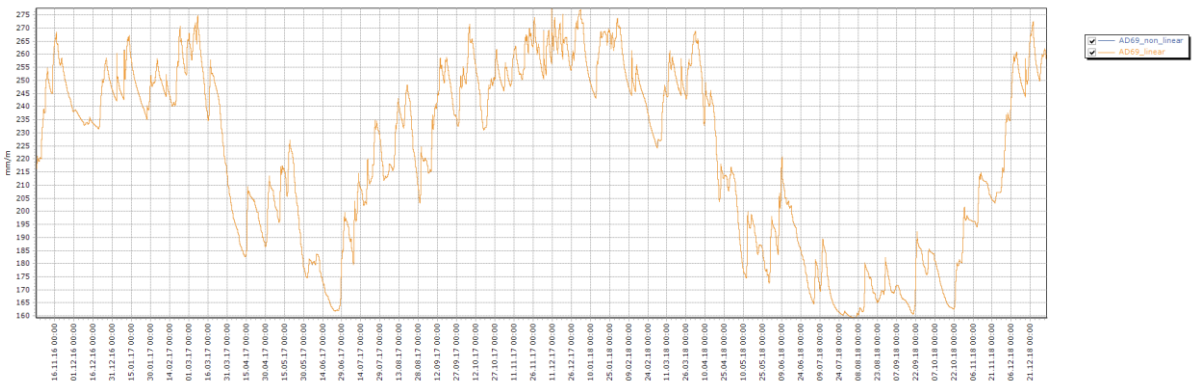

Figure 4.34. Simulated soil moisture - non-linear (blue) and linear (orange) algorithms

Conclusions

Different parameters can be modified based on different model purposes; the emphasis can be either on total volume, low flow, or high peak magnitude. For this case, special attention was given to high peak discharge since the focus is the improvement of flood forecasting, but also for the summer storm events which actually are not well represented by the models.

- By scaling the original value of hydraulic conductivity by half for all soil layers (variant 2), the model presented a better fit in terms of observed soil moisture.
- Variant 2 caused a worsening in terms of total hydrograph volume and low flow; on the other hand, high peak magnitude improved, i.e., high flood events were better captured by reducing the hydraulic conductivity.
- Using a linear algorithm for soil moisture simulation showed no difference with respect to the non-linear approach (low sensitivity to different simulation algorithms).

SWAT

SWAT results show a similar site specific differentiation as the field measurements. Highest soil moisture contents are correctly reproduced by the model at site 1, while site 2 and 3 show lower values as well as less variability in the annual drying and wetting periods. **Figure 4.35**, shows mean simulated SWAT soil moisture contents of all layers, at the respective measurement sites. Sites 2 and 3 show negligible differences in their soil moisture characteristics.

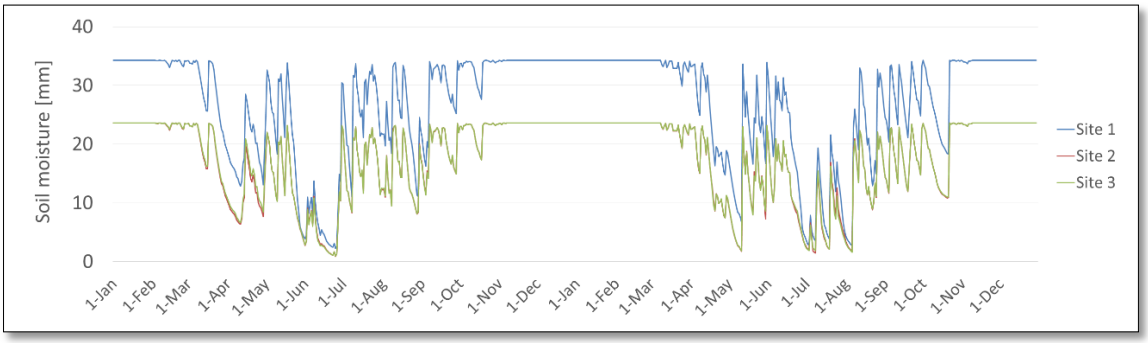

Figure 4.35: Mean daily soil moisture values, simulated by SWAT at all three measuring sites, for 2017-2018.

While the overall temporal annual drying and wetting episodes and the site specific variations are reflected well by SWAT, depth dependent soil moisture variations however, show that the model is not able to correctly reproduce the soil water storage in deeper soil layers. While measurements show a changing vertical moisture distribution, with decreasing soil moisture gradient from top to bottom layer, in winter months and vice versa during summer months, SWAT simulates a constant vertical moisture distribution and a significant moisture decrease with depth. In Figure 4.36 this increasing discrepancy of observed and simulated values by depth is displayed for site 1. The same results can be seen for site 2 and 3 (not displayed).

Apart from the weakly represented vertical soil moisture dynamics, an overall underestimation of soil moisture values by SWAT can be observed. SWAT soil moisture values reach their maximum values (i.e. saturation) in the top layer at about 23% VWC. A further moisture increase is inhibited, which is visualized by the constant upper limit of the SWAT soil moisture curve at approx. 23%. In the lower layers the saturation limit is reached at approx. 5% in layer 2 and 2% in layer 3.

In addition, variations in the daily soil moisture fluxes seem to be overestimated by SWAT.

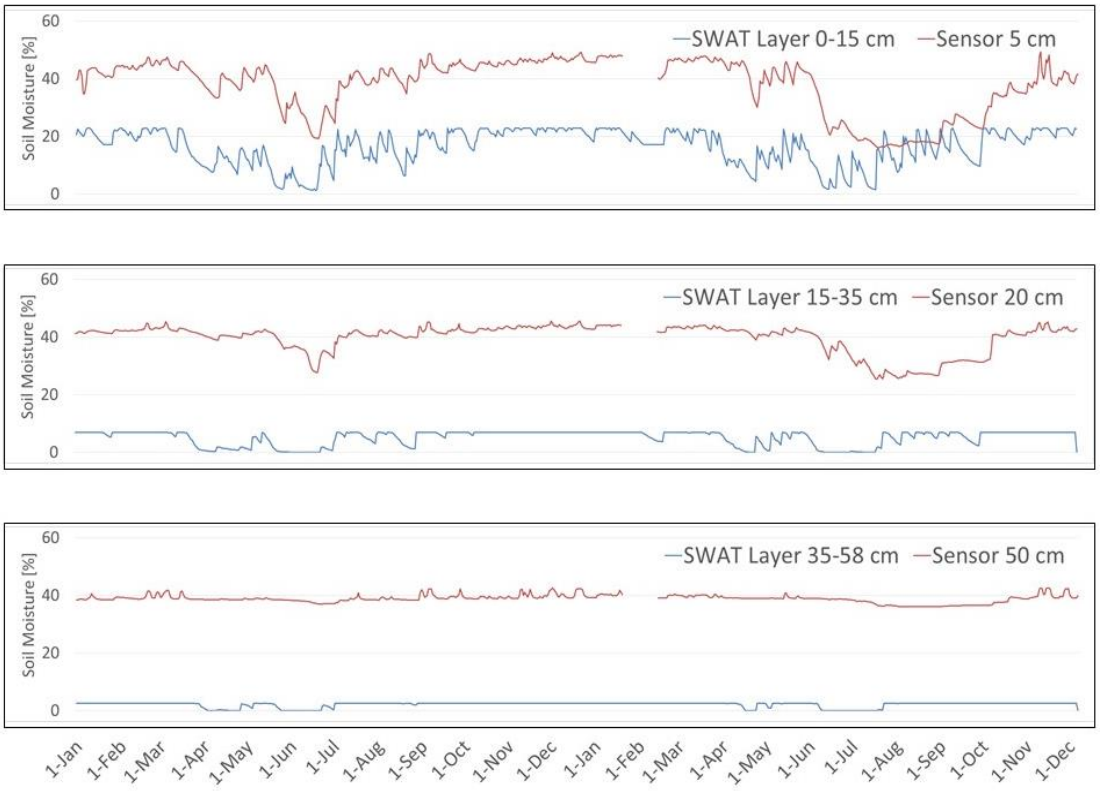

Figure 4.36: The comparison of observed vs. simulated vertical soil moisture distributions for site 1, from January 2017-December 2018, showing increasing discrepancies with depth.

Improvement of the SWAT Model based on field measurements

Based on these findings, we identify the following SWAT model weaknesses which should be considered in a re-calibration procedure and we relate them to specific SWAT model parameters:

1. Soil moisture storage capacities in the lower layers have to be increased, in order to raise soil moisture content in these layers and maintain a nearly constant moisture content throughout the year as well as prevent equal drying throughout the entire soil column.

- We increase the parameter *SOL_K* (hydraulic conductivity) for the upper layers to enable faster infiltration and we decrease the same parameter for the lowest soil layer to prevent fast percolation and reduce fluxes passed the root zone.

2. Soil moisture storage capacities have to be increased, in order to increase the overall soil water content in the SWAT model results and to remove the upper limit of moisture increase
   - We increase *SOL_AWC* (soil water holding capacity) to enable a higher soil water storage.
   - We decrease SOL_BD (bulk density) to increase soil porosity and enable higher water contents

3. To reduce the range of daily variations in soil moisture values, water losses through soil evaporation should be reduced
   - We reduce the parameter *ESCO* (soil evaporation compensation factor) to prevent water from deeper layers to be used to meet the soil evaporative demand.

Table 4.5: Table of pervious parameter values and updated parameter values used for re-calibration, at site 1

Parameter Name	Previous parameter value			Updated parameter value		
	Layer 1	Layer 2	Layer 3	Layer 1	Layer 2	Layer 3
SOL_K [mm/hr]	8.5	5.7	0	10	7	0
SOL_AWC [mm H_2O/mm soil]	0.16	0.07	0	0.18	0.18	0.18
ESCO [-]	0.5			0.1		
SOL_BD [Mg/m^3]	1.6	1.5	1.6	1	1	1

Changes in the SWAT model parameters are done in a step-wise procedure, changing one parameter at a time. Thus sensitivities of each parameter can be addressed separately. Examining the sensitivity of each parameter with respect to changes on soil moisture storage and the vertical moisture gradient, it can be stated that bulk density (SOL_BD) shows the strongest impact on soil moisture content and distribution with depth. Decreasing bulk density increases the porosity of the soil structure and thus leads to a significant increase in maximum soil moisture contents. The previously mentioned “upper limit” could successfully be removed and in addition, the moisture gradient with depth could be modified. Even though the discrepancy between observed and simulated soil moisture is still increasing with depths (Figure 4.38), the overall vertical distribution is now showing a closer match with the vertical moisture distribution of the field measurements. Figure 4.37, shows that during the drying cycle in summer, soil moisture content is maintained in lower layers and is showing higher values than the top layer, as it was seen in the field data.

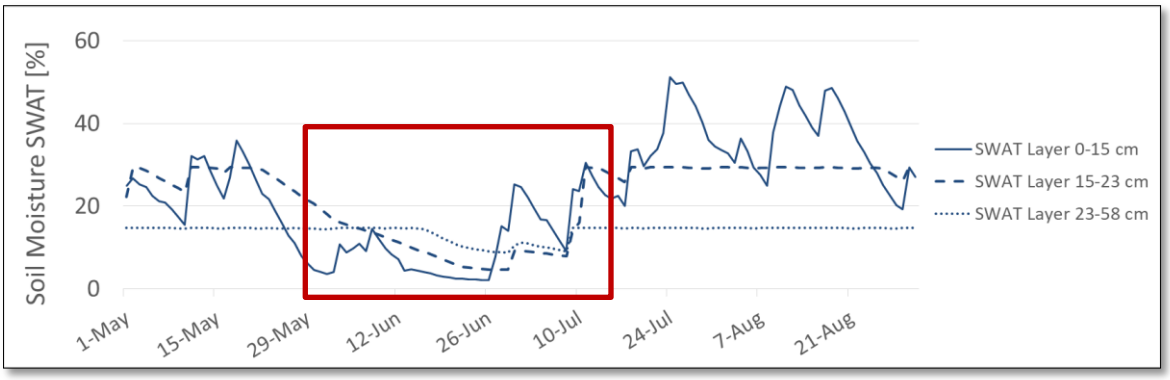

Figure 4.37: Simulated summer soil moisture distribution (May-August, 2017), for each soil layer at measuring site 1, after re-calibrating the SWAT model. Red box: highlighting the correct vertical soil moisture distribution after re-calibration

The soil moisture patterns of each layer compared to the field data, after the parameter adjustments, are shown in Figure 4.38, for measuring site 1:

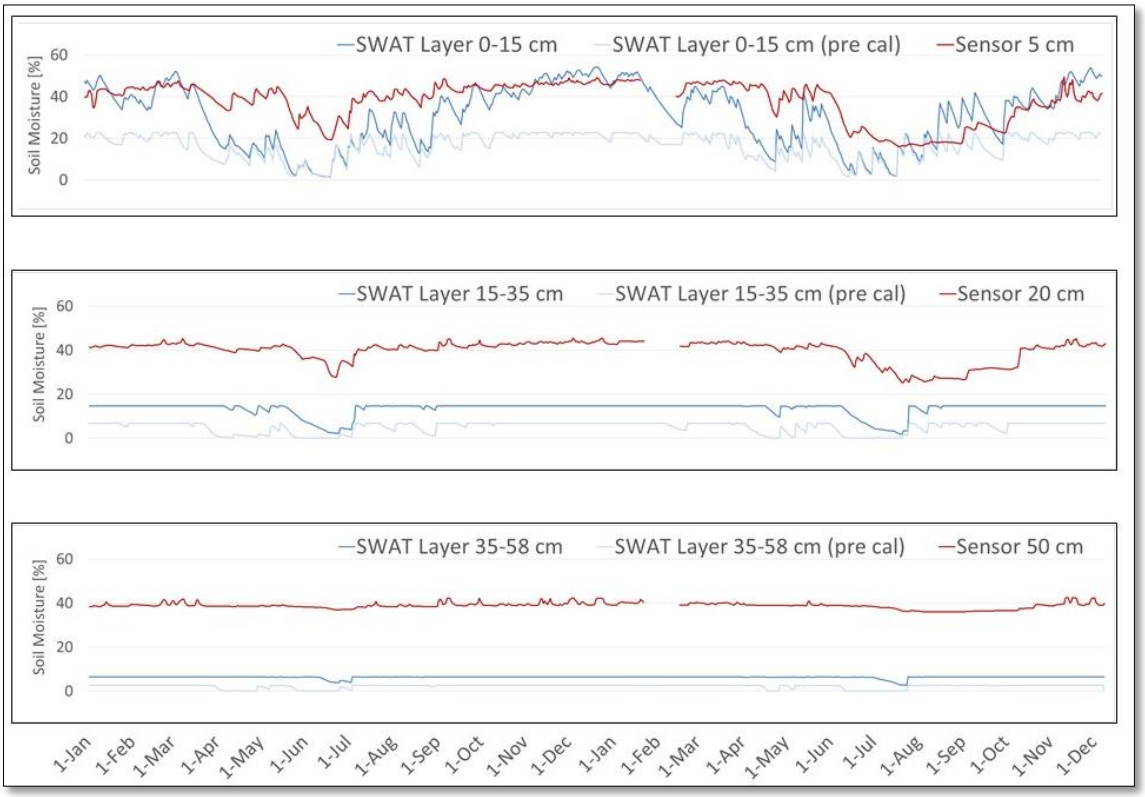

Figure 4.38: Site 1 - Comparison of observed vs. simulated vertical soil moisture distributions, after re-calibration of the SWAT model. The light blue line shows the fit before re-calibration (pre cal)

Especially the upper layer of site 1, could be significantly improved and shows that the re-calibration, using the in-situ data as reference data set, helped to increase soil moisture simulation performance at this site.

Site 2 and 3, are showing a limited success in improving the soil moisture dynamics of the upper soil layer. At both sites, soil moisture variations are highly overestimated, as can be seen for site 2 in (Figure 4.39). The re-calibration was able to increase the overall moisture content but the upper layer still shows a low saturation threshold, which impedes a further improvement of the match between observed and simulated values. Similar results are obtained for site 3 (not displayed). Reasons for this hampered re-calibration

might be the parameter selection for the calibration procedure at these two sites. Due to the dense forest cover and shallow soils, bio-physical parameter might have a bigger influence on soil moisture dynamics, at these sites, than just parameters of physical soil properties. Nevertheless, apart from potential model parameter errors, the weak fit between observed and simulated vertical soil moisture distribution, hints also towards model structural reasons for the low model performance. As mentioned in the model description (see 1.2.3 SWAT), as well as by Rajib and Merwade (2015), SWAT doesn't compute soil moisture balances based on physical parameter but derives them indirectly from surface runoff estimates. The authors point out the weaknesses of the common SCS CN approach used here and the importance of a precise calculation of surface runoff for an accurate soil moisture estimation. In addition, the depths distribution of soil moisture was pointed out as a major model weakness. This might be due to ET depth distribution functions and parameters like EPCO and ESCO, which can be seen as scaling factors for soil and plant ET. A fixed value has to be set for both coefficients, ignoring any temporal variability in soil and plant evapotranspiration. Hence a closer look into model structural aspects is recommended.

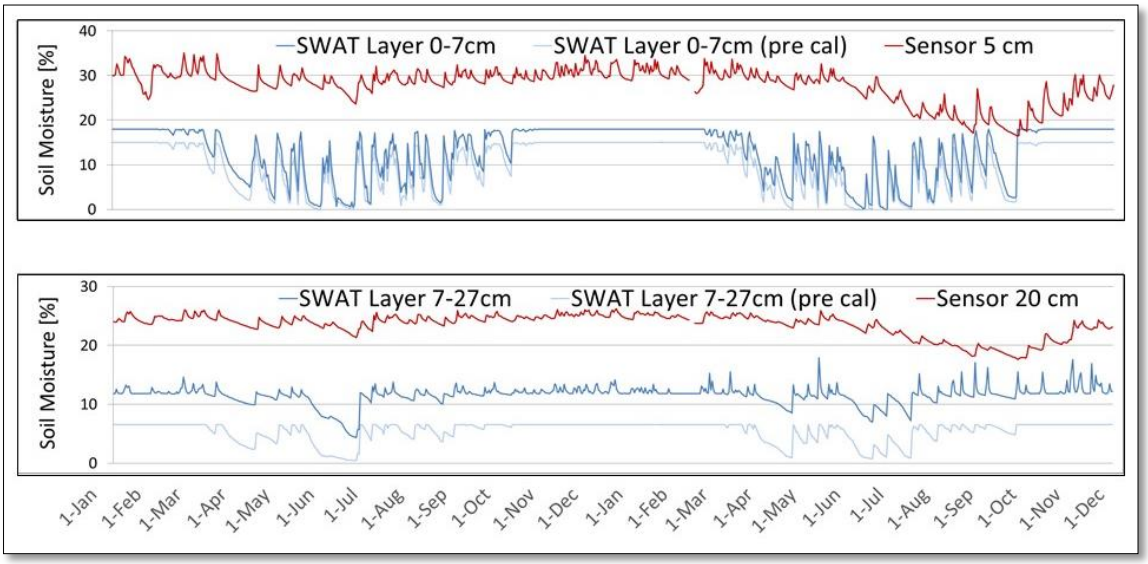

Figure 4.39: Site 2 - Comparison of observed vs. simulated vertical soil moisture distributions, after re-calibration of the SWAT model. The light blue line shows the fit before re-calibration (pre cal)

In a final step, the parameter values found to improve soil moisture characteristics at measuring site 1, are adapted for all HRUs of the same land-use class, the same soil type and the same slope value. Similarly the parameters for sites 2 and 3 are adapted to respective HRUs. The model is re-run for the same time period with the updated parameter values and the resulting discharge is evaluated against measured stream flow data. However, the fit between observed and simulated discharge remains the same and shows no changes (not displayed). Why the modification made to the model can still be regarded as a model improvement is outlined in the following discussion section.

4.4. Discussion

The field measurements of soil moisture at the three test sides in the Obere Dhünn catchment, gave detailed insight into temporal moisture variations as well as vertical moisture distribution patterns. The knowledge gained through the field data helped to optimize the model parameters of the TALSIM and SWAT models, which were modified to improve the models with respect to their soil moisture simulation performance. Even though the calibration procedure was a trial-and-error process with only a limited

number of calibration parameters and model iterations, the field data helped to refine both models and improve their physical accuracy.

However, we acknowledge that some site specific as well as general limitations have to be pointed out:

- Soil types in a river catchment can vary significantly and field data can often times only be collected for a small number of sites. Consequently, changes to main soil parameters can only be made for a limited area. In the Obere Dhünn catchment, the field measurements covered 3 different land-use and 2 different soil types and changes could therefore be made for a vast number of HRUs. Nevertheless the total area benefiting from parameter adjustment was limited. This might also be the reason why changes in the total catchment discharge were negligible. We would recommend to look into possible transfer function which could help to up-scale the limited field data to a larger area. Increasing uncertainty however, might be a problem of this approach and should be given close attention. For this reason the Wupperverband will enhance the soil moisture network to new land use and soil classes, which will give valuable in-situ data for a more complete model refinement (see 4.5 Outlook).

- Field data from soil moisture sensors only give very site specific and depth specific point data. In order to compare this data with model outputs from SWAT and TALSIM, we assumed an equal moisture distribution of this point data over the layer depths specified by the model (Figure 4.9). However, the integration of point soil moisture over the entire soil layer depth represented by the models, might not be adequate. Also, due to the necessary unit conversion from mm to volumetric moisture content, the layer depths is crucial for the final converted soil moisture estimate (in the case of SWAT). This is a large potential for miscalculations in the simulated soil moisture estimates. Therefore, the calibration goal was fitting the temporal as well as vertical soil moisture pattern, rather than matching the absolute values of soil moisture content. Hence we argue, that for evaluating the final model performance, not only volumetric error dependent efficiency criteria (e.g. RMSE, MAE) should be used, but more pattern dependent error functions (e.g. correlation coefficient, NSE, KGE etc.).

- Finally, we recommend that besides soil moisture measurements, field data of a second variable such as ET could be collected. This would enable a further evaluation of the physical correctness of the model and would allow a quantification of the model improvement, even if the previously taken evaluation variable (i.e. discharge) doesn't show any changes in model performance.

The final conclusions are given below:

Input data from the German Soil Service is considered to be similar and sufficient in comparison with soil assessment results, at least for grassland at this part of the study area. Thanks to the soil assessment, the field measurements, and the posterior model enhancement, a better understanding of the model processes regarding soil moisture storage was achieved.

New algorithms were not developed in the framework of BINGO; rather, a new calibration approach was implemented based on the optimization of two observed variables, namely discharge and soil moisture. Implementation of this approach proved to be satisfactory: by fitting soil moisture as an additional criteria, discharge showed a better fit in terms of total simulated hydrograph volume for the TALSIM model.

Field measurements proved to enable the achievement of better soil moisture simulations after using the data for a re-calibration. This improves the hydrological models especially with respect to their flood

forecasting skills, as soil moisture conditions are a dominating factor in controlling surface runoff. An improved forecast by the Wupperverband will benefit relevant stakeholders in the long-term.

Operational use of soil moisture field data is still under investigation. By correlating different indices such as API (Antecedent Precipitation Index), soil moisture, current water level, and precipitation forecast, it will be possible to improve online flood forecasting.

Outlook

On account of the good experience with the soil moisture measurements, Wupperverband will expand the soil moisture network with the installation of five more stations at the drainage area of Unterpilghausen hydrometric station, located at Kleine Dhünn River (inflow to GDT, see Figure 4.40).

For this new installation, different representative combinations between land use units and soil type will be achieved (see Figure 4.40 and Table **4.6**). The process of the exact location of the future five stations is currently carried out by the Wupperverband, considering property owners and adequate field conditions.

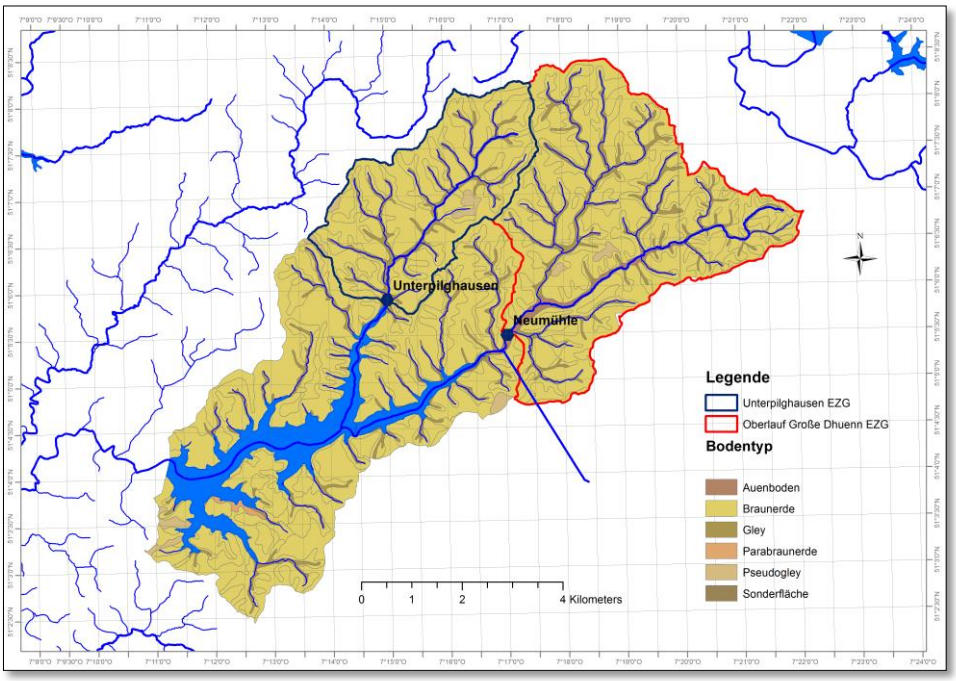

Figure 4.40. Soil moisture network expansion – Soil type

Table 4.6. Representative soil type and land use combination – network expansion

Combination	
Brown earth	Farmland
Brown earth	Grassland
Brown earth	Deciduous forest
Kolluvium	Farmland
Kolluvium	Grassland

Additionally, a new telemetry system is being developed by H. Bogena et al. (SoilNet - Jülich Research Centre), based on the narrowband IoT (NB-IoT) system (see Figure 4.41). With this new system, the coordinator unit will not be necessary anymore, which represents a significant advantage due to lack of

infrastructure at remote areas. Energy supply of the current coordinator unit is carried out via solar energy, causing some data gaps in winter time (around 21.12).

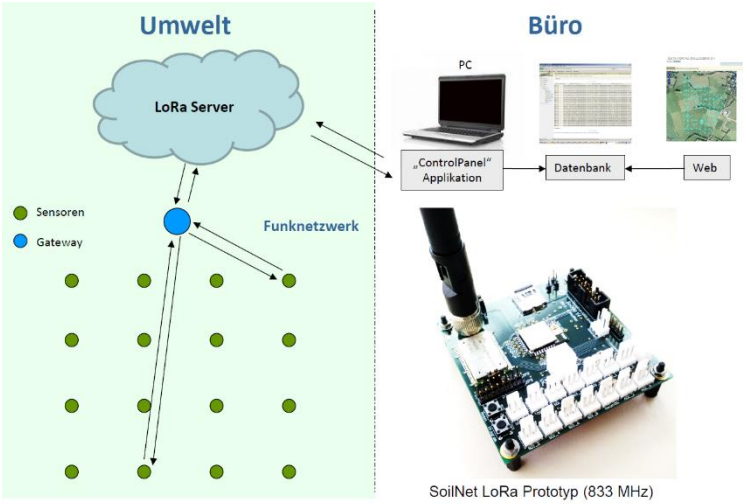

Figure 4.41. New telemetry system – LoRa server (source: Bogena et al., 2016)

In addition, TALSIM developers are adding a new module which enables the possibility of setting up a distributed model. In this manner, each grid cell represents a HRU, and the user has the possibility of defining a fine grid. Therefore, it will be possible to obtain simulated soil moisture output time series per HRU; this will diminish the current drawback of too coarse resulting soil moisture time series. The ultimate goal is to implement operational soil moisture measurements for “online” calibration (override initial states).

4.5. Bibliography

Bogena, H.R, Herbst, M., Huisman, J.A., Rosenbaum, U., Weuthen, A. and Vereecken, H., 2010. Potential of Wireless Sensor Networks for Measuring Soil Water Content Variability. Vadose Zone J. 9:1002–1013 doi:10.2136/vzj2009.0173 Received 30 Nov. 2009. Published online 7 Sept. 2010.

Bogena, H.R, Schilling, B., and Weuthen A., 2016: Das SoilNet Sensornetzwerk für die hydrologische Prozessforschung, Agrosphere Institute, IBG-3, Forschungszentrum Jülich, Germany. Pdf presentation

Decagon, 2016: MPS-2 & MPS-6 Dielectric Water Potential Sensors. Operator’s manual

Neitsch, S.L., Arnold, J.G., Kiniry, J.R., Williams, J.R., 2011: Soil and Water Assessment Tool. Theoretical Documentation. Version 2009. Texas Water Resources Institute Technical Report No. 406.

Rajib, M.A., Merwade, V., 2015. Improving soil moisture accounting and streamflow prediction in SWAT by incorporating a modified time-dependent SCS CN method: SWAT WITH MODIFIED CN METHOD, RAJIB AND MERWADE. Hydrological Processes n/a-n/a. https://doi.org/10.1002/hyp.10639

Rakovec, O., Kumar, R., Attinger, S., Samaniego, L., 2016. Improving the realism of hydrologic model functioning through multivariate parameter estimation: IMPROVING THE REALISM OF HYDROLOGIC MODEL FUNCTIONING. Water Resources Research 52, 7779–7792. https://doi.org/10.1002/2016WR019430

Sutanudjaja, E.H., van Beek, L.P.H., de Jong, S.M., van Geer, F.C., Bierkens, M.F.P., 2014. Calibrating a large-extent high-resolution coupled groundwater-land surface model using soil moisture and discharge data: CALIBRATING GROUNDWATER-LAND SURFACE MODEL. Water Resources Research 50, 687–705. https://doi.org/10.1002/2013WR013807

TALSIM, 2016: Theoretical principles

Truebner, 2016: SMT100 Soil Moisture Sensor & Temperature Meter. User's manual

5. The Netherlands

5.5. Introduction and objectives

The focus within the BINGO project for the Netherlands was on the groundwater of the Veluwe. The Veluwe is a moraine landscape mostly covered by natural vegetation and plantations of pine. It contains a large aquifer of fresh groundwater that is important for the drinking water supply. The amount of available groundwater is determined by the groundwater recharge. In the absence of surface water, this recharge is on average equal to the difference between precipitation and actual evapotranspiration. The actual evapotranspiration is more than half of the precipitation. It is, therefore, very important to have accurate values of the actual evapotranspiration for strategic and operational water management. To correctly assess the effects of the changes in climate and land use that are simulated in BINGO (D3.4) on the groundwater, a reliable simulation of the actual evapotranspiration is even more crucial.

It is, however, very difficult to find accurate measured values for evapotranspiration characteristics of natural vegetation and plantations. Several studies have documented values for different vegetation types (e.g. Schouwenaars 1993, Stuyfzand 1993, Tiktak and Bouten 1994, Spieksma et al. 1996, Moors et al. 1998, Gehrels 1999, Dolman et al. 2000, Elbers et al. 2010, Verhagen 2014, Voortman et al. 2015). However, most of these studies are based on limited field measurements and they are spread over many different conditions. To get an accurate estimate of the evapotranspiration at the Veluwe, six lysimeters were installed at the National Park the Hoge Veluwe in 2015 and 2016. The dominant vegetation of the lysimeters was heather, one of the dominating land use types at the Veluwe.

Within BINGO we have simulated the groundwater heads and evapotranspiration for the Veluwe with AZURE. The aim of the field work at the Veluwe was to evaluate the simulated evapotranspiration and if possible to improve these simulations. For heather, the evaluation was done with the measurements from the lysimeters. For the other land use types, the simulated evapotranspiration was compared with values found in the literature.

Besides the field work at the Veluwe itself, we also set up an experiment on the premises of KWR to measure transpiration and rainfall interception for trees. The most common tree species at the Veluwe were used in this experiment. Measurements at this site started in the summer of 2017 and will end in March 2019. Because of the later start of the experiment and the required time to gather the data, results from this experiment could not be used yet to evaluate the simulated evapotranspiration values from AZURE and adjust the model. The analysis of the data will be done in the coming months.

5.6. Methods

5.6.1. Study site description

The Veluwe research site (ca. 1 250 km^2) is located in the centre of the Netherlands and consists of ice-pushed moraine and fluvio-glacial complexes. It is an elevated sandy area, which contains a large aquifer of fresh groundwater. Most of the area is designated nature reserve and land use mainly consists of forests (predominantly pine), heather and drift-sand. Due to the expanse of the area and its large unsaturated zone, the groundwater system responds slowly to changes in meteorological conditions. Brooks and streams are found at the fringe of the sandy area, where water exfiltrates. Upward seepage also occurs in surrounding lower-lying agricultural areas. No large drainage systems or surface water

bodies exist in the central part of the area. A complete description of the site including historical information can be found in D3.1.

5.6.2. Field work

Field station Hoge Veluwe

Since 2015, six lysimeters (Figure 5.1) were installed at the national park the Hoge Veluwe (location: 52° 3'5.86"N, 5°49'27.42"O). Each lysimeter has different characteristics and dimensions (Table 5.1). Besides the lysimeters, a meteorological station was installed to measure all the relevant meteorological variables (Table 5.1and Figure 5.2). For the evaluation of the model results, measurements were used from April 2015 till July 2017. From the measurements, evapotranspiration values were derived using the AWAT filter (Peters et al. 2014).

Evapotranspiration measurements representative for the surrounding land use type were selected based on the measured surface temperature of the vegetation inside the lysimeters (Figure 5.2) and surface temperature of the vegetation in their surroundings. Measurements were excluded if the temperature difference was larger than 1°C during 2 hours or more while the sun was at an angle of 45 degrees or higher, because this indicates a measurement that is not representative for the surrounding vegetation.

Two different types of lysimeters were installed, free drainage and suction-controlled. In the suction-controlled lysimeter, the suction was set equal to observations from tensiometers, which were installed at the same depth as the bottom of each lysimeter. Since only representative measurements were selected for the parameterisation of the model, there were no differences between observed values from the different lysimeter types.

From the measurements, a crop factor for the transpiration and soil evaporation for the Makkink equation (Makkink 1957) was determined by comparing the measured evapotranspiration to the Makkink reference evapotranspiration on days without interception. The Makkink factor is described as a trapezoid with different values for the summer months and winter months, which are linearly interpolated.

Figure 5.1 Installation of one of the lysimeters at the Hoge Veluwe.

Figure 5.2 Overview of the field station (left) and infra-red sensors for surface temperature.

Table 5.1 Information about the field station at the Hoge Veluwe

Meta data	
Coordinates	52° 3'5.86"N, 5°49'27.42"O
Elevation	42.16 m NAP
Starting date measurements	20150430
Characteristics field site	Heather, dominated with Calluna, a bit of Erica
Soil type	Sand (40 cm organic dark soil, below yellow parent material)
Evaporation measurements	
Start date – End date	
20151218 -	lysimeter free drainage, 50 cm diameter, 50 cm deep
20160419 -	lysimeter free drainage, 50 cm diameter, 50 cm deep
20150430 -	lysimeter suction-controlled, 50 cm diameter, 30 cm deep
20160413 -	lysimeter suction-controlled, 50 cm diameter, 50 cm deep
20160413 -	lysimeter free drainage, 50 cm diameter, 50 cm deep
20160413 -	lysimeter suction-controlled, 50 cm diameter, 50 cm deep
20150507 - 20150915	eddy correlation
Other measurements	**Sensortype**
Air temperature	HMP155A
Rain	ARG100
Wind speed	A100LK
Wind direction	W200P-01
Humidity	HMP155A
In and outgoing shortwave radiation	CMA6
In and outgoing longwave radiation	NetPyrgeometer IRA01_T2
Net radiation	Nrlite2
Surface temperature	7 Apogee SI400
NDVI	7 Decagon SRS
Soil heat flux	2 HFP01SC
Soil moisture and pressure	2 CS616, 6 5TE, 6 MPS6
Soil temperature	2 TCAV

Experiment at KWR, Nieuwegein

An outdoor-experiment was set up on the premises of KWR, Nieuwegein, to measure transpiration and interception from trees. In total, 70 trees were planted in individual pots for measuring transpiration (all trees) and rainfall interception (10 trees). Our species selection consisted of the 10 most common deciduous and coniferous tree species growing on the Veluwe (see Figure 5.3). The actual trees were obtained from a commercial grower. At the moment of purchase the trees were between 3 and 10 years old.

Figure 5.3 Overview of the experiment at KWR with the individual trees in pots, the high resolution weighing balances, the water supply device and the meteorological station.

Out of the 70 trees, 60 trees were individually connected to a water supply device which was designed by KWR for this purpose. This device supplied the amount of water which the tree has used, thereby also measuring the inflow. This way, whole-tree transpiration could be measured on a daily basis. Rain entering the pot was minimized by a custom-made cover. Daily transpiration data were collected from May 2018 until October 2018. The remaining 10 trees were placed on high-resolution weighing balances. The weights were recorded in 1-min intervals. For these trees, both transpiration and rainfall interception were measured by monitoring weight decreases (transpiration) and weight increases (interception). Data were recorded from August 2017 until January 2019.

One of the 60 trees connected to a water supply device was additionally equipped with sensors to measure soil water conditions in the pot. The following sensors were installed at different positions in the pot: 2 tensiometers, 3 volumetric water content sensors, 5 temperature sensors. Data were collected on a datalogger in 5-min intervals. Data were recorded from August 2017 until January 2019.

On site, meteorological conditions were recorded by 2 meteorological stations measuring air temperature, air humidity, air pressure, wind speed, wind direction and solar radiation as well as 3 tipping buckets measuring precipitation. Data were collected on a datalogger in 5-min intervals and recorded from June 2017 until January 2019.

In addition to the measurements of transpiration and interception during occurring meteorological conditions, 30 out of 60 trees were subjected to a drought treatment in August/September 2018. The drought was implemented by closing the water supply of the pot for a period of 3 weeks. In those pots, the volumetric moisture content was monitored 3 times per day with a handheld device (HS2 with 20 cm rods, Campbell Scientific). On a subset, stomatal conductance was measured every second day with a SC-1 leaf porometer (Decagon).

To gather more information about the trees themselves and to gain more insight into the measured transpiration values, additional measurements were done. Leaf samples were collected from all 70 trees during July 2018 and October 2018 for later analysis of, for example, stomata properties and nutrient contents. All 70 trees will be harvested in February and March 2019 to determine aboveground biomasses and to measure wood traits.

5.6.3. Model description

For the Veluwe, the AZURE model (De Lange and Borren 2014) was used to simulate the impact of the climate, land use and water use changes on the water resources. The groundwater part of AZURE is based on MODFLOW (Harbaugh 2005) and it is coupled to MetaSWAP (van Walsum and Groenendijk 2008, van Walsum et al. 2010) for the simulation of the unsaturated zone. MetaSWAP simulates the actual evapotranspiration and groundwater recharge based on water availability, soil properties and land use. The model simulations were done on a 250 by 250 m resolution grid for the Veluwe area and surroundings, in total an area of about 6 500 km^2, and a temporal resolution of 1 day. A detailed description of the model can be found in D3.3.

The field data were used to evaluate the evapotranspiration values of the model. We will, therefore, describe the calculation of the evapotranspiration in the model in more detail. The potential evapotranspiration has been determined by multiplying the Makkink reference crop evapotranspiration (Makkink 1957) with land use specific crop factors. Land use types defined in the model that are important for the Veluwe are pine forest, broadleaf forest and dry nature. Different crop factors are used for transpiration, interception, soil evaporation and ponding. For most land use types, the factors for soil evaporation and ponding are equal to 1.0. Ponding will not be considered, because it almost never occurs at the Veluwe. Other important parameters that need to be defined are vegetation cover (-) and interception capacity (mm). The interception capacity is a fitted parameter and does not have a clear physical meaning. Most parameters are constant throughout the year, except for vegetation cover. The constant parameters are multiplied by the vegetation cover or (1-vegetation cover).

Table 5.2 Crop factors and interception capacity in AZURE

	Transpiration factor (-)	Interception factor (-)	Soil evaporation factor (-)	Interception capacity (mm)
Broadleaf forest	0.85	2.20	1.00	2.8
Pine forest	1.00	1.80	1.00	0.75
Dry nature	1.05	1.20	1.00	0.018-0.034

Actual evapotranspiration is derived from the potential evapotranspiration based on the water availability. Evaporation from interception is calculated with the interception model of Rutter et al. (1971). Soil evaporation is simulated with the model of Boesten and Stroosnijder (1986). This model assumes potential evaporation until the top layer of the soil has become too dry. The actual soil evaporation depends on potential soil evaporation, precipitation patterns and a soil parameter. This means that soil evaporation is determined independently from the unsaturated zone model in AZURE.

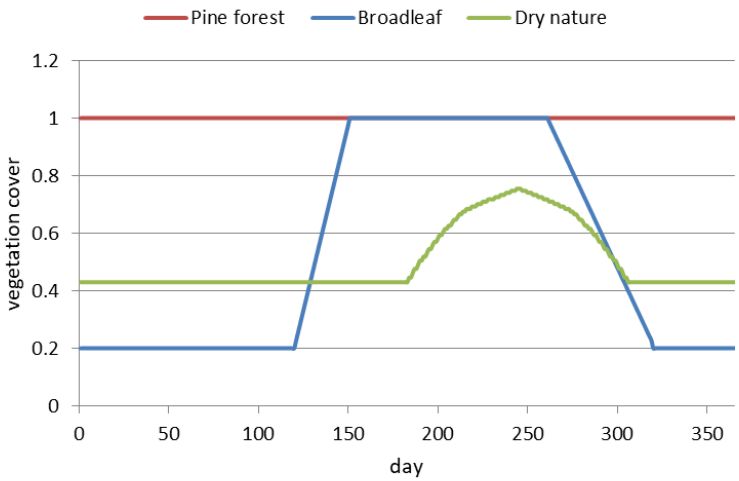

Figure 5.4 Characteristic curve in MetaSWAP of the vegetation cover over the year.

5.7. Results

5.7.1. Field work results

Field station Hoge Veluwe

Actual transpiration heather

The measurements from the lysimeters at the Hoge Veluwe station were used to derive actual evapotranspiration data for heather at the Veluwe (Figure 5.5and Figure 5.6). The average over all 6 lysimeters shows the annual variation in evapotranspiration with maximum values in summer of around 4 mm/d. There are clear differences between the individual lysimeters (Figure 5.6). The long term yearly evapotranspiration varies between 363 mm/y and 473 mm/y for the individual lysimeters, average yearly precipitation in this region is 867 mm/y. This was based on model calculations and measured evapotranspiration. The differences in evapotranspiration values could be caused by differences in vegetation and soil characteristics. The soils were homogenously distributed across the lysimeters, but the viability of the vegetation differed between the individual lysimeters. For example, vegetation in lysimeter 4 was low and this resulted in relatively low evapotranspiration values (**Figure 5.6**). Vegetation in lysimeters 5 and 6, on the other hand, had a denser cover and this resulted in higher values for the evapotranspiration. Large differences in measured evapotranspiration can already occur at the small scale of the lysimeters (50 cm); this should be taken into account when installing lysimeters in the field.

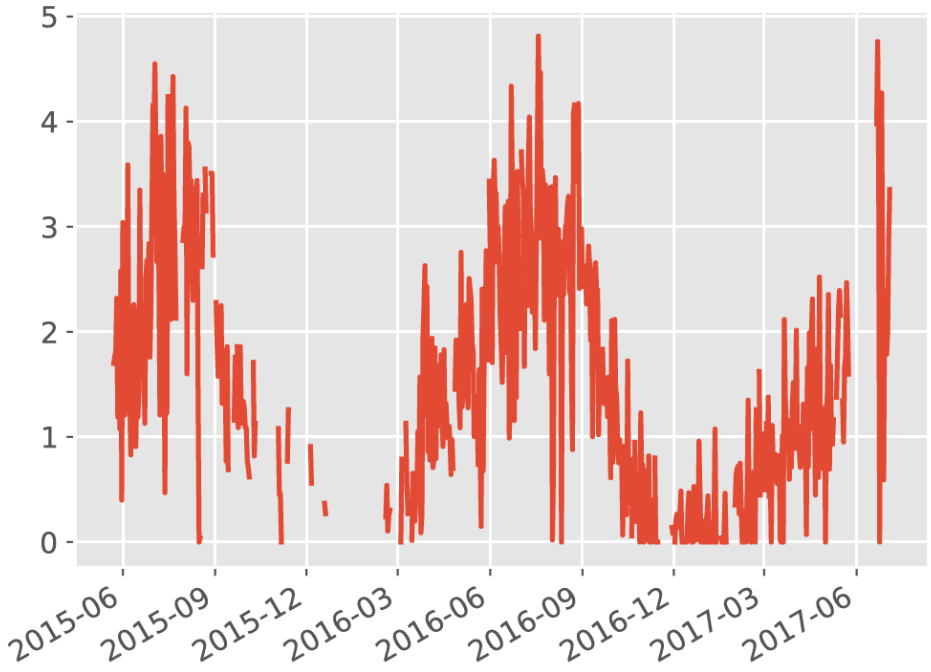

Figure 5.5 Measured evapotranspiration (mm/d) from heather (average over six lysimeters).

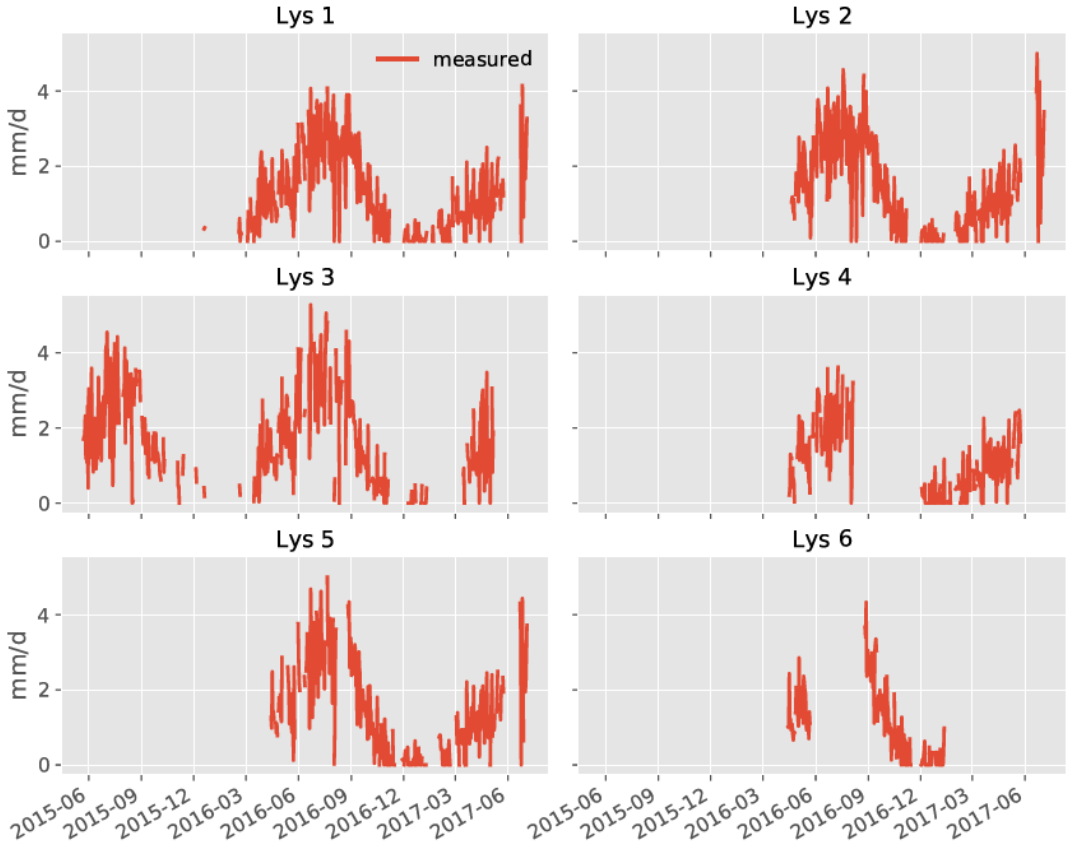

Figure 5.6 Measured evapotranspiration (mm/d) from each individual lysimeter.

Makkink crop factors

Based on the data from the 6 lysimeters, the relation between measured transpiration and soil evaporation and the Makkink reference evapotranspiration was determined (Figure 5.7). This relation is based on the measured evapotranspiration on days without rain and interception. From this relation it is clear that evapotranspiration reaches the maximum values rather late in the season (values becomes 1). The 75th percentile from the relation was used to fit a trapezoid for the combined Makkink crop factor for soil evaporation and transpiration (Figure 5.7).

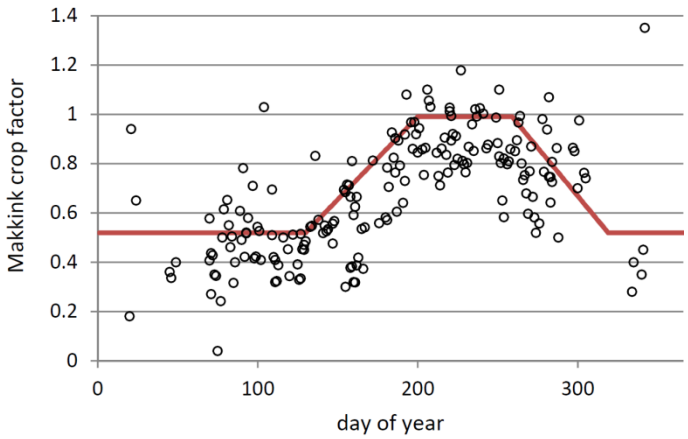

Figure 5.7 Fitted trapezoid on the relation between the measured soil evaporation and transpiration (on days without rain and interception and averaged from all lysimeters) and the Makkink reference evapotranspiration.

This trapezoid is divided into a crop factor for soil evaporation and transpiration, also including the vegetation cover, using expert judgment and a 1D hydrological model. In summer, this had led to a transpiration factor of 0.85 and a soil evaporation factor of 0.14. In winter, the values are 0.05 for the transpiration factor and 0.47 for the soil evaporation factor. The vegetation cover is derived from the soil evaporation factor (1-soil evaporation factor).

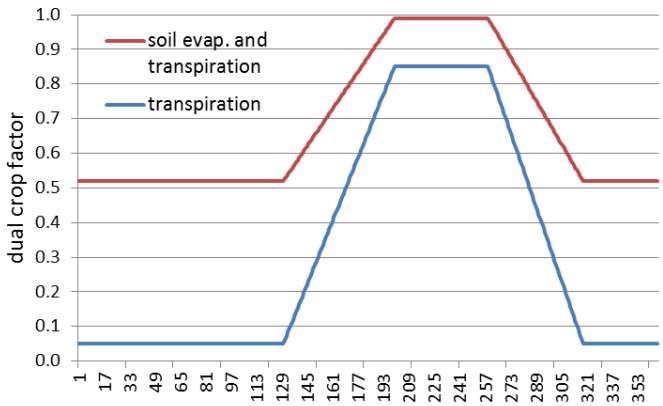

Figure 5.8 Division of total crop factor in soil evaporation and transpiration on each day of the year.

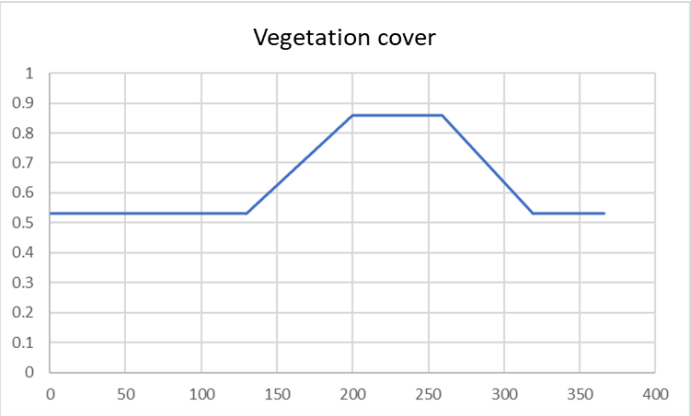

Figure 5.9 Vegetation cover of heather derived from the soil evaporation factor on each day of the year.

Experiment at KWR, Nieuwegein

As mentioned before, most data from this experiment have not been analyzed yet. Here, we will give a very short overview of the analyses that will be done and show some preliminary results.

Transpiration

The data of the whole-tree water use will be used to determine the effect of meteorological variables on daily tree transpiration. We will also analyze whether and how tree species differ in their maximum transpiration rates. Additionally, the explanatory value of plant traits regarding tree transpiration will be derived.

Preliminary results are depicted in Figure 5.10. The positive relationship between the diameter at breast height and tree water use was expected and shows that the water supply device gives reasonable data. It also shows that the trees are functioning well in the pots.

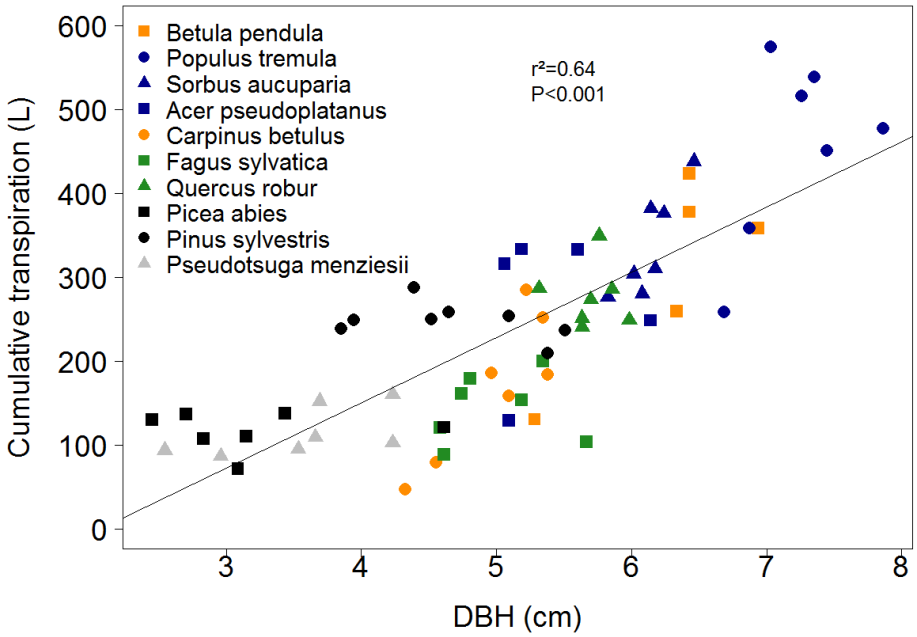

Figure 5.10 Relationship between cumulative transpiration (in L; time period = 24 days) and diameter at breast height (DBH; in cm). Each circle represents one tree (n=67).

Interception

The data files from the weighing balances and the meteorological data have been prepared for further analysis. From the information of the weighing balances and the meteorological data we will determine the effect of meteorological variables on tree transpiration and rainfall interception and the effect of tree traits on rainfall interception. Traits possibly relevant for interception are, for example, branch angles and branch lengths as well as crown depth and width.

Preliminary results for rainfall interception and transpiration for one of the trees are shown in Figure 5.11. At the moments when the tree was watered manually, a sharp increase in weight can be observed (upper figure, purple dots). The transpiration losses in the course of the day are reflected in a drop in the measured weight (upper figure). Rainfall events lead to an increase in the weight of the tree due to intercepted water. The interception by the tree is in good agreement with measured rainfall (lower figure).

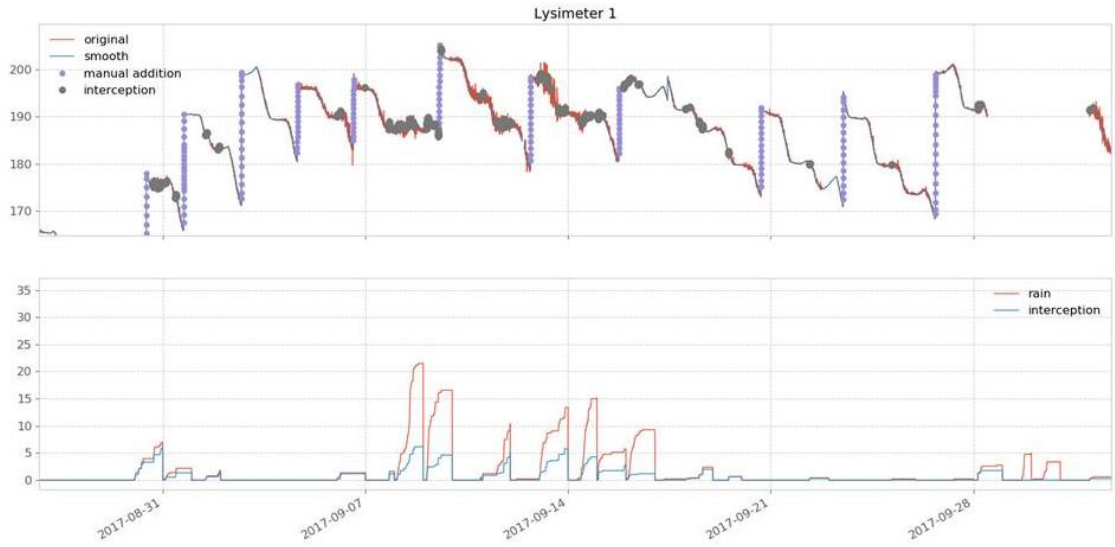

Figure 5.11 Changes in weight (in kg, top graph) and daily cumulative rainfall interception (in mm, lower graph) of one tree for a period of one month.

Drought treatment

From the data collected during the drought treatment, we will determine the relationship between soil water depletion and leaf responses. We will also analyze the differences in drought responses between species.

Preliminary results based on the raw data show that soil water is depleted within a week for the largest trees (that was expected), which also consumed the most water (*Populus tremula*), and that the response at the leaf level (stomatal conductance) differs between species. Visible drought stress (leaf yellowing) occurred within 2 weeks after the onset of the drought.

Leaf and stem traits

The leaf trait data have not been analyzed yet and stem traits will be determined in February/March 2019, when the trees are harvested. We will analyze the explanatory value of traits for tree transpiration.

5.7.2. Model results

Due to the long calculation times of the AZURE model, we only have evapotranspiration values for 2004 and 2005. In 2004 the precipitation was 924 mm and the potential Makkink reference evapotranspiration was 561 mm, in 2005 precipitation was 741 mm and potential Makkink reference evapotranspiration was 599 mm. The simulated actual evapotranspiration in AZURE was, averaged over the two years, 650 mm/y for pine forest, 617 mm/y for broadleaf forest and 494 mm/y for dry nature (Table 5.3).

The soil evaporation for bare ground was calculated directly with the Boesten Stroosnijder model, because soil evaporation is independent from the unsaturated soil model and thus AZURE. The yearly average of the soil evaporation of bare ground is 302 mm/y.

We will compare the simulated evapotranspiration values with values from literature and field measurements for the different land use types.

Table 5.3 Evaporation values from AZURE in mm/y. Interception is included as percentage of the precipitation.

2004. Precipitation: 924 mm, Makkink evapotranspiration 561 mm			
	Broadleaf forest	Pine forest	Dry nature
Interception evaporation	286 (30 %)	296 (32%)	108 (12%)
Transpiration	238	354	182
Soil evaporation	94	0	174
Ponding	0	0	1
Total evapotranspiration	618	650	465
Recharge	306	274	459
2005. Precipitation 741 mm, Makkink evapotranspiration 599 mm			
	Broadleaf forest	Pine forest	Dry nature
Interception evaporation	275 (37%)	323 (44%)	114 (15%)
Transpiration	226	326	203
Soil evaporation	115	0	205
Ponding	0	0	0
Total evapotranspiration	616	649	523
Recharge	125	92	218

Pine forest

The most representative measurements for pine forest at the Veluwe are done in Loobos, Kootwijk. Reported evapotranspiration values for this location are 630 mm/y (average for 1995-1998 (Dolman et al. 2000)) and 550 mm/y (average for 1997-2012 (Verhagen 2014)). These last estimates are done with eddy-correlation measurements without corrections and they underestimate the actual evapotranspiration. When the values are corrected for not closing the energy balance, estimated actual evapotranspiration is 602 mm/y (Voortman et al., 2019). For 2004 and 2005 the estimated values were 673 and 638 mm/y. These values are close to the simulated values with AZURE (difference of -23 mm/y and 11 mm/y). Other measurements for pine forest were done in Castricum (Stuyfzand 1993). The average evapotranspiration measured at this location was 679 mm/y for 1957-1981. This is about 30 mm/y higher than the simulated values from AZURE. This means that evapotranspiration for the pine forest at the Veluwe was well simulated in AZURE.

Broadleaf forest

For the evapotranspiration of broadleaf forest in the Netherlands only a few measurements are available and especially long-term measurements are missing. Evapotranspiration in Castricum was estimated as 517 mm/y for oak trees (Stuyfzand 1993). Other reported values are 558 mm/y for beech trees and 555 mm/y for mixed deciduous forest (Dolman et al. 2000). All these values are lower than the simulated evapotranspiration from AZURE (617 mm/y). It is, however, difficult to make a direct comparison, because measurements were done in a different period.

Dry nature

Dry nature consists of heather areas, grassy heather areas (dominated by purple moor grass, *Molinia caerulea*) and areas with low grassy vegetation and moss. The simulated evapotranspiration values from AZURE (465 mm/y and 523 mm/y) show a good consistency with values for heather from other models (Voortman et al. 2019). For the purple moor grass, some estimates are available in literature ((Schouwenaars 1993, Jansen 1995, Moors et al. 1998), but these studies were based on measurements in areas with shallow groundwater levels. Measurements in an area with deeper groundwater levels (around 20 m below surface level) were done by Gehrels (1999). From these measurements, the actual evapotranspiration was determined for 1994 as 434 mm/y. This value is almost equal to simulated values for heather by Voortman et al. (2019). Evapotranspiration values for purple moor grass and heather thus seem to be very similar and are close to the dry nature values from AZURE.

Although the total actual evapotranspiration values for dry nature in AZURE are similar to measured values for heather and purple moor grass, the division between the different evapotranspiration terms (soil evapotranspiration, transpiration, interception) was different from the expected division based on the field measurements at the Veluwe. The soil evaporation in AZURE was equal to the transpiration, on average 171 mm/y, whereas values derived from the field measurements were about half of the evapotranspiration. Compared to evaporation from bare ground (200-250 mm/y (Stuyfzand 1993, Voortman et al. 2015)) the soil evaporation values from AZURE seem to be an overestimation.

Measured evapotranspiration from areas with low grassy vegetation and moss is about 180-330 mm/y (Voortman et al. 2015, Voortman et al. 2017). In AZURE the evapotranspiration of this type of vegetation is overestimated with 100-250 mm/y.

Based on the comparison with literature values and the measurements, an extra land use type ‘heather’ was added to AZURE. For the parameterisation of the evapotranspiration from heather the Makkink crop factors based on the field measurements were used. Interception parameters were also changed for heather. This resulted in evapotranspiration values around 430 mm/y. The evapotranspiration from dry nature was adjusted in AZURE by lowering the soil evaporation. The potential soil evaporation is now determined by 0.5*Makkink factor. Average yearly soil evaporation for dry nature decreased from 171 mm/y to 104 mm/y after this adjustment.

Bare ground

Evaporation from bare ground was estimated from measurements for a loose sandy soil as 201 mm/y (Stuyfzand 1993) and for a stable sandy soil in the dunes as 258 mm/y (Voortman et al. 2015). In AZURE the simulated evaporation from bare ground was higher (302 mm/y). Therefore, the potential soil

evaporation was lowered by 50% in AZURE. Without further calibration the evaporation from bare ground became 190 mm/y after this adjustment.

Summary

The simulated evapotranspiration values from AZURE were compared with values from literature and the field measurements. For most land use types, AZURE overestimated the evapotranspiration. Based on this comparison, a land use type was added for heather and evapotranspiration factors for heather, dry nature and bare ground were changed in the model.

Table 5.4 Summary of comparison between simulated AZURE evapotranspiration and values from literature and measurements. Positive values mean an overestimation by AZURE, negative values an underestimation by AZURE

Land use type	Difference between AZURE and literature
Pine forest	-23-11 mm/y
Broadleaf forest	36-58 mm/y
Heather (before changes in model)	5-33 mm/y
Low grassy vegetation and moss	100-250 mm/y
Bare ground	100 mm/y

5.8. Discussion

Based on the field measurements in the national park Hoge Veluwe and values from literature, the evapotranspiration part of AZURE has been adjusted. A land use type for heather was added and the overestimation of soil evaporation in AZURE has been corrected. This led to more accurate simulations of the actual evapotranspiration across the Veluwe. Within BINGO a historical analysis of the effect of land use changes on the groundwater levels at the Veluwe was done. The land use type heather is important for this analysis. Historically, heather was the dominant land use type at the Veluwe, implying that measurements of the evapotranspiration of heather are crucial.

Besides insight into the actual evapotranspiration values of heather, the measurements also provided information about the division between the different evapotranspiration components (soil evaporation, transpiration, interception).

The accurate simulation of the evapotranspiration is very important for the Veluwe, because it has a large influence on the groundwater recharge. The groundwater reservoir at the Veluwe is important for the drinking water supply of the Netherlands, but nature at the Veluwe also depends on the groundwater of the Veluwe. To adequately assess the risks of climate change and potential adaptation measures, the simulated evapotranspiration therefore plays an important role. For example, one of the potential measures at the Veluwe is land use change; the effect of this measure depends on the simulated actual evapotranspiration.

Not only the differences in average yearly evapotranspiration between vegetation types are important to assess the effects of land use and climate change, but the yearly variation should also be taken into account. For heather, Voortman et al. (2019) showed that in dry years reduction of the actual transpiration occurs, leading to a lower total actual evapotranspiration. This has consequences for the groundwater recharge. When precipitation mainly occurs in winter, recharge in areas with heather will remain relatively

constant even for years with dry summers, because transpiration decreases. Trees, however, are less affected in dry summers due to their rooting depth. A change from heather to more trees, therefore, means transpiration reduction will occur less frequently in dry summers, leading to higher actual transpiration values and less recharge. In the dry summer of 2018, for example, trees at the Veluwe did not show much water stress, whereas heather areas suffered from the conditions. The consequences of more extreme conditions for the groundwater recharge are thus dependant on the land use type and accurate estimates of evapotranspiration from model results are important.

5.9. Bibliography

Boesten, J. J. T. I. and L. Stroosnijder (1986). "Simple model for daily evaporation from fallow tilled soil under spring conditions in a temperate climate." Netherlands Journal of Agricultural Science **34**: 75-90.

De Lange, W. and W. Borren (2014). Grondwatermodel AZURE versie 1.0. Actueel instrumentarium voor de Zuiderzee Regio, Deltares.

Dolman, H., E. Moors, J. Elbers, W. Snijders and P. Hamaker (2000). Het waterverbruik van bossen in Nederland. Wageningen, Alterra.

Elbers, J., E. J. Moors and C. Jacobs (2010). Gemeten actuele verdamping voor twaalf locaties in Nederland, Stowa.

Gehrels, H. (1999). Groundwater level fluctuations, Separation of natural from anthropogenic influences and determination of groundwater recharge in the Veluwe area, The Netherlands, Free University of Amsterdam.

Harbaugh, A. W. (2005). MODFLOW-2005, the U.S. Geological Survey modular ground-water model -- the Ground-Water Flow Process. U.S. Geological Survey Techniques and Methods 6-A16.

Jansen, P. C. (1995). "Verdamping van korte vegetaties in natte natuurgebieden." H2O : tijdschrift voor watervoorziening en afvalwaterbehandeling **28**(15): 467-471.

Makkink, G. F. (1957). "Testing the Penman formula by means of lysimeters." J. Inst. of Water Eng. **11**: 277-288.

Moors, E. J., J. N. M. Stricker and G. D. van den Abeele (1998). Evapotranspiration of cut over bog covered by Molinia caerulea. Afd. Waterhuishouding, Wageningen Univ. **73**.

Peters, A., T. Nehls, H. Schonsky and G. Wessolek (2014). "Separating precipitation and evapotranspiration from noise - a new filter routine for high-resolution lysimeter data." Hydrol. Earth Syst. Sci. **18**(3): 1189-1198.

Rutter, A. J., K. A. Kershaw, P. C. Robins and A. J. Morton (1971). "A predictive model of rainfall interception in forests, 1. Derivation of the model from observations in a plantation of Corsican pine." Agricultural Meteorology **9**: 367-384.

Schouwenaars, J. M. (1993). "Verdamping van pijpestrootje (Molinia caerulea) en veenmos (Sphagnum papillosum) in hoogveengebieden en haar betekenis voor het waterbeheer." H2O **26**: 375-382.

Spieksma, J. F. M., A. J. Dolman and J. M. Schouwenaars (1996). De parametrisatie van de verdamping van natuurterreinen in hydrologische modellen, RU Groningen [etc.].

Stuyfzand, P. J. (1993). Hydrochemistry and hydrology of the coastal dune area of the Western Netherlands. PhD PhD, Vrije Universiteit Amsterdam.

Tiktak, A. and W. Bouten (1994). "Soil water dynamics and long-term water balances of a Douglas fir stand in the Netherlands." Journal of Hydrology **156**(1): 265-283.

van Walsum, P. E. V. and P. Groenendijk (2008). "Quasi steady-state simulation of the unsaturated zone in groundwater modeling of lowland regions." Vadose Zone Journal **7**(2): 769-781.

van Walsum, P. E. V., A. A. Veldhuizen and P. Groenendijk (2010). SIMGRO 7.1. 0, Theory and model implementation. Wageningen, Alterra. **913**.

Verhagen, F., Spek, T., Witte, J.P.M., Voortman, B.R., Moors, E.J., Querner, E., Eertwegh, G., Bakel, J. (2014). "Expertdialoog de Veluwe: Begrijpen we het watersysteem? ." Stromingen **20**: 49-64.

Voortman, B. R., R. P. Bartholomeus, S. E. A. T. M. van der Zee, M. F. P. Bierkens and J. P. M. Witte (2015). "Quantifying energy and water fluxes in dry dune ecosystems of the Netherlands." Hydrol. Earth Syst. Sci. **19**(9): 3787-3805.

Voortman, B. R., Y. Fujita, R. P. Bartholomeus, C. J. S. Aggenbach and J. P. M. Witte (2017). "How the evaporation of dry dune grasslands evolves during the concerted succession of soil and vegetation." Ecohydrology **10**(4): e1848-n/a.

Voortman, B. R., M. H. J. van Huijgevoort and J.-P. M. Witte (2019). Verdamping van natuurterreinen berekend met AZURE. De parametrisatie van heide op basis van lysimetermetingen en een vergelijking met literatuurcijfers. KWR2019.015. Nieuwegein.

6. Norway

Model frameworks

The BINGO modelling objectives in Norway have been twofold, dealing with 1) urban drainage and 2) drinking water supply (BINGO D3.1) systems in Bergen city. With respect to these objectives, a SWMM (Storm Water Management Model) model has been set up for the urban drainage system at the Damsgård research site, and an existing excel-based model framework has been used for hydrological inflow and surface reservoir balance. (see BINGO D3.1-D3.4 for detailed description of study sites, objectives, models and model results). The existing model framework adopted for water supply assessment did not comprise any model development task; consequently, no fieldwork has been envisaged. All efforts to conduct field measurements concentrated on the urban drainage system and were conducted by re-using equipment from previous projects. A summary of the performed fieldwork is presented in the following sections.

6.5. Introduction and objectives [Urban drainage]

A SWMM model has been set up for the urban drainage system in Damsgaard, Bergen. Over the past few decades, SWMM has been successfully applied for planning, designing and analyzing urban drainage systems (Rossman, 2015). Like most mathematical modelling exercises, calibration and validation of SWMM model (both event-based or a continuous) are carried out using manual or automated techniques. The SWMM model set up for the Damsgaard area comprises of two main components, which can be run separately. These are: 1) a runoff component: for establishing precipitation-runoff relationship on subcatchment scale, and 2) a routing component: for transporting the runoff through the hydraulic network. This two-step model execution was important to circumvent the computational constraints a continuous high-temporal-resolution simulation of the system posed (see BINGO D3.4 and D3.6 for details). In order to calibrate this model, flow records from an existing database was used. The database was created during flow monitoring campaigns the municipality conducted in the period 2001 – 2008 using an area-velocity flow meter (Triton, ADS). As outlined in D3.3, further field measurements were contemplated in order to overcome the challenging data scarcity posed. Accordingly, two activities for collecting field data has been conducted during the time-frame of BINGO:

1) collection of rainfall data from a network of temporary rain gauges distributed within the Damsgård area for better understanding of topographic influence on precipitation patterns.
2) collection of stormwater flow data for verifying model results to increase reliability of the model simulations

6.6. Methods

6.6.1. Study site description

The Damsgård area is located at the foot of Mount Løvstakken close to the city center and is characterized by its steep slopes. A combined sewer system handles the stormwater runoff generated in the urban area and the less developed area on top of the mountain. Please refer to BINGO D3.1 for further details. CSOs are present in the downstream parts of the system, discharging mixed stormwater and sewage to the subjacent fjord, Puddefjorden during heavy rains.

6.6.2. Field work

The rainfall measurements were collected using a network of six portable rain gauges, distributed within the urban drainage study area. The rain gauges are equipped with tipping buckets of 0.2 mm resolution. Sub-zero temperatures are damaging to the batteries of the rain gauges; hence, they were not operable during the winter seasons. The measurement periods lasted from May to October/November of 2016 and 2017. The rain gauges were placed following the wind direction over the mountainous area of Damsgaard. A south-west wind direction causes an orographic lift over the Bergen mountains and is decisive for the precipitation in Bergen city. In addition, some gauges were distributed in the north-easterly direction to cover a bigger area of the study cite.

Stormwater flow measurements were collected using and ADS Triton+® flow meter. The flow meter was installed in a stormwater pipe in the upper parts of urban area, which is close to an inlet where the runoff from one of the headwater subcatchments on the mountainous enters the stormwater system. The distance to temporary rain gauges (described below) was also considered when selecting the location of the stormwater pipe in order to be able to capture the orographic effects and large local variations in precipitation amounts observed in Bergen.

The rain gauges and flow meter used were instruments re-used from previous projects.

Figure 6.1 Map showing the locations of the main weather station in Bergen (Florida), the temporary rain gauges (Irene, Gyldenpris, Frelsesarmeen, Terreng 1, Terreng 2, Terreng 3) and the flow meter.

6.6.3. Model description

The urban drainage model set up for the Damsgård area is a SWMM model comprising a hydrological routine for surface water coupled with a hydraulic model of the combined sewer system in the area. It is calibrated using the aforementioned campaign measurements and a parameter regionalization technique (see BINGO D3.3 and Mittet (2016) for details).

6.7. Results

6.7.1. Field work results

Rain gauges:

An analysis of the collected rainfall data is performed. The analysis takes the spatial dependencies between the temporary rain gauges into account and compares them with those of the main official weather station, Florida, in Bergen. Results of the analyses are presented in a student's project attached in Appendix I to this report (Kleiven 2016). Due to large local variations in precipitation amounts in Bergen, caused by aforementioned orographic effects, the main objectives of the analyses were to investigate the spatial precipitation patterns at the Damsgaard area and to determine whether or not the official weather station Florida could be a predictor for local precipitation at the Damsgaard area. The investigation was based on extreme precipitation (90^{th} percentile) and comprised of: 1) Difference between daily, hour and minute precipitation; 2) Correlation between the stations; 3) Difference in precipitation amounts; 4) Relationship between Florida and the other stations; 5) Validation, 6) Data quality evaluation (Appendix I). The main results are:

1) Strong correlation between stations for daily data and weaker correlations for smaller durations indicating a temporal shift (due to wind direction and topography) of rain events.
2) Gauges located close to each other show the best event correlation. For some stations this logical, for others not. Terreng 3 is located on the other side of the mountain than the rest, and should, theoretically not have the same correlation to the other stations than the other stations have to each other. This indicate a 'spill-over' effect of the mountains (also supported by literature: Jonassen et al. 2013)
3) In terms of cumulative precipitation, short distance to the Florida station does not imply strong correlation. This can be seen in Figure 6.2, where e.g. Gyldenpris (which is closest to Florida in linear distance) has the second weakest correlation to Florida. This is likely caused by the gages' location relative to mountains (e.g. located by the foot of mountain or in the shadow of a mountain).
4) The relationship between Florida and the temporary gauges during rain events of different durations and magnitudes were investigated to determine whether or not observations at Florida could be a predictor for local precipitation at Damsgaard. Based on the collected data, a linear relationship between the main weather station Florida and the temporary stations could not be found (Figure 6.3).

Details of the methods and more results are found in Kleiven 2016 (Appendix I).

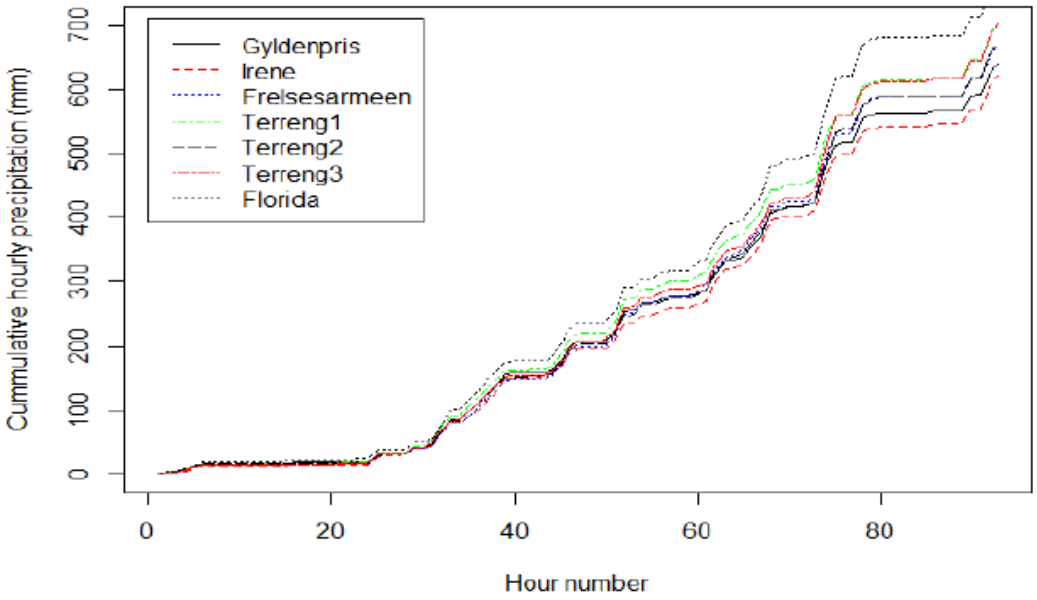

Figure 6.2 Re-print from Appendix X): Daily cumulative mass plot for all the investigated rain gauges.

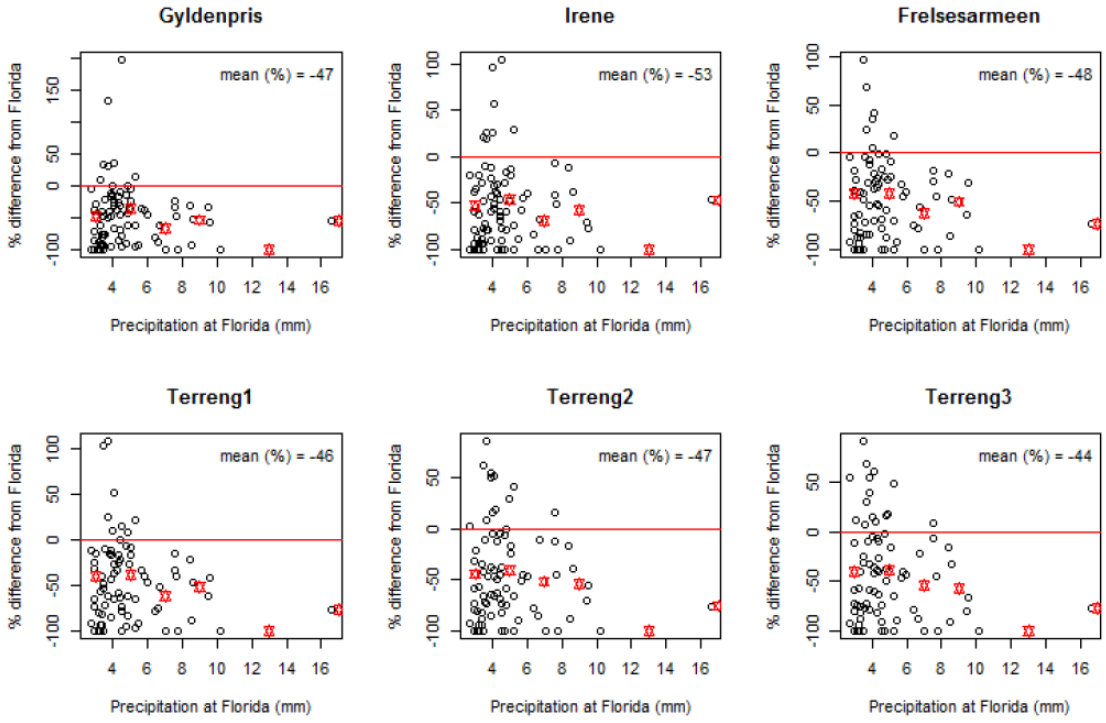

Figure 6.3 (Re-print from Appendix X): Percentage difference from Florida (hourly data), showing the mean for all the extreme precipitation, and the mean for different intervals (red dots).

Flow meter:

On the other hand, even though the flow meter was successfully installed at the selected site, it has not contributed towards the intended outcome. Retrieving the records was the main challenge encountered. The plan during installation of the device was to retrieve the flow records remotely. Either incapability of

the equipment or issue of compatibility with the Norwegian telecommunication networks hampered the fruition of the plan. Thus, no usable measurements have, at the present time, been obtained and analyzed.

6.7.2. Model results

The field data collection in the Bergen case came about as a result of discussion during the early project phase and was not planned in the project proposal. The field data collection was a result of opportunities based on equipment form previous projects among the partners. Analysis of the precipitation records from the rain gauges added provided valuable information and insight into the local rainfall distribution in the area. In addition to the above described utilization, it provided students with a thorough grounding in hydrology through complementary student research projects. The flow data series could not be utilized for the above described circumstances.

6.8. Discussion

The collection of spatially distributed precipitation data resulted in a better understanding of how the rainfall distributes over the study site. Potentially, the spatial relationships between stations could be used to improve projections of future climate over the study site through e.g. statistical methods. This would, however, require longer observational series in order to establish such relationships. Installation of more permanent gauges, that also could be operable during the winter season, would be beneficial in order to achieve this.

The field work covering flow measurements did not result in an updated model. However, it is not unlikely that the data could eventually be accessed. The municipality would then be equipped with observations of stormwater amounts generated in the mountainous parts of the study site due to the flow meter's location. This could be valuable when designing climate adaptation measures, as the municipality is considering measures to reduce the amount of stormwater runoff from mountainous areas to enter the combined sewer system in the lower parts of the site.

6.9. Bibliography

Jonassen, M.O.; Ólafsson, H.; Valved, A.S.; Reuder, J.; Olseth, J.A. Simulations of the Bergen orographic wind shelter. **2013**, *1*, 1–17. DOI: 10.3402/tellusa.v65i0.19206.

Kleiven, Guro Heimstad. "Statistical Downscaling of Global Climate Models for Use in Stormwater Management in Bergen". Student specialization project, NTNU, Trondheim, Norway, 2016. (Appendix I)

Mittet, J. A regionalisation technique for urban ungauged catchments. Master Thesis, Department of Civil and Environmental Engineering, NTNU, 2017.

Rossman, L. Storm Water Management Model Reference Manual Volume I – Hydrology, EPA/600/R-15/162 www2.epa.gov/water-research, 2015.

7. Portugal

Model frameworks

The Portuguese contribution to the BINGO objectives of testing different systems' vulnerabilities to climate change is fourfold:

1. Anticipate climate change impacts in the Tagus estuary bordering lands where expected sea level rise associated with more frequent storm surges and salt water intrusion are the driving forces;

2. Determine how potential reduction in aquifers recharge and, in coastal lowland areas, possible saltwater intrusion, may reduce the availability of groundwater for agricultural uses and water supply;

3. Estimate how vulnerable communities will become to increases in flood frequency and magnitude in urban areas;

4. Assess how the potential changes in surface water flow regimes will jeopardize the current and future water use.

The field work described in this chapter was carried out in the Tagus estuary and contributes to the first objective mentioned above.

7.5. Introduction and objectives [Tagus estuary]

Two main problems in the Tagus estuary are tackled in BINGO concerning the Lezíria Grande Public Irrigation Perimeter (Lezíria Grande PIP, Figure 7.1): i) the inundation of rich agricultural lands by the combined action of tides and storm surges; and ii) the salt water intrusion in the upper reaches of the estuary where a major water intake for irrigation is located. For each of these two problems, we aimed to implement, calibrate and validate appropriate process based-models (see D3.3) and to use those models to evaluate future scenarios (see D3.4). However, in the upper Tagus estuary, where the BINGO project is focused, the available data regarding water levels and salinity are scarce. Thus, the field work performed aimed to verify the model results and to improve the understanding of the modelled processes.

The field work included:

- the maintenance of two monitoring stations located along the estuary – Station 1 located in the Parque das Nações Marina and Station 2 located in Alcântara (Figure 7.1) – these data helped to validate the model results regarding water levels and salinity and to improve the understanding of the salinity dynamics, in particular in the medium-upper estuary (see Figure 1 for the location of the Tagus estuary in light blue and of the Lezíria Grande PIP in grey);
- one field campaign performed in November 2017, after a long dry period; these data helped to understand the salinity dynamics in the upper estuary.

The equipment of the two online monitoring stations and their installation in the Tagus estuary was supported by other research projects (Rodrigues et al., 2014; Rodrigues et al., 2017). The maintenance of these stations was partly supported by BINGO. During the project a malfunction and damage of the equipment of the Parque das Nações station occurred and the equipment was replaced. The new equipment was funded by BINGO.

Figure 7.1 The Tagus River and estuary (in light blue) and the Lezíria Grande Public Irrigation Perimeter (in grey). Locations of the online monitoring stations St1 and St2 (medium-upper estuary),the Cascais station and the Almourol flow monitoring station.

7.6. Methods

7.6.1. Study site description

The Tagus estuary is one of Europe's largest estuaries, with a surface area of about 320 km^2. The estuary has a deep, long and narrow tidal inlet connecting the Atlantic Ocean to a shallow, tide-dominated basin. About 40 km upstream, the estuary markedly narrows at the bay head. In this area, the estuary is bordered by low elevation terrains extensively used for agriculture and often protected by dykes. A detailed description of this estuary and its margins is presented in a previous report (see D3.1).

7.6.2. Field work

The Parque das Nações monitoring station (station 1) is located in the Tagus estuary in the Parque das Nações Marina (38º45'15.27'' N, 9º05'34.17'' W; Figure 7.1). This monitoring station is equipped with a SEBA MPS D3 multiparameter probe, which measures water pressure, conductivity and water temperature, and a SEBA Slimcom2 data logger, for data acquisition and transmission (Figure 7.2). Water elevations and salinity can be evaluated from the water pressure and conductivity, respectively. Salinity is given in Pratical Salinity Units (PSU), which is a unit based on the properties of sea water conductivity.

The probe and the data logger are supported and protected by a PVC tube, which is located near the gates of the marina (Figure 7.2).

This station is in operation since January 14, 2016. Data are measured continuously at the monitoring station with 10 minutes intervals, transmitted once a day to LNEC and stored in databases (Rodrigues et al., 2017).

During the period to which this report refers, maintenance procedures were undertaken to guarantee the safety of the equipment, the acquisition of the data and their quality. Damage to the data logger, which required factory repairing, prevented the acquisition of data between July 2016 and December 2016. Moreover, abnormal water temperature values were observed from April 2016 onwards, which remained even after the calibration of the sensor. The probe was reinstalled in January 2017 and measured water pressure until June 2017. After this date, a malfunction and damage of the probe was confirmed. A new probe was acquired and installed in February 2019, which is currently in operation.

In the scope of an agreement between the private company SenZ2 and LNEC, a sensor to measure water levels was also installed in the Parque das Nações (Figure 7.3). This sensor was installed in August 2017 and is currently operational, measuring water levels with 5 minutes intervals. This sensor measures the distance between the sensor and the water surface. During low tide of high spring tides, the location below the sensor dries out, and the sensor measures the distance to the bottom, rather than to the water surface.

Figure 7.2 General overview of the Parque das Nações station and SEBA MPS D3 multiparameter probe with SEBA Slimcom2 data logger.

Figure 7.3 General overview of the sensor SenZ2 installed in the Parque das Nações Marina.

The Alcântara monitoring station (station 2) is located in the Tagus estuary at the Alcântara pier (38°41'52.7"N; 9°10'31.7"W; Figure 7.1. This monitoring station is equipped with S::CAN probes, including a conductivity meter (Condu::lyser S::CAN) which data (conductivity, temperature, salinity) was analysed in

BINGO and a Con::cube S::CAN data logger. The probes are supported and protected by a structure suspended from the pier (Figure 7.4).

This station is in operation since October 2013, although it was reinstalled several times due to damage of the equipment or of the supporting structures. Data are measured continuously at the monitoring station with 2 to 5 minutes intervals, transmitted to LNEC and stored in databases (Rodrigues et al., 2014).

During the period to which this report refers, maintenance procedures were undertaken to guarantee the safety of the equipment, the acquisition of the data and their quality. The station was reinstalled in April 2016 and was in operation until November 2017, although with some flaws in the data acquisition. Due to large damage to the shelter that protects some of the equipment, the station was totally dismantled in December 2017. The Alcântara on-line monitoring station was then reinstalled in August 2018 and is in operation since then.

Figure 7.4 General overview of the Alcântara station and supporting structure of the probes.

In order to understand the salinity dynamics in the upper estuary during a drought situation, salinity and water level were measured in two locations, Vila Franca de Xira and Carregado, in November 2017 after a long dry period (Figure 7.5). The salinity was measured with a conductivity and temperature meter (YSI Professional Plus) and the water level with a gauge pole (Figure 7.6). The data was acquired with 10 minutes frequency during 3.5 hours (November 13, 2017) and 3 hours (November 15, 2017) to cover the peak of salinity. Tidal range in Lisbon was 2.07 m and 2.35 m, respectively.

Figure 7.5. Location of the salinity monitoring points in the upper Tagus estuary.

Figure 7.6. Overview of the salinity and level data acquisition in Vila Franca de Xira station.

7.6.3. Model description

The dynamics of the Tagus estuary were simulated with the community model SCHISM (Zhang et al., 2016). In order to properly represent all the relevant physical processes, the model domain includes the whole estuary, from the river to the ocean. The simulation of tides, surges and waves further requires regional models covering large parts of the Atlantic Ocean. SCHISM is forced by surface water elevations at the ocean boundary and river flow at the river boundaries. For the simulation of the storm events, the model is run in 2D and wind and atmospheric pressure are imposed at the water surface. Depth-averaged velocities and waves are also imposed at the ocean boundary. For the salinity intrusion simulations, the

model is run in 3D baroclinic mode and the atmospheric forcing is imposed at the surface. See D3.3 and D3.4 for further details.

7.7. Results

7.7.1. Field work results

Water levels and salinity data acquired at the Parque das Nações station between January 2016 and February 2019 are presented below (Figure 7.7, Figure 7.8, Figure 7.9 and Figure 10).

In general, the water levels obtained with the two sensors are very similar, as they are located a few tens of meters apart. The major difference is the lack of data during low spring tide at the distance sensor, due to the drying of the estuary below the sensor. This similitude allows us to use the distance sensor when the pressure sensor fails.

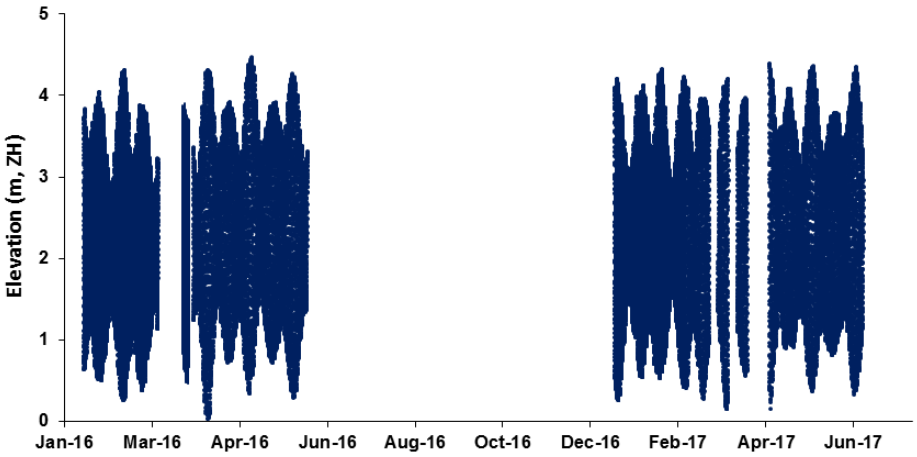

Figure 7.7 Water levels observed at the Parque das Nações pressure sensor between January 2016 and June 2017.

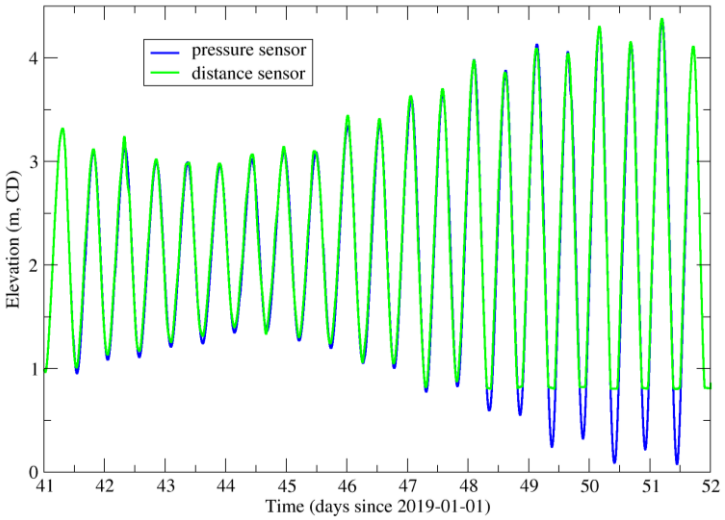

Figure 7.8. Comparison between water levels obtained with the pressure sensor and the distance sensor at the Parque das Nações station during February 2019.

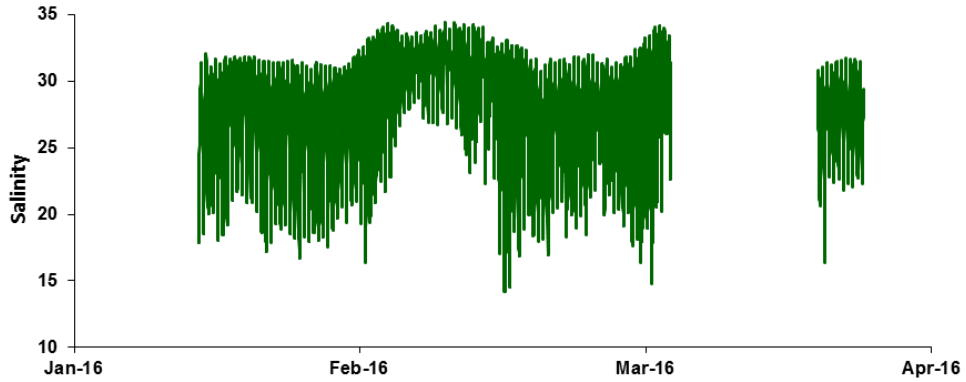

Figure 7.9. Salinity (psu) observed at the Parque das Nações station between January 2016 and March 2016.

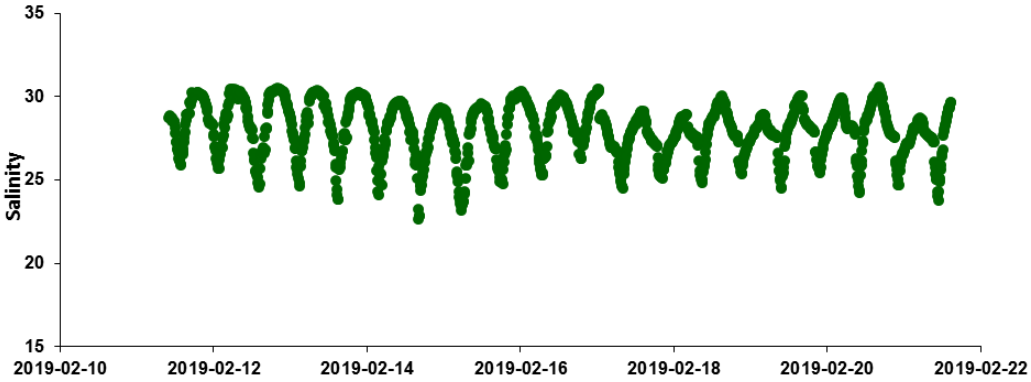

Figure 7.10. Salinity (psu) observed at the Parque das Nações station in February 2019.

Salinity data acquired at the Alcântara station between June 2016 and February 2019 are presented in Figure 7.11 and Figure 7.12.

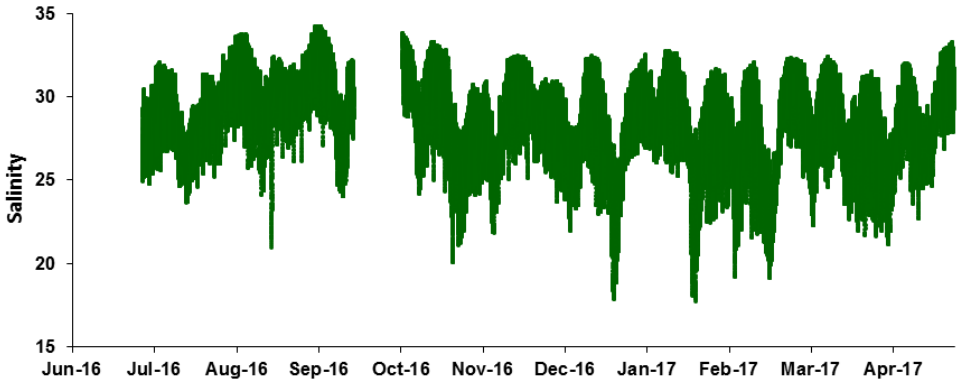

Figure 7.11. Salinity (psu) observed at the Alcântara station between June 2016 and April 2017.

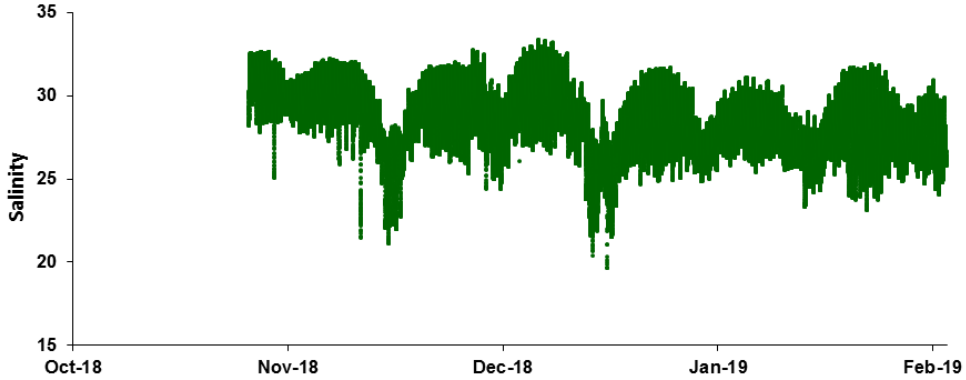

Figure 7.12. Salinity (psu) observed at the Alcântara station between October 2018 and February 2019 (after the reinstallation of the station).

During low tide salinity presented a horizontal gradient between the two monitoring stations with higher values at the Alcântara station (located further downstream in the estuary). At this station, salinity typically ranged between 25 PSU and 32 PSU (percentiles 5 and 95, respectively) with mean values of 28 PSU. It should be noted that this station is located in the vicinity of the largest urban discharge entering the estuary, the discharge from the Alcântara wastewater treatment plant (David et al., 2014). At the Parque das Nações station, salinity typically ranged between 20 PSU and 32 PSU (percentiles 5 and 95, respectively) with mean values of 28 PSU. The river flow influenced the salinity variation in the estuary. Salinity reached higher values during periods of lower freshwater discharge (Figure 7.13). The influence of the river flow is particularly evident during low tide.

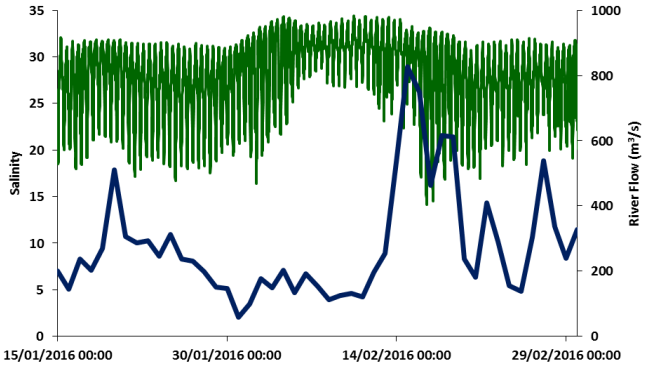

Figure 7.13. Salinity (PSU) at Parque das Nações and river flow (Almourol) variation. Daily mean river flow data were obtained from SNIRH (http://snirh.pt).

Water salinity and levels acquired in Vila Franca de Xira and Carregado in November 2017 are presented in Figure 7.14 and Figure 7.15. Salinity reached 9.3 PSU in Vila Franca de Xira, about 45 km from the estuary mouth, and 1.6 in Carregado 10 km further upstream. These results show that values of water salinity unacceptable for irrigation (above 1) can occur further upstream than Vila Franca de Xira, particularly in drought conditions.

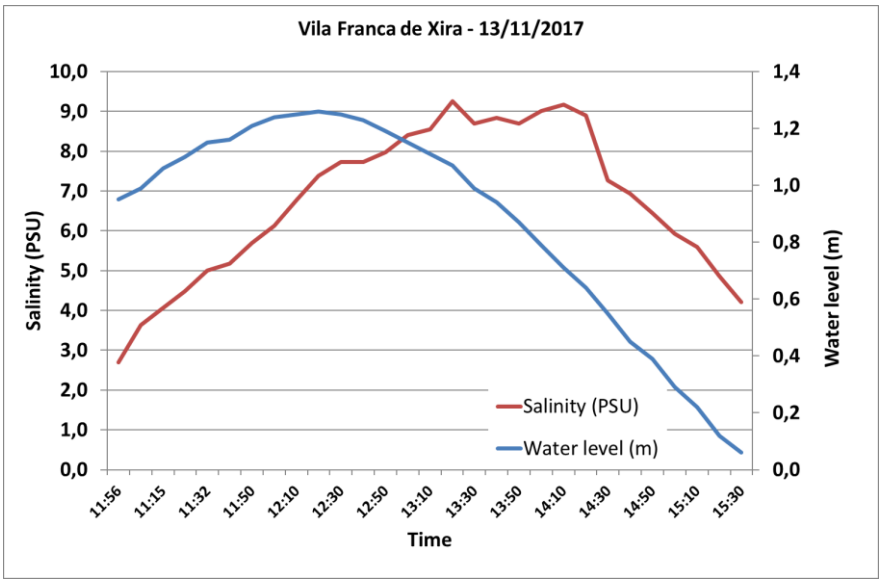

Figure 7.14. Salinity and local water level (m, MSL – mean sea level) in Vila Franca de Xira.

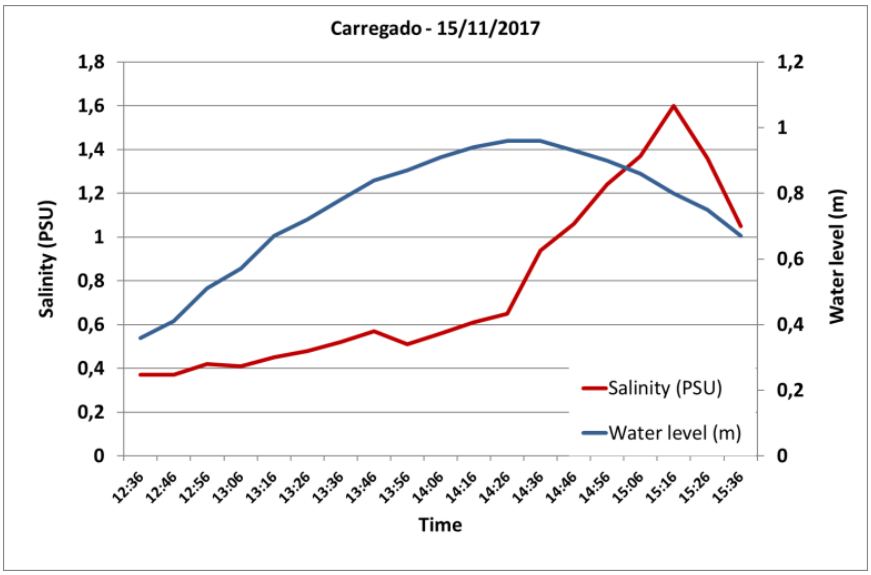

Figure 7.15. Salinity and local water level (m, MSL – mean sea level) in Carregado.

7.7.2. Model results

Previous validations of the circulation model used data from 13 tide gauges installed in the estuary in 1972 and measured sea surface elevations for the whole year (see D3.3). These data are used to predict present tides at the same locations, using standard harmonic analysis and synthesis procedures. Predicted tides are then compared with model results.

In general, the accuracy decreased from the ocean towards the head of the estuary. For instance, unbiased root mean square errors increased from about 4 cm close to the coast to over 12 cm upstream. This increase may have two different causes. Firstly, the errors at the coast primarily reflect errors in the boundary conditions, whereas errors inside the estuary are also affected by the accuracy with which the model propagates the tidal signal. Secondly, tides are affected by the bathymetric evolution. For instance, Fortunato et al. (1999) analysed the evolution of the major tidal constituent (M2) between 1972 and 1986

at three stations in the Tagus estuary. These authors showed that at the upstream station (Vila Franca de Xira) there was a significant decrease of the amplitude and an increase of the phase, while both the amplitude and the phase remained unchanged at the coastal station (Cascais). It is therefore likely that the 1972 tidal data at the upstream stations are outdated, thereby partially explaining the discrepancies between the data and the model results.

To distinguish between the two sources of errors, the model was run between December 15, 2018 and January 31, 2019. Model errors at Cascais (a coastal station) and the Parque das Nações station were computed. The model was run in forecast mode, forced by atmospheric predictions from Météo France (Arpège model) and the regional model of Fortunato et al. (2017). Selected error measures are shown in Table 7.1: the bias, the root mean square error (RMSE), and the root mean square error at high tide (HT-RMSE).

Results indicate that the model errors are mostly explained by the errors at the boundaries. The exception is the root mean square error, which may be affected by the fact that the location of the Parque das Nações dries out at low tide on spring tides. At high tide the errors are almost the same at the two stations. These results suggest that the model is more accurate than previously believed based on the comparison with data from 1972. Due to their unique coverage, these data have been used extensively by many authors to evaluate hydrodynamic models of the Tagus estuary. The new results indicate that more recent data, such as those used herein, should be used for model validation.

Table 7.1. Errors (in cm) of the model at the coast (Cascais station) and inside the estuary (Parque das Nações station).

Cascais			Marina		
Bias	RMSE	HT error	Bias	RMSE	HT error
-5.2	6.1	5.5	-6.3	13.0	6.0

To verify the SCHISM 3D model implemented in the Tagus estuary (see D3.3 for further details regarding model setup and validation) a simulation was performed to compare the model results with water levels and salinity data from the Parque das Nações station. Data from the Alcântara station were not used for this purpose, because, as mentioned above, this station is in the vicinity of an urban discharge and this freshwater source is not implemented in this version of the model. Moreover, the study area (Lezíria Grande de Vila de Xira) is located further upstream in the Tagus estuary. The simulation was performed for a period of 40 days, starting on January 15, 2016. The model was forced as follows: i) at the oceanic boundary by tides from the regional model of Fortunato et al. (2016); ii) at the Tagus river by river flow data from the Almourol station available at SNIRH (http://snirh.pt, Figure 7.13) and at the Sorraia river by river flow data estimated as 5% of the Tagus river (see D3.3); iii) at the surface by atmospheric data from NCEP-NCAR Reanalysis (Kalnay et al., 1996), since only decadal predictions from BINGO were available for the analyzed period. Climatology was used to force salinity and water temperature at the ocean and river boundaries.

Results show that the model is able to represent adequately the water levels (Figure 7.16) and the salinity (Figure 7.17). Unbiased root mean square errors are 13 cm for elevations and 2.9 PSU for salinity, respectively, at the Parque das Nações station. The differences observed may be due to the uncertainty in

the river flow, as discussed in D3.4. Moreover the bathymetry used in the simulations is not contemporary of the data and in the upstream area of the domain the bathymetric data are scarce, which may affect the model results regarding the river flow and tidal propagation, and consequently the salinity. Further discussion regarding this issue is presented below.

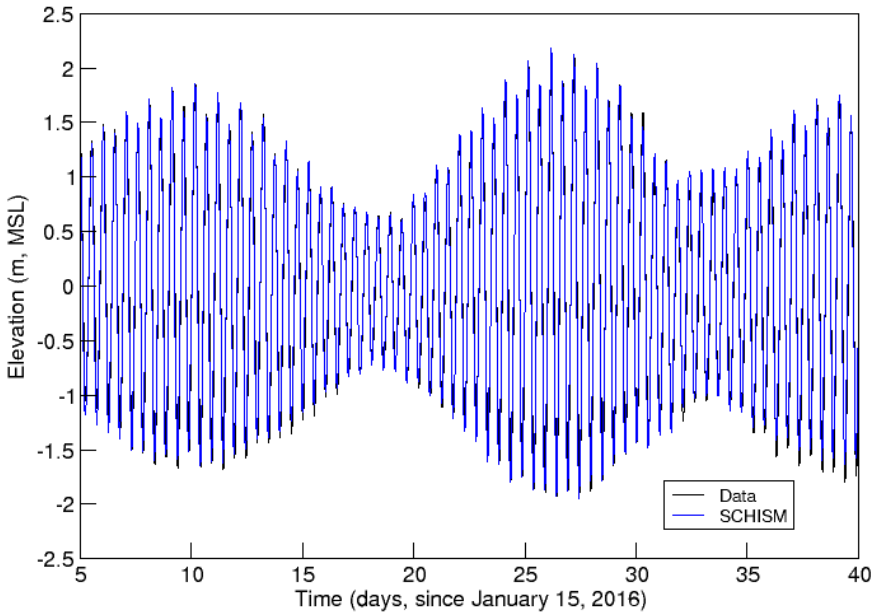

Figure 7.16 Comparison between water levels data and model results (Parque das Nações station).

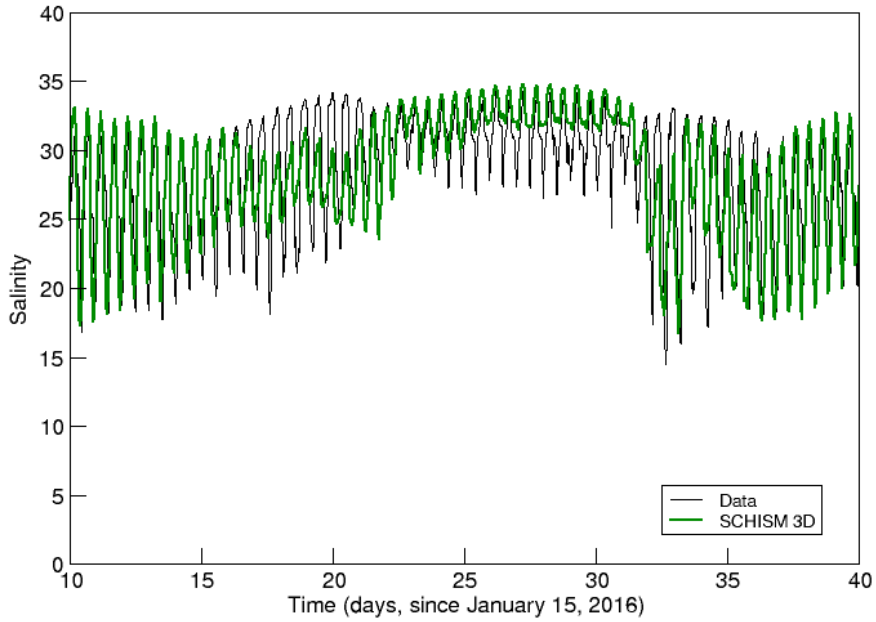

Figure 7.17. Comparison between salinity (psu) data and model results (Parque das Nações station).

7.8. Discussion

The validation of the 2D model using the new data highlights that the model errors are primarily due to the ocean boundary conditions. The errors increase only marginally inside the estuary, contradictory to our

previous interpretation based on data that are probably outdated. This conclusion provides further confidence in the model results.

The validation of the 3D model using the field data acquired during the project shows the model ability to adequately represent the main patterns regarding water levels and salinity dynamics in the Tagus estuary. As discussed in D3.4, based on a validation for drought conditions for the period of July 2017, errors in the river flow data, used to specify the boundary conditions, constitute a major source of uncertainty in the model results. The simplified representation of the bathymetry upstream of Vila Franca de Xira (rectangular cross-sections with varying width and depth were used), associated to the lack of detailed bathymetric data, was also pointed out as an additional source of errors. To evaluate the influence of the bathymetry, a new approach was used to represent the bathymetry upstream of Vila Franca de Xira and the 2017 simulation was repeated using a different bathymetry. A sophisticated approach to transform the cross-sectional data into a 2D bathymetry was developed, loosely based on Caviedes-Voullieme et al. (2014), whereby the bathymetry is interpolated along the streamlines. Results show that the differences between the two simulations are minor (Figure 7.18), with mean absolute difference less than 0.1 (range 0-0.7), suggesting that the river flow is the main source of uncertainty in the model results.

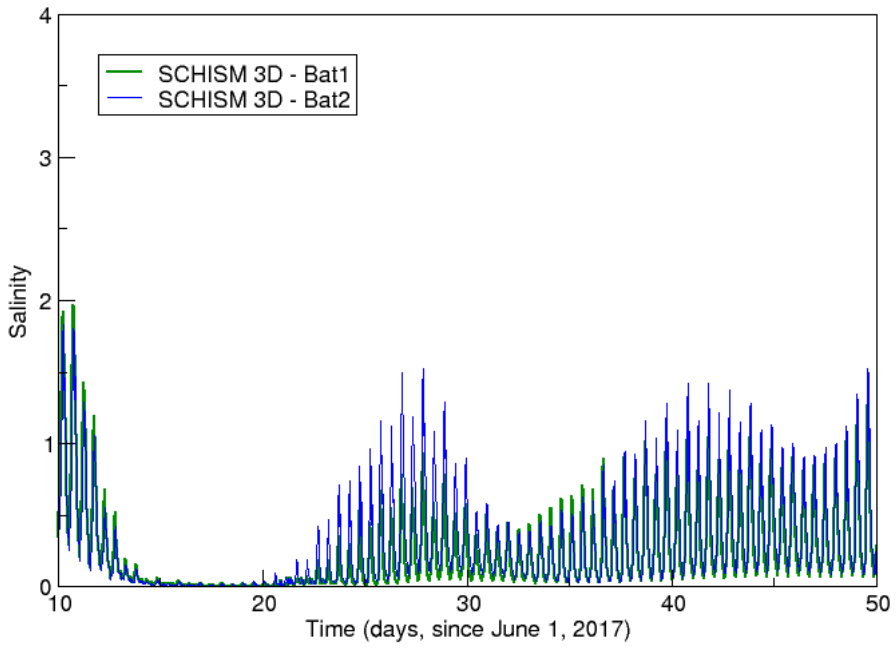

Figure 7.18 Influence of the upstream bathymetry in the salinity (psu) results at the Conchoso station.

7.9. Bibliography

Caviedes-Voullieme, D., Morales-Hernandez, M., Lopez-Marijuan, I., Garcia-Navarro, P. (2014). Reconstruction of 2D river beds by appropriate interpolation of 1D cross-sectional information for flood simulation. *Environmental Modelling & Software*, 61, 206-228

David, L.M., Oliveira, A., Rodrigues, M., Fortunato, A.B., Rogeiro, J., Jesus , G., Mota, T., Costa, J., Gomes, J., Menaia, J., Póvoa, P., David, C., Ferreira, F., Matos, J.S., Matos, R.S. (2014). Real-time monitoring and forecasting system for early warning of recreational waters contamination. Proceedings of the 13th IWA/IAHR International Conference on Urban Drainage 2014 (Sarawak, Malaysian Borneo), 9 pp.

Fortunato, A.B., Li ,K., Bertin, X., Rodrigues ,M., Miguez, B.M. (2016). Determination of extreme sea levels along the Iberian Atlantic coast. *Ocean Engineering*, 111/1, 471-482.

Fortunato, A.B., Oliveira, A., Rogeiro, J., Tavares da Costa, R., Gomes, J.L, Li, K., Jesus, G, Freire, P., Rilo, A., Mendes, A., Rodrigues, M., Azevedo, A. (2017). Operational forecast framework applied to extreme sea levels at regional and local scales, *Journal of Operational Oceanography* 10, 1: 1 - 15.

Kalnay et al. (1996).The NCEP/NCAR 40-year reanalysis project, Bull. Amer. Meteor. Soc., 77, 437-470.

Rodrigues, M., David, L.M., Oliveira, A., Fortunato, A.B., Menaia, J., Costa, J., Mota, T., Rogeiro, J., Jesus, G., Morais, P., Palma, J., Matos, R. (2015). On-line monitoring of CSO: sewer and receiving waters. Climate Change, Water Supply and Sanitation: Risk Assessment, Management, Mitigation and Reduction, IWA Publishing, Hulsmann A. et al. (eds), Chapter 3 - Real Time Monitoring and Modelling, Tools, Methodologies and Models , subchapter 3.9, pages 69-74, ISBN13: 9781780404998, eISBN: 9781780405001.

Rodrigues, M., Freire, P., Rogeiro, J., Fortunato, A.B. (2017). Online monitoring in the Tagus Estuary: Parque das Nações station, Installation and operation between January 2016 and February 2017. Report 131/2017 – DHA/NEC, LNEC.

Zhang, Y.J., Ye, F., Stanev, E.V., Grashorn, S. (2016). Seamless cross-scale modeling with SCHISM, *Ocean Modelling*, 102, 64-81.

8. Spain

Model frameworks

The aim of the WP3 BINGO case study of Badalona is to develop a full hazard assessment for both flooding and Combined Sewer Overflows (CSOs) through the development and calibration of advanced models to simulate the combined behavior of sewer system and urban surfaces in case of flood events and the sea water quality conditions of Badalona bathing waters due to the CSO spills produced during rain events. In this context, D3.1 described the main characteristics of the case study, D3.2 the future land use and water use scenarios, D3.3 the integrated model setup and calibration, and D3.4 the model results in terms of simulation results and hazard maps. This deliverable D3.5 presents the field work research related to the developed models in order to improve their performances. Part of the fieldwork was already presented in D3.3 and D3.4. Table 8.1 summarizes all the equipment and field campaigns that were carried out during the Bingo project.

Table 8.1. Resume of the fieldwork activities and equipments in Bingo

	Measured variables	**Period**	**BINGO funded**
14 water level sensors	Water level in the sewer	2015-present	no
4 pluviometers	Rainfall intensity	2013-present	no
5 sea water level campaigns	E. Coli concentrations Enterococci Intestinalis concentrations Salinity Suspended Solids Oxidability Turbidity	2016-2018	yes
2 sewer sediment campaigns	Content of organic matter Specific density Sediment size	2017-2018	yes
2 sediment campaign in the upstream rural areas	Sediment traps status	2016-2017	no
4 temperature, 2 water level, and 2 turbidity sensors at 2 CSO monitoring points.	Turbidity Temperature Water level	2017-present	yes
2 bottle samplers at 2 CSO monitoring points	E. Coli concentrations	2017-2018	no
Photos and videos	Flood videos and photos CSO videos and photos	continous	no

8.5. Introduction and objectives [Flood Risk Assessment]

Framework 1 concerns the flood risk assessment that was made based on a hydrological and hydraulic model. As described in detail in D3.3, the flood model is a coupled 1D/2D model (urban drainage network / surface runoff) setup in InfoWorks ICM.

State of the art urban flood analysis is performed using urban drainage network models (1D) coupled to surface runoff models (2D) (Russo et al., 2015). These models are setup using detailed information of the physical system (topography, manhole location and dimensions, pipe length and diameter, inlet location and type, etc.) and information about the hydrological process to be modeled (rainfall inputs, land use data, soil properties, pipe and surface roughness, etc.). Further, model calibration and validation should use both quantitative and visual performance metrics (Bennett et al., 2013; Hauduc et al., 2015). Therefore, a significant amount of local field data collected by field work and local measuring stations are required in order to simulate urban floods.

Field work and station measurements were essential for several reasons:

- To calibrate and validate the 1D/2D model. A sediment transport model was also calibrated as part of the 1D/2D model.
- To verify the model results
- To improve the understanding of the local hydraulic and hydrological processes of the drainage infrastructure
- To continuously update the models with new data
- To improve model reliability among the project stakeholders.

The objective of the flood framework is to develop a full flood risk assessment. Particularly, to produce spatially distributed risk maps for pedestrians, vehicles and buildings as part of WP4. This is done using the 1D/2D model that aims at simulating the spatial distribution of maximum surface flow velocities and depths in Badalona during selected design rainfall events.

8.6. Methods

8.6.1. Study site description

The detailed description of the Badalona catchment is presented in D3.1. Here only the main features relevant for the flood risk assessment are summarized.

Badalona (21.2 Km^2) has a highly urbanized urban area facing the Mediterranean Sea and is surrounded by mountains/hills with steep slopes. The urbanized area mostly occupies the low lying parts of the municipality with heights of few tens of meters above sea levels, whereas the surrounding hills can reach few hundreds of meters. The urban area of Badalona is prone to flash flood risk caused by the combination of both surface runoff coming from the hilly areas and limited urban drainage capacity.

8.6.2. Field work

Different types of field work were conducted in order to collect observation data useful for the flood analysis. In this section both data coming from measuring stations or sensors and field campaign are summarized.

Rainfall data. 4 different rainfall gauges collects rainfall data in Badalona. 3 rain gauges were installed by the municipality of Badalona using BINGO funds; while 1 rainfall gauge was already owned by the municipality. Figure 8.1 shows the location of the rain gauges in Badalona.

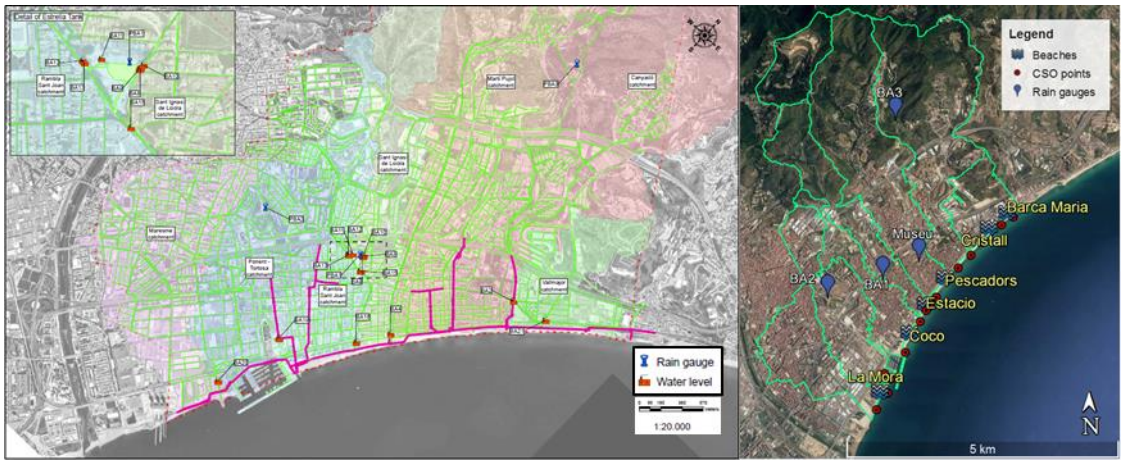

Figure 8.1. (Left) Location of the fourteen water level sensors in Badalona. (Right) Location of the rain gauges, CSO ponts and rain gauges.

Water level sensors in the drainage network. Fourteen water levels sensors were installed by AQUATEC. These sensors collected 5 minutes time step series of water levels at specific points of the drainage network (at manholes and pipes). These data were useful to calibrate and validate the 1D/2D model. Figure 8.1 shows the location of the water level sensors.

Sediment data. 2 different field campaigns were carried out in order to collect sediment data at 6 different points of the sewer network on two different days (one after a dry period and one after a wet period). The campaign consisted in manually collect deposited material samples (1dm^3 approximately) from selected sewer pipes by physically accessing specific manholes. Then, the geotechnical laboratory of the Polytechnic University of Catalonia analyzed the samples to provide: specific density of sediment [kg/m3], organic matter content of the sample and the representative diameter (D_{50}) of the sediments. These data were useful to improve knowledge about the origin of the sediments (urban or undeveloped areas) in the sewer network and to properly select sediment model parameters. Moreover, two inspections (during two different days after two different rainfalls) with photos and measurements of sediment traps located at the inlets of the drainage piped network that are located upstream the densely urbanized area (downstream the hilly rural areas) were performed. These dates were used to calibrate the sediment transport model of the rural areas. Finally, turbidity and suspended solids concentrations measurements were collected using sensors located at two selected CSO structures together with temperature and water level sensors. Figure 8.2 shows some of the sampling facilities and campaigns. These campaigns and measuring devices were funded by BINGO and other projects.

Photos and videos from local people and from information media. Photos and videos of surface floods during several different rain events over several years were used to improve the 1D/2D model, particularly the 2D surface runoff model. Figure 8.3 an example of the calibration process of the surface runoff 2D model using photos and videos from an event that generated surface flood.

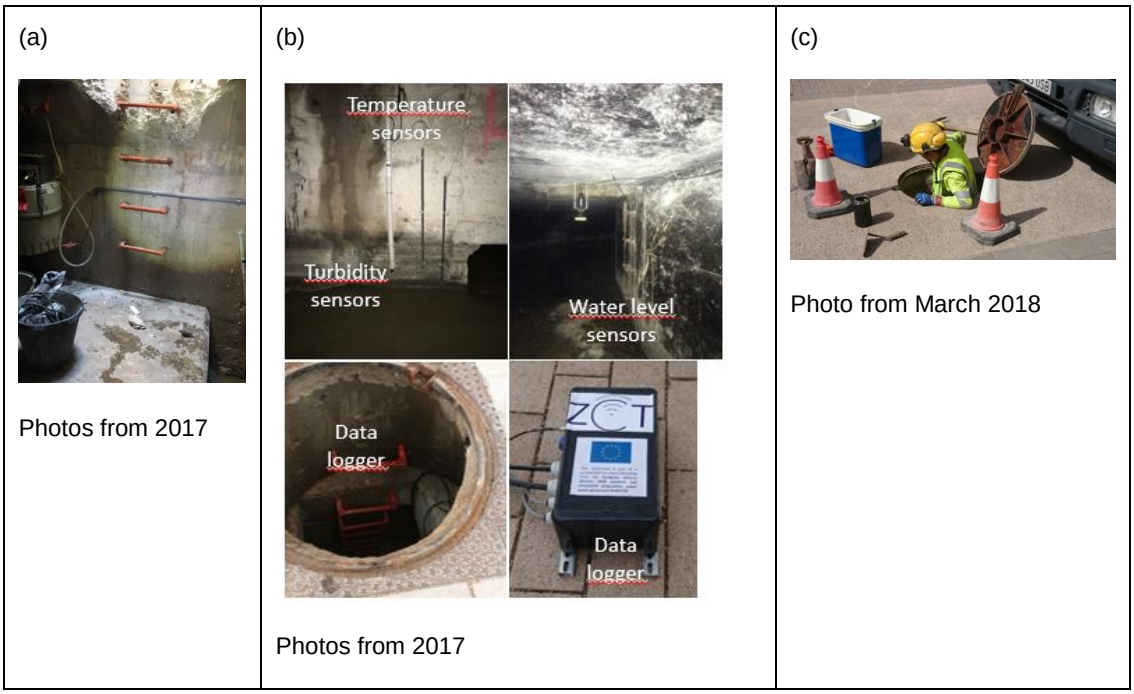

Figure 8.2. (a) Automatic samplers; (b) sensors installed at the CSO structures; (c) sampling of deposited sediments in the drainage netowrk.

Figure 8.3. Visual surface flood calibration process using photos and videos. Event of July 2018

8.6.3. Model description

The 1D/2D model was modified and improved (see D3.3) by including the new data presented in the previous section:

- Rainfall data. The rainfall time series from 3 of the 4 rain gauges were used to improve the description of the rainfall spatial distribution when simulating single flood events. Thiessen polygons were used to spatially distribute the observed rainfall from the rain gauges in the 1D/2D model. Also, the climate models from WP2 used these time series to downscale regional rainfall in order to better reproduce local rainfall intensity and volume distribution.
- Water level data. The detailed time series of water levels from the 14 water level sensors installed throughout the drainage network were used to calibrate the 1D/2D model. Four different rain

events were chosen for calibration and one event for validation. Figure 8.4shows the characteristics of the calibration and validation events. The modelled hydraulic and hydrological processes that were improved thanks to the new data were (D3.3):

- Hydrological losses, particularly the continuous losses (the initial losses were in the order of 1 mm and not considered to be an influential variable). The continuous losses, mainly from infiltration were simulated using the Horton model. The Horton models parameters were adjusted to improve the water balance coming from the undeveloped hilly areas of the catchment.
- 2D surface runoff routing. The surface roughness coefficients for both impervious and rural areas were fixed to properly reproduce surface water velocity, depth and timing of peak flows.
- 1D Pipe flow routing. The pipe roughness coefficient (Manning) was calibrated to properly reproduce pipe water velocity, depth and timing of peak flows.

Date event	Cumulative rainfall (mm)	Max. Rainfall intensity in 20min (mm/h)	Max. Rainfall intensity in 5min (mm/h)	Function
22/08/2014	25.5	42.6 (T=0.4)	74.4 (T=0.6)	Calibration
28/07/2014	46.5	56.4 (T=0.8)	91.2 (T=0.8)	Calibration
03/10/2015	34.1	81 (T=2.1)	122.4 (T=1.1)	Calibration
14/09/2016	21.7	64.5 (T=1.1)	142.8 (T=6.1)	Calibration
18/06/2016	24.6	60.3 (T=0.8)	105.6 (T=0.9)	Validation

Figure 8.4 Selected model calibration and valibdation events.

- Photos and videos of surface water floods. These data were used to improve the 2D surface runoff model. Particularly, by improving the simulation of surface water flow and accumulation areas. This was achieved by introducing in the models surface obstacles (walls, bumps, sidewalks and other obstacles to surface water flow) that could not be detected by the 2D surface runoff computational grid. This obstacles were simulated as no-flow 1D walls (with zero gradient boundary conditions) of either infinite or limited height depending on the characteristics of the real obstacle (i.e. backyard walls or impermeable fences).

Two different sediment models were used: one HEC-HMS model specific for the rural areas and an InfoWorks ICM for the rural and the urban areas and for the drainage network (see D3.3). The HEC-HMS model were used to estimate the sediment erosion from the upstream rural areas of the catchment. The results were used as sediment input time series to the urban drainage model. The InfoWorks ICM model was used for both the generation of sediment in the urban areas and for the sediment transport in the urban drainage network. The sediment models were modified and improved by including the new data presented in the previous section:

- Sediment data. The sediment data were used to estimate the sediment transport model parameters. Particularly, the representative diameter (D_{50}). The other data, the density of the sediment and the organic matter content helped us to improve our understanding of the origin of the sediments deposited in the piped drainage network. The suspended solid sensors were used for a preliminary calibration of the InfoWorks ICM sediment transport model and particularly, the sediment buildup parameters, wash-off parameters and the Velikanov model parameters. The turbidity data were used in other projects to correlate total suspended sediments with turbidity

data. The data from the 2 field campaigns on the sediment traps were used to calibrate the HEC-HMS model of the rural areas during the 2 observation rain events.

8.7. Results

8.7.1. Field work results

The rain gauges collected high resolution rainfall time series (every 0.1 mm rainfall depth) between 2013 and 2019. The statistical properties of rainfall intensities and accumulated volumes were verified to be similar to the neighboring Barcelona stations.

The water level sensor and sediment data were shown together with the calibration results in D3.3 and in the example shown in Figure 8.4.

8.7.2. Model results

All the model results together with the model performance criteria selected were shown in D3.3 and D3.4. The model performance parameters used for the calibration of the 1D/2D model were: the coefficient of determination (R^2), the root mean squared error (RMSE), the peak error (PE) and time to peak error (TPE). In some cases the data are sparse and calibration was made using only visualization metrics, i.e. the calibration of total suspended solids in the InfoWork ICM (D3.3) sediment transport model and the calibration of total sediment loads in the HEC-HMS models (D3.3).

Figure 8.5shows some of the calibration and validation results. The results show the simulated and observed water levels at different locations in the sewer network during a selected rain event.

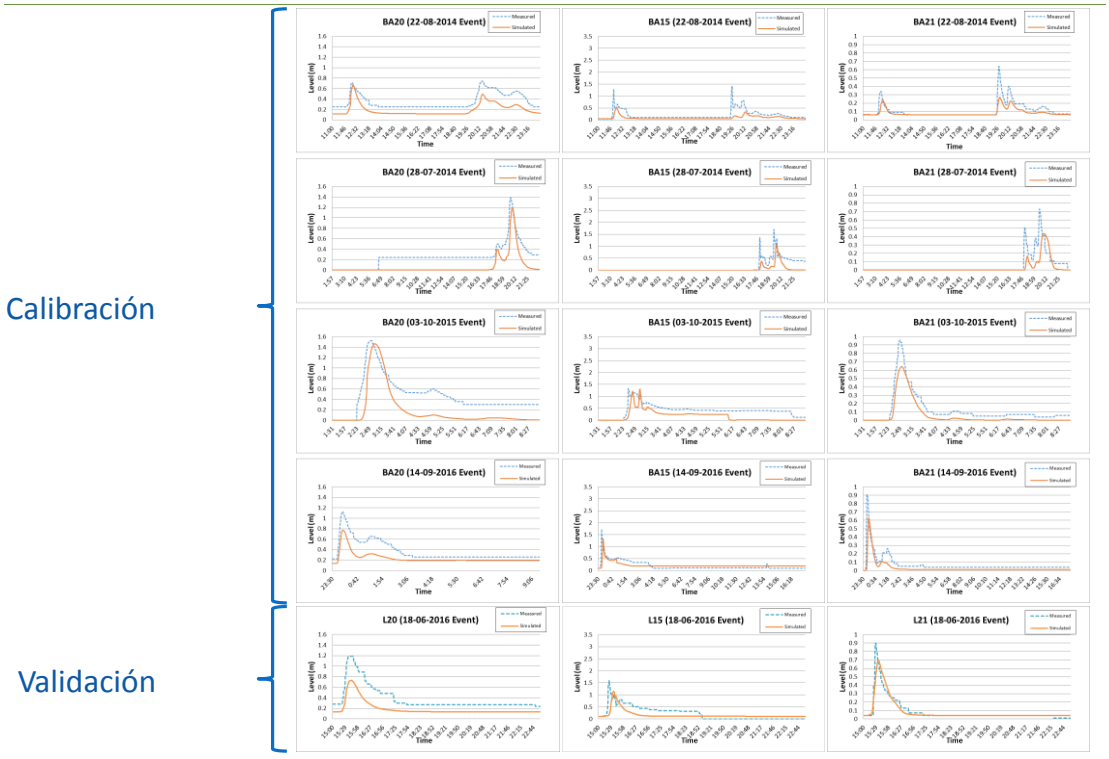

Figure 8.5 1D/2D model calibration and validation

Figure 8.6 shows the results of a preliminary TSS model calibration at the CSO point of Maria Auxiliadora (further results in D3.3). The observed data are sparse and the attempted model calibration gave poor

visual matching between observed and simulated values. For these reasons, no quantitative model performance metrics were computed and the TSS model would not be used in further analysis.

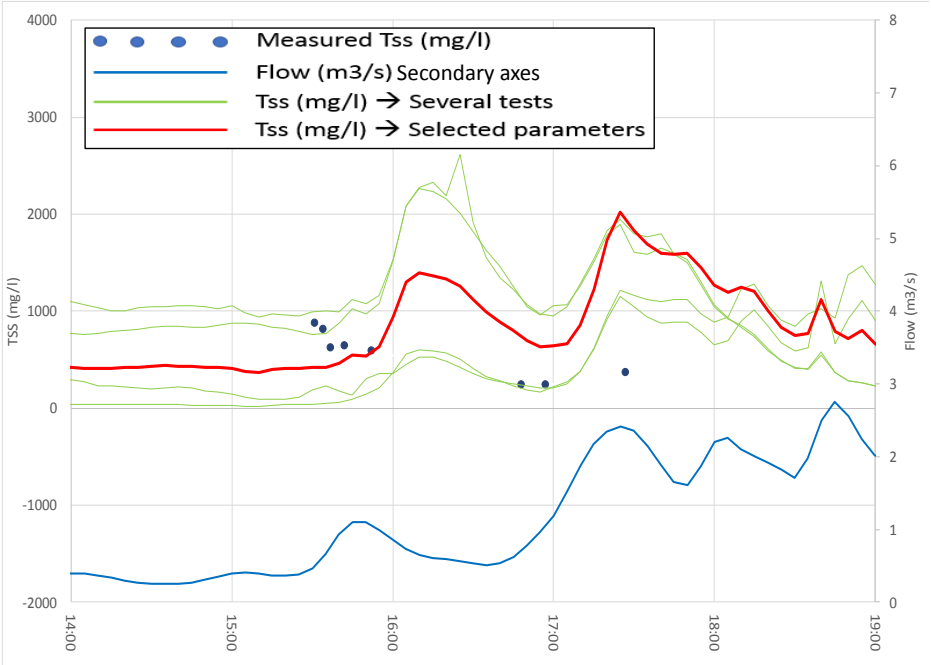

Figure 8.6. Example of a prelimiary calibration of the TSS model at the CSO point of Maria Auxiliadora (24/03/2017). Simulated vs observed Total Suspended Solid concentrations. The simulated flow is also shown.

8.8. Discussion

The observed data helped improving the model performances through new calibration results, better process understanding, new selection of model parameters and more precise model inputs. The improved model simulations concern:

- the extent of the urban flood areas and surface water fluxes;
- the urban drainage network flows;
- the sediment transport processes in the rural and urban areas and in the drainage network of Badalona.

The new model results obtained in the BINGO project will be used by the municipality to publish on-line flood risk maps and to update the master drainage plans of the municipality.

Overall, the new data collected improved the flood model reliability and confidence of all the project stakeholders.

8.9. Bibliography

Bennett, N.D., Croke, B.F.W., Guariso, G., Guillaume, J.H.A., Hamilton, S.H., Jakeman, A.J., Marsili-Libelli, S., Newham, L.T.H., Norton, J.P., Perrin, C., Pierce, S.A., Robson, B., Seppelt, R., Voinov, A.A., Fath, B.D., Andreassian, V., 2013. Characterising performance of environmental models. Environ. Model. Softw. 40, 1–20.

Hauduc, H., Neumann, M.B., Muschalla, D., Gamerith, V., Gillot, S., Vanrolleghem, P.A., 2015. Efficiency criteria for environmental model quality assessment: Areview and its application to wastewater treatment. Environ. Model. Softw. 68, 196–204.

Russo, B., Sunyer, D., Velasco, M., Djordjević, S., 2015. Analysis of extreme flooding events through a calibrated 1D/2D coupled model: the case of Barcelona (Spain). J. Hydroinformatics 17, 473.

8.10. Introduction and objectives [Combined Sewer Overflows]

Framework 2 relates to Combined Sewer Overflows (CSOs). Particularly, it focuses on the development of a health risk assessment for people bathing in sea waters contaminated from CSOs. Such assessment was based on bathing water quality model simulations. As described in detail in D3.3, the bathing water quality model integrates the 1D/2D urban drainage model (described in Framework 1) and a 3D hydrodynamic model of the of the Mediterranean Sea close to Badalona. The hydrodynamic model simulated both the near-shore hydrodynamics and the contaminant fate and transport processes of bacterial contaminants coming from Combined Sewer Overflows (CSOs). The model was used to estimate both the seasonal time duration of unacceptable bathing water quality and the single event contamination duration as a function of the rainfall volume.

State of the art models couple urban drainage models to hydrodynamic and sea water quality models of receiving water bodies (Andersen et al., 2013; Marchis et al., 2013; Scroccaro et al., 2010; Suñer et al., 2008). Urban drainage models predict the hydraulic and contaminant CSOs loads of and the hydrodynamic models of the receiving water bodies computes the spatial and temporal distribution of bacterial contamination. Further, models need to be calibrated and validated. Therefore, a significant amount of local field data collected by field work and local measuring stations are required in order to simulate bathing water quality.

Field work and station measurements were essential for several reasons:

- To improve the 1D/2D model simulation of CSOs.
- To verify the model results
- To improve the understanding of the local hydraulic and hydrological processes of CSOs
- To continuously update the models updated with new data
- To improve model reliability among the project stakeholders.

Some of the data used also came from other projects: EFFIDRAIN (EU LIFE Project) and from local authorities: Agència Catalana de l'Aigua and the municipality of Badalona.

8.11. Methods

8.11.1. Study site description

The detailed description of the Badalona catchment is presented in D3.1. Here only the main features relevant for the risks derived from CSOs are presented.

Badalona (21.2 Km^2) has a highly urbanized urban area facing the Mediterranean Sea and is surrounded by mountains/hills with steep slopes. It has approximately 5 km of bathing sandy beaches facing the Mediterranean Sea. Several CSO points discharge combined sewers along the beaches. Generally, all rainfall events larger than few mm cause CSOs that can compromise bathing water quality up to 2-3 days after CSO events, and during the bathing season, bathing is forbidden during at least 24 hours after CSO events.

8.11.2. Field work

Different types of field work were conducted in order to collect observation data useful for the bathing water analysis. In this section both data coming from measuring stations or sensors and field campaign are summarized.

Rainfall data. These data were presented in the flood analysis framework 1.

Sensors at the CSO points. A water level, a temperature and a turbidity sensor were installed by AQUATEC at each of the 2 selected CSO points of Badalona (Riera Canyado and M. Auxiliadora) (Figure 8.2b). These sensors collected detailed time series of water levels at of CSOs. These data were useful to adjust the CSO hydrograph simulated by the 1D/2D model at the 2 monitored CSO points. These sensors were funded by BINGO.

Automatic samplers at 2 CSO points. Two automatic samplers made of 12 sampling bottles each were installed at each of the 2 monitored CSO points (Figure 8.2a). Data about Total Suspended Solids and Escherichia Coli concentrations were collected. These data are useful to define the pollutographs that are used as input to the water quality model of the receiving water body. These samplers were funded by the LIFE EFFIDRAIN project (LIFE14 ENV/ES/000860).

Water quality manual sampling of sea water. A total of 5 different CSO field campaigns after 5 different CSO events were carried out. Each campaign consisted in manual collection of water samples at 3 different points in the sea in front of Badalona (Figure 8.7). One sample per day at each sampling point was taken from the moment the CSO was detected until the measured concentrations of E. Coli and Enterococci Intestinalis were below regulating thresholds. Each measurement was analyzed by the municipal laboratory of Badalona to estimate: E. Coli, Enterococci Intestinalis, Salinity, suspended solids, Turbidity and oxidability. The values of E. Coli, Enterococci Intestinalis, Salinity were used to calibrate and validate the sea water quality model. Figure 8.7 shows examples of the sea water quality measurements. These measurements were made by the municipality of Badalona through BINGO funds.

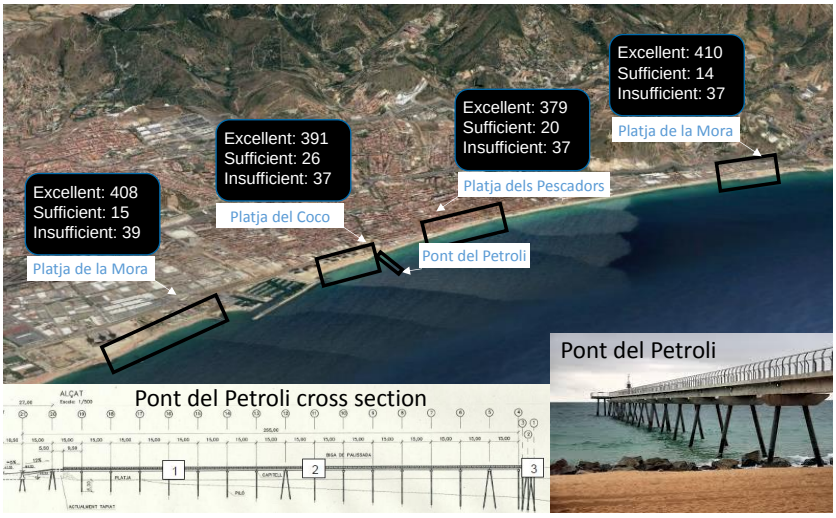

Figure 8.7 Sea water quality sampling locations. The 'Pont del Petroli' cross section shows the three sampling locations.

Photos and videos from local people and from information media. Photos and videos of Combined Sewer Overflows and contaminant plumes in the sea water of Badalona during several different rain events over several years were used to visually validate the sea water quality model.

8.11.3. Model description

The 1D/2D model and the sea water quality model were modified and improved (see D3.3) by including the new data presented in the previous section:

- Rainfall data. The rainfall time series from 4 rain gauges were used to improve the description of the rainfall spatial distribution when simulating the observed CSO events. Thyssen polygons were used to spatially distribute the observed rainfall from the rain gauges in the 1D/2D model. Also, the climate models from WP2 used these time series to downscale regional rainfall in order to better reproduce local rainfall intensity and volume distribution.
- Sensors at the CSO points. The time series of water levels from the 2 CSO points were used to adjust the simulated CSO hydrographs and total volumes at the 2 observed CSO points. Only manual calibration without quantification of model performance indicators was performed. The manual calibration of these 2 CSO points (out of more than 10 CSO points) was assumed not to affect the model performance of the previously calibrated urban drainage model of the whole Badalona area.
- Automatic samplers at 2 CSO points. The data from automatic samplers provided E. Coli concentrations at the CSO points during different CSOs. These data were used to extract Event Mean Concentrations that were used as input to the sea water quality model.
- Water quality manual sampling of sea water. The time series of salinity, E. Coli, and Enterococci Intestinalis at the 3 different sampling points were used to calibrate and validate the sea water quality model.
- Photos and videos of surface water floods. These data were used to visualize the extent of the contamination plumes originated from CSOs.

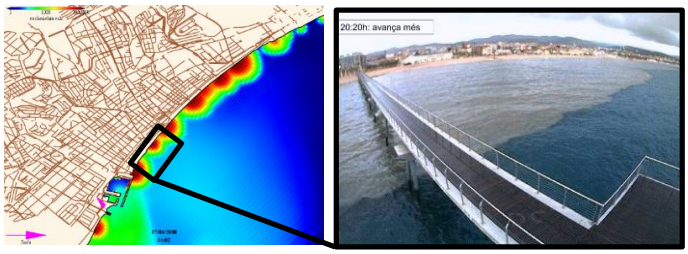

Figure 8.8 Example of visual validation of CSO contaminant plumes in the sea. Photo from July 2018.

8.12. Results

8.12.1. Field work results

All the data presented in the previous section were shown together with the calibration results in D3.3. shows an example of the laboratory results from the municipality of Badalona about measured sea water quality indicators.

Núm. registre	29	30	31
Punt/Paràmetre	1 Línia costa	2 Centre pont	3 Extrem pont
Escherichia coli (ufc/100 ml) (PNT-M-6, M-29, M-49)	**$4.9x10^3$**	**$1.9x10^3$**	**$7.8x10^2$**
Enterococs intestinals (ufc/100 ml) (PNT-M-6, M-20)	**$3.8x10^2$**	**$2.3x10^2$**	**90**
Salinitat (‰) (PNT-Q-68)	**37.6**	**37.9**	**37.9**
MES (mg/l) (PNT-Q-13)	**22**	**15**	**10**
Oxidabilitat (mg O_2/l) (PNT-Q-21)	**37**	**46**	**59**
Terbolesa (UNT) (PNT-Q-71)	**11.0**	**4.3**	**2.6**

Figure 8.9. Laboratory results of the measured water quality variables. Results from February 2018.

8.12.2. Model results

All the model results together with the model performance criteria selected were shown in D3.3 and D3.4. The sea water quality model calibration was made using only visualization metrics because of the sparse observations that were considered to be insufficient for a reasonable quantitative performance metric. Figure 8.10 shows examples of model simulations of both E. Coli and salinity concentrations in sea water after CSO events.

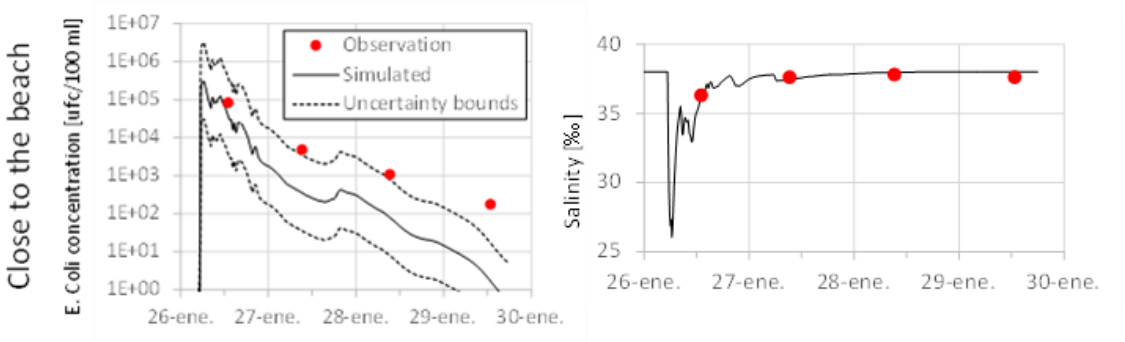

Figure 8.10 Examples of model performances in terms of E. Coli (left) and salinity (right) contentrations in sea water after CSO events. Observations and results from an observed event in January 2018.

8.13. Discussion

The observed data helped improving the model performances through new calibration results, better process understanding, new selection of model parameters and more precise model inputs. The improved model simulations concern:

- the spatial and temporal distribution of sea water bacterial contamination caused by CSOs in Badalona;
- the simulation of CSOs from the 1D/2D model. Particularly, the inclusion of the structural details about the crest levels of the CSO weirs and the water level sensor data from the 2 monitored CSO points allowed a new calibration of the CSO hydrographs so that the model that can also simulate small rain events.

The new model results obtained in the BINGO project will be used by the municipality to improve the prediction of the duration of insufficient bathing water quality after CSOs.

Overall, the new data collected improved the model reliability and confidence of all the project stakeholders.

8.14. Bibliography

Andersen, S.T., Erichsen, A.C., Mark, O., Albrechtsen, H.J., 2013. Effects of a 20 year rain event: A quantitative microbial risk assessment of a case of contaminated bathing water in Copenhagen, Denmark. J. Water Health 11, 636–646.

Marchis, M. De, Freni, G., Napoli, E., 2013. Modelling of E. coli distribution in coastal areas subjected to combined sewer overflows. Water Sci. Technol. 68, 1123–1136.

Scroccaro, I., Ostoich, M., Umgiesser, G., De Pascalis, F., Colugnati, L., Mattassi, G., Vazzoler, M., Cuomo, M., 2010. Submarine wastewater discharges: Dispersion modelling in the Northern Adriatic Sea. Environ. Sci. Pollut. Res. 17, 844–855.

Suñer, D.; Malgrat, P.; Leitão, P.; Clochard, B., 2008. COWAMA - Integrated and real time management system of urban drainage to protect the bathing waters. 11th International Conference on Urban Drainage (ICUD), Edinburgh, Scotland.

9. Conclusions and outlook

In Cyprus, sapflow of pine trees, soil moisture, throughfall, meteorology and streamflow observations during 2015-2018 improved our understanding of forest water use and streamflow generation for the watersheds along the northern slopes of the Troodos Mountains. The evapotranspiration of the *Pinus brutia* forest was found to amount to 86 to 90% of the annual rainfall. The majority of the transpiration is extracted from the fractured bedrock. During the 2007 drought year, evapotranspiration exceeded the incoming rainfall, with trees relying on moisture from the bedrock fractures until transpiration nearly ceded towards the end of October. Interception, which is included in the evapotranspiration, comprises 15-19% of the annual rainfall. The lumped, daily GR4J model was modified for automatic calibration on the normalized monthly evapotranspiration observations for the Peristerona Watershed. The model calibrations showed that the observed evapotranspiration is captured better when the streamflow exchange parameter is set to zero. A Nash Sutcliff Efficiency of 0.82 was obtained for the long-term calibration (1995-2010) and 0.71 for the validation (1980-1995). The calibrated GR4J model will be used for the long-term simulations of future streamflow, which is crucial for the recharge of the downstream aquifers. Streamflow observations will continue, to improve our understanding of groundwater recharge in these complex and fractured geological formations.

In the Wupper Research Site (Germany) a better understanding of the hydrologic model processes was obtained through soil physical sampling and analysis, soil moisture monitoring and trial and error model calibrations. Soil moisture observations in grassland, pine and deciduous forests gave insight in the temporal moisture variations and vertical moisture distribution patterns. The data were used for the re-calibration of the TALSIM and SWAT hydrologic models. For the SWAT model the soil moisture calibration was found to have no effect on the streamflow simulations. The new model parameterization of the physically-based, lumped TALSIM model, which is used for flood forecasting, gave a better fit of observed soil moisture and peak flows. However, the model performance for low flow and total flow worsened. Wupperverband will expand the soil moisture network with the installation of five new stations at representative combinations of land uses and soil types, based on the good experience obtained. Valuable modelling experience was also gained through the use of both SWAT and TALSIM models and further model calibrations are foreseen. The TALSIM developers are currently adding a new module that will enable the set-up of a distributed model, where grid cells represent Hydrologic Response Units. This will facilitate the simulation of soil moisture per HRU. The ultimate goal is to assimilate soil moisture observations in the operational flood forecasting modeling.

In the Veluwe, evapotranspiration field measurements from automated lysimeters and data from published research were compared with the simulated evapotranspiration values from the AZURE groundwater model. For most land use types, AZURE overestimated the evapotranspiration. Based on this comparison, a land use type was added for heather and evapotranspiration factors for heather, dry nature and bare ground were changed in the model. A large pot analysis experiment showed a single linear relation between transpiration and the tree diameter of 10 different species that grow at the Veluwe. The analysis of interception, leaf and stem traits of the experiment is ongoing. The accurate simulation of the evapotranspiration has a large influence on the groundwater recharge in the Veluwe. Variations in rainfall also affect different species and evapotranspiration in different ways. The understanding and simulation of evapotranspiration is important for analysing potential land use changes as climate adaptation measures.

In Bergen (Norway) stormwater runoff generated in the urban area and the less developed upstream area is handled by a combined sewer system. In the downstream area, CSOs discharge mixed stormwater and

sewage to the Puddefjorden during heavy rains. A network of six temporary tipping-bucket rain gauges was distributed within the steeply sloping Damsgård area to obtain a better understanding of topographic influence on precipitation patterns. A flow meter was installed in a stormwater pipe in the upper parts of urban area, close to an inlet from the mountainous headwater catchment. Rainfall data showed the effect of wind direction and topography on the rainfall. Strong correlation between stations for daily data and weaker correlations for shorter durations were found. No linear relation between the main rainfall station and the temporary rainfall station could be found. The flowmeter data were not accessible, but is expected to be used for future model applications.

In the downstream Tagus Basin (Portugal), sea level rise and storm surges threaten agricultural land. Water level and salinity observations in the estuary showed that errors in the 2D SCHISM model are primarily due to the ocean boundary conditions. The validation of the 3D SCHISM model with the field data acquired during the project shows the model ability to adequately represent the main patterns regarding water levels and salinity dynamics in the Tagus estuary. To evaluate the influence of the bathymetry, a sophisticated approach was developed to transform the cross-sectional data into a 2D bathymetry, through interpolation along the streamlines. Results show that the differences between the two simulations are minor, suggesting that the river flow is the main source of uncertainty in the model results.

The development and calibration of advanced models to simulate the combined behavior of sewer system and urban flooding and sea water quality conditions of bathing waters in Badalona (Spain) was supported by new CSO water level, temperature, turbidity and sediment observations. The observed field data helped to improve the model performances through new calibration results, better process understanding, new selection of model parameters and more precise model inputs. The improved model simulations included the spatial and temporal distribution of sea water bacterial contamination caused by CSOs in Badalona and the simulation of CSOs from the 1D/2D model. Particularly, the inclusion of the structural details about the crest levels of the CSO weirs and the water level sensor data from the 2 monitored CSO points allowed a new calibration of the CSO hydrographs so that the model can also simulate small rain events. The new model results obtained in the BINGO project will be used by the municipality to improve the prediction of the duration of insufficient bathing water quality after CSOs.

Throughout the project, field research knowledge and methods were exchanged between the research sites, through the project meetings, WP3 workshops and field trips. Valuable experience was gained by all project partners and concepts and ideas for further monitoring and modelling research have been developed. The monitoring and analysis of water balance components led to an improved understanding of hydrologic processes and an improved capacity to model climate change impacts and adaptation options.

Appendix I: Statistical Downscaling of Global Climate Models for Use in Stormwater Management in Bergen

Guro Heimstad Kleiven

Statistical Downscaling of Global Climate Models for Use in Stormwater Management in Bergen

Trondheim, 22.12.2016

NTNU
Norwegian University of Science and Technology
Faculty of Engineering Science and Technology
Department of Hydraulic and Environmental Engineering

Specialization Project in TVM 4510

NTNU
Kunnskap for en bedre verden

Abstract

Climate change is expected to lead to higher precipitation amounts, in addition to more intense and frequent events. This can give stormwater problems and flooding. Adapting to climate change therefore is essential. This study investigates the applicability of statistical downscaling of Global Climate Models (GCMs) for assessing the effects of climate change on stormwater systems in the mountainous city Bergen. For this purpose, a literature review of the precipitation in Bergen and on statistical downscaling theory is done. In addition, is the local precipitation variations investigated by analyzing the precipitation at seven stations. Big local variations in precipitation are identified, and it is found that the topography influences the precipitation. Statistical downscaling methods seem to be able to transfer the results from GCMs to a sub-daily time step useful for stormwater management. Further may the methods be useful in mountainous areas like Bergen because they give detailed climate information. Representing spatial variations, however, is problematic when using statistical downscaling methods.

Preface

This thesis is submitted to the Norwegian University of Science and Technology (NTNU). It is a product of the course *TVM4510 Water and wastewater engineering, Specialization Project*, which is mandatory for fulfilling the master degree at NTNU. The study has been done at the Department of Hydraulic and Environmental Engineering, and is a part of the EU project BINGO: Bringing INovation to onGOing water management – a better future under climate change. Continuation of the work will be done in my master thesis in spring 2017.

I would like to express my gratefulness to Erle Kristvik for supervision throughout the work with the thesis. Thank you for supporting me by email or in person whenever I have had questions or have needed to discuss a topic. I would also like to thank Tone Muthanna for being my supervisor and for letting me participate on the course *Statistical Downscaling of Global Climate Models using SDSM 5.2.* The course clearly improved my understanding of the topic.

Trondheim, 22.12.2016

Guro Heimstad Kleiven

Contents

List of figures

List of tables

1. Introduction

1.1. Background

The coastal city Bergen is famous its high precipitation amounts. Because of climate change is even higher precipitation amounts and more frequent storm events with higher intensity expected in the future, according to reports like The Fifth Assessment Report (IPCC, 2013) and Klimaprofil Hordaland (NorskKlimaservicesenter, 2016). Heavier rainfall in combination with urbanization and a poor condition on the water and waste water networks can lead to problems with handling the stormwater and by this an increased probability of flood damages (Nilsen et al., 2011). This is an unwanted situation for the Municipality of Bergen, and they are eager to adapt their stormwater management to climate change.

To do so, applying General Circulation Models (GCMs), which simulate the future climate, is a possibility. The GCMs simulate the future climate on a global scale, but the models are too coarse to reproduce detailed climate predictions at the temporal and spatial scale necessary for hydrological assessments (Herath et al., 2016). In other words, they do not give the information the Municipality of Bergen needs to adapt their stormwater systems to climate change. To bridge the gap between the GCMs and the smaller scale, downscaling techniques for translating the large-scale climate to the local scale with high temporal resolution have been developed.

Statistical downscaling methods are widely used for this purpose (see e.g. Benestad et al., 2007; Wilby and Dawson, 2013). They have the advantage of requiring little computer capacity, being cheap and relatively easy to apply. However, these methods are based on statistical relationships between the global climate predictions and the small-scale climate. The complex topography in Bergen, giving local precipitation variations, may limit the applicability of statistical downscaling methods. Therefore, the aim of this thesis is to investigate whether statistical downscaling methods can be used for downscaling GCMs to the spatial and temporal resolution required for stormwater management in the mountainous city Bergen. In addition, an investigation of local variations in precipitation amounts in Bergen will be done. The work is done in relation to EU's project BINGO - *Bringing INovation to onGOing water management – a better future under climate change*. The Damsgård area is the study site in the BINGO project, and the analysis of local precipitation variation is therefore conducted for that area.

1.2. Objectives

The main objectives of the project are:

1) Literature review of:
    a. Precipitation in Bergen
    b. Downscaling (mainly statistical downscaling) to sub-daily time steps
    c. Use of downscaled climate projections in the support of stormwater management
2) Investigation of local variations in precipitation amounts by analyzing measurements from a network of precipitation gauges located in Bergen.
3) Investigate whether statistical downscaling can be used for downscaling precipitation in Bergen to a sub-daily time step useful for stormwater management.

1.3. Thesis structure

The thesis is divided into six parts:

1. **Introduction:** Illuminate the background and motivation for doing the study, in addition to the objectives.
2. **Literature review:** Consists of literature review of (1) The precipitation in Bergen; (2) Projecting climate change; (3) - (7) Downscaling, with focus on statistical downscaling; (8) Use of statistical downscaling in stormwater management.
3. **The study site and data:** The study site, Damsgård, and data availability at the site is presented.
4. **Methodology:** The methodology for investigating local precipitation amounts at the study site is presented.
5. **Results and discussion:** Consists of two parts: (1) Results from the investigation of local precipitation amounts and discussion of the results. (2) A discussion on whether statistical downscaling to sub-daily time step useful in stormwater management can be done in general and in Bergen.
6. **Conclusion:** This part concludes the work done and an outline further work

2. Literature review

2.1. The precipitation in Bergen

Bergen is the second largest city in Norway and is located in Hordaland, at the west coast of the country (Figure 2.1). The city is well-known for its large amount of rainfall, with an annual mean rainfall of 2250 mm (Jonassen et al., 2013). Still, Bergen seems to be experiencing more precipitation than ever, with three rainfall records this summer. July 2016 became the wettest month since 1995, according to Meteorologisk Institutt (NRK, 2016).

The reason for the high precipitation amounts in Bergen can be explained to be the combination of winds and topography. At the coast of Norway, and in Bergen, there is an overweight of winds from the west (Skartveit and Grønås, 2009) and this way winds coming from the open sea. The air is often moisty due to evaporation from the sea. When the air hits the Norwegian mainland, it ascends and the vapor condenses. This is the main reason for the large precipitation amounts at the West Coast and in Bergen, according to Skartveit and Grønås (2009). In the area around Bergen there are steep mountains, making the incoming wind rising higher and therefore giving more precipitation. Bergen has about twice as much annual average precipitation (2250 mm) as Stavanger, with a flatter topography (1250 mm) (Jonassen et al., 2013).

Figure 2.1 The location of Bergen. From Google Maps (Google)

The precipitation in Bergen is not only characterized by large amounts, but also great variations within the city (e.g. Johansen, 2016; Kolstad, 2016). As explained, the topography affects the precipitation at a large scale, but Jonassen et al. (2013) found that because of the strong winds in Bergen, the effect of local mountains is dominating over the larger scale topography. Precipitation caused by the mountains pressing the moist air up and condensation due to temperature differences happens at a large-scale, as explained above, but also at a local scale. In addition, can mountains increase precipitation on the downstream side when the moist air is transported with the wind over the mountain tops, the precipitation elements form, and water fall to the ground. Jonassen et al. (2013) found that this is the case in Bergen, where the largest precipitation amount was found downstream of local mountain tops. Twice as much precipitation was modelled in the city centre as at the top of the mountain Løvstakken. However, removing the mountain Løvstakken in the model, gave lower and more equally distributed precipitation in most parts of the city centre. In other words, the local topography causes big local variations in the precipitation.

There is also a seasonal variation in the precipitation in Bergen, with the most precipitation during autumn (Johansen, 2016). Johansen (2016) found that the winter season has the second most precipitation, whereas whether spring or summer precipitation is highest varies within the city.

2.1.1. Future precipitation in the Bergen region

The report Klimaprofil Hordaland (NorskKlimaservicesenter, 2016) indicate that annual precipitation in Hordaland is expected to increase by approximately 15% at the end of this century. Further it is expected that coastal areas with already high annual precipitation will get the biggest increase. This imply that Bergen can expect even more precipitation in the future than today. In addition, the events with high rainfall intensity will increase in frequency, and also get more intense (NorskKlimaservicesenter, 2016).

2.2. Projecting climate change

According to FN's climate panel are human activities most likely the cause of the climate change that has been seen since 1950 (Hanssen-Bauer et al., 2015). The climate change is also likely to continue in the future (IPCC, 2013). To give an estimate of the future climate, Global Climate Models (GCMs) are developed. GCMs are models that describe processes and interactions in the climatic system (e.g. ocean, atmosphere, land, and soil) using mathematical equations. In the GCMs the climatic system is divided into grid cells with a typical size of 200 x 200 km^2. They simulate the internal variations in the climatic system, in addition to the changes due to the unbalance in the energy exchange with space (Hanssen-Bauer et al., 2015).

The unbalance in the energy exchange with space is due to natural causes (e.g. changes in solar radiation) and human activity (e.g. greenhouse gas emissions and emissions of aerosols). The future human emissions are taken into account in *Representative Concentration Pathways* (RCPs) (IPCC, 2013). Since many factors (e.g. population growth, developments in technology and politics) drive the level of future emissions, is it impossible to know how the emissions will be in the future. Therefore, are RCPs for different scenarios made. The RCPs are numbered after the extra energy the emission scenario will give to the atmosphere. For example, will RCP4.5 give 4.5 W/m^2 extra energy in the atmosphere. The different emission scenarios are fed into the GCMs and give different climatic consequences, exemplified in Figure 2.2.

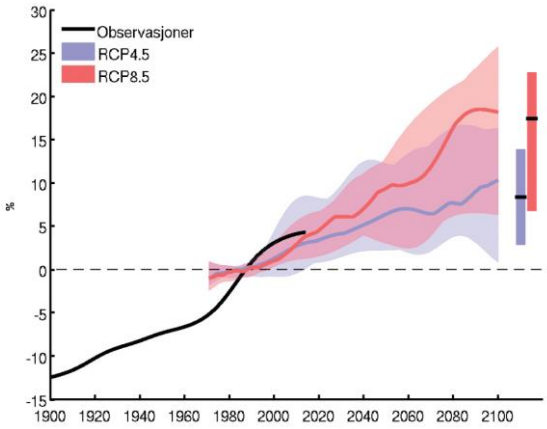

Figure 2.2 Annual precipitation in Norway, given as percent difference from 1971-2000. RCP4.5 represents slightly increased emissions to 2040, and then a reduction. RCP8.5 represents continuously increase in the emissions. From Klima i Norge 2100 (Hanssen-Bauer et al., 2015)

2.3. Downscaling of GCMs

A link between large scale climate and local climate can be obtained by the process of downscaling. Benestad et al. (2007) define downscaling as "the process of making the link between the state of some variable representing the large scale and the state of some variable representing a much smaller scale."

There are two approaches for downscaling: dynamical and statistical. Dynamical modelling is a computer intensive approach which involve making a higher resolution climate model based on the properties, or boundary conditions, of the coarser resolution GCM (Wilby et al., 2002). The higher resolution climate model, also called Regional Climate Model (RCM) describe the modelled area more in detail than the GCM. The other approach, statistical modelling, which is less computationally demanding, utilizes the statistical relationship between the large-scale climate and the local climate to simulate the future climate at a local scale (Benestad et al., 2007). Statistical and dynamical downscaling both have strengths and weaknesses. Those are presented in Table 2.1.

Table 2.1 Strengths and weaknesses by statistical and dynamical downscaling (Modified from Wilby et al., 2002)

	Statistical downscaling	Dynamical downscaling
Strengths	• Station-scale (site specific) climate information from GCM-scale output. Can get point projections • Cheap, computationally undemanding, and readily transferable • Ensembles of climate scenarios permit risk/uncertainty analyses • Flexibility	• 10 – 50 km resolution climate information from GCM-scale output • Respond in physically consistent ways to different external forcing • Resolve atmospheric processes such as orographic precipitation • Consistency with GCM
Weaknesses	• Dependent on the realism of GCM boundary forcing • Choice of domain size and location affects the results • Require high-quality data for model calibration • Predictor-predictand relationships are often non-stationary • Choice of predictor variables affects the results • Choice of empirical transfer scheme affects the results • Low-frequency climate variability problematic	• Dependent on the realism of GCM boundary forcing • Choice of domain size and location affects the results • Require significant computing resources • Ensembles of climate scenarios seldom produced • Initial boundary conditions affect the results • Choice of cloud/convection scheme affects (precipitation) results • Not readily transferred to new regions

2.4. Statistical downscaling

Statistical downscaling assumes that two factors govern the local climate. These are the large-scale climate state and the local physiographic features like topography, land-sea distribution etc. (Wilby et al., 2004). Therefore, local climate information is derived by determining a statistical model which relates large-scale variables to local variables. The large-scale variables are typically called “predictors” in the context of statistical downscaling, while the local variables are called “predictands” (Benestad et al., 2007).

When the statistical model describing the relationship between the predictand and the predictor is determined, the large-scale output from the GCM (predictor) is used in the statistical model to estimate the local climate characteristics (the predictand) (Wilby et al., 2004).

2.4.1. Assumptions behind statistical downscaling

Benestad et al. (2007) present four key assumptions that must be fulfilled for statistical downscaling:

1) *Strong relationship:*
   There is a strong relationship between the large-scale predictor and the small-scale predictand
2) *Model representation:*
   The models must simulate the predictor well. If the predictor is unrealistic, the downscaling results will be wrong
3) *Description of change:*
   The predictor parameter must respond to changes in a similar way as the predictand. Otherwise the statistical downscaling results will not show the changes
4) *Stationarity*
   The statistical relationship between predictor and predictand does not change over time

2.4.2. Main types of statistical downscaling techniques

A widely-used way of classifying statistical downscaling techniques are into the tree groups "weather classification", "regression models", and "weather generators" (Wilby et al., 2002; Wilby et al., 2004). The groups are briefly explained in this section.

Weather typing

Weather typing, or weather classification methods, group local, meteorological variables in relation to different classes of atmospheric circulation (Wilby et al., 2002). The weather patterns are grouped according to the similarities with the nearest neighbors or a reference set (Wilby et al., 2004). Future local climate scenarios are then produced by either resampling from the observed variable distribution, or first generating a new sequence of weather pattern and then resample from the data observed (Wilby et al., 2002).

Weather generators

Weather generators are explained by Wilby et al. (2004). By these models the attributes of a local climate variable are reproduced. Examples of such attributes are mean and variance. The models simulate precipitation occurrence using Markov chains for wet/dry day sequences. Wet-day amounts, temperature and solar radiation are often found based on precipitation occurrence. An example is that dry days may have more sunshine than wet days. Weather generators can be used in downscaling by conditioning the parameters on the large-scale predictors, weather states or precipitation properties.

Regression models

Regression models represent linear or non-linear relationships between the local-scale predictands and the large-scale predictors (Wilby et al., 2004). The different regression models differ from each other by choice of mathematical transfer function, procedure of the statistical fitting, and the choice of predictor variables.

2.5. Sub-daily time step: Temporal downscaling

Downscaling is, as explained, to find a linkage between the global and the local scale climate. What the methods described have in common, is that the smallest temporal resolution they give is on daily basis (Hassan et al., 2014; Herath et al., 2015). For the results from the downscaling to be useful for design of stormwater systems and climate change assessments in regards to stormwater, a higher temporal resolution is necessary (Nilsen et al., 2011). Temporal downscaling, or disaggregation, is a way of converting the output from the statistical downscaling models to the necessary sub-daily temporal resolution.

A possible method for temporal downscaling is Generalized Extreme Value (GEV) distribution. GEV distribution has been widely used to model extreme rainfall events (Herath et al., 2016).

2.6. Correcting for extremes: Bias correction

Statistical downscaling techniques are often most successful at reproducing the mean and represent variability and extremes poorly (Wilby et al., 2004). However, spatially downscaled maximum rainfall can be bias corrected to gain better accuracy for the maximum rainfall series (Herath et al., 2016). In other words, bias-correction can make statistical downscaling methods that best present average values able to also simulate the extreme precipitation better.

2.7. Tools for statistical downscaling

There exist different tools for statistical downscaling. The tools apply one method, or a combination of methods. Examples can be found in literature (e.g. Wilby et al., 2009; Hassan et al., 2014), and are amongst others *Long Ashton Research Station Weather Generator* (*LARS-WG), Statistical Downscaling Model (SDSM)* and *clim.pact*. The last has been further developed and is now called *esd*. They are all freely available tools**.** esd utilizes functions in R, a software for statistical computing, and downscale monthly and daily mean climate scenarios (Wilby et al., 2009). LARS-WG is a stochastic weather generator (Hassan et al., 2014) and it is a tool for producing time series of climate variables at a single site (Wilby et al., 2009). SDSM is also primarily used for single-site downscaling and can be used for downscaling to a daily time resolution (Herath et al., 2016; Wilby and Dawson, 2013).

2.8. Use of statistical downscaling in the support of stormwater management

In this section the possible use of downscaled precipitation in stormwater management will be presented. In general, the downscaled climate projections can give an impression of what can be expected as future design rainfall and this way help assessing what needs to be done to maintain a given performance on the stormwater and sewer network (Arnbjerg-Nielsen, 2008).

The output from the downscaling can be used to make IDF curves, climate factors or a time series for future precipitation (Arnbjerg-Nielsen, 2008; Herath et al., 2016; Nilsen et al., 2011). Climate factors and IDF curves for the future can be used for designing new stormwater and sewer systems. The future IDF curves can be used directly to find design rainfall, and the climate factors can be used for design by multiplying them to the design rainfall given by the present IDF curves.

IDF curves for the future and climate factors can also be used to assess the impact of climate change on current stormwater systems and other hydrological designs (Herath et al., 2016). If combined with runoff models, IDF curves can be used for simulating future runoff, both peaks and volumes, in urban areas (Nguyen et al., 2010). This can further be used e.g. for investigating whether a stormwater pipe will have sufficient capacity in the future or whether flooding can be expected.

Time series for future precipitation can also be used for assessing the climate change's impact on today's infrastructure. Nilsen et al. (2011) downscaled climate projections and made a time

series for future precipitation. The time series was used, in combination with a runoff model, to investigate what can be expected of combined sewer overflows in the future. Having assessed the impacts, Nilsen et al. (2011) proposed solutions for reducing the damage by stormwater in the future.

The results from downscaling is also applicable for use for evaluating the effects of proposed stormwater solutions, like those proposed by Nilsen et al. (2011) (disconnection of roof drains, use of green infrastructure etc.). Wilby and Dawson (2013) state that the best use of downscaled scenarios is for sensitivity testing and adaption options assessments. Assessments of whether e.g. opening a stream will have the desired effect can be done. Solutions can be compared, and the best single solution or combination of solutions can be chosen. The downscaled scenarios can in other words make it possible to estimate which solutions will handle the future precipitation best.

In summary, downscaled future precipitation scenarios can give an impression of consequences of the climate change on today's stormwater systems, be used in design of future stormwater systems, and help assessing the performance of alternative solutions. This way it can contribute in the decision of which solution is best for handling the future precipitation.

3. The study site and data

Damsgård is a residential area in Bergen located close to the city centre and below the mountains Damsgårdsfjellet and Løvstakken (Figure 3.1). It is a focus area in the BINGO project because it is prone to high amounts of runoff, coming both from the mountains above and from the residential area itself. Therefore, the stormwater management in this area is of importance. Local variations are of interest in stormwater management, and therefore are six temporal precipitation stations placed in the area (Figure 3.1), giving the area a higher density of precipitation stations than what is commonly found in Norway.

To investigate the local variations in precipitation, the Damsgård area and the six temporal precipitation stations located there are used. The investigation is done with downscaling GCMs in mind. Therefore, a nearby station in Bergen, at Florida, is used as reference station. This is because Florida station has the longest data record in Bergen, and is therefore most suitable to use in the downscaling process. For stormwater management, however, it is beneficial to have projections of future precipitation other places in Bergen as well. To be able to use the downscaled results from Florida at other places in Bergen, it is desired to find a relationship between Florida and the other stations. Therefore, an investigation of the local variations in general and on the relationship between Florida and stations at Damsgård is done, the last with focus of finding the percentage difference. The percentage difference can easily be used for estimating precipitation other places based on the precipitation at Florida. Special attention is payed to the extreme precipitation as this is what can cause stormwater problems for Bergen Municipality.

3.1. The data

In total seven precipitation stations are used in the analysis. The six stations Gyldenpris, Irene, Frelsesarmeen, Terreng1, Terreng2 and Terreng3 are located at Damsgård. In addition is Florida station at Florida used (Figure 3.1).

Data from the Florida station is from VA-etaten, Bergen kommune, while data from the other stations, placed in relation to the BINGO project, is found at *Regnbyge.no*. Continuous data from all stations is available from May 3rd 2016 to September 27th 2016. The analyzes are done based on data from May 27th to August 27th. One month of data (August 28th to September 27th) is left for validation.

The precipitation data is investigated with a daily, hourly and minute step. Daily data for Florida was not found. Therefore, the hourly precipitation at the station during one day was summarized. Daily precipitation (from midnight to midnight) was by this calculated.

Figure 3.1 The Damsgård area and the precipitation stations used in the study

4. Methodology

4.1. Investigation of local variations in precipitation amounts

A script in R (a programming language for statistical computing) was developed to analyze the data (Appendix J). The same analyzes were done for the daily, hourly and minute data.

The study can be divided into six parts: (1) Difference between daily, hour and minute precipitation; (2) Correlation between the stations; (3) Differences in precipitation amounts; (4) Relationship between Florida and the other stations; (5) Validation; (6) Data quality evaluation.

1) Difference between daily, hour and minute precipitation

Correlation matrices were developed for daily, hourly and minute precipitation (see Table A.1-Table A.3), and differences in correlation between daily, hourly and minute precipitation were compared. In addition, was percentage difference in precipitation between Florida and the other stations found and compared between the time steps (see Figure D.1-Figure D.3 and Figure E.1-Figure E.3). This was done for all the precipitation, and for the extreme precipitation. Ten percent of the rainfall data was assumed to be extreme. The percentage difference was found by first removing days, hours, and minutes with zero precipitation. Afterwards the data was ranked from least to most precipitation at Florida station. The corresponding measurements for the other stations followed the ranking at Florida. For example, follows the precipitation measurements at day number 5 at Gyldenpris the ranking of day number 5 at Florida. The ranked difference in precipitation between Florida and the other stations was calculated, and the percentage difference was found with the following formula:

$$\frac{difference\ between\ the\ stations}{precipitation\ at\ Florida} \times 100\%$$

Finally, the ranked percentage difference between the stations at Damsgård and Florida was plotted.

2) Correlation between the stations

The stations with best and worst correlations were identified by using the correlation matrices developed in step 1).

3) Differences in precipitation amounts

Cumulative mass plots were made to investigate the rainfall amounts (Figure B.1 - Figure B.3).

4) Relationship between Florida and the other stations

The relationship between Florida station and the other stations was investigated for all precipitation, normal precipitation, and extreme precipitation[1]. The ranked precipitation at the stations at Damsgård (found in part 1) was plotted against the precipitation at Florida. So was the ranked difference between the stations at Damsgård and at Florida (found in part1). Further were mean percentage difference for the extremes and mean percentage difference for different precipitation intervals was found (Table G.1 - Table G.3, Figure G.1 - Figure G.3). The applied precipitation intervals are as following:

Table 4.1 Precipitation intervals

Day	**Hour**	**Minute**
0-10 mm	0-2 mm	0-0.5 mm
10-20 mm	2-4 mm	0.5-1.0 mm
20-30 mm	4-6 mm	1.0-1.5 mm
30-40 mm	6-8 mm	over 1.5 mm
40-50 mm	8-10 mm	
50-60 mm	10-16 mm	
over 60 mm	over 16 mm	

5) Validation

The percentage difference in precipitation between Florida and the other stations was validated using data from August 28th to September 27th. The same R scripts and precipitation intervals as for the original data sets were used. In addition, was the percentage difference for the validation data and for the original data compared by plotting them together (see Figure H.1 - Figure H.3). A new script was made for this (Appendix J).

6) Data quality evaluation

The cumulative mass plots were used to see whether the stations follow the same rainfall patterns (Figure B.1 - Figure B.3). Double mass plots were also made to check the consistency of the data (Figure C.1 - Figure C.3)

[1] 10% of the precipitation is assumed to be extreme

5. Results and discussion

5.1. Investigation of local variations in precipitation amounts

5.1.1. Difference between daily, hour and minute precipitation

The daily precipitation at the different stations correlate well with each other (>0.964) (Table A.1). The correlation is best for daily precipitation, whereas the correlation between the stations for minute precipitation is generally poor (<0.459) (Table A.3). The correlation level for hourly precipitation is between the correlations for daily and minute (0.564 < correlation < 0.970) (Table A.2). The reason for the poorer correlation at hourly, and especially minute precipitation, might be that the rain event is coming from one direction, giving rain at one place before another. Even though it will rain approximately the same at all stations during a day, this is not reflected in the correlation for minute precipitation as the weather might be moving, giving different intensities at different time at the stations. The percent difference in precipitation from Florida is in average bigger at hourly basis than at daily basis for all stations, exemplified by Terreng2 in Figure 5.1. (See also Figure F.1 - Figure F.3.) This can be argued to underline the statement of that it is raining differently at different places at the same time.

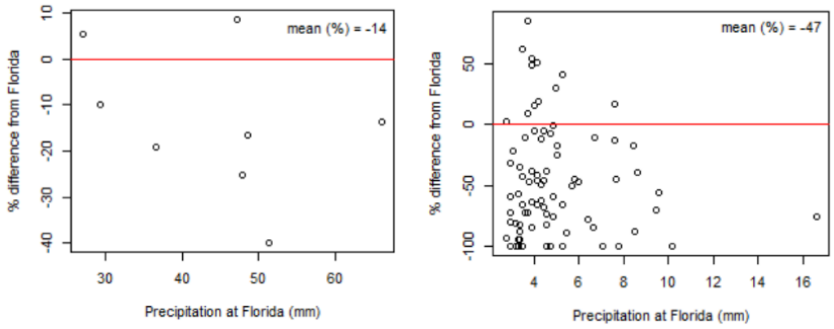

Figure 5.1 Percentage difference in extreme precipitation between Terreng2 and Florida. Left: Daily extreme precipitation. Right: Hourly extreme precipitation

5.1.2. How location matters – correlation between the stations

Gyldenpris has the best correlation to Florida (Table A.1 - Table A.3), and is also the station located closest to Florida (Figure 3.1). Irene, on the other hand, has the poorest correlation to Florida (Table A.1 -Table A.3). Terreng1, Terreng2 and Frelsesarmeen have the best or amongst the best correlations, and are located close to each other at the north-eastern side of the Løvstakken mountain. Terreng3 correlate best to Terreng2, and after that to Terreng1 and Frelsesarmeen. These are the closest stations to Terreng3, but Terreng3 is located at the other side of the mountain. If the weather is coming from west (section 2.1), there is a valley in the mountain where it seems like the weather can pass (Figure 3.1). This can explain the good

correlation. Irene, which is located north-west for the other stations, correlate best to the station closest, Gyldenpris. Irene correlate worst to Terreng1, 2 and 3. Overall it is seen that the stations closest to each other correlate best.

5.1.3. How location matters – precipitation amounts

The cumulative mass plots for daily, hourly and minute precipitation give similar results. All the stations follow the same precipitation pattern, but the amount of precipitation is varying (see Figure 5.2, Figure B.1and Figure B.3). It is seen in section 5.1.2 that the stations closest to each other correlate best. For the precipitation amounts, however, it is not that simple. First, Florida has the most precipitation even though the closest station, Gyledenpris, has the second least precipitation. The precipitation amounts at Florida will be further commented in section 0. Irene has the least precipitation. This might be explained by Damsgårdfjellet being a barrier for the weather coming from west (section 2.1 and Figure 3.1). The same effect can be seen for Gyldenpris and Frelsesarmeen, having Løvstakken as barriers. They are both amongst the stations with the least precipitation. What is interesting, is that Terreng3 and 1 have almost the same precipitation amounts, whereas Terreng2, which is located between them, has less precipitation (Figure 5.2). This means that distance between the stations is not the only thing that matters for the precipitation relationships. Terreng2 is located at a hill top, and Terreng3 and 1 at each side of the same hill. This indicates that the topography may be important for the precipitation amounts.

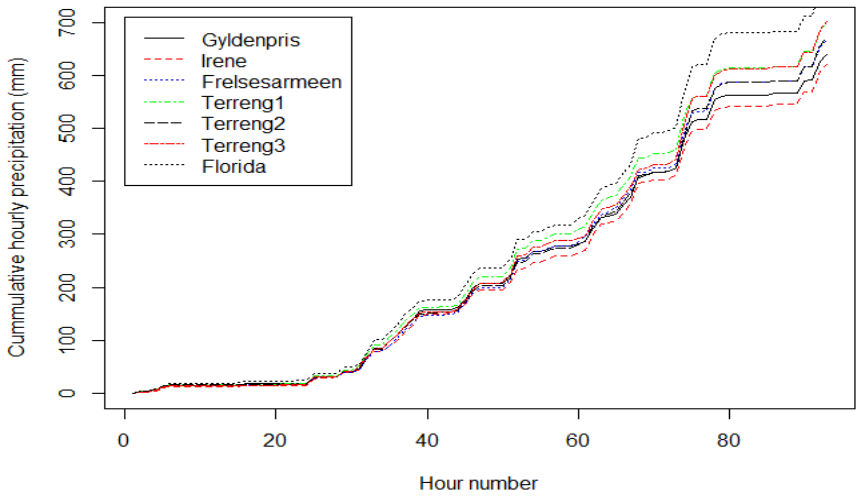

Figure 5.2 Daily cumulative mass plot for all the investigated weather stations

5.1.4. Relationship between Florida and the other stations

For all the stations the difference in precipitation compared to Florida increase with more intense events, while the percentage difference decrease with higher intensity (exemplified with Gyldenpris in Figure 5.3, see also Appendix D and Appendix E). The trend is seen for daily, hourly and minute precipitation. This makes sense as a small difference can be a big part of the rainfall when the rainfall amount is small. E.g. is the percentage difference between 0.2 mm and 0 mm big even though the absolute difference is small.

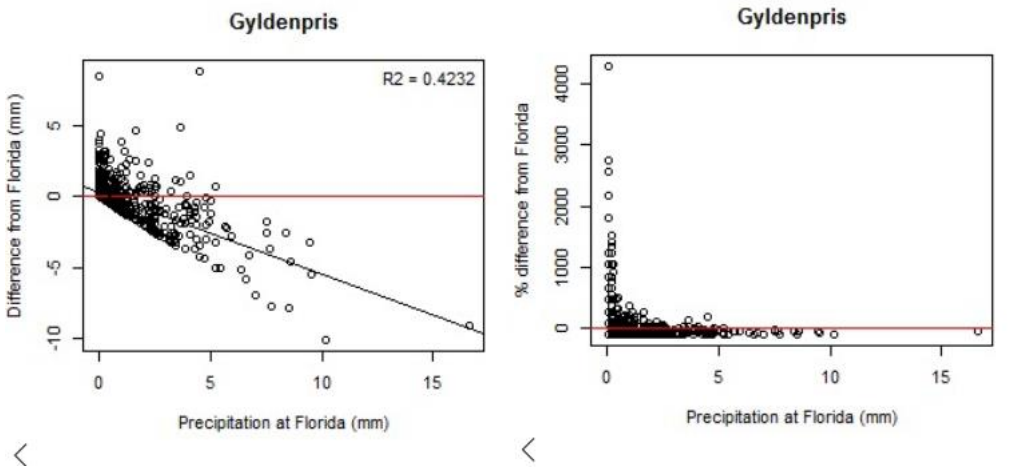

Figure 5.3 Left: Difference in precipitation from Florida (hours). Right: Percentage difference in precipitation from Florida. The trend is the same for all stations, for daily, hourly and minute precipitation, see Appendix D and Appendix E.

However, the relationship between Florida and the other stations is most interesting for the extreme precipitation, as this is what can give the Municipality in Bergen problems with stormwater handling. The relationship expressed as mean difference for all the extreme precipitation was found too coarse as it will not reflect the variation in percentage difference for different intensities (e.g. Figure 5.4). Using the average difference for different precipitation intervals reflect the variation better (see Figure 5.4, Figure E.1 and Figure E.3). In addition, is the range which is described as extreme large, e.g. ca. 3 mm – over 16 mm for daily precipitation. Dividing into smaller intervals therefore seems reasonable. However, one can comment on that the average this way will be more influenced by single observations since few observations are used in the analysis. In addition, even though the precipitation is divided into intervals, there is still a large range in the percentage difference within the intervals. As Figure 5.4 shows, using the mean percentage difference does not reflect the temporal variations in percentage difference between Florida and the other stations. Using this relationship can therefore lead to underestimations of the variations. This implies that the relationship might

not be beneficial to use in combination with statistical downscaling to describe the spatial variations in precipitation for stormwater purposes.

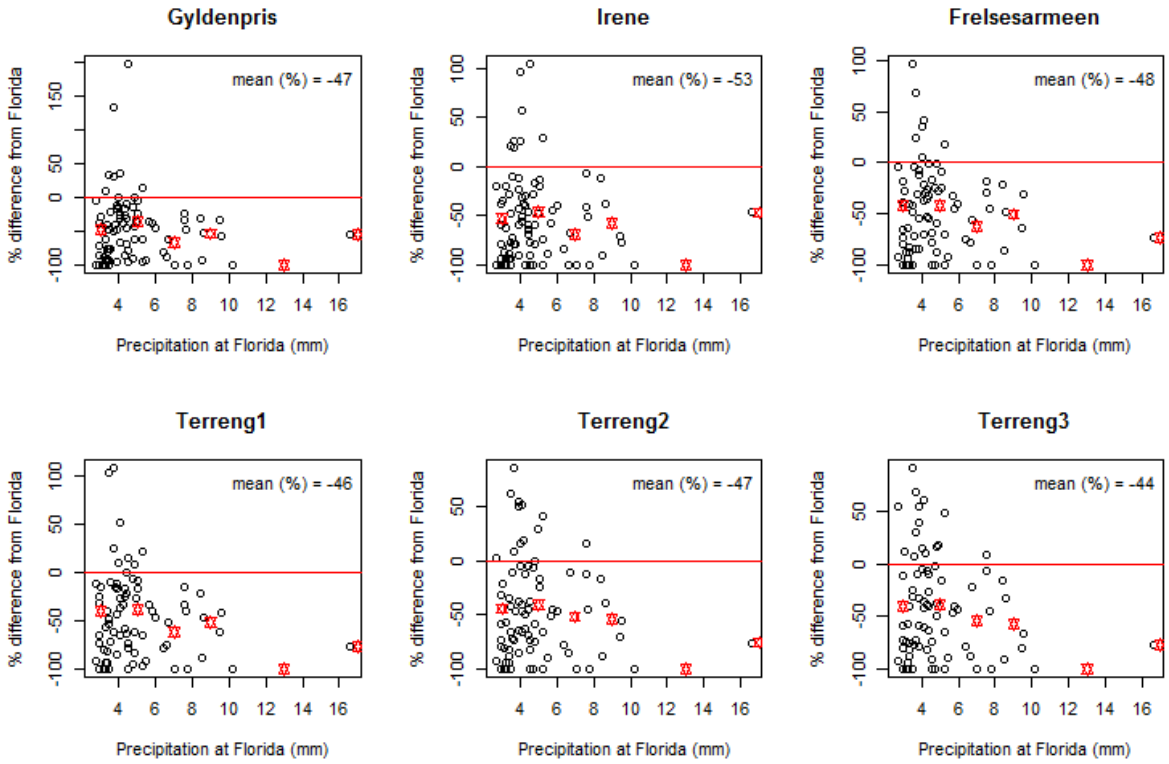

Figure 5.4 Percentage difference from Florida (hourly data), showing the mean for all the extreme precipitation, and the mean for different intervals (red dots).

5.1.5. Validation

The data used for validation gave different interval means than the first data period (Table H.1 - Table H.3, Figure H.1 - Figure H.3). This strengthens the statement of that using a factor like percentage difference for representing the relationship between the stations may not be accurate enough for use in stormwater management. The difference between original and validation data is bigger for minute precipitation than for hour and daily precipitation. This underlies that it might be raining one place and not another at a short period, but that this will be evened out during a longer period.

5.1.6. Limitations of the work

Data quality

Raw data from all stations is used. Because of time limitations a proper quality control and correction of the data was not done. In addition, the strongest doubt regarding data quality is to Florida, and data from this station will be corrected by MET in the future. Therefore, the focus was on developing good scripts which can be used for analyzes on corrected data later rather than on correcting the data.

Florida has much higher cumulative precipitation than the other stations (Figure B.1 - Figure B.3). The double mass plots give indications of somewhat poor quality of the Florida data (Appendix C). The double mass plots indicate that some changes in gauging conditions at Florida might be happening at approximately 70 mm precipitation and 500 mm precipitation because there are some shifts in the double mass plots. This is especially evident for the minute precipitation (Figure C.3). The cumulative mass curve for minute precipitation indicate the same: it has a sudden shift, where Florida suddenly has higher precipitation than the other stations (Figure B.3). This is confirmed by the correlation for hourly precipitation, where Florida correlates poorer than the other stations to each other.

Data period

The period with data available is short (under five months). It was chosen not to use data from the first days of the measuring period. This was done to avoid using wrong measurements due to initial problems, and to get exactly four months' investigation period. In addition, there was little rainfall in May, meaning that the days not included in the analysis did not give valuable information anyway.

The short investigation period limits the confidence of the results because

- The data only represent the rainfall during summer and autumn
- The precipitation variations only in 2016 is evaluated. Since data from one single year is used, variations between different years are not reflected

5.2. Downscaling to a resolution useful for stormwater management in Bergen

A discussion of whether statistical downscaling can be used for downscaling precipitation in Bergen to a sub-daily time step useful for stormwater management is presented in this section. The discussion is based on the literature review and the conducted study of precipitation variations in Bergen.

5.2.1. Uncertainties

Dynamical and statistical downscaling methods are equally good on estimating weather variables under current climate conditions (Wilby et al., 2002). The major challenge when projecting future climate, however, is the GCMs. A weakness for both downscaling approaches is that the results are very dependent on the chosen GCM(s) (Table 2.1). As described in section 2.2, the GCMs are developed based on RCPs, representing different emission scenarios, which have uncertainties connected to them. Several authors (e.g. Herath et al., 2016; Nilsen et al., 2011) present the GCMs and emission scenario selection as one of the main sources of uncertainty in projection of future climate. Nilsen et al. (2011) relate this especially to that only one single GCM, based on one single emission scenario was used. Wilby et al. (2004) state that multiple GCM outputs must be used to make the downscaling applicable for impact studies. From that it can be argued that there are big uncertainties connected to the GCMs, but that they can be reduced by using several GCMs and emission scenarios as inputs for the downscaling.

One of the main assumptions of statistical downscaling is stationarity. It is assumed that the same statistical relationships will apply in the future as in present (and past) (section 2.4.1). This is not verifiable and is the major theoretical weakness of statistical downscaling (Wilby et al., 2004). However, the authors further explain that this is a limitation that applies for the physical parameterization of dynamical models as well. Hence, this limitation is not an argument for choosing either dynamical or statistical downscaling over the other, it is rather an assumption that increases the uncertainty of downscaling in general.

From what is seen above, downscaling adds spatial precision, but of a questionable accuracy due to the biases in the climate models and uncertainties in the downscaling process. This does not mean that downscaling is value-less, but it should affect how the models are used (Wilby and Dawson, 2013).

5.2.2. Usefulness for stormwater management

The spatial resolution obtained by dynamical and statistical downscaling differs the two methods. GCMs have resolution of hundreds of kilometers whilst RCMs can have resolutions down to tens of kilometers (Table 2.1). The needed spatial resolution for stormwater assessments is however one to five km^2 (Nilsen et al., 2011). Since statistical downscaling can give point projections (Table 2.1), this approach can be argued to be the most suited for stormwater assessments. It gives the spatial resolution needed for stormwater management.

Another advantage of statistical downscaling methods is the little computer capacity required (section 2.3). This facilitate the use of the methods by others than climate researchers. Statistical downscaling methods can therefore be used e.g. by water engineers for stormwater assessments.

Nevertheless, as described in section 2.6, the statistical downscaling approaches are not describing extremes well. In stormwater management however, the extremes might be what is most interesting. Bias correction makes the extremes better represented (section 2.6), and can therefore make statistical downscaling more applicable for stormwater management.

As stated in section 2.5, describing the extreme rainfall properly is not the only important aspect in downscaling climate projections for use in stormwater management. The temporal resolution is also of importance. Many of the statistical downscaling methods do not give the sub-daily temporal resolution necessary for stormwater management assessments. Therefore, temporal disaggregation can be useful (section 2.5). Temporal disaggregation is applied in literature (e.g. Arnbjerg-Nielsen, 2008; Herath et al., 2016) and suggests that statistical downscaling combined with a temporal disaggregation can give output useful for stormwater management.

5.2.3. Applicability in Bergen

Bergen is a mountainous city. The current and other studies show that this highly influences the precipitation. Big local variations are found even within a small area like Damsgård (section 5.1). Therefore, the question of whether statistical downscaling can be used for stormwater management purposes in Bergen arises.

Due to the complex topography of the Alps, a study from this site (Schmidli et al., 2007) may be representing for Bergen. Schmidli et al. (2007) found that RCMs performed generally better than or equal to the statistical methods. Because of divergent results for the RCMs and statistical downscaling methods during summer, the authors raise the question of whether the

RCM changes are mainly governed by local physical processes like orographic precipitation and land use, and not the large-scale circulation changes. As the statistical methods mainly focus on the statistical relationship between the large and local scale climate, the physical processes may not be reflected. Statistical methods reflect e.g. not land-use changes. The importance of land-use change and other local physical processes can be argued to be determining for whether statistical downscaling can be used in Bergen.

From this, it may seem like statistical downscaling will be inaccurate in describing the climate in Bergen. On the other hand, Schmidli et al. (2007) suggest that details of the downscaling are of high importance during summer because of stochastic mesoscale processes. This can be an argument for that downscaling to the high resolution useful in stormwater management is more accurate than the coarse resolution downscaled to in the study conducted by Schmidli et al. (2007). This is underlined by Wilby et al. (2004), who state that statistical downscaling methods are particularly useful in heterogeneous environments like mountainous areas. This is because statistical downscaling methods give site-specific information, and therefore will reflect the detailed processes at this point. Statistical downscaling to a point-scale therefore is argued to be more accurate than using RCMs in mountainous areas.

Nevertheless, even though accurate information can be gained at the downscaling point, the spatial variations in the area will not be reflected by downscaling to one point. To capture the variations, it might therefore be useful to downscale to several points in the area of interest. However, this might be problematic since statistical downscaling only is possible with high-quality climate data available (Table 2.1). Having several climate stations with long records within a small area might not be realistic. Therefore, an alternative might be to downscale to one station with quality data and convert the results to other locations. A perquisite is that a good relationship between the downscaling station and other locations is found. For obtaining this, different stations across the area with reasonable time record is needed (the temporal stations at Damsgård might e.g. not have long enough record, see 5.1.6). Therefore, it seems like spatial variations in precipitation can be captured if high-quality data from several stations across the area is available. In Bergen, there is a reasonable number of high-quality stations, but since there are big variations even between locations that are spatially close (5.1), there might not be enough stations to reflect the big local variations accurately.

6. Conclusion

Statistical downscaling methods can bridge the gap between the large scale GCMs and the local scale climate. The aim of this thesis was to investigate whether statistical downscaling methods can be used for downscaling to the spatial and temporal resolution required for stormwater management in the mountainous city Bergen. The study consisted of three parts: (1) a literature review of the precipitation in Bergen and downscaling (mainly statistical) theory, (2) an investigation of local precipitation variations at Damsgård, Bergen, using the programming language R, and (3) an investigation of whether statistical downscaling can be used for downscaling precipitation in Bergen to a sub-daily time step.

From the literature review it is seen that there are great local variations in the precipitation in Bergen. The precipitation analyses conducted in this study show the same, but at a smaller scale. There are big variations also within a small area like Damsgård. Further it appears that the stations closest to each other correlate best, but the precipitation amounts also seem to be influenced by topography. Florida is the station with most precipitation. Representing the relationship between Florida and the other stations as percentage difference seems to not reflect the temporal variation in precipitation differences well. It is therefore concluded to not be beneficial to use this relationship in combination with statistical downscaling to describe the spatial variations for stormwater purposes.

It seems like statistical downscaling can be used for translating GCMs to a sub-daily time step useful for stormwater management if a combination of statistical downscaling, bias-correction and temporal downscaling is used. Nevertheless, it is important to be aware that there are great uncertainties related to the GCMs and the downscaling process. However, the uncertainties can be somewhat reduced e.g. by using several GCM inputs in the downscaling. Being aware of the uncertainties and using the results as a guidance rather than a truth also seem to be important.

Further it seems like statistical downscaling methods are appropriate to use mountainous areas like Bergen because statistical downscaling captures the detailed climate and temporal variation at the downscaling point. However, this does not reflect the spatial variation in the area. To reflect the spatial variation, one can downscale to different points, or transfer the downscaled results to other locations using a developed relationship between the locations. For this, several high-quality stations are needed. Some exist in Bergen, but it might not enough to

reflect the high spatial variations identified in this study. The spatial variations will therefore not be represented as accurate as necessary for stormwater management, even though some indications of the variations can be obtained. Another limitation with statistical downscaling seems to be that it does not reflect changes in physical processes like land-use. It can be concluded that statistical downscaling methods can give the sub-daily time scale necessary for stormwater purposes, but there are challenges connected to representing the spatial precipitation variations in Bergen well.

6.1. Further work

6.1.1. In general

Further work on representing the spatial precipitation variations seems beneficial. This can be done by establishing and operating more precipitation stations for a longer period, and by this getting high-quality data. Further work is also suggested on establishing a good relationship between e.g. Florida and other already existing stations in order to downscale climate projections to one station, and then transfer the results to other locations. Since the precipitation in Bergen is to a high extent driven by topography and winds, investigating the relationship based on e.g. different wind directions might be of interest. To make the results more useful in a stormwater management perspective, the intensity and duration of the rainfall events could also be considered when developing a relationship.

6.1.2. In the master thesis

The tool SDSM (section 2.7) is intended to be used to downscale GCMs statistically to Florida station. This will give a point-scale spatial resolution. Temporal disaggregation will be done to get a sub-daily time scale. The results will be used to evaluate the design criteria for a raingarden under future climate conditions.

Appendix A Correlation matrices

Table A.1 Correlation matrix for daily precipitation

	Gyldenpris	Irene	Frelsesarmeen	Terreng1	Terreng2	Terreng3	Florida
Gyldenpris	1.000						
Irene	0.989	1.000					
Frelsesarmeen	0.983	0.970	1.000				
Terreng1	0.989	0.978	0.996	1.000			
Terreng2	0.973	0.964	0.981	0.981	1.000		
Terreng3	0.973	0.965	0.982	0.982	0.997	1.000	
Florida	0.991	0.977	0.985	0.987	0.979	0.978	1.000

Table A.2 Correlation matrix for hourly precipitation

	Gyldenpris	Irene	Frelsesarmeen	Terreng1	Terreng2	Terreng3	Florida
Gyldenpris	1.000						
Irene	0.910	1.000					
Frelsesarmeen	0.914	0.860	1.000				
Terreng1	0.932	0.876	0.983	1.000			
Terreng2	0.904	0.867	0.962	0.970	1.000		
Terreng3	0.881	0.860	0.939	0.946	0.970	1.000	
Florida	0.603	0.564	0.599	0.582	0.589	0.579	1.000

Table A.3 Correlation matrix for minute precipitation

	Gyldenpris	*Irene*	*Frelsesarmeen*	*Terreng1*	*Terreng2*	*Terreng3*	*Florida*
Gyldenpris	1.000						
Irene	0.255	1.000					
Frelsesarmeen	0.321	0.216	1.000				
Terreng1	0.353	0.233	0.428	1.000			
Terreng2	0.331	0.236	0.408	0.459	1.000		
Terreng3	0.294	0.230	0.310	0.315	0.349	1.000	
Florida	0.356	0.260	0.328	0.341	0.301	0.267	1.000

Appendix B Cumulative mass plots

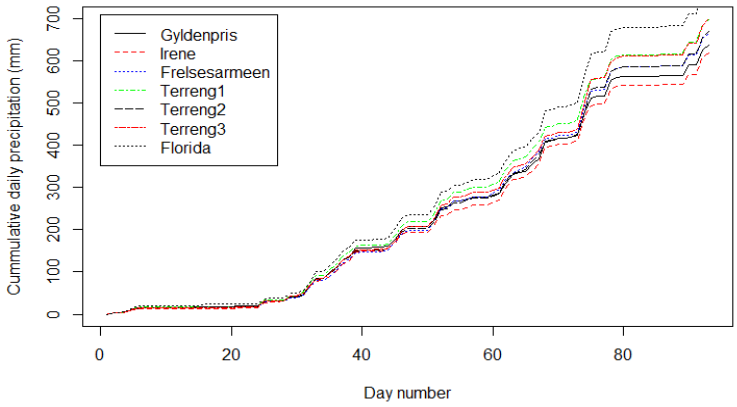

Figure B.1 Cumulative mass plot for daily precipitation

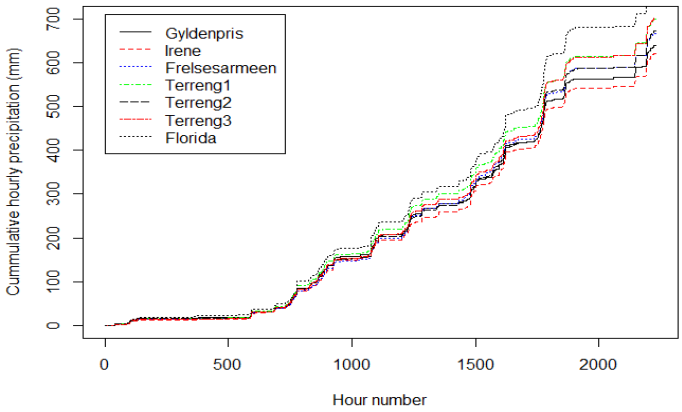

Figure B.2 Cumulative mass plot for hourly precipitation

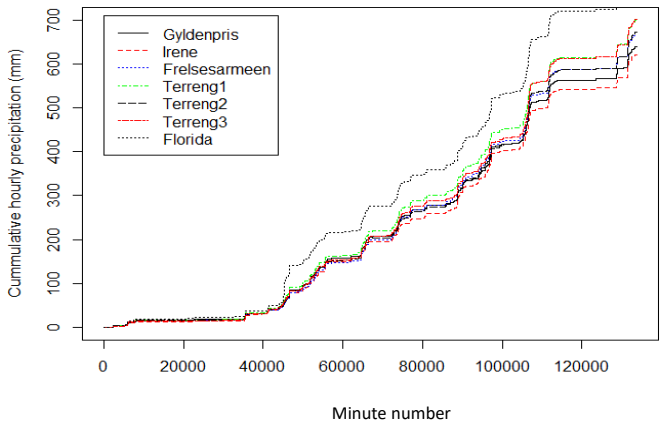

Figure B.3 Cumulative mass plot for minute precipitation

Appendix C Double mass plots

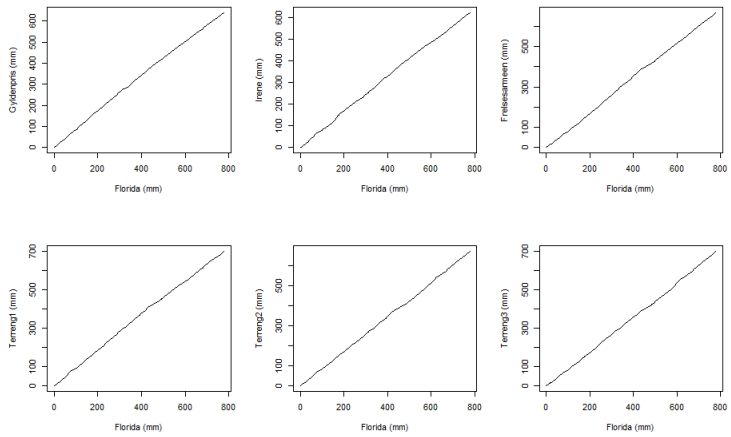

Figure C.1 Double mass plots for daily precipitation

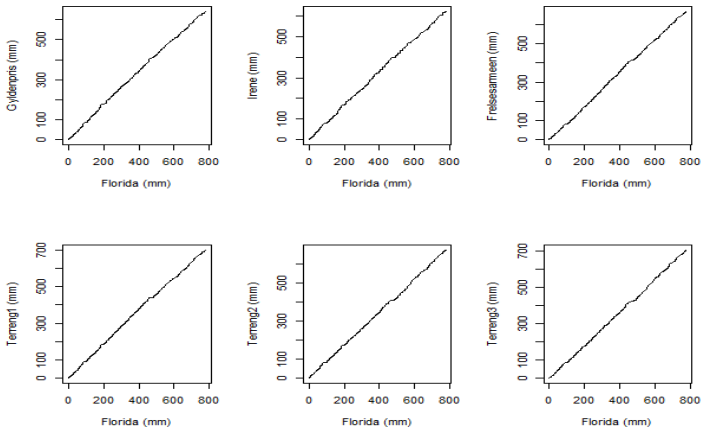

Figure C.2 Double mass plots for hourly precipitation

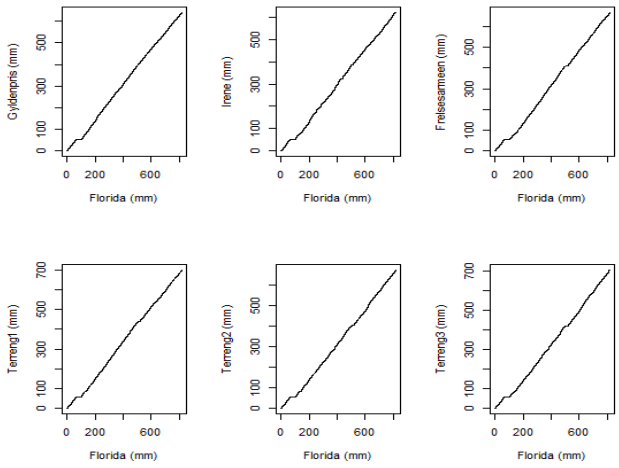

Figure C.3 Double mass plots for minute precipitation

Appendix D Difference in precipitation between Florida and the other stations

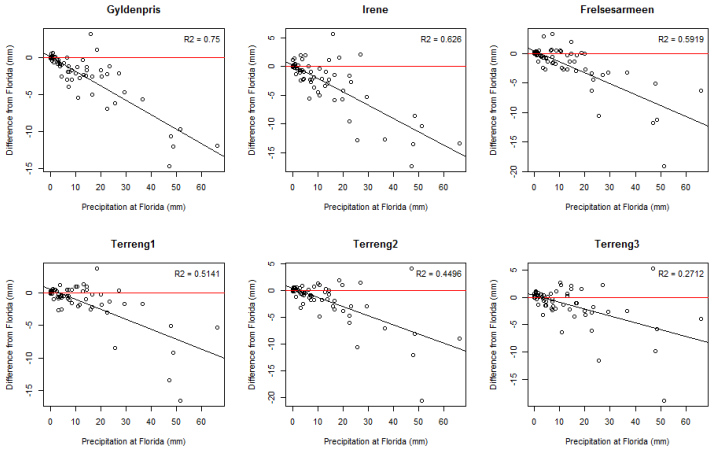

Figure D.1 Difference in daily precipitation between Florida and the other stations

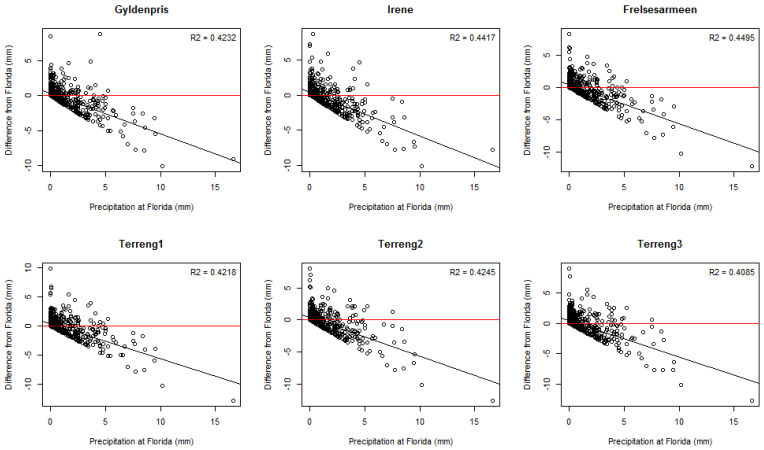

Figure D.2 Difference in hourly precipitation between Florida and the other stations

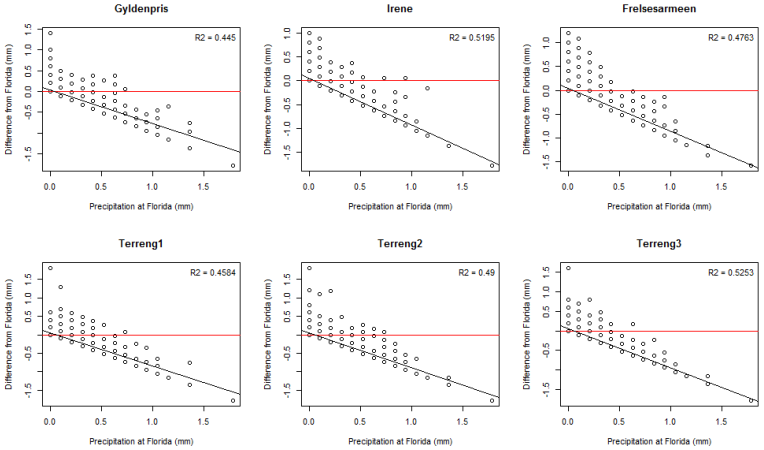

Figure D.3 Difference in minute precipitation between Florida and the other stations

Appendix E Percentage difference in precipitation between Florida and other stations

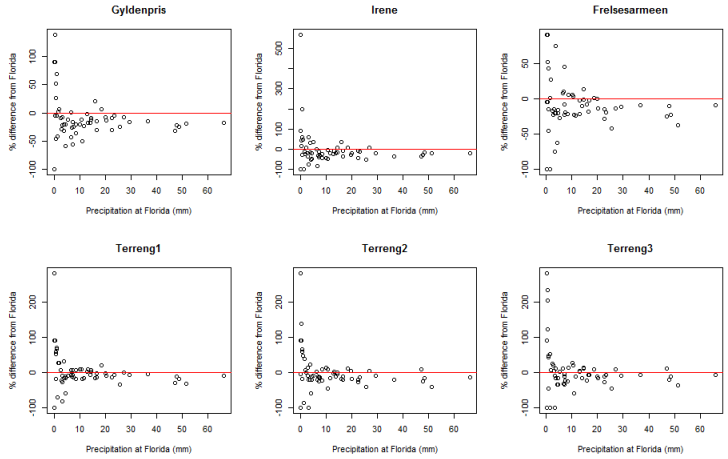

Figure E.1 Percentage daily precipitation difference between Florida and other stations

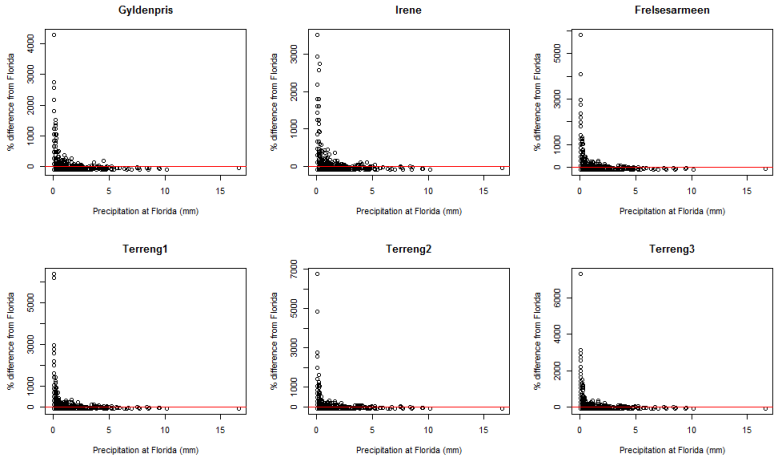

Figure E.2 Percentage hourly precipitation difference between Florida and other stations

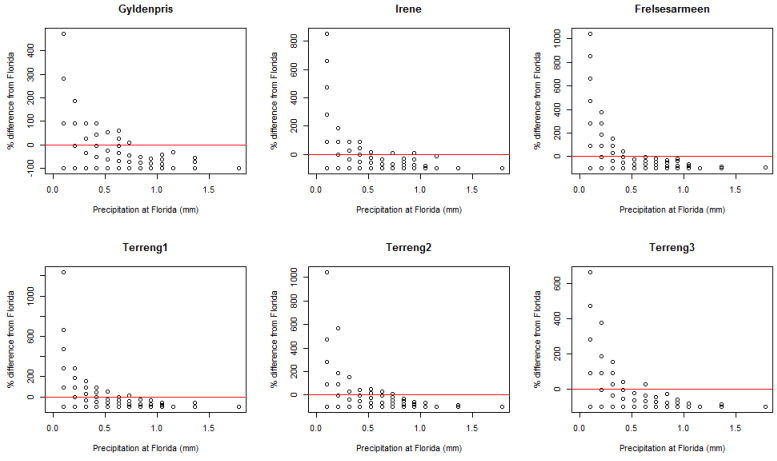

Figure E.3 Percentage minute precipitation difference between Florida and other stations

Appendix F Percentage difference for extreme precipitation

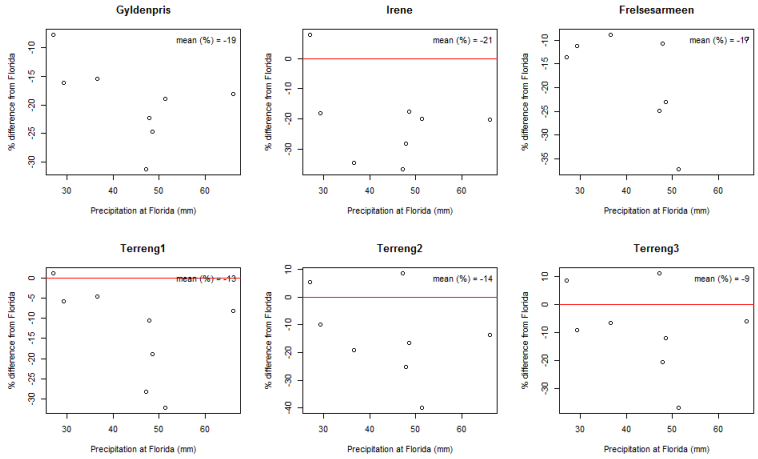

Figure F.1 Daily percentage difference in precipitation compared to Florida

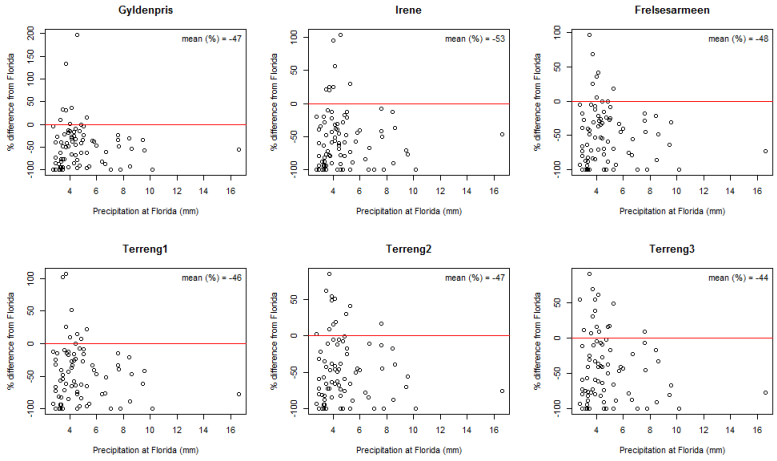

Figure F.2 Hourly percentage difference in precipitation compared to Florida

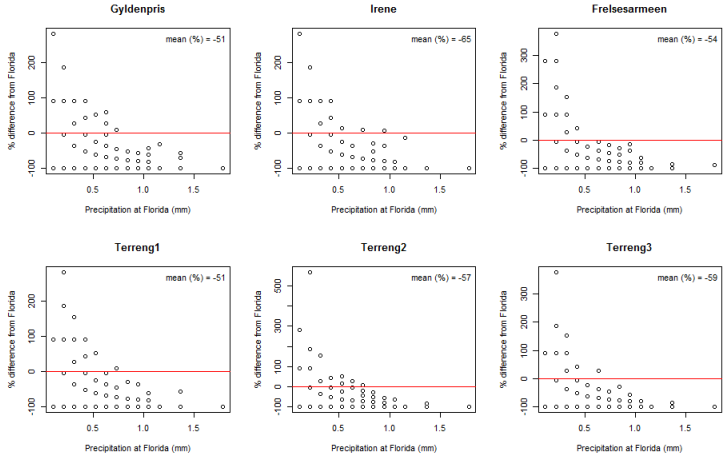

Figure F.3 Minute percentage difference in precipitation compared to Florida

Appendix G Mean percentage difference for different intervals

Table G.1 Daily mean percentage difference in precipitation from Florida

	Gyldenpris	Irene	Frelsesarmeen	Terreng1	Terreng2	Terreng3
0-10 mm	-8.3	9.8	4.9	8.8	5.5	21.7
10-20 mm	-13.6	-14.6	-6.1	-0.9	-6.5	-3.2
20-30 mm	-15.1	-20.3	-20.4	-11.2	-17.8	-15.5
30-40 mm	-15.4	-34.5	-8.9	-4.5	-19.2	-6.7
40-50 mm	-26.1	-27.6	-19.5	-19.3	-11.0	-7.1
50-60 mm	-19.0	-20.1	-37.3	-32.2	-40.0	-36.9
over 60 mm	-18.1	-20.2	-9.6	-8.1	-13.5	-6.0

Table G.2 Hourly mean percentage difference in precipitation from Florida

	Gyldenpris	Irene	Frelsesarmeen	Terreng1	Terreng2	Terreng3
0-2 mm	93.2	94.5	117.6	130.4	123.0	127.6
2-4 mm	-47.5	-53.0	-42.2	-40.6	-44.1	-40.2
4-6 mm	-36.0	-46.2	-42.1	-38.8	-41.1	-38.8
6-8 mm	-66.9	-68.9	-62.6	-61.9	-51.9	-54.1
8-10 mm	-54.0	-57.4	-50.2	-51.9	-54.2	-57.5
10-16 mm	-100.0	-100.0	-100.0	-100.0	-100.0	-100.0
over 16 mm	-55.4	-47.0	-73.5	-77.1	-75.9	-77.1

Table G.3 Minute mean percentage difference in precipitation from Florida

	Gyldenpris	Irene	Frelsesarmeen	Terreng1	Terreng2	Terreng3
0-0.5 mm	-53.0	-59.8	-52.1	-49.7	-53.1	-54.1
0.5-1.0 mm	-76.1	-85.8	-79.8	-76.7	-77.8	-86.8
1.0-1.5 mm	-87.8	-94.1	-95.7	-94.3	-97.5	-98.4
over 1.5 mm	-100.0	-100.0	-88.8	-100.0	-100.0	-100.0

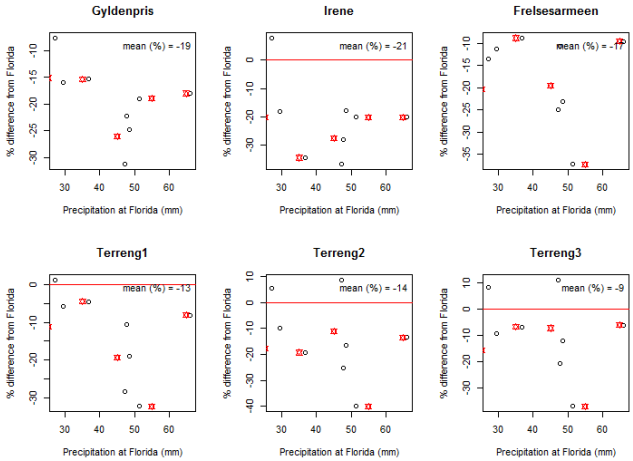

Figure G.1 Daily mean percentage difference in extreme precipitation compared to Florida. Showing the mean for all the extreme precipitation, and the mean for different intervals (red dots).

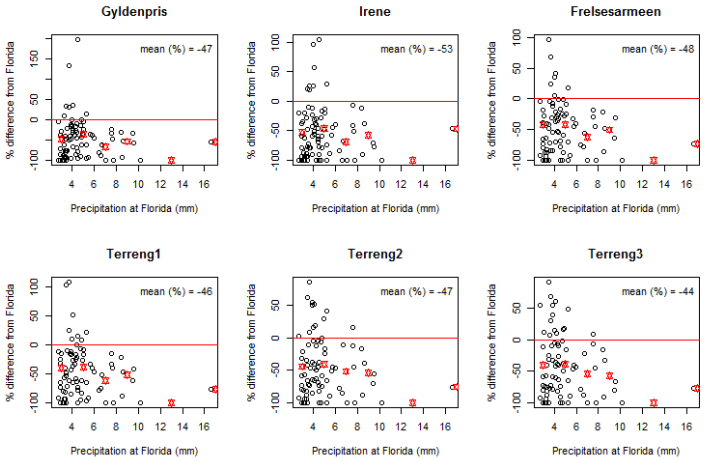

Figure G.2 Hourly mean percentage difference in precipitation compared to Florida. Showing the mean for all the extreme precipitation, and the mean for different intervals (red dots).

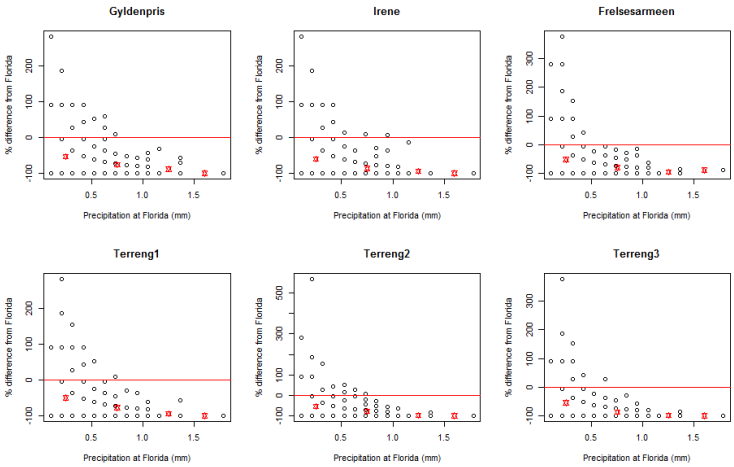

Figure G.3 Minute mean percentage difference in extreme precipitation compared to Florida

Appendix H Validation

Table H.1 Daily mean percentage difference in precipitation from Florida (validation data)

	Gyldenpris	Irene	Frelsesarmeen	Terreng1	Terreng2	Terreng3
0-10 mm	-13.92586	-19.1158	-22.52842901	15.02084	0.2143712	-19.75631
10-20 mm	-22.05023	-20.61629	-11.87404125	-9.818546	-9.862191	-8.626417
20-30 mm	-17.26473	-19.35837	3.121201964	2.1546523	-8.012489	0.1923798
over 60 mm	-7.91078	-21.10737	-15.36971957	-7.623897	-7.050133	-6.476368

Table H.2 Hourly mean percentage difference in precipitation from Florida (validation data)

	Gyldenpris	Irene	Frelsesarmeen	Terreng1	Terreng2	Terreng3
0-2 mm	60.394332	56.789508	71.51100186	83.899266	75.157525	93.729476
2-4 mm	-21.2034	-26.07205	-8.365176734	-8.955536	-12.36907	-7.091942
4-6 mm	-32.75857	-32.48088	-29.64637172	-28.71053	-29.43954	-26.3878
6-8 mm	-67.4913	-72.38054	-73.53816401	-69.65673	-72.53035	-70.51473
8-10 mm	-95.671	-95.671	-94.58874459	-95.671	-95.671	-96.75325
10-16 mm	-94.59459	-97.2973	-90.54054054	-93.24324	-93.24324	-93.24324

Table H.3 Minute mean percentage difference in precipitation from Florida (validation data)

	Gyldenpris	Irene	Frelsesarmeen	Terreng1	Terreng2	Terreng3
0-0.5 mm	174.79413	178.01647	212.7461511	232.9753	224.02435	231.60282
0.5-1.0 mm	-14.78962	-19.48381	-5.638227513	-6.497229	-12.31182	-10.38675
1.0-1.5 mm	-20.08424	-19.87432	-24.87058645	-17.74422	-22.44236	-22.91009
over 1.5 mm	-44.13913	-47.87203	-39.77273455	-37.51515	-40.31749	-38.59041

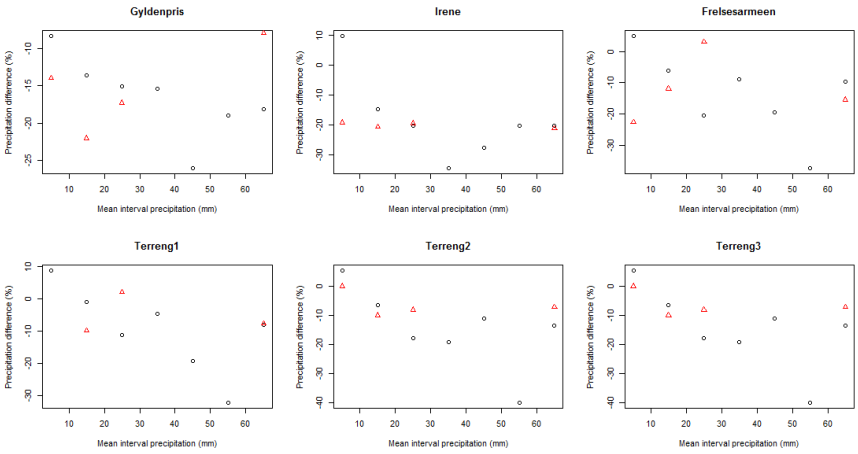

Figure H.1 The percentage difference for different precipitation intervals, daily values. Black: original data. Red: validation data

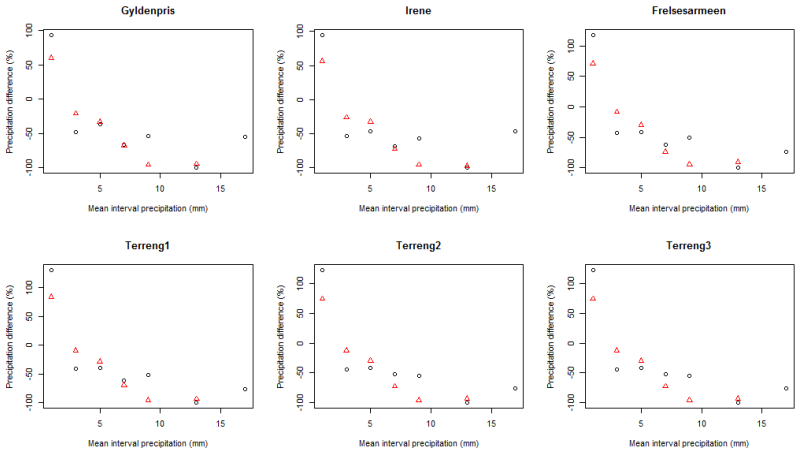

Figure H.2 The percentage difference for different precipitation intervals, hourly values. Black: original data. Red: validation data

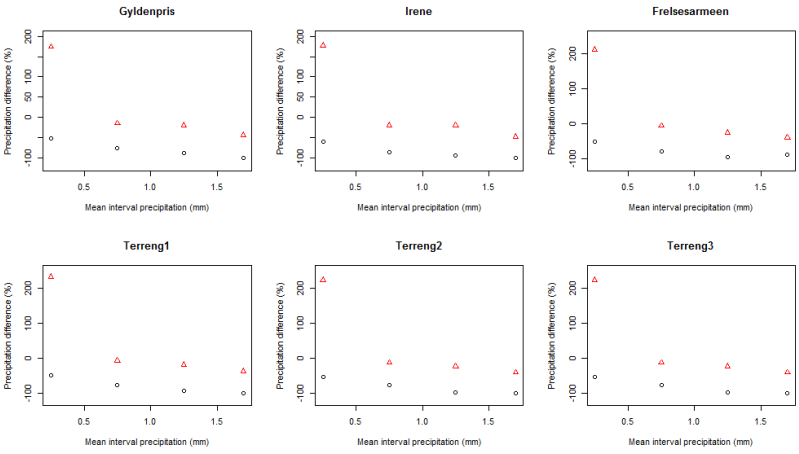

Figure H.3 The percentage difference for different precipitation intervals, minute values. Black: original data. Red: validation data

Appendix I Comment on the plots for minute precipitation

The plots for minute precipitation (e.g. Figure F.3, Figure D.3 and Figure E.3) have few points. Considering that there are more measurements (data points) for minute precipitation than for hourly and daily precipitation, one could expect plots with more points for minute precipitation than for hourly and daily. However, by visual inspection of the data, it seems like the precipitation is too small for the gauges to measure the differences well. Therefore, the stations measure only for example 0.2 mm, 0.4 mm, 0.6 mm etc. This way many of the observations will be represented as the same dot in the graph.

Appendix J R-scripts

The analysis

The following script was used for analyzing the daily, hourly and minute precipitation. It was also used for validation.

```
# Local variations in precipitation in Bergen
# 04.11.2016

# The excel sheet must be saved as csv.
#Remember to change axis name on plots when changing analyzed data
#Remember to change setwd and read.csv file

setwd('C:/Users/Bruker/OneDrive - NTNU/Prosjektoppgave/Local variations in precipitation amounts/Skal bruke/Alle')

# Make a dataframe
dams <- read.csv(file = 'Minutt_Alle.csv', header = TRUE, sep = ';')

# DATA QUALITY CONTROL

# Plot cummulative rainfall to control variation patterns between the stations
par(mfrow = c(1,1))
plot(cumsum(dams$Gyldenpris), type = "n", lty = 1, col = 'black', xlab = 'Hour number',
     ylab = 'Cummulative hourly precipitation (mm)', ylim =c(0,700))
lines(cumsum(dams$Gyldenpris),  lty = 1, col = 'black')
lines(cumsum(dams$Irene), lty = 2, col = 'red')
lines(cumsum(dams$Frelsesarmeen), lty = 3, col = 'blue')
lines(cumsum(dams$Terreng1), lty = 4, col = 'green')
lines(cumsum(dams$Terreng2), lty = 5, col = 'black')
lines(cumsum(dams$Terreng3), lty = 6, col = 'red')
lines(cumsum(dams$Florida), lty = 3, col = 'black')
legend(0, 710, lty = c(1, 2, 3, 4, 5, 6, 3),
       col = c('black', 'red', 'blue','green', 'black', 'red', 'black'),
       c('Gyldenpris', 'Irene','Frelsesarmeen','Terreng1', 'Terreng2', 'Terreng3', 'Florida'))

# Make Double mass plot to control the quality of the data
{par(mfrow = c(2,3))
  plot(cumsum(dams$Florida), cumsum(dams$Gyldenpris), type = "line", ylab = 'Gyldenpris (mm)', xlab = 'Florida (mm)')
  plot(cumsum(dams$Florida), cumsum(dams$Irene),type = "line", ylab = 'Irene (mm)', xlab = 'Florida (mm)')
  plot(cumsum(dams$Florida), cumsum(dams$Frelsesarmeen), type = "line", ylab = 'Frelsesarmeen (mm)',xlab = 'Florida (mm)')
  plot(cumsum(dams$Florida), cumsum(dams$Terreng1),type = "line", ylab = 'Terreng1 (mm)', xlab = 'Florida (mm)')
  plot(cumsum(dams$Florida), cumsum(dams$Terreng2), type = "line", ylab = 'Terreng2 (mm)', xlab = 'Florida (mm)')
  plot(cumsum(dams$Florida), cumsum(dams$Terreng3), type = "line", ylab = 'Terreng3 (mm)', xlab = 'Florida (mm)')
  }

# INVESTIGATION OF LOCAL VARIANCES

# Plot daily precipitation at all stations
par(mfrow = c(1,1))
plot(dams$Gyldenpris, type = 'p', pch = 20, col = 'black', xlab = 'Minute number',
     ylab = 'Minute precipitation (mm/d)')
  lines(dams$Irene, type = 'p', pch = 0, col = 'red')
  lines(dams$Frelsesarmeen, type = 'p', pch = 6, col = 'blue')
  lines(dams$Terreng1, type = 'p', pch = 18, col = 'green')
  lines(dams$Terreng2, type = 'p', pch = 24, col = 'black')
  lines(dams$Terreng3, type = 'p', pch = 4, col = 'black')
  lines(dams$Florida, type = 'p', pch = 8, col = 62)
  legend("topleft", pch = c(20, 0, 6, 18, 24, 4, 8),
         col = c('black', 'red', 'blue','green', 'black', 'black', 62),
         c('Gyldenpris', 'Irene','Frelsesarmeen','Terreng1', 'Terreng2', 'Terreng3', 'Florida'))

# Find the difference in precipiation between Florida and the other stations
g.diff <- dams$Gyldenpris - dams$Florida
i.diff <- dams$Irene - dams$Florida
f.diff <- dams$Frelsesarmeen - dams$Florida
t1.diff <- dams$Terreng1 - dams$Florida
t2.diff <- dams$Terreng2 - dams$Florida
t3.diff <- dams$Terreng3 - dams$Florida

diff <- data.frame(i.diff, f.diff, t1.diff, t2.diff, t3.diff)

# Rank the precipitation at Florida
dams_to_rank1 <- data.frame(dams$Florida, dams$Gyldenpris, dams$Irene, dams$Frelsesarmeen, dams$Terreng1, dams$Terreng2, dams$Terreng3, dams$Florida)
dams_to_rank <- dams_to_rank1[!apply(dams_to_rank1[, -c(1,2)], 1, function(row) all(row == 0)), ]
ranked <- dams_to_rank[order(dams_to_rank$dams.Florida),]

# Plot the ranked precipitation at each station relative
# to Florida
{par(mfrow = c(2,3))
  plot(ranked$dams.Florida, ranked$dams.Gyldenpris, type = 'p', main = 'Gyldenpris',
       xlab = 'Precipitation at Florida (mm)', ylab = 'Precipitation at Gyldenpris (mm)')
  abline(fit.g <- lm(ranked$dams.Gyldenpris ~ ranked$dams.Florida))
  legend("topright", bty="n", legend=paste("R2 =",
                                           format(summary(fit.g)$adj.r.squared, digits=4)))
  plot(ranked$dams.Florida, ranked$dams.Irene, type = 'p', main = 'Irene',
       xlab = 'Precipitation at Florida (mm)', ylab = 'Precipitation at Irene (mm)')
  abline(fit.i <- lm(ranked$dams.Irene ~ ranked$dams.Florida))
  legend("topright", bty="n", legend=paste("R2 =",
                                           format(summary(fit.i)$adj.r.squared, digits=4)))
   plot(ranked$dams.Florida, ranked$dams.Frelsesarmeen,  type = 'p', main = 'Frelsesarmeen',
       xlab = 'Precipitation at Florida (mm)', ylab = 'Precipitation at Frelsesarmeen (mm)')
   abline(fit.f <- lm(ranked$dams.Frelsesarmeen ~ ranked$dams.Florida))
   legend("topright", bty="n", legend=paste("R2 =",
                                            format(summary(fit.f)$adj.r.squared, digits=4)))
   plot(ranked$dams.Florida, ranked$dams.Terreng1,  type = 'p', main = 'Terreng1',
       xlab = 'Precipitation at Florida (mm)', ylab = 'Precipitation at Terreng1 (mm)')
   abline(fit.t1 <- lm(ranked$dams.Terreng1 ~ ranked$dams.Florida))
   legend("topright", bty="n", legend=paste("R2 =",
                                            format(summary(fit.t1)$adj.r.squared, digits=4)))
   plot(ranked$dams.Florida, ranked$dams.Terreng2,  type = 'p', main = 'Terreng2',
       xlab = 'Precipitation at Florida (mm)', ylab = 'Precipitation at Terreng2 (mm)')
   abline(fit.t2 <- lm(ranked$dams.Terreng2 ~ ranked$dams.Florida))
   legend("topright", bty="n", legend=paste("R2 =",
                                            format(summary(fit.t2)$adj.r.squared, digits=4)))
   plot(ranked$dams.Florida, ranked$dams.Terreng3,  type = 'p', main = 'Terreng3',
       xlab = 'Precipitation at Florida (mm)', ylab = 'Precipitation at Terreng3 (mm)')
   abline(fit.t3 <- lm(ranked$dams.Terreng3 ~ ranked$dams.Florida))
   legend("topright", bty="n", legend=paste("R2 =",
                                            format(summary(fit.t3)$adj.r.squared, digits=4)))
  }
```

```
# Find the ranked difference between the stations
g.diff.ranked <- ranked$dams.Gyldenpris - ranked$dams.Florida
i.diff.ranked <- ranked$dams.Irene - ranked$dams.Florida
f.diff.ranked <- ranked$dams.Frelsesarmeen - ranked$dams.Florida
t1.diff.ranked <- ranked$dams.Terreng1 - ranked$dams.Florida
t2.diff.ranked <- ranked$dams.Terreng2 - ranked$dams.Florida
t3.diff.ranked <- ranked$dams.Terreng3 - ranked$dams.Florida

ranked.diff <- data.frame(g.diff.ranked, i.diff.ranked, f.diff.ranked, t1.diff.ranked, t2.diff.ranked, t3.diff.ranked)

# Plot to see that the absolute difference increase with increasing precipitation
par(mfrow = c(2,3))
plot(ranked$dams.Florida, g.diff.ranked, type = 'p', main = 'Gyldenpris',
     xlab = 'Precipitation at Florida (mm)', ylab = 'Difference from Florida (mm)')
abline(h = 0, col = 'red')
abline(fit.diff.g <- lm(g.diff.ranked ~ ranked$dams.Florida))
# Få r2 til å vises i plottet:
legend("topright", bty="n", legend=paste("R2 =",
                    format(summary(fit.diff.g)$adj.r.squared, digits=4)))
plot(ranked$dams.Florida, i.diff.ranked, type = 'p', main = 'Irene',
     xlab = 'Precipitation at Florida (mm)', ylab = 'Difference from Florida (mm)')
abline(h = 0, col = 'red')



abline(fit.diff.i <- lm(i.diff.ranked ~ ranked$dams.Florida))
legend("topright", bty="n", legend=paste("R2 =",
                                         format(summary(fit.diff.i)$adj.r.squared, digits=4)))
plot(ranked$dams.Florida, f.diff.ranked,  type = 'p', main = 'Frelsesarmeen',
     xlab = 'Precipitation at Florida (mm)', ylab = 'Difference from Florida (mm)')
abline(h = 0, col = 'red')
abline(fit.diff.f <- lm(f.diff.ranked ~ ranked$dams.Florida ))
legend("topright", bty="n", legend=paste("R2 =",
                                         format(summary(fit.diff.f)$adj.r.squared, digits=4)))
plot(ranked$dams.Florida, t1.diff.ranked,  type = 'p', main = 'Terreng1',
     xlab = 'Precipitation at Florida (mm)', ylab = 'Difference from Florida (mm)')
abline(h = 0, col = 'red')
abline(fit.diff.t1 <- lm(t1.diff.ranked ~ ranked$dams.Florida))
legend("topright", bty="n", legend=paste("R2 =",
                                         format(summary(fit.diff.t1)$adj.r.squared, digits=4)))
plot(ranked$dams.Florida, t2.diff.ranked,  type = 'p', main = 'Terreng2',
     xlab = 'Precipitation at Florida (mm)', ylab = 'Difference from Florida (mm)')
abline(h = 0, col = 'red')
abline(fit.diff.t2 <- lm(t2.diff.ranked ~ ranked$dams.Florida ))
legend("topright", bty="n", legend=paste("R2 =",
                                         format(summary(fit.diff.t2)$adj.r.squared, digits=4)))
plot(ranked$dams.Florida, t3.diff.ranked,  type = 'p', main = 'Terreng3',
     xlab = 'Precipitation at Florida (mm)', ylab = 'Difference from Florida (mm)')
abline(h = 0, col = 'red')
abline(fit.diff.t3 <- lm(t3.diff.ranked ~ ranked$dams.Florida))
legend("topright", bty="n", legend=paste("R2 =",
                                         format(summary(fit.diff.t3)$adj.r.squared, digits=4)))


# Find the % difference (using ranked data)
g.percent <- g.diff.ranked/ranked$dams.Florida*100
i.percent <- i.diff.ranked/ranked$dams.Florida*100
f.percent <- f.diff.ranked/ranked$dams.Florida*100
t1.percent <- t1.diff.ranked/ranked$dams.Florida*100
t2.percent <- t2.diff.ranked/ranked$dams.Florida*100
t3.percent <- t3.diff.ranked/ranked$dams.Florida*100

percent.diff <- data.frame(g.percent, i.percent, f.percent, t1.percent, t2.percent, t3.percent)

# Plot the % difference against the precipitation at Florida
{par(mfrow = c(2,3))
plot(ranked$dams.Florida, g.percent, type = 'p', main = 'Gyldenpris',
     xlab = 'Precipitation at Florida (mm)', ylab = '% difference from Florida')
  abline(h = 0, col = 'red')
plot(ranked$dams.Florida, i.percent, type = 'p', main = 'Irene',
     xlab = 'Precipitation at Florida (mm)', ylab = '% difference from Florida')
  abline(h = 0, col = 'red')
plot(ranked$dams.Florida, f.percent,  type = 'p', main = 'Frelsesarmeen',
     xlab = 'Precipitation at Florida (mm)', ylab = '% difference from Florida')
  abline(h = 0, col = 'red')
plot(ranked$dams.Florida, t1.percent,  type = 'p', main = 'Terreng1',
     xlab = 'Precipitation at Florida (mm)', ylab = '% difference from Florida')
  abline(h = 0, col = 'red')
plot(ranked$dams.Florida, t2.percent,  type = 'p', main = 'Terreng2',
     xlab = 'Precipitation at Florida (mm)', ylab = '% difference from Florida')
  abline(h = 0, col = 'red')
plot(ranked$dams.Florida, t3.percent,  type = 'p', main = 'Terreng3',
     xlab = 'Precipitation at Florida (mm)', ylab = '% difference from Florida')
abline(h = 0, col = 'red')
}

# DIVIDE INTO PRECIPITATION INTERVALS

# Find the mean precipitation in each interval
ranked$cut <- cut(ranked$dams.Florida,
                  breaks = c(- Inf, 0.5, 1, 1.5, Inf),
                  labels = c("0-0.5 mm", "0.5-1.0 mm", "1.0-1.5 mm", "over 1.5 mm"),
                  right = FALSE)

cut <- data.frame(ranked$cut, ranked$dams.Gyldenpris, ranked$dams.Irene, ranked$dams.Frelsesarmeen,
                  ranked$dams.Terreng1, ranked$dams.Terreng2, ranked$dams.Terreng3, ranked$dams.Terreng3,
                  ranked$dams.Florida)

cut.mean <- aggregate(cut[, 2:9], list(cut$ranked.cut), mean)

# Make a data.frame with precipitation intervals and belonging percent difference
cut.percent <- data.frame(ranked$cut, g.percent, i.percent, f.percent, t1.percent, t2.percent, t3.percent)
# Remove NaN and Inf values
cut.p <- data.frame(cut.percent[is.finite(cut.percent$g.percent) & is.finite(cut.percent$i.percent) &
                                is.finite(cut.percent$f.percent) & is.finite(cut.percent$t1.percent) &
                                is.finite(cut.percent$t2.percent) & is.finite(cut.percent$t3.percent), ])

#Find the average differance in each group
cut.p.mean <- aggregate(cut.p[, 2:7], list(cut.p$ranked.cut), mean)

write.table(cut.p.mean, file = 'Minutt mean percent diff validering.txt')

intervals <- c(0.25, 0.75, 1.25, 1.6)
cut.m.p <- data.frame(intervals, cut.p.mean$g.percent, cut.p.mean$i.percent, cut.p.mean$f.percent,
                      cut.p.mean$t1.percent, cut.p.mean$t2.percent, cut.p.mean$t3.percent)
```

```
#Plot the averages in each group (lines)

plot(cut.p.mean$Group.1, cut.p.mean$g.percent, type = "n", lty = 1, col = 'black', xlab = 'Precipitation at Florida (mm)',
     ylab = 'Mean difference from Florida (mm)', ylim = c(-120, 0))
lines(cut.p.mean$Group.1, cut.p.mean$g.percent, lty = 1)
lines(cut.p.mean$Group.1, cut.p.mean$i.percent, lty = 2, col = 'red')
lines(cut.p.mean$Group.1, cut.p.mean$f.percent, lty = 3, col = 'blue')
lines(cut.p.mean$Group.1, cut.p.mean$t1.percent, lty = 4, col = 'green')
lines(cut.p.mean$Group.1, cut.p.mean$t2.percent, lty = 5, col = 'black')
lines(cut.p.mean$Group.1, cut.p.mean$t3.percent, lty = 6, col = 'black')
  abline(h = 0, col = 'red')
  legend("topright", lty = c(1, 2, 3, 4, 5, 6),
         col = c('black', 'red', 'blue','green', 'black', 'black'),
         c('Gyldenpris', 'Irene','Frelsesarmeen','Terreng1', 'Terreng2', 'Terreng3'))

#Plot the averages in each group (points)
plot(cut.p.mean$Group.1, cut.p.mean$g.percent, type = "n", lty = 1, col = 'black', xlab = 'Precipitation at Florida (mm)',
       ylab = 'Mean difference from Florida (mm)', ylim = c(-120, 0))
  points(cut.p.mean$Group.1, cut.p.mean$g.percent, pch = 1)
  points(cut.p.mean$Group.1, cut.p.mean$i.percent, pch = 2, col = 'red')
  points(cut.p.mean$Group.1, cut.p.mean$f.percent, pch = 3, col = 'blue')
  points(cut.p.mean$Group.1, cut.p.mean$t1.percent, pch = 4, col = 'green')
  points(cut.p.mean$Group.1, cut.p.mean$t2.percent, pch = 5, col = 'black')
  points(cut.p.mean$Group.1, cut.p.mean$t3.percent, pch = 6, col = 'black')
  abline(h = 0, col = 'red')
  legend("topright", lty = c(1, 2, 3, 4, 5, 6),
         col = c('black', 'red', 'blue','green', 'black', 'black'),
         c('Gyldenpris', 'Irene','Frelsesarmeen','Terreng1', 'Terreng2', 'Terreng3'))


#REMOVE THE EXTREMES (10%)

n <- as.numeric(nrow(ranked))
x <- round(0.1*n)

extremes <- ranked[(n-x):n,]
normals <- ranked[0:(n-x-1),]




# Analyze the normal precipitation

# Plot the ranked precipitation at each station relative
# to Florida
{par(mfrow = c(2,3))
  plot(normals$dams.Florida, normals$dams.Gyldenpris, type = 'p', main = 'Gyldenpris',
       xlab = 'Precipitation at Florida (mm)', ylab = 'Precipitation at Gyldenpris (mm)')
  abline(fit.n.g <- lm(normals$dams.Gyldenpris ~ normals$dams.Florida))
  legend("topright", bty="n", legend=paste("R2 =",
                                           format(summary(fit.n.g)$adj.r.squared, digits=4)))
  plot(normals$dams.Florida, normals$dams.Irene, type = 'p', main = 'Irene',
       xlab = 'Precipitation at Florida (mm)', ylab = 'Precipitation at Irene (mm)')
  abline(fit.n.i <- lm(normals$dams.Irene ~ normals$dams.Florida))
  legend("topright", bty="n", legend=paste("R2 =",
                                           format(summary(fit.n.i)$adj.r.squared, digits=4)))
  plot(normals$dams.Florida, normals$dams.Frelsesarmeen,  type = 'p', main = 'Frelsesarmeen',
       xlab = 'Precipitation at Florida (mm)', ylab = 'Precipitation at Frelsesarmeen (mm)')
  abline(fit.n.f <- lm(normals$dams.Frelsesarmeen ~ normals$dams.Florida))
  legend("topright", bty="n", legend=paste("R2 =",
                                           format(summary(fit.n.f)$adj.r.squared, digits=4)))
  plot(normals$dams.Florida, normals$dams.Terreng1,  type = 'p', main = 'Terreng1',
       xlab = 'Precipitation at Florida (mm)', ylab = 'Precipitation at Terreng1 (mm)')
  abline(fit.n.t1 <- lm(normals$dams.Terreng1 ~ normals$dams.Florida))
  legend("topright", bty="n", legend=paste("R2 =",
                                           format(summary(fit.n.t1)$adj.r.squared, digits=4)))
  plot(normals$dams.Florida, normals$dams.Terreng2,  type = 'p', main = 'Terreng2',
       xlab = 'Precipitation at Florida (mm)', ylab = 'Precipitation at Terreng2 (mm)')
  abline(fit.n.t2 <- lm(normals$dams.Terreng2 ~ normals$dams.Florida))
  legend("topright", bty="n", legend=paste("R2 =",
                                           format(summary(fit.n.t2)$adj.r.squared, digits=4)))
  plot(normals$dams.Florida, normals$dams.Terreng3,  type = 'p', main = 'Terreng3',
       xlab = 'Precipitation at Florida (mm)', ylab = 'Precipitation at Terreng3 (mm)')
  abline(fit.n.t3 <- lm(normals$dams.Terreng3 ~ normals$dams.Florida))
  legend("topright", bty="n", legend=paste("R2 =",
                                           format(summary(fit.n.t3)$adj.r.squared, digits=4)))
}

# Find the ranked difference between the stations
g.diff.normals <- normals$dams.Gyldenpris - normals$dams.Florida
i.diff.normals <- normals$dams.Irene - normals$dams.Florida
f.diff.normals <- normals$dams.Frelsesarmeen - normals$dams.Florida
t1.diff.normals <- normals$dams.Terreng1 - normals$dams.Florida
t2.diff.normals <- normals$dams.Terreng2 - normals$dams.Florida
t3.diff.normals <- normals$dams.Terreng3 - normals$dams.Florida

normals.diff <- data.frame(g.diff.normals, i.diff.normals, f.diff.normals, t1.diff.normals, t2.diff.normals, t3.diff.normals)
```

```
# Plot to see that the absolute difference increase with increasing precipitation
{par(mfrow = c(2,3))
  plot(normals$dams.Florida, g.diff.normals, type = 'p', main = 'Gyldenpris',
       xlab = 'Precipitation at Florida (mm)', ylab = 'Difference from Florida (mm)')
  abline(h = 0, col = 'red')
  abline(fit.diff.n.g <- lm(g.diff.normals ~ normals$dams.Florida))
  legend("topright", bty="n", legend=paste("R2 =",
                                           format(summary(fit.diff.n.g)$adj.r.squared, digits=4)))
  plot(normals$dams.Florida, i.diff.normals, type = 'p', main = 'Irene',
       xlab = 'Precipitation at Florida (mm)', ylab = 'Difference from Florida (mm)')
  abline(h = 0, col = 'red')
  abline(fit.diff.n.i <- lm(i.diff.normals ~ normals$dams.Florida))
  legend("topright", bty="n", legend=paste("R2 =",
                                           format(summary(fit.diff.n.i)$adj.r.squared, digits=4)))
  plot(normals$dams.Florida, f.diff.normals,  type = 'p', main = 'Frelsesarmeen',
       xlab = 'Precipitation at Florida (mm)', ylab = 'Difference from Florida (mm)')
  abline(h = 0, col = 'red')
  abline(fit.diff.n.f <- lm(f.diff.normals ~ normals$dams.Florida ))
  legend("topright", bty="n", legend=paste("R2 =",
                                           format(summary(fit.diff.n.f)$adj.r.squared, digits=4)))
  plot(normals$dams.Florida, t1.diff.normals,  type = 'p', main = 'Terreng1',
       xlab = 'Precipitation at Florida (mm)', ylab = 'Difference from Florida (mm)')
  abline(h = 0, col = 'red')
  abline(fit.diff.n.t1 <- lm(t1.diff.normals ~ normals$dams.Florida.))
  legend("topright", bty="n", legend=paste("R2 =",
                                           format(summary(fit.diff.n.t1)$adj.r.squared, digits=4)))
  plot(normals$dams.Florida, t2.diff.normals,  type = 'p', main = 'Terreng2',
       xlab = 'Precipitation at Florida (mm)', ylab = 'Difference from Florida (mm)')
  abline(h = 0, col = 'red')
  abline(fit.diff.n.t2 <- lm(t2.diff.normals ~ normals$dams.Florida ))
  legend("topright", bty="n", legend=paste("R2 =",
                                           format(summary(fit.diff.n.t2)$adj.r.squared, digits=4)))
  plot(normals$dams.Florida, t3.diff.normals,  type = 'p', main = 'Terreng3',
       xlab = 'Precipitation at Florida (mm)', ylab = 'Difference from Florida (mm)')
  abline(h = 0, col = 'red')
  abline(fit.diff.n.t3 <- lm(t3.diff.normals ~ normals$dams.Florida ))
  legend("topright", bty="n", legend=paste("R2 =",
                                           format(summary(fit.diff.n.t3)$adj.r.squared, digits=4)))
}

# Find the % difference (using ranked data)
g.percent.n <- g.diff.normals/normals$dams.Florida.*100
i.percent.n <- i.diff.normals/normals$dams.Florida.*100
f.percent.n <- f.diff.normals/normals$dams.Florida.*100
t1.percent.n <- t1.diff.normals/normals$dams.Florida*100
t2.percent.n <- t2.diff.normals/normals$dams.Florida*100
t3.percent.n <- t3.diff.normals/normals$dams.Florida*100

percent.diff.n <- data.frame(g.percent.n, i.percent.n, f.percent.n, t1.percent.n, t2.percent.n, t3.percent.n)

# Plot the % difference against the precipitation at Florida
{par(mfrow = c(2,3))
  plot(normals$dams.Florida, g.percent.n, type = 'p', main = 'Gyldenpris',
       xlab = 'Precipitation at Florida (mm)', ylab = '% difference from Florida')
  abline(h = 0, col = 'red')
  plot(normals$dams.Florida, i.percent.n, type = 'p', main = 'Irene',
       xlab = 'Precipitation at Florida (mm)', ylab = '% difference from Florida')
  abline(h = 0, col = 'red')
  plot(normals$dams.Florida, f.percent.n,  type = 'p', main = 'Frelsesarmeen',
       xlab = 'Precipitation at Florida (mm)', ylab = '% difference from Florida')
  abline(h = 0, col = 'red')
  plot(normals$dams.Florida, t1.percent.n,  type = 'p', main = 'Terreng1',
       xlab = 'Precipitation at Florida (mm)', ylab = '% difference from Florida')
  abline(h = 0, col = 'red')
  plot(normals$dams.Florida, t2.percent.n,  type = 'p', main = 'Terreng2',
       xlab = 'Precipitation at Florida (mm)', ylab = '% difference from Florida')
  abline(h = 0, col = 'red')
  plot(normals$dams.Florida, t3.percent.n,  type = 'p', main = 'Terreng3',
       xlab = 'Precipitation at Florida (mm)', ylab = '% difference from Florida')
  abline(h = 0, col = 'red')
}

# Analyze the extreme precipitation

# Plot the ranked precipitation at each station relative
# to Florida
{par(mfrow = c(2,3))
  plot(extremes$dams.Florida, extremes$dams.Gyldenpris, type = 'p', main = 'Gyldenpris',
       xlab = 'Precipitation at Florida (mm)', ylab = 'Precipitation at Gyldenpris (mm)')
  abline(fit.e.g <- lm(extremes$dams.Gyldenpris ~ extremes$dams.Florida))
```

```
  legend("topright", bty="n", legend=paste("R2 =",
                                           format(summary(fit.e.g)$adj.r.squared, digits=4)))
  plot(extremes$dams.Florida, extremes$dams.Irene, type = 'p', main = 'Irene',
       xlab = 'Precipitation at Florida (mm)', ylab = 'Precipitation at Irene (mm)')
  abline(fit.e.i <- lm(extremes$dams.Irene ~ extremes$dams.Florida))
  legend("topright", bty="n", legend=paste("R2 =",
                                           format(summary(fit.e.i)$adj.r.squared, digits=4)))
  plot(extremes$dams.Florida, extremes$dams.Frelsesarmeen,  type = 'p', main = 'Frelsesarmeen',
       xlab = 'Precipitation at Florida (mm)', ylab = 'Precipitation at Frelsesarmeen (mm)')
  abline(fit.e.f <- lm(extremes$dams.Frelsesarmeen ~ extremes$dams.Florida))
  legend("topright", bty="n", legend=paste("R2 =",
                                           format(summary(fit.e.f)$adj.r.squared, digits=4)))
  plot(extremes$dams.Florida, extremes$dams.Terreng1,  type = 'p', main = 'Terreng1',
       xlab = 'Precipitation at Florida (mm)', ylab = 'Precipitation at Terreng1 (mm)')
  abline(fit.e.t1 <- lm(extremes$dams.Terreng1 ~ extremes$dams.Florida))
  legend("topright", bty="n", legend=paste("R2 =",
                                           format(summary(fit.e.t1)$adj.r.squared, digits=4)))
  plot(extremes$dams.Florida, extremes$dams.Terreng2,  type = 'p', main = 'Terreng2',
       xlab = 'Precipitation at Florida (mm)', ylab = 'Precipitation at Terreng2 (mm)')
  abline(fit.e.t2 <- lm(extremes$dams.Terreng2 ~ extremes$dams.Florida))
  legend("topright", bty="n", legend=paste("R2 =",
                                           format(summary(fit.e.t2)$adj.r.squared, digits=4)))
  plot(extremes$dams.Florida, extremes$dams.Terreng3,  type = 'p', main = 'Terreng3',
       xlab = 'Precipitation at Florida (mm)', ylab = 'Precipitation at Terreng3 (mm)')
  abline(fit.e.t3 <- lm(extremes$dams.Terreng3 ~ extremes$dams.Florida))
  legend("topright", bty="n", legend=paste("R2 =",
                                           format(summary(fit.e.t3)$adj.r.squared, digits=4)))
}

# Find the ranked difference between the stations
g.diff.extremes <- extremes$dams.Gyldenpris - extremes$dams.Florida
i.diff.extremes <- extremes$dams.Irene - extremes$dams.Florida
f.diff.extremes <- extremes$dams.Frelsesarmeen - extremes$dams.Florida
t1.diff.extremes <- extremes$dams.Terreng1 - extremes$dams.Florida
t2.diff.extremes <- extremes$dams.Terreng2 - extremes$dams.Florida
t3.diff.extremes <- extremes$dams.Terreng3 - extremes$dams.Florida

normals.diff.e <- data.frame(g.diff.extremes, i.diff.extremes, f.diff.extremes, t1.diff.extremes, t2.diff.extremes, t3.diff.extremes)

# Plot to see that the absolute difference increase with increasing precipitation
{par(mfrow = c(2,3))
  plot(extremes$dams.Florida, g.diff.extremes, type = 'p', main = 'Gyldenpris',
       xlab = 'Precipitation at Florida (mm)', ylab = 'Difference from Florida (mm)')
  #abline(h = 0, col = 'red')
  abline(fit.diff.e.g <- lm(g.diff.extremes ~ extremes$dams.Florida))
  legend("topright", bty="n", legend=paste("R2 =",
                                           format(summary(fit.diff.e.g)$adj.r.squared, digits=4)))
  plot(extremes$dams.Florida, i.diff.extremes, type = 'p', main = 'Irene',
       xlab = 'Precipitation at Florida (mm)', ylab = 'Difference from Florida (mm)')
 # abline(h = 0, col = 'red')
  abline(fit.diff.e.i <- lm(i.diff.extremes ~ extremes$dams.Florida ))
  legend("topright", bty="n", legend=paste("R2 =",
                                           format(summary(fit.diff.e.i)$adj.r.squared, digits=4)))
  plot(extremes$dams.Florida, f.diff.extremes,  type = 'p', main = 'Frelsesarmeen',
       xlab = 'Precipitation at Florida (mm)', ylab = 'Difference from Florida (mm)')
  #abline(h = 0, col = 'red')
  abline(fit.diff.e.f <- lm(f.diff.extremes ~ extremes$dams.Florida ))
  legend("topright", bty="n", legend=paste("R2 =",
                                           format(summary(fit.diff.e.f)$adj.r.squared, digits=4)))
  plot(extremes$dams.Florida, t1.diff.extremes,  type = 'p', main = 'Terreng1',
       xlab = 'Precipitation at Florida (mm)', ylab = 'Difference from Florida (mm)')
  #abline(h = 0, col = 'red')
  abline(fit.diff.e.t1 <- lm(t1.diff.extremes ~ extremes$dams.Florida ))
  legend("topright", bty="n", legend=paste("R2 =",
                                           format(summary(fit.diff.e.t1)$adj.r.squared, digits=4)))
  plot(extremes$dams.Florida, t2.diff.extremes,  type = 'p', main = 'Terreng2',
       xlab = 'Precipitation at Florida (mm)', ylab = 'Difference from Florida (mm)')
  #abline(h = 0, col = 'red')
  abline(fit.diff.e.t2 <- lm(t2.diff.extremes ~ extremes$dams.Florida ))
  legend("topright", bty="n", legend=paste("R2 =",
                                           format(summary(fit.diff.e.t2)$adj.r.squared, digits=4)))
  plot(extremes$dams.Florida, t3.diff.extremes,  type = 'p', main = 'Terreng3',
       xlab = 'Precipitation at Florida (mm)', ylab = 'Difference from Florida (mm)')
  #abline(h = 0, col = 'red')
  abline(fit.diff.e.t3 <- lm(t3.diff.extremes ~ extremes$dams.Florida))
  legend("topright", bty="n", legend=paste("R2 =",
                                           format(summary(fit.diff.e.t3)$adj.r.squared, digits=4)))
}

# Find the % difference (using ranked data)
g.percent.e <- g.diff.extremes/extremes$dams.Florida*100
i.percent.e <- i.diff.extremes/extremes$dams.Florida*100
f.percent.e <- f.diff.extremes/extremes$dams.Florida*100
t1.percent.e <- t1.diff.extremes/extremes$dams.Florida*100
t2.percent.e <- t2.diff.extremes/extremes$dams.Florida*100
t3.percent.e <- t3.diff.extremes/extremes$dams.Florida*100

percent.diff.e <- data.frame(g.percent.e, i.percent.e, f.percent.e, t1.percent.e, t2.percent.e, t3.percent.e)

# Find the mean percent differance
mean.g <- mean(percent.diff.e$g.percent.e)
mean.i <- mean(percent.diff.e$i.percent.e)
mean.f <- mean(percent.diff.e$f.percent.e)
mean.t1 <- mean(percent.diff.e$t1.percent.e)
mean.t2 <- mean(percent.diff.e$t2.percent.e)
mean.t3 <- mean(percent.diff.e$t3.percent.e)

m.g <- round(mean.g)
m.i <- round(mean.i)
m.f <- round(mean.f)
m.t1 <- round(mean.t1)
m.t2 <- round(mean.t2)
m.t3 <- round(mean.t3)

lines(extremes$dams.Florida, rsum.g)

# Plot the % difference against the precipitation at Florida
par(mfrow = c(2,3))
plot(extremes$dams.Florida, g.percent.e, type = 'p', main = 'Gyldenpris',
     xlab = 'Precipitation at Florida (mm)', ylab = '% difference from Florida')
abline(h = 0, col = 'red')
legend("topright", bty = "n", legend = paste("mean (%) =", m.g))
plot(extremes$dams.Florida, i.percent.e, type = 'p', main = 'Irene',
     xlab = 'Precipitation at Florida (mm)', ylab = '% difference from Florida')
abline(h = 0, col = 'red')
legend("topright", bty = "n", legend = paste("mean (%) =", m.i))
plot(extremes$dams.Florida, f.percent.e,  type = 'p', main = 'Frelsesarmeen',
     xlab = 'Precipitation at Florida (mm)', ylab = '% difference from Florida')
abline(h = 0, col = 'red')
legend("topright", bty = "n", legend = paste("mean (%) =", m.f))
plot(extremes$dams.Florida, t1.percent.e,  type = 'p', main = 'Terreng1',
     xlab = 'Precipitation at Florida (mm)', ylab = '% difference from Florida')
abline(h = 0, col = 'red')
legend("topright", bty = "n", legend = paste("mean (%) =", m.t1))
plot(extremes$dams.Florida, t2.percent.e,  type = 'p', main = 'Terreng2',
     xlab = 'Precipitation at Florida (mm)', ylab = '% difference from Florida')
abline(h = 0, col = 'red')
legend("topright", bty = "n", legend = paste("mean (%) =", m.t2))
```

```
plot(extremes$dams.Florida, t3.percent.e,  type = 'p', main = 'Terreng3',
     xlab = 'Precipitation at Florida (mm)', ylab = '% difference from Florida')
abline(h = 0, col = 'red')
legend("topright", bty = "n", legend = paste("mean (%) =", m.t3))


# Plot the % difference against the precipitation at Florida
par(mfrow = c(2,3))
plot(extremes$dams.Florida, g.percent.e, type = 'p', main = 'Gyldenpris',
     xlab = 'Precipitation at Florida (mm)', ylab = '% difference from Florida')
abline(h = 0, col = 'red')
points(cut.m.p$intervals, cut.m.p$cut.p.mean.g.percent, pch = 11, col ='red')
plot(extremes$dams.Florida, i.percent.e, type = 'p', main = 'Irene',
     xlab = 'Precipitation at Florida (mm)', ylab = '% difference from Florida')
abline(h = 0, col = 'red')
points(cut.m.p$intervals, cut.m.p$cut.p.mean.i.percent, pch = 11, col ='red')
plot(extremes$dams.Florida, f.percent.e,  type = 'p', main = 'Frelsesarmeen',
     xlab = 'Precipitation at Florida (mm)', ylab = '% difference from Florida')
abline(h = 0, col = 'red')
points(cut.m.p$intervals, cut.m.p$cut.p.mean.f.percent, pch = 11, col ='red')
plot(extremes$dams.Florida, t1.percent.e,  type = 'p', main = 'Terreng1',
     xlab = 'Precipitation at Florida (mm)', ylab = '% difference from Florida')
abline(h = 0, col = 'red')
points(cut.m.p$intervals, cut.m.p$cut.p.mean.t1.percent, pch = 11, col ='red')
plot(extremes$dams.Florida, t2.percent.e,  type = 'p', main = 'Terreng2',
     xlab = 'Precipitation at Florida (mm)', ylab = '% difference from Florida')
abline(h = 0, col = 'red')
points(cut.m.p$intervals, cut.m.p$cut.p.mean.t2.percent, pch = 11, col ='red')
plot(extremes$dams.Florida, t3.percent.e,  type = 'p', main = 'Terreng3',
     xlab = 'Precipitation at Florida (mm)', ylab = '% difference from Florida')
abline(h = 0, col = 'red')
points(cut.m.p$intervals, cut.m.p$cut.p.mean.t3.percent, pch = 11, col ='red')
cut.m.p <- data.frame(intervals, cut.p.mean$g.percent, cut.p.mean$i.percent, cut.p.mean$f.percent,
                      cut.p.mean$t1.percent, cut.p.mean$t2.percent, cut.p.mean$t3.percent)

# Find corrolation between all stations stations
dams_matrix <- data.matrix(dams[2:8])
correlation <- cor(dams_matrix)

# Find corrolation between the stations with extremes and normal precipitation
extremes_matrix <- data.matrix(extremes[2:8])
correlation_extremes <- cor(extremes_matrix)

# Find corrolation between stations with normal precipitation
normals_matrix <- data.matrix(normals[2:8])
correlation_normals <- cor(normals_matrix)

write.table(correlation_normals, file = 'correlation normals.txt')
```

Extra script for validation

The following script was used to compare the mean precipitation difference from the original data period and validation period.

```
#Validation

setwd('C:/Users/Bruker/OneDrive - NTNU/Prosjektoppgave/Local variations in precipitation amounts/Skal bruke/Alle/Validering')

# Make a dataframe
val <- read.csv(file = 'Dag mean alle validering.csv', header = TRUE, sep = ';')


par(mfrow = c(2,3))
  plot(val$X, val$Gyldenpris, type = 'l')
  lines(val$X, val$VGyldenpris, col = 'red', lty = 2)
  plot(val$X, val$Irene, type = 'l')
  lines(val$X, val$VIrene, col = 'red', lty = 2)
  plot(val$X, val$Frelsesarmeen, type = 'l')
  lines(val$X, val$VFrelsesarmeen, col = 'red', lty = 2)
  plot(val$X, val$Terreng1, type = 'l')
  lines(val$X, val$VTerreng1, col = 'red', lty = 2)
  plot(val$X, val$Terreng2, type = 'l')
  lines(val$X, val$VTerreng2, col = 'red', lty = 2)
  plot(val$X, val$Terreng2, type = 'l')
  lines(val$X, val$VTerreng2, col = 'red', lty = 2)

  par(mfrow = c(2,3))
  plot(val$X, val$Gyldenpris, type = 'p', xlab = 'Mean interval precipitation (mm)', ylab = 'Precipitation difference (%)', main = 'Gyldenpris')
  points(val$X, val$VGyldenpris, col = 'red', pch = 2)
  plot(val$X, val$Irene, type = 'p', xlab = 'Mean interval precipitation (mm)', ylab = 'Precipitation difference (%)', main = 'Irene')
  points(val$X, val$VIrene, col = 'red', pch = 2)
  plot(val$X, val$Frelsesarmeen, type = 'p', xlab = 'Mean interval precipitation (mm)', ylab = 'Precipitation difference (%)', main = 'Frelsesarmeen')
  points(val$X, val$VFrelsesarmeen, col = 'red', pch = 2)
  plot(val$X, val$Terreng1, type = 'p',, xlab = 'Mean interval precipitation (mm)', ylab = 'Precipitation difference (%)', main = 'Terreng1')
  points(val$X, val$VTerreng1, col = 'red', pch = 2)
  plot(val$X, val$Terreng2, type = 'p', xlab = 'Mean interval precipitation (mm)', ylab = 'Precipitation difference (%)', main = 'Terreng2')
  points(val$X, val$VTerreng2, col = 'red', pch = 2)
  plot(val$X, val$Terreng2, type = 'p', xlab = 'Mean interval precipitation (mm)', ylab = 'Precipitation difference (%)', main = 'Terreng3')
  points(val$X, val$VTerreng2, col = 'red', pch = 2)
```

Appendix K Description of Project Thesis fall 2016

Candidate name: Guro Kleiven

Subject: Statistical downscaling / stormwater

Title: Statistical Downscaling of Global Climate Models for Use in Stormwater Management in Bergen

Start:

Due date:

Background

The city of Bergen is renowned for its plentiful rainfall. This precipitation is primarily caused by the combination of winds coming in from the west and the pronounced topography surrounding the city (e.g. Jonassen et al. 2013) The municipality in Bergen continuously work on ensuring a secure handling of the stormwater resulting from this precipitation.

Recent reports on future climate, such as the Fifth Assessment Report (IPCC 2013) and KLIMA 2100 (Hanssen-Bauer E.J., Haddeland, I., Hisdal, H., Mayer, S. 2015) ,indicate an increased risk for more heavy and frequent precipitation extremes. These projections are of great concern to the city of Bergen as the infrastructure they design and manage today also should be sufficient in the future.

Although the municipality in Bergen is eager to adapt to climate change, the large-scale projections reflected in the abovementioned reports does not provide enough information to do so. This is mainly due to the coarse spatial and temporal resolution of the projections

In order to bridge this gap, techniques for translating the large-scale climate to the local scale has been developed (Maraun et al. 2010). Empirical-statistical downscaling (ESD) is a widely applied method for this purpose (see e.g. Benestad et al. 2008). The benefits of ESD is that it is easy to use and does not require much computer capacity. However, being based only on statistics, the method is challenged when applied to areas such as Bergen where local properties (e.g. pronounced topography) has a great influence on the precipitation patterns and cause high local variations.

The aim of this project work will be to investigate the applicability of ESD of precipitation in areas with high local variations and to sub-daily time steps.

References:

Benestad, R.E., Hanssen-Bauer, I. & Chen, D., 2008. *Empirical-statistical downscaling*, World Scientific.

Hanssen-Bauer E.J., Haddeland, I., Hisdal, H., Mayer, S., I.F., 2015. Klima i Norge 2100., (2).

IPCC, 2013. *Climate Change 2013: The Physical Science Basis. Contribution of Working Group I to the Fifth Assessment Report of the Intergovernmental Panel on Climate Change*, Cambridge, United Kingdom and New York, NY, USA: Cambridge University Press. Available at: www.climatechange2013.org.

Jonassen, M.O. et al., 2013. Simulations of the Bergen orographic wind shelter. , 1, pp.1–17.

Maraun, D. et al., 2010. Precipitation downscaling under climate change: Recent developements to bridge the gap between dynamical models and the end user. *Reviews of Geophysics*, 48(2009RG000314), pp.1–38.

Objectives

The main objectives of the project are:

1) Literature review of:
    a. Precipitation in Bergen
    b. Downscaling (mainly statistical downscaling) to sub-daily time steps
    c. Use of downscaled climate projections in the support of stormwater management.
2) Investigation of local variations in precipitation amounts by analyzing measurements from a network of precipitation gauges located in Bergen.
3) Investigate whether statistical downscaling can be used for downscaling precipitation in Bergen to a sub-daily time step.

Collaboration partners: BINGO, Bergen Kommune

Location: The project thesis will be conducted at the Department of Hydraulic and Environmental Engineering. The candidate should have regular meetings with advisors(s) and collaboration partners.

Advisors: Erle Kristvik, Tone Merete Muthanna

Bibliography

Arnbjerg-Nielsen, K. A. 2008. Quantification of climate change impacts on extreme precipitation used for design of sewer systems. *Proceedings of the 11th International Conference on Urban Drainage* 31(

Benestad, R. E., Chen, D. & Hanssen-Bauer, I. 2007. *Empirical-Statistical Downscaling*.

Google. Available: https://www.google.no/maps/@59.8649422,4.8082643,6.75z [Accessed 22.12. 2016].

Hanssen-Bauer, I., Førland, E. J., Haddeland, I., Hisdal, H., Mayer, S., Nesje, A., Nilsen, J. E. Ø., Sandven, S., Sandø, A. B., Sorteberg, A. & Ådlandsvik, B. 2015. Klima i Norge 2100, klimasservicesenter, N.

Hassan, Z., Shamsudin, S. & Harun, S. 2014. Application of SDSM and LARS-WG for simulating and downscaling of rainfall and temperature. *Theoretical and Applied Climatology,* 116(1-2)**,** pp 243-257.

Herath, H., Sarukkalige, P. R. & Nguyen, V. T. V. 2015. Downscaling approach to develop future sub-daily IDF relations for Canberra Airport Region, Australia. Joint Inter-Association Symposium on Extreme Hydrological Events, Jun 22-Jul 02 2015 Prague, CZECH REPUBLIC. GOTTINGEN: Copernicus Gesellschaft Mbh, 147-155.

Herath, S. M., Sarukkalige, P. R. & Nguyen, V. T. V. 2016. A spatial temporal downscaling approach to development of IDF relations for Perth airport region in the context of climate change. *Hydrological Sciences Journal-Journal Des Sciences Hydrologiques,* 61(11)**,** pp 2061-2070.

IPCC. 2013. Climate change 2013: The Physical Science Basis. Contribution of Working Group I to the Fifth Assessment Report of the Intergevernmental Panel on Climate Change, [Stocker, T. F., D. Qin, G.-K. Plattner, M., Tignor, S. K. A., J. Boschung, A. Nauels, Y. Xia, V. Bex and P.M. Midgley & (eds.)] (Cambridge University Press, Cambridge, United Kingdom and New York, NY, USA,).

Johansen, S. 2016. *Ekstremverdianalyse av nedbør og oppdatering av intensitet - varighet - frekvenskurver i Bergen Kommune.* Master, Universitetet i Bergen.

Jonassen, M. O., Olafsson, H., Valved, A. S., Reuder, J. & Olseth, J. A. 2013. Simulations of the Bergen orographic wind shelter. *Tellus Series a-Dynamic Meteorology and Oceanography,* 65(17.

Kolstad, E. W. 2016. *Kronikk i BT om klimatjenester* [Online]. Bjerknessenteret for klimaforskning. Available: https://erikwkn.wordpress.com/2016/01/08/kronikk-i-bt-om-klimatjenester/ [Accessed 28.10. 2016].

Nguyen, V. T. V., Desramaut, N. & Nguyen, T. D. 2010. Optimal rainfall temporal patterns for urban drainage design in the context of climate change. *Water Science and Technology,* 62(5)**,** pp 1170-1176.

Nilsen, V., Lier, J. A., Bjerkholt, J. T. & Lindholm, O. G. 2011. Analysing urban floods and combined sewer overflows in a changing climate. *Journal of Water and Climate Change,* 2(4)**,** pp 260-271.

NorskKlimaservicesenter. 2016. Klimaprofil Hordaland.

NRK. 2016. *Ny nedbørsrekord i Bergen* [Online]. Available: https://www.nrk.no/hordaland/ny-nedborsrekord-i-bergen-1.13063470 [Accessed 10.11. 2016].

Schmidli, J., Goodess, C. M., Frei, C., Haylock, M. R., Hundecha, Y., Ribalaygua, J. & Schmith, T. 2007. Statistical and dynamical downscaling of precipitation: An evaluation and comparison of scenarios for the European Alps. *Journal of Geophysical Research-Atmospheres,* 112(D4)**,** pp 20.

Skartveit, A. & Grønås, S. 2009. *Hvorfor regner det så mye i Bergen?* [Online]. Universitetet i Bergen. Available: http://www.uib.no/gfi/56974/hvorfor-regner-det-s%C3%A5-mye-i-bergen [Accessed 28.10. 2016].

Wilby, R., Charles, S., Zorita, E., Timbal, B., Whetton, P. & Mearns, L. 2004. Guidelines for use of climate scenarios developed from statistical downscaling methods. TGICA IPCC August)**,** pp.

Wilby, R. L., A Troni, J., A Biot, Y., A Tedd, L., A Hewitson, B. C., A Smith, D. M. & A Sutton, R. T. 2009. A review of climate risk information for adaptation and development. *International Journal of Climatology,* 29(1193-1215)**,** pp.

Wilby, R. L. & Dawson, C. W. 2013. The Statistical DownScaling Model: insights from one decade of application. *International Journal of Climatology,* 33(7)**,** pp 1707-1719.

Wilby, R. L., Dawson, C. W. & Barrow, E. M. 2002. SDSM - a decision support tool for the assessment of regional climate change impacts. *Environmental Modelling & Software,* 17(2)**,** pp 147-159.

NTNU

Kunnskap for en bedre verden